PATHWAYS OF ABIOTIC HUMIFICATION AS CATALYZED BY MINERAL COLLOIDS

A thesis submitted to the College of Graduate Studies and Research
in partial fulfillment of the requirements for the degree of Doctor of Philosophy
in the Department of Soil Science, University of Saskatchewan, Saskatoon, Canada

By

Ailsa Ghillainé Hardie

Keywords: abiotic humification pathways, polyphenol-Maillard reaction, soil mineral colloids, biomolecules, humic substances, rhodochrosite, catalysis, NEXAFS

PERMISSION TO USE

In presenting this thesis/dissertation in partial fulfillment of the requirements for a Postgraduate degree from the University of Saskatchewan, I agree that the Libraries of this University may make it freely available for inspection. I further agree that permission for copying of this thesis/dissertation in any manner, in whole or in part, for scholarly purposes may be granted by the professor or professors who supervised my thesis/dissertation work or, in their absence, by the Head of the Department or the Dean of the College in which my thesis work was done. It is understood that any copying or publication or use of this thesis/dissertation or parts thereof for financial gain shall not be allowed without my written permission. It is also understood that due recognition shall be given to me and to the University of Saskatchewan in any scholarly use which may be made of any material in my thesis/dissertation.

Requests for permission to copy or to make other uses of materials in this thesis/dissertation in whole or part should be addressed to:

Head of the Department of Soil Science
University of Saskatchewan
51 Campus Drive
Saskatoon, Saskatchewan S7N 5A8
Canada

ABSTRACT

The polyphenol pathway and Maillard reaction (polycondensation of sugars and amino acids) are regarded as important pathways in natural humification. The significance of linking the Maillard reaction and polyphenol pathways into an integrated humification pathway has been addressed. However, the ability of mineral colloids commonly occurring in tropical and temperate environments to promote the Maillard reaction and integrated polyphenol-Maillard humification pathways remained to be uncovered. Furthermore, the effect of the nature and relative abundance of biomolecules on humification and associated reaction products remained to be studied.

The results of this study show that the structure of polyphenols and the relative molar ratio of polyphenol, glucose and glycine, significantly affected humification processes and the associated carbonate formation in the integrated polyphenol-Maillard reaction catalyzed by birnessite. Increasing the molar ratio of *ortho*-polyphenols (catechol and pyrogallol) to Maillard reagents in the polyphenol-Maillard pathway catalyzed by birnessite enhanced humification while suppressing the formation of rhodochrosite ($MnCO_3$). The opposite trend of $MnCO_3$ formation was observed in the *meta*-polyphenol (resorcinol)-Maillard reaction system. Increasing the amount of glucose in the integrated catechol-Maillard system under the catalysis of birnessite promoted the formation of Maillard reaction-type humic acid in the supernatant and $MnCO_3$ in the solid phase.

The catalytic abilities of commonly occurring mineral colloids from temperate and tropical regions greatly differed in influencing humification processes and products in the Maillard reaction and integrated polyphenol-Maillard pathways. Compared with layer silicate colloids, the poorly ordered Fe and Mn oxides were by far the strongest catalysts of humification reactions in

the Maillard and catechol-Maillard pathways. This accounted for the significant difference in reactivity between the sesquioxide-rich Oxisol clay from the high rainfall region of South Africa and the Mollisol clay from the Canadian Prairies. Furthermore, the nature of the mineral colloids also affected the extent of organic C accumulation in the solid phase upon humification, and related mineral surface alteration. The metal oxide- and Oxisol clay-catalyzed Maillard and catechol-Maillard reaction systems had the highest accumulation of organic C in the solid phase, indicating their significance in contributing to C sequestration in the environment.

The findings obtained in this study are of fundamental significance in understanding the influence of the atomic bonding, structural configuration and related surface properties of mineral colloids, and the nature and abundance of biomolecules on the abiotic humification pathways and related reaction products in natural environments.

ACKNOWLEDGEMENTS

I would like to thank my supervisor, Dr P.M. Huang, for giving me this opportunity and for all his guidance and encouragement throughout this project. I wish to thank all the members of my PhD Advisory Committee, Drs D.W. Anderson, D.E. Ward, D. Peak and L.M. Kozak, for their invaluable suggestions and inputs. I would like to thank The Natural Sciences and Engineering Research Council of Canada for financial support and the University of Saskatchewan for the awards of PhD Tuition Scholarship and PhD Devolved Scholarship.

The NEXAFS spectroscopy research described in this thesis was performed at the Canadian Light Source (CLS), which is supported by NSERC, NRC, CIHR, and the University of Saskatchewan. I would like to thank J.J. Dynes, Environment Canada/McMaster University, for assisting me with the NEXAFS spectroscopy data collection at the CLS. I would like to thank Edwige Otero, Department of Chemistry, University of Saskatchewan, for helping to prepare the gold-coated silicon mounts used in the NEXAFS experiments. I would like to thank the SGM beamline staff, Tom Regier and Robert Blyth, and the PGM beamline staff, Yongfeng Hu and Lucia Zuin, at the CLS for their assistance with the NEXAFS experiments.

I would like to thank Barry Goetz for his assistance using the atomic absorption spectrometer. I would like to thank Arlette Seib and Lori Phillips for training me and assisting me with the aseptic techniques used in my experiments. I would like to thank my fellow graduate students at the University of Saskatchewan, Mohammad Tahir, Dani Xu, Christian Dedzoe and Adam Gillespie, for all their help and suggestions during my project.

DEDICATION

To my parents, Caryle and Stewart Hardie.

TABLE OF CONTENTS

LIST OF TABLES

LIST OF FIGURES

1 INTRODUCTION

In the environment, humification is pivotal in transforming biomolecules originating from organized structures typical of organisms to randomly polymerized, heterogeneous humic substances characteristic of biogeochemical systems. Humic substances are formed through both selected preservation processes and biotic (enzymatic) and abiotic (mineral) catalytic synthesis mechanisms (Bollag et al. 1998; Huang 2004; Clapp et al. 2005; Schaumann 2006a, 2006b). The dark colour of humic substances can be attributed to oxidative browning reactions between biomolecules such as sugars, polyphenols, lipids, amino acids and proteins (Rouet-Mayer et al. 1990; Hidalgo and Zamora 2000; Zamora and Hidalgo 2005; Bittner 2006). These browning reactions mostly involve carbonyl-amine reactions and result in the generation of highly coloured, high and low molecular weight polymers (Hidalgo and Zamora 2000). Abundant research evidence at the molecular level shows that enzymes and mineral colloids can enhance the polymerization and/or polycondensation of biomolecules such as amino acids, sugars, and polyphenols, derived from the breakdown of biological residues and from biological metabolites (Stevenson 1994; Bollag et al. 1998; Huang 2000, 2004).

Soil mineral colloids, such as metal oxides and layer silicates, have been shown to catalyze the transformations of natural and synthetic organic compounds (Huang 2000). Poorly ordered Fe- and especially Mn-oxides are the most reactive in facilitating transformations of organic compounds. This includes catalysis of the ring cleavage of polyphenols, the deamination, decarboxylation, and dealkylation of amino acids, the polymerization of phenolic compounds and their polycondensation with amino acids, and the Maillard reaction (Shindo and Huang 1982, 1984a, 1984b; Bollag et al. 1995; Huang 2000; Majecher et al. 2000; Wang and Huang 2000b, 2003; Jokic et al. 2004a).

Abundant scientific evidence at the molecular level shows the significance of the polyphenol pathway in humification (Stevenson 1994; Bollag et al. 1998; Huang 2000, 2004). The surfaces of metal oxides and layer silicates are able to promote the polymerization of phenolic compounds. Redox reactive metal oxides act as oxidants, while Al oxides and layer silicate clays act as Lewis acids, by accepting electrons from hydroxyphenolics, leading to the formation of highly reactive semiquinone radicals which readily undergo coupling reactions with

other semiquinones, phenolics, amino compounds or existing humus (Dec and Bollag 2000; Huang 2000)

The Maillard reaction, involving condensation reactions between sugars and amino acids (Maillard 1913), is regarded as an important pathway in natural humification processes (Ikan et al. 1996). The appeal of the Maillard reaction in understanding humification processes lies in the two proposed precursors (sugars and amino acids) being among the most abundant biomolecules of terrestrial and aquatic environments (Anderson et al. 1989). Although the potential energy barrier of the Maillard reaction is high (Jokic et al. 2001c), Jokic et al. (2001b) reported that birnessite (δ-MnO_2), which is commonly present in the environment, decreases the energy barrier and thus enhances the reaction rates by one to two orders of magnitude under environmentally relevant temperatures (25 and 45° C) and a neutral pH (7.00). Furthermore, Jokic et al. (2004a) clearly showed, using N K-edge NEXAFS, that the Maillard reaction, involving glucose and glycine, catalyzed by birnessite under environmentally relevant conditions not only produces heterocyclic N but also a significant amount of amide N. This provides an explanation for one of the pathways for the formation of heterocyclic N and amide N found in humic substances in the environment.

In nature it is most likely that the Maillard reaction and polyphenol pathways do not occur separately but rather interact with each other as sugars, amino acids and polyphenols coexist in soil solutions and natural waters. Jokic et al. (2004b) were the first to study an abiotic integrated Maillard reaction and polyphenol pathway of humification, using equimolar amounts of catechol, glucose and glycine and birnessite (δ-MnO_2) as catalyst. Their data showed that the ubiquitous soil mineral, birnessite significantly accelerates humification processes in an integrated polyphenol-Maillard reaction system under pH and temperature conditions typical of natural environments. The relative abundance of biomolecules varies with vegetation, microbial community and the environment (Stevenson 1994; Kögel-Knabner 2002). The effects of the type of polyphenol, and the molar ratio of polyphenol to Maillard reactants on the integrated polyphenol-Maillard humification pathway remained to be investigated. Hence, the first objective of this study was to elucidate the role of polyphenols in the integrated polyphenol-Maillard humification pathway under the catalysis of birnessite, by comparing the effect of structurally different polyphenols (catechol, resorcinol, pyrogallol), as well as, the effect of

varying the molar ratio of polyphenol to Maillard reagents (glucose and glycine) on the humification processes and reaction products, including organic and inorganic C.

Glucose is one of the primary decomposition products arising from the natural degradation of cellulose (Koivula and Hanninen 2001), one of the most abundant substrates in the terrestrial environment. However, the role that sugar plays in abiotic humification reactions was not yet fully understood. The influence of glucose in the polyphenol humification pathway and integrated polyphenol-Maillard humification pathway as catalyzed by birnessite remained to be uncovered. Therefore, the second objective of this study was to examine the effect of the molar ratio of glucose to catechol on catechol-humification processes and the effect of the molar ratio of glucose to catechol and glycine in the integrated polyphenol-Maillard humification pathway as catalyzed by birnessite.

The abiotic catalytic ability of soils in the formation of humic substances is attributable to the reactive components, namely Mn, Fe, and Al oxides, (oxy)hydroxides, and short-range ordered mineral colloids, clay-size layer silicates, and some reactive primary minerals (Huang 2000). The Maillard reaction pathway has only been previously investigated using birnessite (Jokic et al. 2001b), smectites and crystalline goethite (Gonzalez and Laird 2004) as catalysts under environmentally relevant conditions, while the integrated polyphenol-Maillard pathway has been investigated using birnessite (Jokic et al. 2004b). Thus far, only the polyphenol theory of abiotic humic substance formation and copolymerization of polyphenols with amino acids have been investigated using natural soils and soil clays (Wang et al. 1983a; Pohlman and McColl 1989; Wang and Huang 1989a, 2003). The catalytic ability of poorly ordered Fe and Al oxides, 1:1 and 2:1 layer silicate clays, and natural soil clays on the Maillard reaction and integrated polyphenol-Maillard reaction humification pathways remained to be studied. Furthermore, little was known on the effect of abiotic humification on the surface chemistry of mineral colloids. Therefore, the third objective of this study was to examine the Maillard reaction and integrated polyphenol-Maillard reaction humification pathways as catalyzed by representative mineral colloids commonly occurring in temperate and tropical soils and sediments, namely, poorly ordered metal oxides (Al, Fe and Mn oxides), pure clay-sized layer silicates (nontronite and kaolinite), as well as, natural soil clays from temperate and tropical environments (Mollisol and Oxisol).

The overall objective of this study was to investigate the catalytic abilities of a wide range of mineral colloids, commonly occurring in soils and sediments, in the Maillard reaction and integrated polyphenol-Maillard humification pathways, as well as, the effect of the nature and relative abundance of the biomolecules on humification and associated reactions.

2 LITERATURE REVIEW

2.1 Introduction

Soil and related environments are both an important natural habitat of biota and a natural reservoir of biotic debris consisting of plant remains and dead animals and microorganisms. With time, dead remains are subject to continuous turnover, either mineralized or transformed to diverse organic components which are termed *humus*. This process is referred to as humification. Humus is composed of *humic substances* plus *non-humic substances* that have become stabilized, and are thus an integral part of soil and related environments (Table 2.1).

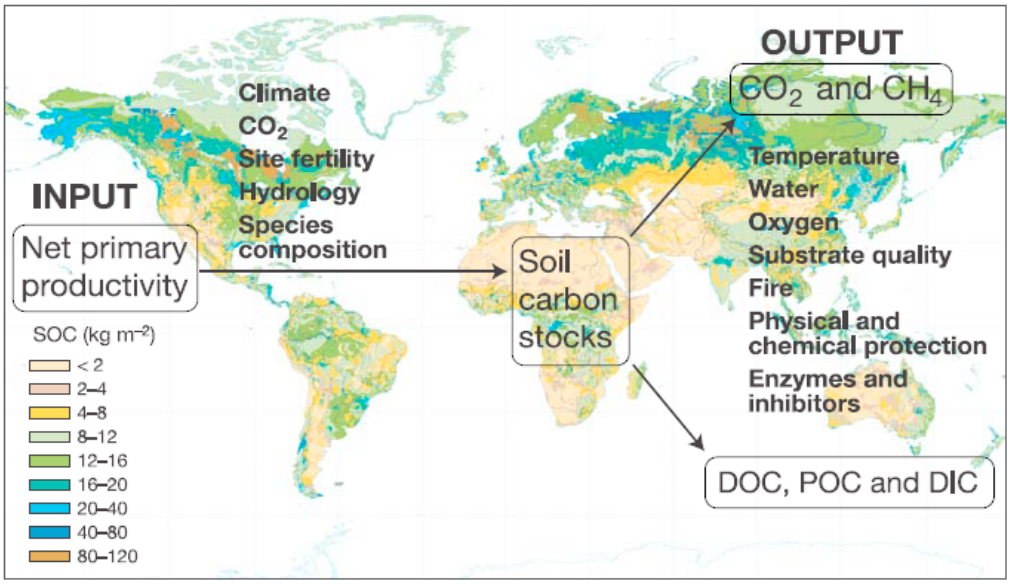

Figure 2.1 Diagram of factors controlling the main inputs and outputs of soil carbon, superimposed over a global map of soil organic carbon stocks (Davison and Janssens 2006). DOC, POC and DIC stand for dissolved organic C, particulate organic C and dissolved inorganic C, respectively (Miller Projection; 1:100,000,000).

The stocks of organic matter in soils results from the balance between inputs and outputs of organic C within the below ground environment (Fig. 2.1). Inputs are primarily controlled by net primary productivity; outputs are dominated by the efflux of carbon dioxide (CO_2) from the soil surface, although methane (CH_4) efflux and hydrologic leaching of dissolved organic and inorganic and particulate organic C compounds can also be important (Davison and Janssens 2006). During the turnover process of organic C, organic matter may become physically

protected in the interior of soil aggregates (Oades 1988; Six et al. 2002), where microorganisms and their enzymes may have limited access and where O_2 concentration may also be low. Similarly, organic compounds can be physically protected from degradation by water-soluble enzymes if they have low water solubility or if they occur in hydrophobic domains of humified organic matter (Spaccini et al. 2002). Furthermore, organic matter may become adsorbed onto surfaces of minerals, especially short-range ordered Al and Fe (oxy)hydroxides through complexation, thus chemically protecting it from decomposition (Oades 1988; Torn et al. 1997; Huang 2004; Rasmussen et al. 2005).

The transformation of biotic debris to humus proceeds in two stages (Hayes 1991; Stevenson 1994; Bollag et al. 1998). The first stage involves degradation processes that lead to the formation of biological residues, their "partial decomposition" products, and substrates (simpler structural units), which are primarily mediated by microorganisms and free enzymes (Haider et al. 1975; Bollag et al. 1998). The prevailing vegetation greatly affects the amount and type of biomolecules released during decomposition processes, which in turn will affect the nature of substances and the amount of CO_2 released. Climate and microbial populations affect the rate of decomposition of biological residues. Recent studies show that: (1) the biotic community is able to disintegrate any organic matter of natural origin, (2) molecular recalcitrance of organic matter is relative rather than absolute, (3) recalcitrance is only important during early decomposition and in active surface soils, and (4) during late decomposition and in subsoils, the relevance of spatial inaccessibility and organo-mineral interactions for soil organic matter increases (von Lützow et al. 2006). In the second stage of the transformation, the substrates are further transformed by synthetic processes catalyzed by enzymes (biotic catalysts) (Stevenson 1994; Bollag et al. 1998) and mineral particles (abiotic catalysts) (Shindo and Huang 1982, 1984b; Wang and Huang 1986; Wang et al. 1986; Huang 1990; Bollag et al. 1998; Huang 2004; Jokic et al. 2004b). Environmental mineralogy and surface chemistry greatly influence the turnover and storage of organic matter (Torn et al. 1997; Guggenberger and Haider 2002; Huang et al. 2005). Biotic and abiotic catalysts in humification all have significant roles to play; one cannot be considered more important than the other, as they interact with each other to influence humification which is one of the most important processes in the C cycle.

Table 2.1 Definitions of environmental organic matter and humic substances (Modified from Stevenson 1994).

Term	Definition
Litter	Macroorganic matter (e.g., plant residues) that lies on the soil surface
Light fraction	Undecayed plant and animal tissues and their partial decomposition products that occur within soil proper and that can be recovered by flotation with a liquid of high density
Biomass	Organic matter present as organisms
Humus[†]	Total of the diverse organic components in the environment exclusive of undecayed plant and animal tissues, their "partial decomposition" products, and the soil biomass
Soil organic matter	Same as humus
Humic substances	A series of relatively high-molecular-weight, yellow to black coloured substances formed by secondary synthesis reactions. The term is used as a generic name to describe the coloured material or its fractions obtained on the basis of solubility characteristics. These materials are distinctive to the soil (or sediment) environment in that they are dissimilar to the biopolymers of microorganisms and higher plants (including lignin)
Nonhumic substances	Compounds belonging to known classes of biochemistry, such as amino acids, carbohydrates, fats, waxes, resins, organic acids, etc. Humus probably contains most, if not all, of the biochemical compounds synthesized by living organisms
Humin	The alkali insoluble fraction of soil organic matter
Humic acid	The dark-coloured organic material that can be extracted from soil by dilute alkali and other reagents and is insoluble in dilute acid
Hymatomelanic acid	Alcohol-soluble portion of humic acid
Fulvic acid	Fraction of soil organic matter that is soluble in both alkali and acid
Generic fulvic acid	Pigmented material in the fulvic acid fraction

[†] The term humus is generally used synonymously with soil organic matter and refers to those organic substances that do not occur in the form of plant residues or their decay products (i.e. the "light fraction") (Waksman 1936; Stevenson 1994). The "light fraction" is sometimes included with the definition of "soil organic matter" in which case the term "humus" has a restricted meaning and refers to humic substances plus resynthesis products that have become stabilized, and is thus an integral part of soil and related environments. However, the absolute demarcation is blurred and it should be noted that strict adherence to the definitions will not always be possible. Furthermore, humic polymers may anchor and encapsulate unstable biomolecules by various adsorption forces or chemical binding (Bollag et al. 1998). Any biomolecules intimately associated with humic substances, that cannot be separated effectively by chemical and physical methods, may be considered as humic components (Sutton and Sposito 2005). Therefore, many unstable biological constituents may survive in humus in the environment for a significant length of time in the humification process (Bollag et al. 1998).

In the environment, humification is pivotal in transforming biomolecules originating from organized structures typical of organisms to randomly polymerized, heterogeneous humic

substances characteristic of biogeochemical systems. The objective of this chapter is to integrate the existing information on our understanding of the mechanisms of the transformation of biological debris and the resultant formation of humic substances in soils and related environments. It is hoped that this review would provide a well balanced view on this subject matter and lead the way to further advancement on our knowledge on this very important and exciting area of science.

2.2 Current Concepts on the Nature of Humic Substances

Traditionally humic substances (HS) were viewed as heterogeneous, high molecular weight polymers, for example, the widely accepted definition according to Aiken et al. (1985), "HS are a category of naturally occurring, biogenic, heterogeneous organic substances that can be generally characterized as being yellow-to-black in colour, of high molecular weight, and refractory". MacCarthy (2001) provided a broader definition for the term: "HS refers to a category of naturally occurring materials found in or extracted from soils, sediments, and natural waters. They result from the decomposition of plant and animal residues." Despite the important role of HS in the sustainability of life, their chemical nature and reactivities still remain poorly understood and there remains some contention with regards to their molecular structures.

One school of thought states that HS are collections of diverse, relatively low molecular mass organic components forming dynamic supramolecular associations stabilized by hydrophobic interactions and hydrogen bonds (Burdon 2001; Piccolo 2001; Simpson 2002; Diallo et al. 2003; Sutton and Sposito 2005; Kelleher and Simpson 2006). Another widely known school of thought states that HS are formed by polymerization and polycondensation of simple biomolecules derived from the degradation of biological residues (Schnitzer 1986; Stevenson 1994; Huang 2004; Jokic et al. 2004b; Allison 2006a). However, there is no conclusive evidence to disprove either view (Clapp et al. 2005; Schaumann 2006a). A number of reports support the polymer-sorption model for HAs (Xia and Pignatello 2001; Xing 2001; Lu and Pignatello 2002, 2004). Sorption nonlinearity in the undissolved phase is attributed to polymer properties of the sorbent; hysteresis and conditional effects can up to now only be explained with the polymer analogy (Schaumann 2006a). According to the chemical terminology of the International Union of Pure and Applied Chemistry (IUPAC), a

macromolecule (polymer molecule) is a molecule of high relative molecular mass, the structure of which essentially comprises the multiple repetition of units derived, actually or conceptually, from molecules of low relative molecular mass (McNaught and Wilkison 1997). Polymer molecules do not have a definite formula since they consist of chains of different lengths (Daintith 1990). The IUPAC definition of a supramolecule is a system of two or more molecular entities held together and organized by means of intermolecular (noncovalent) binding interactions. Macromolecules as well as small molecules tend to form supramolecular structures, the properties of which largely determine the chemical and physical nature of the whole material (Steed and Atwood 2000). Although the supramolecular model has not explicitly been shown for unfractionated dissolved organic matter (DOM) and unaltered humic substances including humin, the combination of all studies suggests supramolecular as well as macromolecular characteristics of natural organic matter (NOM) (Schaumann 2006a). Neither macromolecules nor supramolecules can be excluded in solid and dissolved NOM.

Recent studies have shown that the soil biotic community is able to disintegrate any organic matter of natural origin including black C unless it is physically inaccessible and/or chemically protected (von Lützow et al. 2006). Therefore, mere associations of biological residues and metabolites would not be able to make up the stable environmental HS and to account for their darkness in colour. Mere hydrophobic interactions and hydrogen bonding between colourless biomolecules such as lipids, proteins, and polysaccharides cannot provide a logical explanation of the browning reaction and the resultant dark colour of HS. Browning of biomolecules during oxidative degradative processes is produced by five known biochemical pathways in nature: (i) the Maillard reaction (condensation reaction of reducing sugars and amino compounds to produce melanoidins), (ii) oxidation of polyphenols to produce quinones and subsequent polymerization reactions of quinones (enzymatic and non-enzymatic reactions), (iii) quinone-amine polycondensation reactions (iv) ascorbic acid browning, and (v) oxidative lipid-protein polycondensation reactions (Rouet-Mayer et al. 1990; Hidalgo and Zamora 2000; Zamora and Hidalgo 2005; Bittner 2006). Most of these browning reactions involve carbonyl-amine reactions which result in the formation of highly coloured high and low molecular weight polymers (Hidalgo and Zamora 2000). Quinones are produced during the decomposition of lignin and by the oxidation of polyphenols; they are highly unstable and very reactive in aqueous media (Stevenson 1994; Filley et al. 2002; Telysheva et al. 2007). They readily combine with

amine, sulfydryl, phenol, indole and imidazole groups of amino acids, peptides and proteins to give even more intensely coloured products than simple quinones or phenol polymers (Bittner 2006). Abundant research evidence at the molecular level shows that biomolecules such as amino acids, sugars, and polyphenols, derived from the breakdown of biological residues and from biological metabolites, undergo polymerization and/or polycondensation especially by catalysis of enzymes and mineral particles (clay minerals, short-range ordered Mn, Fe, and Al oxides and (oxy)hydroxides, and primary minerals) (e.g., Stevenson 1994; Bollag et al. 1998; Huang 2000; Jokic et al. 2001b; Wang and Huang 2003; Jokic et al. 2004a, 2004b; Wang and Huang 2005). These reactions evidently account for the browning reaction and the darkness in colour of HS. Furthermore, HS are known to contain free radicals, as shown by electron paramagnetic resonance studies (Schnitzer 1978). Free radicals drive polymerization reactions with other biomolecules and organic pollutants. Black C is another possible contributor to the colour of HS in soils, which forms as a result of condensation of aromatic structures of organic residues during the burning process.

Most biomolecules, such as polysaccharides, simple sugars, lipids and proteins are crystalline (International Centre for Diffraction Data 2006). If HS consist merely of associations of biological residues, they should have characteristic crystal structures which can be rigorously studied and identified by x-ray diffraction analysis. However, the research evidence clearly shows that environmental organic matter has to be considered as highly amorphous material, which additionally contains microcrystalline regions like polymethylene crystallite (Hu et al. 2000; Schaumann 2006b).

Environmental organic matter is a composite of humic and non-humic substances, which is formed through operation of various biotic and abiotic mechanisms, with differing importance. The relative importance of these mechanisms and the nature and properties of the resultant organic matter vary with natural vegetation, microbial populations and activities, enzymatic activities, mineralogical composition and surface chemistry, management practices, and the environment. Therefore, the formation of environmental organic matter is a result of concerted reactions of various biotic and abiotic processes.

2.3 Decomposition of Organic Residues in the Environment

Plants are the primary source of organic matter in soil and related environments while microorganisms and fauna, which facilitate plant residue decomposition, are considered secondary sources of degradable organic matter. Kassim et al. (1981) estimated that microbial biomass contributed 1-4% of the soil organic carbon, while the total edaphon only contributed about 10%. Only a small portion of the organic residues entering the soil is finally transformed into stable humic substances. Schlesinger (1990) estimated that only 0.7% of the annual terrestrial net primary production is transformed into refractory humic substances. Organic matter entering the soil can be divided into four major groups of biomolecules, namely, polysaccharides (e.g., cellulose, hemicellulose, chitin), proteins, lipids/aliphatic materials (e.g., waxes, cutin, suberin), and lignins. The relative amounts of these biomolecules vary greatly between plant species (Kögel-Knabner 2002). Biomolecules, such as lipids and lignins (recalcitrant fractions) take longer to be degraded than polysaccharides, sugars and proteins (labile fractions), and can accumulate during the initial phase of organic residue decomposition (Kalbitz et al. 2003). However, soil microbial communities can and will degrade any type of organic residues entering the soil, even black carbon (Bird et al. 1999; Hamer et al. 2004), provided that it is physically accessible to them and that there is enough oxygen and moisture present (von Lützow et al. 2006).

2.3.1 Organisms Involved in Degradation Processes

Microbes and fauna are primarily responsible for the decomposition of organic residues in the environment. Megafauna (e.g., rodents), macrofauna (e.g., earthworms, beetle larvae, termites), and mesofauna (e.g., collemboles and mites), are known as primary decomposers. They are responsible for physically breaking the plant litter and other organic residues into smaller pieces, redistributing it in the soil profile, enzymatically altering plant tissues in the gut and ultimately exposing the larger biomolecules in the residues to further chemical attack by the secondary decomposers (Wolters 2000). Large amounts of litter have to be consumed by invertebrates because of its low nutritional value. Earthworms have been observed to consume up to 90% of the annual leaf fall litter in a single month of spring (Knollenberg et al. 1985). In general, litter that contains high amounts of carbohydrates and N-containing biomolecules is preferentially ingested, while litter containing large amounts of lignin polyphenols and tannins is

avoided; thus, this can lead to an enrichment of recalcitrant biomolecules (Wolters 2000). Ingested soil, organic residues, and stabilizing compounds are thoroughly mixed in invertebrate digestive tracts and this can lead to the exposure of lignocellulose to microflora in the gut (Hammel 1997), as well as, to the formation of stable organo-mineral complexes (Barois et al. 1993). In general, soil fauna are not able to digest lignin, cellulose and other large highly aliphatic or aromatic compounds. Some of them do possess gut microflora which are able to partially degrade resistant organic matter, but even these species primarily assimilate C from less recalcitrant forms of organic matter (Wolters 2000). Some saprophytic fungi and protozoa are also important in the primary decomposition process because these organisms produce extracellular enzymes that catalyze the dissolution of outer protective tissues.

Microorganisms are known as secondary decomposers. Secondary decomposition is performed exclusively by microorganisms, which include most of the saprophytic bacteria and fungi (Ross 1989), by means of extracellular enzymes. These microorganisms are able to further degrade and utilize the decomposition products of the primary decomposers. They are specialized to facilitate the chemical degradation of large biomolecules, such as lignin and cellulose, into their constituent biochemical subunits which can provide substrates for further reaction with soil enzymes or minerals to form humic polymers (Stevenson 1994). Although soil fauna are primary decomposers, decomposition of organic matter in soils is predominantly mediated by microorganisms, with only about 10-15% of organic C energy utilized by soil fauna (Wolters 2000). Plants, however, serve as the major source of biomass in the humification process. All other organisms contribute as a minor source of biomass after death.

Extracellular enzymes play a fundamental role in the global carbon cycle. Microorganisms must produce extracellular enzymes of the correct structural specificity to hydrolyze the high-molecular weight substrates, such as polysaccharides and lignin, so that they are small enough (generally less than 600 Da) to be taken up and metabolized by their cells (Weiss et al. 1991). Fungi are the most efficient degraders of lignin and cellulose, in particular white rot and brown rot species from the basidiomycetes and ascomycetes groups. These fungi are able to break down the large recalcitrant biomolecules by producing extracellular oxidoreductive enzymes, such as laccase and peroxidase, and biochelators containing redox reactive metals (ten Have and Theunissen 2001; Xu and Goodell 2001). White rot fungi are the only species capable of completely degrading lignin to CO_2 and water (Kirk and Farrell 1987),

whereas brown rot fungi are only able to modify lignin through demethylation and demethoxylation (Eriksson et al. 1990). The microorganisms responsible for the breakdown of organic residues are virtually found in all soils, differing only in numbers and proportions, even in the deepest layers up to 500 m below the surface (Bollag et al. 1998).

2.3.2 Degradation Processes in the Formation of Substrates and Preservation Products

The rate of organic residue decomposition in soils and related environments is ultimately controlled by its biological stability, which is a function of the following four main factors, namely, (i) its biochemical recalcitrance, (ii) the biological capability and capacity of the environment, (iii) decomposition rate modifiers (e.g. temperature, moisture, exposure time) and (iv) physical protection mechanisms (Baldock et al. 2004). Recent studies have shown that the physical protection mechanisms, such as the spatial inaccessibility of organic matter in soil micropores, are the most important factors in controlling the stability of organic matter in soils (Mikutta et al. 2006; von Lützow et al. 2006).

Table 2.2 Mechanisms of chemical recalcitrance of primary and secondary sources of organic matter (adapted from von Lützow et al. 2006).

Specific mechanism	Cause	Compounds and precursors
Primary recalcitrance: Plant litter and rhizodeposition	C-C bonds	n-fatty acids, n-alkanes, branched alkanes, n-alkenes, n-alcohols, sterines, mono-, di- , tri-esters
	C-O-C-, C-C, R-C-R bonding, aromatic polymers structure	Lignin
	Aromatic polymer structure	Tannins
Secondary recalcitrance: Microbial and faunal products	Macromolecular structure	Chitin (N-acetyl-D-glucosamine in β-(1-4)- glycosidic bonds)
	Aromatic polymer structure	Melanin
	Macromolecular structure	Murein (peptidoglucan)
	C-C bonding	Phospholipids (n-C4:0 to n-C26:0 fatty acids)
	Macromolecular structure	Ceratin (scleroprotein)

Biochemical recalcitrance of biomolecules is related to their molecular weight and complexity, as well as, to the presence of ether-bridges, quaternary and tertiary C-atoms, amide groups, phenyl- and heterocyclic N-groups, long-chain hydrocarbons and polymerized aromatic groups (Haider and Martin 1981; von Lützow et al. 2006). Table 2.2, adapted from von Lützow et al. (2006), summarizes the mechanisms of chemical recalcitrance from primary and secondary sources of organic matter. The compounds most resistant to degradation are those containing polymerized aromatic rings, such as lignin, and compounds containing polymethylenic structures, such as lipids and waxes (Derenne and Largeau 2001).

2.3.2.1 Decomposition phases

Organic matter entering the soil and related environments goes through a number of stages of degradation. Baldock and Skjemstad (2000) studied the changes that occur in organic matter during the decomposition process using physical fractionation and solid-state ^{13}C NMR spectroscopy (Figure 2.2). Initially the organic residues have a chemical structure (denoted by chemical shift in ppm) and C/N ratio similar to that of the materials from which they were derived and a particle size >20 μm. The NMR spectrum reveals that the residues are rich in O-alkyl groups (50-100 ppm), which is typical for material rich in polysaccharides, such as fresh plant tissues. The first phase of decomposition involves a decrease in the particle size (2-20 μm) of the residues and a rapid and preferential consumption and degradation of the labile fraction (proteins, sugars, polysaccharides) by fauna and microorganisms. This relatively rapid process (weeks to months) involves assimilation of the labile fraction's C, N, P and S (about 5-10%) by the fauna and microbes and results in the release of CO_2, and other inorganic species such as ammonium, phosphates and sulfates (about 70%) (Haider 1992). It also results in the accumulation of recalcitrant forms of organic matter, such as lignin and alkyl structures. Figure 2.2 shows the accumulation of aromatic lignin (100-200 ppm) and alkyl structures (below 50 ppm) in the residues from the first decomposition stage (2-20 μm). At the same time the O-alkyl C peaks (50-100 ppm) remain dominant because of the assimilation of plant C into O-alkyl microbial structures. In the second phase of decomposition the accumulated lignin is slowly decomposed, primarily by white-rot fungi. These organisms do not actually derive energy or assimilate C from the lignin degradation but benefit from an exposure of labile O-alkyl C (holocellulose) buried in the lignin structures (Haider 1992; ten Have and Theunissen 2001). The

decomposition of lignin results in a decrease in the amount of aromatic C, which is seen in Figure 2.2 in the NMR spectrum of the final decomposition product, where the aromatic features have significantly decreased (100-200 ppm). In Figure 2.2 it can also be seen that in the final decomposition stage, the alkyl-C fraction has become the most prominent fraction (0-50 ppm), which Baldock and Skjemstad (2000) speculated was due to its highly recalcitrant nature. However, recent NMR studies have shown that a significant fraction of the stable lipids (alkyl-C) found in the soil actually originate from the microbial biomass rather than plant derived carbon (Poirer et al. 2006; Quénéa et al. 2006b).

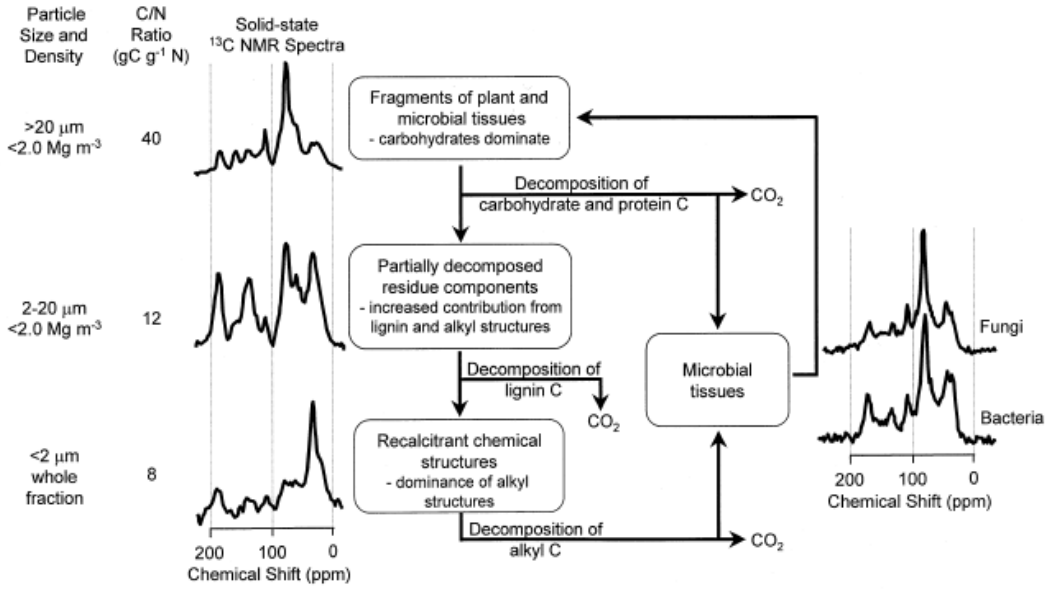

Figure 2.2 Changes in particle size, C/N ratio and chemical composition of organic matter in mineral soil with increasing extent of oxidative decomposition (Baldock and Skjemstad 2000).

2.3.2.2 Breakdown processes

Sugar and amino acid monomers can be rapidly degraded, within hours, by fauna or microorganisms which use these compounds as their primary energy source. Even though polysaccharides and proteins are large heteropolymers, they are also easily degraded even within weeks or months. This is because they contain hydrolytic bonds which are decomposed by a ubiquitous group of enzymes known as hydrolases (e.g., glucosidase, amidase, pectinase,

xylanase, proteases, chitinase) which are able to hydrolyse ester-, glycoside-, ether-, peptide and other C-N bonds (von Lützow et al. 2006).

Cellulose and hemicellulose

Cellulose is a linear and highly ordered polymer of cellobiose (D-glucopyranosyl-β-1,4-D-glucopyranose) and is the most abundant biopolymer found in plant residues. Hemicellulose is the second most abundant biopolymer and is a complex polysaccharide with a lower molecular weight than cellulose. It consists of D-xylose, D-mannose, D-galactose, D-glucose, L-arabinose, 4-O-methyl-glucuronic, D-galacturonic and D-glucuronic acids, linked together by β-1,4- and occasionally β-1,3-glycosidic bonds. Cellulose and hemicellulose are often found together strongly bonded with lignin in woody tissues, and is thus known as lignocellulose (Pérez et al. 2002). A host of fungi, in particular white-rot, brown-rot and soft-rot fungi, and selected bacteria are able to break-down cellulose and hemicellulose using a variety of hydrolytic and oxidoreductive enzymes. All the enzymatic decomposition reactions occurs exocellularly as the biopolymers are insoluble (Pérez et al. 2002).

Microorganisms that degrade cellulose produce a variety of hydrolytic enzymes that work together to breakdown the polymers. This includes cellulases, which are responsible for hydrolyzing the β-1,4-glycosidic linkages of cellulose. Two classes of cellulases exist, namely endoglucanases and cellobiohydrolases. Endoglucanases can hydrolyse internal bonds in amorphous regions while cellobiohydrolases act on existing chain ends. Once the β-1,4-glycosidic linkages are broken, cellobiose molecules are released, which are further broken down by β-glucosidases into two glucose molecules (Pérez et al. 2002). The released glucose can then be utilized by the cellulolytic microorganisms or other microbes as sources of energy. Thus, the final products of decomposition under aerobic conditions are CO_2 and water, or methane and water under anaerobic conditions (Béguin and Aubert 1994; Leschine 1995).

Brown-rot basidiomycetes fungi are one of the most common degraders of cellulose and hemicellulose in the Northern Hemisphere, being the dominant wood decay fungi in coniferous forests (Xu and Goodell 2001; Filley et al. 2002). The brown-rot fungi are only able to demethylate and slightly depolymerize lignin, as well as, being able to oxidize its side chains, unlike white-rot fungi which are able to completely degrade lignin and cellulose at the same time (Filley et al. 2002). In the past it was thought that the degradation of cellulose by brown-rot fungi

was merely an enzymatic process. It was later realized that the degradation does not only occur in the vicinity of the hyphae but also deeper into the wood cells, indicating a non-enzymatic process since enzymes are too large to penetrate unmodified wood cells (Xu and Goodell 2001). The exact mechanism of brown rot decay has not yet been established, but it is known that iron, hydrogen peroxide, biochelators and oxalate each play an important role in the process. The initial stage of decomposition is thought to involve Fenton chemistry (Eq. 2.1), as the fungi are known to produce extracellular H_2O_2 and the wood substrate contains iron, which after reaction result in the production of hydroxyl anions and free radicals (Koenigs 1974; Xu and Goodell 2001).

$$Fe^{2+} + H_2O_2 \rightarrow Fe^{3+} + OH^- + HO\cdot \qquad (2.1)$$

The resultant hydroxyl radicals are able to cleave long chain cellulose polymers and thus help to initiate and accelerate decay. The fungi also produce low molecular weight (1500-5000 Da) *ortho*-dihydroxy phenolic compounds (catecholates) which act as Fe(III) iron chelators and as a source of electrons for iron reduction (Goodell et al. 1997; Paszczynski et al. 1999). These biochelators are small enough to penetrate the unmodified wood's lignocellulose tissue and to initiate cellulose decomposition. It has also been shown that the brown *ortho*-dihydroxy-rich lignin residues produced by the fungi, can be enriched in metals, particularly calcium, iron, manganese, and magnesium (Ostrofsky et al. 1997). This is of particular relevance to synthetic humification reactions, as polyphenols, particularly *ortho*-polyphenols, are very reactive in participating in polymerization and polycondensation reactions with amino compounds especially in the presence of redox reactive metals (Huang 2000).

Hemicellulose degradation requires a host of enzymes working together, mainly from the glycosidase family of enzymes, due to its complex and heterogeneous structure. These include β-mannases, β-xylanases, β-mannosidase, β-xylosidase, β-glycosidase, α-galactosidases, and accessory hemicellulases, xylan esterases, ferulic and *p*-courmaric esterases, α-l-arabinofuranosidases and α-4-O-methyl glucuronosidases. The degradation of a common hemicellulose, O-acetyl-4-O-methylglucuronxylan, requires the synergistic action of endoxylanase, acetyl esterase, α-glucuronidase and β-xylosidase. The products of hemicellulose decomposition are monomeric sugars and acetic acid (Pérez et al. 2002).

Lignin

Lignin is a large insoluble, amorphous heteropolymer that consists of phenylpropane units, i.e., coniferyl alcohol (guaiacyl propanol), coumaryl alcohol (*p*-hydroxyphenylpropanol), and sinapyl alcohol (syringyl propanol), that are randomly joined together by C-C and aryl-ether linkages. Lignin contains no hydrolytic bonds and is highly resistant to biological and chemical degradation (Martínez et al. 2005).

The first stage in lignin degradation involves the production of non-specific, extracellular oxidoreductive enzymes by basidiomycetes fungi, in particular white-rot fungi. The microorganisms do not actually metabolize the lignin C, but rather utilize holocellulose that is exposed during the decomposition process (Haider 1992). There are two major classes of oxidoreductase enzymes that are involved in lignin degradation, namely, peroxidases (EC 1.11.1) and laccases (EC 1.10.3.2). The peroxidases are considered true lignases because they have a high redox potential and are able to degrade phenolic as well as non-phenolic lignin units, whereas, the laccases have a low redox potential and are only able to degrade phenolic lignin units, which often constitute less than 10% of the whole lignin polymer (Martínez et al. 2005). Aryl alcohol oxidase and glyoxal oxidase are also considered important oxidoreductase enzymes in lignin degradation as they generate H_2O_2 for the peroxidases, and have also been shown to inhibit polymerization reactions of the phenolic lignin fragments (Galliano et al. 1991; Ander and Marzullo 1997).

White-rot fungi produce three peroxidases that are involved in lignin degradation, namely, lignin peroxidase (LiP) and manganese peroxidase (MnP) first discovered in *Phanerochaete chrysosporium* in the 1980s, and versatile peroxidase (VP) recently discovered in *Pleurotus* and *Bjerkandera* species (Martínez 2002). Lignin peroxidase has a heme group in its active center, and it catalyzes a variety of oxidations, all of which are dependent on H_2O_2. These include Cα-Cβ cleavage of the propyl side chains of lignin, hydroxylation of benzylic methylene groups, oxidation of benzyl alcohols to the corresponding aldehydes or ketones, oxidation of aromatic ethers, phenol oxidation and even aromatic ring cleavage of non-phenolic lignin model compounds (Cullen 1997; Pérez et al. 2002). Manganese peroxidase is also a heme protein like LiP, except it attacks aromatic lignin structure indirectly using Mn(III) chelates and the associated free radicals which form during the process. It functions by oxidizing Mn^{2+} to Mn^{3+}.

White-rot fungi secrete oxalic and other organic acids that form Mn(III) chelates which stabilize the Mn(III) and allow it to diffuse in solution so that it can oxidize phenolic compounds. Low molecular-weight redox mediators play an important role during the initial steps of lignin degradation since the compact molecular architecture of the intact plant cell-wall prevents the penetration of enzymes to be in direct contact with lignin (Martínez 2002). The recently discovered versatile peroxidase (VP) has the combined catalytic properties of LiP, MnP, and plant/microbial peroxidases oxidizing phenolic compounds.

Laccases are blue-copper phenoloxidases that catalyze one-electron oxidation reactions, mainly the oxidation of phenolic lignin structures to phenoxy radicals in the presence of mediators (Leonowicz et al. 2001). They also catalyze the demethylation of lignin, methoxyphenol acids and methoxyaromatics (Burton 2003). Laccases are also able to catalyze the polymerization of lignin monomers, and *o*- and *p*- polyphenols, and so could also play an important role in synthetic humification reactions (Bollag et al. 1998). Laccases have been found in mainly wood rotting fungi, but also in *Aspergillus*, thermophilic fungi and even bacteria (Pérez et al. 2002).

Since lignin is such a large and complex heteropolymer, it is reasonable that it would require the action of many enzymes working together to break it down, rather than just one enzyme, such as LiP. Leonowicz et al. (2001) proposed an integrated lignocellulose degradation mechanism (Figure 2.3), whereby the degradation pathway of polysaccharides, cellulose and hemicellulose is incorporated into the degradation pathway of lignin. In their proposed mechanism, glucose oxidase operates as a feedback system where lignin and manganese peroxidase function as the initial lignin attacking enzymes, and laccase as the demethylating factor. Glucose, produced by cellulose and hemicellulose hydrolysis, becomes the substrate for glucose oxidase. Quinones, produced by laccase from lignin oligomers, can serve as a replacement for the O_2 required by glucose oxidase. D-gluconolactone is formed as a result of glucose oxidation, which is used as a fungal metabolite. Hydrogen peroxide produced in the reaction catalyzed by glucose oxidase, in turn, activates LiP and MnP. Lignin exposed to the activated peroxidases undergoes decomposition into lower molecular weight fragments containing methoxyl groups. Laccase demethylates these oligomers while peroxidases degrade them further into even smaller fragments. Demethylation by laccase after the initial activity of the peroxidases is an important step, as it prevents the inhibition of the depolymerizing activity

of LiP by the phenolic groups of native lignin (Ander and Marzullo 1997). Generation of excess quinones and resulting repolymerization could be counterbalanced by glucose oxidase, which reduces them to the respective phenols. The phenols could then be utilized as substrates by microbes to form ketoacids via deoxygenases, however, it has been shown that less than 1% lignin carbon is incorporated into new biomass (Haider and Martin 1981). The phenols can also become substrates for synthetic humification reactions (Bollag et al. 1998; Yavmetidinov et al. 2003; Telysheva et al. 2007). Polyphenols are the most reactive biomolecules in participating in polymerization and polycondensation humification reactions, especially in the presence of enzymes such as laccase and abiotic catalysts, such as Fe and Mn oxides (Bollag et al., 1998). Telysheva et al (2007) studied the degradation of lignin in planted soils using a range of chemical and spectroscopic analytical techniques. They found that initially the carbohydrate component of the lignin was preferentially degraded, followed by the oxidative decomposition of the lignin moieties which involved removal of side chains (demethylation and demethoxylation). They also observed a progressive decrease in the acidity of lignin phenolic groups which was directly linked to increasing quinone and phenoxy radical formation and subsequent aromatization and condensation (polymerization) of the lignin structures during the degradation processes.

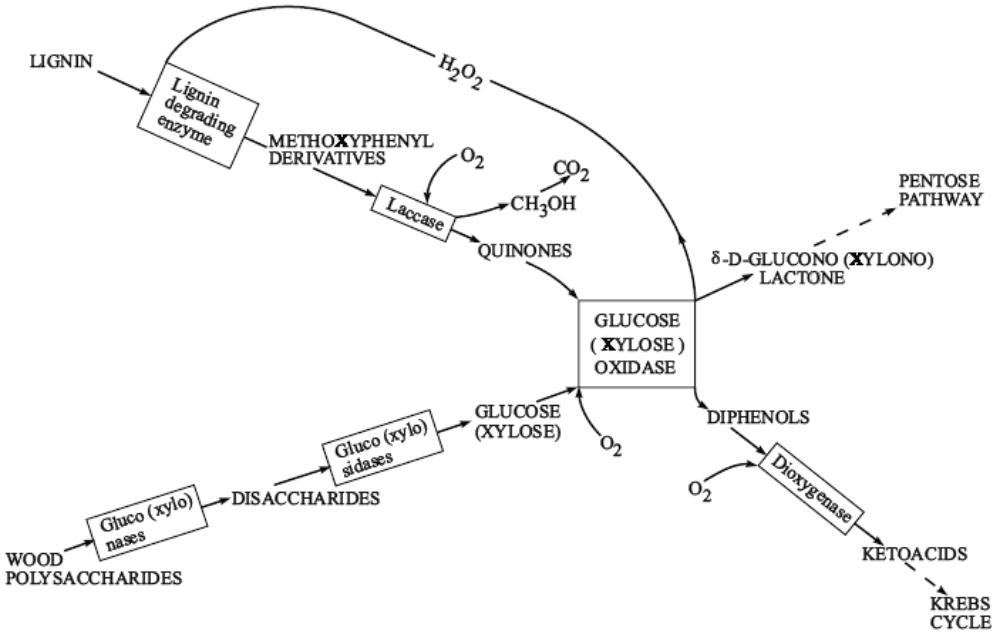

Figure 2.3 Hypothetical mechanism of lignocellulose transformation by enzymes of white-rot fungi. The initial products of partial wood hydrolysis distinctly induce enzymatic systems accelerating the degradation processes (Leonowicz et al. 2001).

2.3.2.3 Physical and chemical protection

Soil mineral colloids, especially short-range ordered (SRO) Al and Fe (oxy)hydroxides, which are virtually noncrystalline, have the ability to complex with organic matter and control the turnover rate and storage of organic C in the soil and related environments (Huang 1990; Torn et al. 1997; Huang et al. 2002; Rasmussen et al. 2005). Figure 2.4 (Torn et al. 1997) demonstrates the positive relationship between noncrystalline minerals and the turnover rate [Δ ^{14}C of SOM (‰)] and soil organic C storage. Ramussen et al. (2005) reported that SRO Al mineral species variation explains nearly all of the variation in C contents in Bt horizons in a California Conifer forest soil (Table 2.3). This SRO Al consists of the precipitated Al-humus complexes and SRO-Al-OH species within interlayers and on edges and external planar surfaces of soil mineral colloids. Short-range ordered Al species possess considerable reactive surface area and microporosity that may contribute to adsorption of organic matter and physical protection within micropore structures (Huang et al. 2002; Yu et al. 2006) and also promote aggregation and occlusion of organic matter in aggregate structures (Baldock 2002). The results of Rasmussen et al. (2005) are similar to those of Percival et al. (2000) who found that the pyrophosphate extractable Al (Alp) is the best predictor of New Zealand C stocks in grassland soils and Veldkamp (1994) who found a high correlation between soil C mean residence time (MRT) and Alp and SRO aluminosilicates. Therefore, chemical protection of organic materials and physical protection of plant-like material within aggregates merit close attention in understanding the degradation of biological residues.

Lignin is relatively resistant to biodegradation (Rasse et al. 2006). It may, thus, stabilize reactive components such as cellulose, hemicellulose, or proteins by forming chemical or physical linkage to these molecules (Alexander 1997). Soil humus polymers may anchor unstable plant constituents by various adsorptive forces or chemical binding (Allison 1973; Bollag et al. 1998). Highly degradable proteins, for example, may be protected against rapid biodegradation by their nucleophilic addition to aromatic polymers through free NH_2 or SH groups and/or by adsorption on humus and mineral colloids (Huang 1990; Bollag et al. 1998; Adani et al. 2006). As a result of the acquired stability, the plant components may not be completely mineralized during the initial rapid decomposition phase. Therefore, many relatively unstable plant constituents, such as polysaccharides, proteins, soluble sugars, and amino acids,

can survive in the soil and related environments for a sufficient length of time in the humification process.

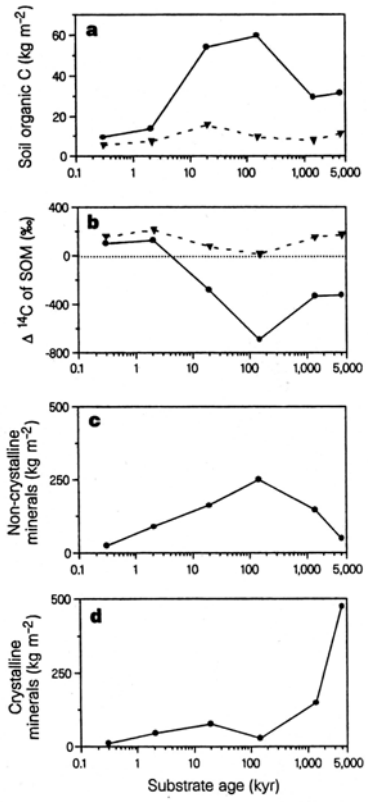

Figure 2.4 Soil inventory carbon in soil organic matter (SOM) (a), $\Delta^{14}C$ of SOM (b), non-crystalline minerals (c), and crystalline minerals (d) versus age of soil substrate. Filled circles, total profile; filled triangles, surface (O and A) horizons (Torn et al. 1997).

Table 2.3 Regression analyses for combined andesite-granite (AN) and granite (GR) data explaining total C content (n = 6)[†] (Rasmussen et al. 2005).

Horizon	Equation	Adjusted R^2
A1[‡]	—	
A2	$C = 6.83Al_p^{\#} - 1.73$	0.80**
Bt1	$C = 1.54Al_o^{\S} - 1.73$	0.89***
Bt2	$C = 1.64Al_o - 0.56$	0.998***
BC	$C = 1.66Al_p + 0.27$	0.99***

*Significant at the probability level < 0.05
**Significant at the probability level < 0.01
***Significant at the probability level < 0.001
[†]All values are kg m^{-2}
[‡]No significant regression found with mineral variables
[#]Al_p stands for pyrophosphate extractable Al
[§]Al_o stands for oxalate extractable Al

2.3.3 Decomposition of Organic Material by Fire and Charcoal Formation

Fire plays an important role in C cycling in many regions, particularly in the Boreal forest and peatlands (Preston and Schmidt 2006). Fire converts biomass and detrital C mainly to gaseous C, predominantly CO_2, and 1-3% to pyrogenic C, which is characterized by condensed aromatic structures. Fire affects soil organic matter (SOM) by decreasing the proportion of HA and increasing the insoluble humin fraction. There is loss of carbohydrates and O-containing functional groups and an increase in the aromatic C. The proportion of alkyl C may increase and is often associated with the formation of hydrophobicity in the upper soil (Preston and Schmidt 2006). Fire also leads to a change in the N speciation of SOM, most notably a decrease in amide N (dominant species in fire unaffected soils) and an increase in heterocyclic N (Knicker et al. 2005). Generally speaking, fire causes an increase in the recalcitrant forms of C and N in soils.

Black C is defined as the finer fraction of pyrogenic C that exhibits chemical resistance to oxidation, as it is the most condensed (has relatively little or no O- and H-containing functional groups) (Preston and Schmidt 2006). Black C can also be extracted by conventional methods used to isolate humic and fulvic acids from soils (Skjemstad et al. 1996). Ponomarenko and Anderson (2001) found that as much as 60% of the organic C fraction in Black Chernozem soils from Saskatchewan, Canada, was resistant to UV oxidation, which indicated a significant presence of black C. Their study highlighted the important contribution of black C to the formation of Black Chernozem soils and a need for a better understanding of the role of black C in carbon sequestration in these soils. Rumpel et al. (2006) showed that the black C content of tropical soils subjected to slash and burn treatment was positively correlated with the organic C contents, suggesting that black C is a component strongly influencing organic carbon sequestration in these types of tropical soils.

Black C has generally been considered inert because of its resistance to oxidation; however, it does eventually degrade, but much more slowly than other plant residues. It has been shown that with aging (decades to millennia) the surfaces of black C become increasingly oxidized which increases potential for degradation by microorganisms (Schmidt et al. 2002). Bird et al. (1999) found that black C could be degraded in the range of tens to hundreds of years. A number of incubation studies have shown that black C can be microbially degraded at a relatively slow rate. Baldock and Smernick (2002) showed that 2% of wood char was mineralized after 120 days. Brodowski (2004) found that 5-50% of the black carbon in wheat and

rice char was degraded within the first 6 months of incubation. Hamer et al. (2004) showed that the presence of a readily available source of C (glucose) significantly increased the rate of microbial degradation of maize char.

Shindo et al. (2004; , 2005) recently suggested that charred plant remains serve as an important source of carbon for the formation of humic substances through oxidative degradative processes in Japanese volcanic ash soils, based on evidence of $\delta^{13}C$ values (Table 2.4). The formation of humic substances from the degradation of charred plant residues would be of particular significance in regions where annual burning of crop residues is practiced, or where frequent fires or volcanic activity occur.

Table 2.4 Correlation of $\delta^{13}C$ values of charred plant fragments, humic and fulvic acids, and whole soils (Shindo et al. 2005).

Whole soil and constituent	Charred plant fragments	Humic acid	Fulvic acid	Whole soil
Charred plant fragments	1			
Humic acid	0.951†	1		
Fulvic acid	0.792‡	0.740¶	1	
Whole soil	0.968†	0.947†	0.900†	1

†Significant at 0.1% level
‡Significant at 1% level
¶Significant at 5% level

2.4 Pathways of Humic Substance Formation

2.4.1 Selective preservation pathways of humification

The modified lignin pathway was one of the first theories of humus formation. Waksman (1936) popularized this theory, which proposes that humic acids resulted from the condensation of lignin with microbially produced protein (Figure 2.5). Waksman's theory was primarily based on the observation that (i) lignin is a recalcitrant fraction of plant residues that accumulates during the first stages of organic residue decomposition, and (ii) lignin decomposition (as opposed to cellulose decomposition) gives rise to aromatic products, and humic acids also contain aromatic compounds. Hatcher and Spiker (1988) proposed a modified version of Waksman's lignin-protein theory, which included other refractory macromolecules such as cutin, suberin and microbial melanins. They also proposed the degradative formation of humic and

fulvic acids from refractory biopolymers (humin), whereby increasing degradation of biopolymers leads to the formation of macromolecules enriched in carboxylic and phenolic functional groups. This increase in acidic functional groups promotes increased solubility in alkali and thus the development of humic acids and then fulvic acids. Bacteria and fungi, in particular white-rot fungi, are known to be able to effectively degrade humic substances (Haider and Martin 1988; Gramss et al. 1999; Steffen et al. 2002; Granit et al. 2007). Gramss et al. (1999) found that large humic acid molecules were more readily degraded than the smaller fulvic acid molecules by the fungal species and eubacteria studied, and that the humic substances served as a sole source of carbon and energy for the microorganisms in the systems they studied.

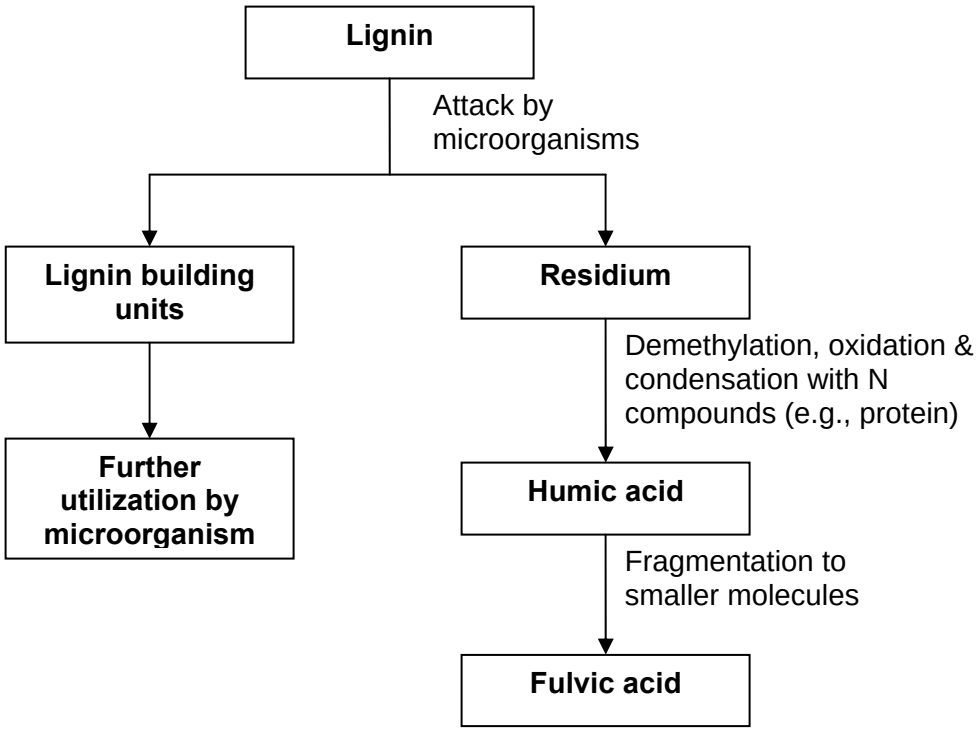

Figure 2.5 Schematic representation of the modified lignin theory of humus formation (adapted from Stevenson 1994).

Selective preservation theories have been questioned by several authors (O'Brien and Stout 1978; Nadelhoffer and Fry 1988; Melillo et al. 1989) based on the fact that $\delta^{13}C$ values generally increase with depth in soils, whereas lignin and fatty acids and waxes have depleted $\delta^{13}C$ values relative to other plant components. Preston et al. (2006) further confirmed this hypothesis by demonstrating that increasing amounts of lignin-derived residues resulted in lower

$\delta^{13}C$ values, by studying the lignin-rich residues produced by brown-rot fungi acting on wood debris. Although lignin is less easily attacked by microorganisms than other plant components, mechanisms do exist in nature for its complete aerobic breakdown; otherwise the earth would be deeply buried in undecomposed plant residues (Stevenson 1994). Recent studies have shown that lignin is quickly degraded in the soil (Rasse et al. 2006). Plant lipids have also been shown to be rapidly degraded in cultivated soil; a significant portion of the stable lipids found in the soil originate from the microbial biomass rather than plant derived carbon (Poirer et al. 2006; Quénéa et al. 2006b). It has been suggested that the selective preservation pathway would play a more important role in humification processes in poorly drained soils and lake sediments, because of the lack of the fungi that are responsible for lignin degradation and the lack of oxygen which is necessary for this process (Stevenson 1994).

2.4.1.1 The Lignin Theory Pathway

Lignin is one of the most abundant constituents of vascular plant tissues and has long been considered to be a major source of stable C in soils. As discussed above, Waksman's modified lignin pathway was one of the earliest theories of humic substance formation. Recent studies using pyrolysis- and TMAH thermochemolysis-GC/MS, and multidimensional liquid NMR techniques have confirmed the presence of plant derived lignin structures in bulk soils and humic acid fractions from agricultural and forest soils (Chefetz et al. 2002; Simpson 2002; Simpson et al. 2003; Kelleher and Simpson 2006). A number of studies have shown that lignin residues accumulate and are stabilized by covalent linking to humic substances during mineralization processes in soils (Haider et al. 1977; Almendros et al. 2000; Tuomela et al. 2002). The polymerization of lignin residues to the existing humic acid fraction is promoted by oxidoreductase enzymes such as laccase, which are secreted by white-rot fungi when decomposing lignin (Dec and Bollag 1990; Tuomela et al. 2002). It has also been suggested that humic polymers can physically encapsulate partially degraded biological residues (Bollag et al. 1998; Sutton and Sposito 2005). The physical inaccessibility of the lignin residue accompanied by the inactivating effect of the presence of humic substances and minerals on extracellular enzymes can slow the rate of lignin degradation in soils (Tuomela et al. 2002; Allison 2006b). Tuomela et al. (2002) observed that the presence of soil significantly decreased the ability of white-rot fungi species to degrade lignin. However, they found that the white-rot fungi were

nonetheless able to degrade the ^{14}C labeled lignin that was bound to the humic acid fraction of a soil. It is well established that bacteria and fungi can degrade humic substances (Gramms et al., 1999).

Adani et al. (2007) investigated the contribution of lignin to the formation of humic acid from Maize plants using pyrolysis GC/MS. They found that there was a substantial preservation of lignin in plant residues incubated with soil in the short term. However, they also observed the modification of the syringyl/guaiacyl ratio and oxidation of the side chains of lignin, which suggested a turnover of lignin-derived molecules in the soil humic acid fraction. Other studies have shown that lignin is degraded relatively quickly in the soil and does not appear to be stabilized in the soil in the long term (Baldock and Nelson 2000; Kögel-Knabner 2002; Kiem and Kögel-Knabner 2003; Rasse et al. 2006). Rasse et al. (2006) estimated that the turnover rate for lignin in a temperate loamy soil was 1.9 $year^{-1}$ (the turnover rate obeys the first-order rate equation). They also found that about 92% of the lignin was mineralized to CO_2 or assimilated to microbial C, thus only 8% was incorporated in the stabile fraction.

2.4.1.2 Preservation of other refractory biologically derived polymers

Plant derived polymers with polymethylenic structures such as lipids, waxes, cutin, suberin and other microbially-derived lipids are considered the fraction of organic C that is most resistant to degradation (Derenne and Largeau 2001). It has been hypothesized that the hydrophobicity of these components prevents enzymes from directly interacting with them. Furthermore, clay stabilization of alkyl C components either by surface association or intercalation has also been suggested as a reason for the accumulation of alkyl C in finer fractions (von Lützow et al. 2006). The humin fraction of soil C, which usually accounts for more than 50%, is known to be rich in alkyl C (Rice 2001). Quénéa et al. (2006b) studied the lipids in particle size fractions of previously forested soil that had been cultivated with maize for 22 years and compared it to a similar continuously forested soil from the same region. They found that microbial reworking of lipid components increased with decreasing particle size in the cultivated soil. They also found that the lipids of the cultivated soil were dominated by microbial lipids while the forest soil contained more plant derived lipids. This indicates that the persistence of plant lipids is also related to type of vegetation as well as management practices. In a related study of the same soils, Quénéa et al. (2006a) studied the so called "refractory organic

macromolecular" fraction of the soils, which is defined as the fraction which is resistant to drastic laboratory hydrolysis. They found that this fraction (20% of TOC) consisted of heterogeneous macromolecules that contained altered lignin, polysaccharides, suberans, bacterial and plant fatty acids, suberin and melanoidin-type components. Feng and Simpson (2007) studied the distribution of organic C in subsoil horizons in Alberta grasslands, and found that aliphatic molecules derived from cutin and suberin were preferentially preserved in deeper horizons in comparison to lignin, and that trehalose, a fungal polysaccharide, was detected in significant abundance in the subsoil horizons. They concluded that non-plant biomass and eluviation strongly contributed to the composition of organic C in these subsoils. Similarly, Kiem and Kögel-Knabner (2003) showed that microbially produced polysaccharides were stabilized over the long-term within the fine fraction of arable soils, while lignin was not. It would appear that microbial resynthesis products persist for longer periods as they are closely associated with the fine fraction of soils and hence physically protected.

2.4.2 Synthesis pathways of humification

There is a large volume of work documenting the polycondensation and polymerization of simple biomolecules (e.g., polyphenols, amino acids, and sugars), as catalyzed by enzymes and soil minerals, leading to the formation of humified substances (Bollag et al. 1998; Huang 2000, 2004). Since these catalysts are ubiquitous in soil environments, and the substrate biomolecules are readily available from the continuous decomposition of organic residues as discussed in section 2.3, it is certain that these reactions occur in the natural environment. Furthermore, these reactions are responsible for browning reaction of biomolecules observed during oxidative decomposition, and provide an explanation for the dark colour of humic substances in soils. The following section reviews the major synthetic pathways that have been investigated.

2.4.2.1 Polyphenol Pathway

According to polyphenol pathway humification theory, quinones of lignin and microbial origin are the major building blocks of humic substances. In this model, the first step is the breakdown of all plant biopolymers into their structural units, some of which polymerize enzymatically or by means of mineral colloid catalysis to form humic molecules of various

complexities (Shindo and Huang 1982; Wang et al. 1986; Stevenson 1994; Bollag et al. 1998). For both biotic and abiotic catalysts, polyvalent metals such as Cu, Mn and Fe facilitate the transformation of phenolic compounds by acting as electron acceptors. The order of formation of humic substances by the polyphenol pathway is: fulvic acid → humic acid → components of humin (Stevenson 1994). The formation of brown-coloured polymers by reactions involving quinones and amino acids and proteins, is a well-known phenomenon that occurs in plants following mechanical injury or during disintegration of cells (Bittner 2006), and is also observed when brown-rot fungi decompose wood and leave behind aromatic dihydroxy-rich residues (Filley et al. 2002). Polyphenols, originating from lignin, tannins, microorganisms, root exudates, glycosides and anthropogenic contaminants, can be oxidized, by means of oxidoreductase enzymes or mineral colloids, to form highly reactive semiquinone free radicals and/or quinones, which readily participate in polymerization and/or polycondensation reactions with amino compounds to form humic substances (Wang et al. 1986; Stevenson 1994).

Dec et al. (2003) investigated oxidative coupling (polymerization) reactions of a number of polyphenolic compounds, including vanillic acid, as catalyzed by the enzymes, laccase and peroxidase, and birnessite (δ-MnO_2). The first step of the oxidative coupling reactions involves oxidation of susceptible polyphenols to form unstable free radicals. This involves the removal of a hydrogen ion and an electron from the hydroxyl group, generating an alkoxy free radical. The free radical intermediate then reacts with positions *ortho* and *para* to the hydroxyl group to form a dimer, and ultimately polymers. This reaction results in the formation of C-C and C-O bonds between phenolic species (Bollag et al. 1995). If the potential of the oxidant is high enough, C-C coupled dimers can be oxidized to form extended quinones. In the presence of certain enzymes and particularly strong oxidants such as Mn oxides, phenolic compounds can also be oxidized to the extent that ring cleavage occurs, allowing the cleavage products to be further degraded by enzymatic activity or mineral catalysis to CO_2 or incorporated into humic substance structures (Wang and Huang 1992; Majecher et al. 2000; Wang and Huang 2000b, 2005). Another effect of oxidative coupling is dehalogenation, decarboxylation or demethoxylation of the phenolic substrates (Dec et al. 2003). This only occurs if the substituent is attached to a C atom involved in coupling. Electron-withdrawing substituents, such as -COOH and -Cl, are more susceptible to release than electron-donating ones such as OCH_3 and CH_3. The release of organic substituents during oxidative coupling reactions leads to the production of CO_2. Oxidative coupling and

degradation are considered environmentally beneficial pathways, as they lead to detoxification of hazardous xenobiotic substrates.

Although self-condensation of quinones or free radicals can occur under soil conditions, these types of reactions are greatly enhanced in the presence of amino compounds, such as amino acids or amino sugars (Bittner 2006). The condensation reaction between catechol and glycine is shown in Figure 2.6. The reaction of glycine with a quinone C=O group leads to the degradation of glycine and the formation of an aryl amine. Thus, part of the amino acid-N becomes incorporated into the polymer. The condensation of hydroquinone and glycine to form nitrogen complexes is substantially enhanced by mineral colloids such as δ-MnO_2 in the pH range commonly found in the environment (Shindo and Huang 1984b). The findings indicate that Mn oxides merit close attention in the abiotic formation of organic N complexes from nitrogenous substances and polyphenols and the subsequent turnover of N in the environment.

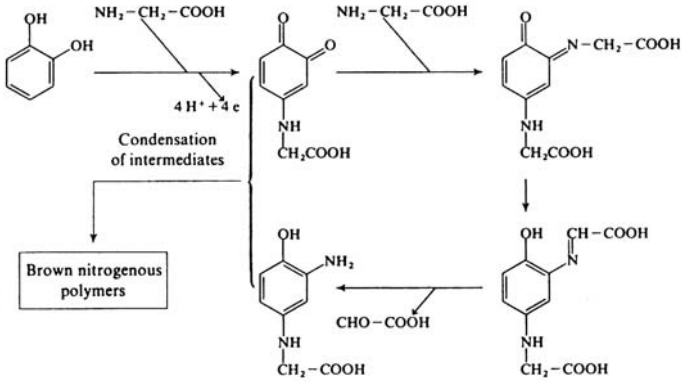

Figure 2.6 Formation of humic substances from quinones and amino acids, as illustrated by the reaction between catechol and glycine (Stevenson 1994).

2.4.2.2 Maillard Reaction Pathway

The Maillard reaction (Maillard 1913), involving condensation reactions between reducing sugars and amino acids, is considered to be an important pathway in natural humification (Ikan et al. 1996). Sugars and amino acids are among the most abundant constituents of terrestrial and aquatic environments (Anderson et al. 1989). The Maillard reaction consists of a cascade of complex pathways involving interactions between degradation products of the precursor sugars and amino acids, and reaction intermediates, known as Amadori and Heyns compounds (Yaylayan 1997).

The initial reaction in the Maillard reaction involves condensation between the α-hydroxy carbonyl group of a reducing sugar and the amino group from an amino acid with the formation of a Schiff base which rearranges to form either Amadori or Heyns compounds (Figure 2.7). Aldohexoses generate Amadori compounds while ketohexoses generate Heyns products (Yaylayan 1997). These compounds can undergo retroaldolization reactions forming α-dicarbonyl and α-hydroxyketone compounds (Figure 2.7). All of these compounds are highly reactive and readily polymerize in the presence of amino compounds to form brown-coloured melanoidins. Amino acids can react with the α-dicarbonyl compounds, undergoing the Strecker degradation and then forming α-amino ketones. The α-amino ketones may then condense resulting in the formation of pyrazines (Ho 1996; Yaylayan 1997). In addition, the Maillard reaction can result in the formation of polyphenols, such as catechol, resorcinol, hydroquinone and pyrogallol, which can enhance the degree of browning during the Maillard reaction by affecting the redox potential of the system (Haffenden and Yaylayan 2005) and undergoing polymerization and polycondensation (Wang and Huang 2005).

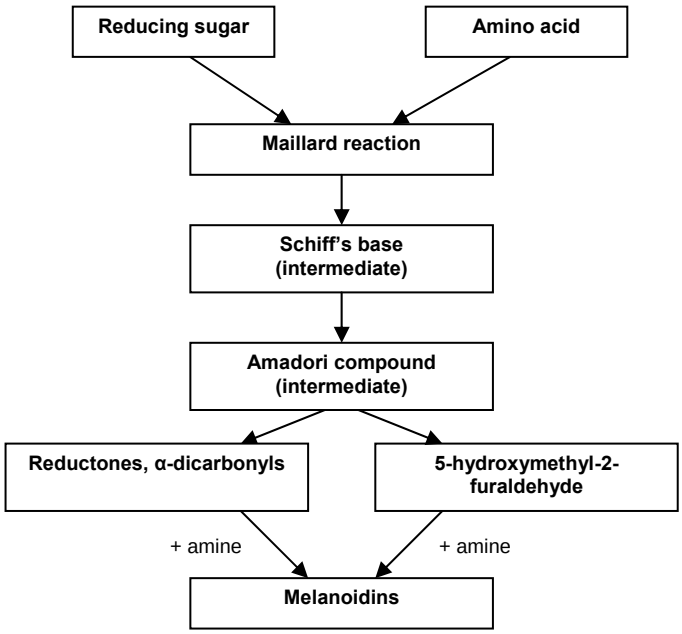

Figure 2.7 A schematic representation of the Maillard reaction (adapted from Ikan et al. 1996).

There has been some recent criticism of the Maillard reaction as a possible humification pathway (Burdon 2001; Sutton and Sposito 2005; von Lützow et al. 2006). Firstly, the critics

argue that the Maillard reaction results in the formation of heterocyclic N, whereas soil N consists primarily of amide N based on ^{15}N CPMAS NMR (Knicker and Lüdemann 1995; Knicker 2004) and N K-edge XANES (Vairavamurthy and Wang 2002) studies. However, Jokic et al. (2004b) clearly showed, using N K-edge XANES, that the Maillard reaction catalyzed by birnessite under ambient temperature conditions and environmentally relevant pH not only produces heterocyclic N but also a significant amount of amide N (Figure 2.8).

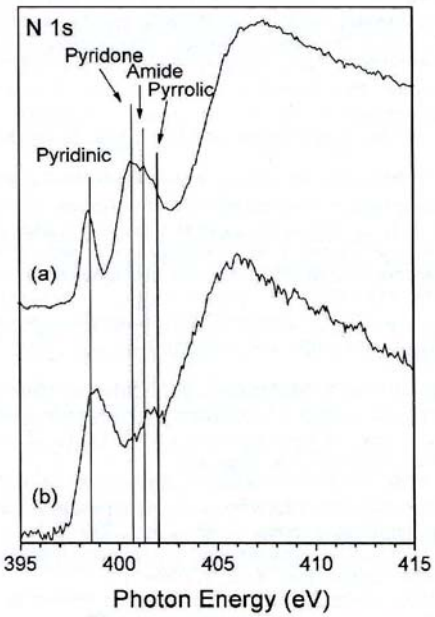

Figure 2.8 N 1s XANES spectra of (a) fulvic acid isolated from a glucose-glycine-δ-MnO_2 system and (b) the lyophilized solid phase. The peaks are assigned to pyridinic (398.6 eV), pyridone (400.7 eV), amide (401.3 eV) and pyrrolic (402.0 eV) moieties (Jokic et al. 2004a).

The spectrum of the fulvic acid is similar to that of asphaltene (Mitra-Kirtley et al. 1993), which has implications with regard to the formation of sedimentary organic matter such as HS, fossil fuels, and kerogen. Pyrrolic N and pyrinilic N are the dominant fractions in fossil fuels (Gorbaty and Kelemen 2001). The action of birnessite on glucose should promote the autoxidation of glucose which results in the generation of reactive dicarbonyl compounds, hydrogen peroxide and hydroxylating agents (Wolff 1996) (Fig. 2.9). These reactive dicarbonyl compounds would then react with ammonia formed by the known deamination of glycine catalyzed by birnessite (Wang and Huang 1987), as proposed by Vairavamurthy and Wang (2002), or with glycine (undergoing the Strecker degradation), resulting in either case in the formation of heterocyclic N compounds (Wong and Shibamoto 1996), as illustrated in Figure

2.10. Ammonium ions are known to react with compounds containing reactive carboxyl groups to form pyridinic structures (Steelink 1994). Carboxylic acids are produced during the Strecker degradation of amino acids (Wong and Shibamoto 1996), or by the action of manganese dioxides on simple carbohydrates (Bose et al. 1959). When heated, carboxylic acids react with ammonia to form amides (Smith and March 2001). The scheme for possible amide formation is shown in Figure 2.11.

The study of Jokic et al. (2004a) reveals that the Maillard (sugar-amino acid condensation) reaction, catalyzed by birnessite, is an abiotic pathway for the formation of biogeomacromolecules containing organic N originally derived from amino acids under ambient environmental conditions. Their data provided for the first time unequivocal evidence that the Maillard reaction catalyzed by birnessite, which is common in soil and sediment environments, produces: (1) amides which are the dominant N types in humic substances, soils, and sediments, and (2) heterocyclic N compounds which are often referred to as *unknown* N. In fact, the N XANES study by Vairavamurthy and Wang (2002) showed that heterocyclic N accounted for at least 20-30% of the total N in the humic substances investigated. Furthermore, it has been shown that ^{15}N CPMAS NMR is insensitive to detecting heterocyclic N. Smernik and Baldock (2005) showed that 20–50% of the soil N was not detected by this technique, which they stated belonged to unprotonated, heterocyclic N functional groups.

A second criticism of the Maillard reaction as a potential humification pathway is that it requires a high temperature and pH to proceed as it is highly unfavourable under ambient soil conditions. In order to elucidate some details of this process, Jokic et al. (2001c) applied molecular shape analysis to investigate the initial reaction between D-glucose and glycine to form the Amadori compound fructosylglycine. This initial part of the Maillard reaction is a complex one which involves an intermediate phase resulting in the formation of the Amadori compound and the splitting off of a molecule of water. The structure of the Amadori compound was optimized at a quantum mechanical level and its ground state electron energy calculated. Molecular Isodensity Contours (MIDCO's) and electron density contour surfaces of constant electron density were constructed for D-glucose, glycine, and fructosylglycine in order to study the steric conditions for the reaction. The calculations of Jokic et al. (2001c) showed that the Amadori compound and water on one hand and the separate entities D-glucose and glycine on the other hand are very similar to each other in terms of their ground state energy. Their results

indicated that the potential energy barrier of this reaction is high and therefore, the reaction between D-glucose and glycine alone to form fructosylglycine is very slow at room temperature, which is in accord with the experimental observation (Jokic et al. 2001b). In order to decrease the energy barrier, Jokic et al. (2001b) used birnessite, which is commonly present in the environment, as catalyst to enhance the reaction rate. Their data showed that the presence of a redox reactive mineral, in this case birnessite, significantly accelerated the reaction by one to two orders of magnitude under environmentally relevant temperatures (25 and 45° C) and a neutral pH (7.00).

A number of studies have detected Maillard reaction products (melanoidins) in refractory organic matter from natural environments, for example from sediments from a west African upwelling (Zegouagh et al. 1999) and archeological plant remains (Evershed et al. 1997). Poirier et al. (2000, 2002) and Quénéa et al. (2006a) showed that the refractory organic matter isolated from different soils consists in part of cross-linked melanoidins poorly resolved by ^{13}C NMR spectroscopy. The presence of amide structures in soil as elucidated by ^{15}N NMR is ascribed to either preserved proteinacious structures or melanoidin type macromolecules (Derenne and Largeau 2001).

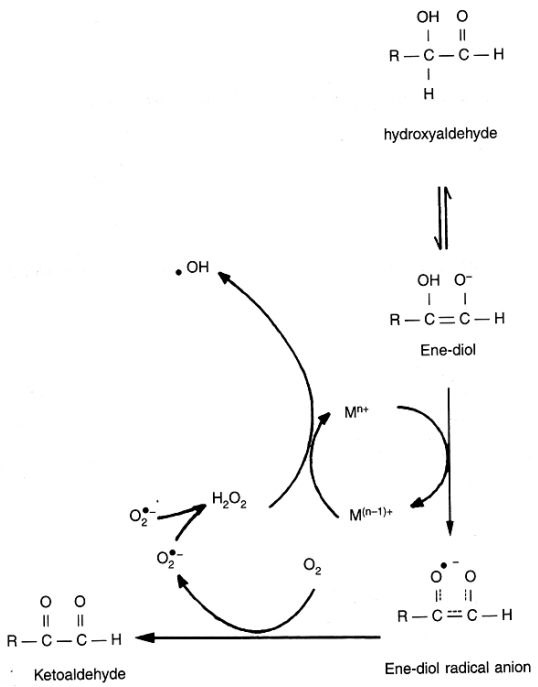

Figure 2.9 Glucose can enolize and reduce transition metals thereby generating reactive dicarbonyl compounds, hydrogen peroxide (H_2O_2) and hydroxyl radicals (•OH) (adapted from Wolff 1996).

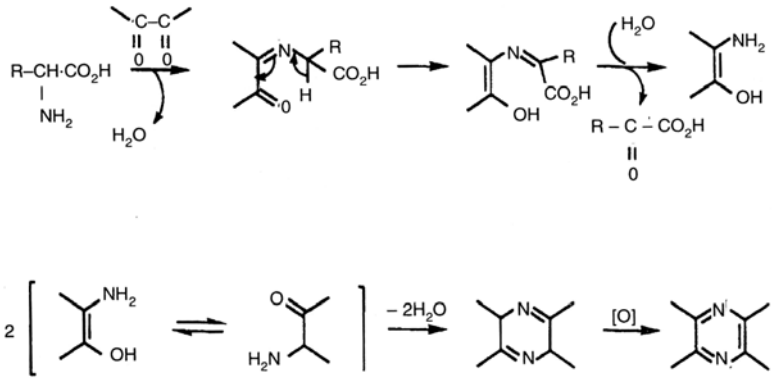

Figure 2.10 Strecker degradation of amino acids and α-dicarbonyls to form heterocyclic compounds. For glycine, R = H (Wong and Shibamoto 1996).

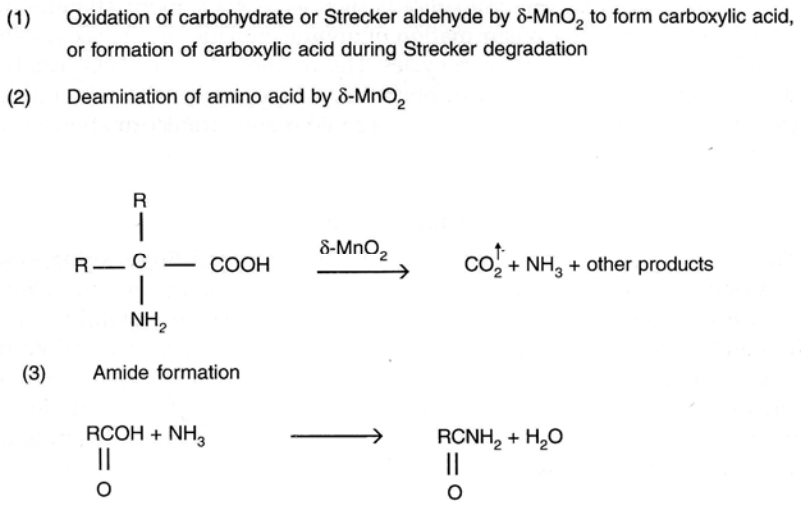

Figure 2.11 Possible amide formation pathway including the key role of MnO_2 (Jokic et al. 2005).

2.4.2.3 Integrated Polyphenol-Maillard Reaction Pathway

Jokic et al. (2004b) were the first to study an integrated Maillard reaction and polyphenol (glucose, glycine and catechol) pathway of humification, using birnessite as catalyst. Their data showed that the ubiquitous soil mineral, birnessite significantly accelerates humification processes in an integrated polyphenol-Maillard reaction system under ambient conditions. In nature it is unlikely that the Maillard reaction and polyphenol pathways occur separately, but rather interact closely, since sugars, amino acids and polyphenols all coexist in soil solutions and

natural waters. Jokic et al. (2004b) also showed that the integrated polyphenol-Maillard reaction system is more effective in generating humic polymers than the Maillard reaction alone.

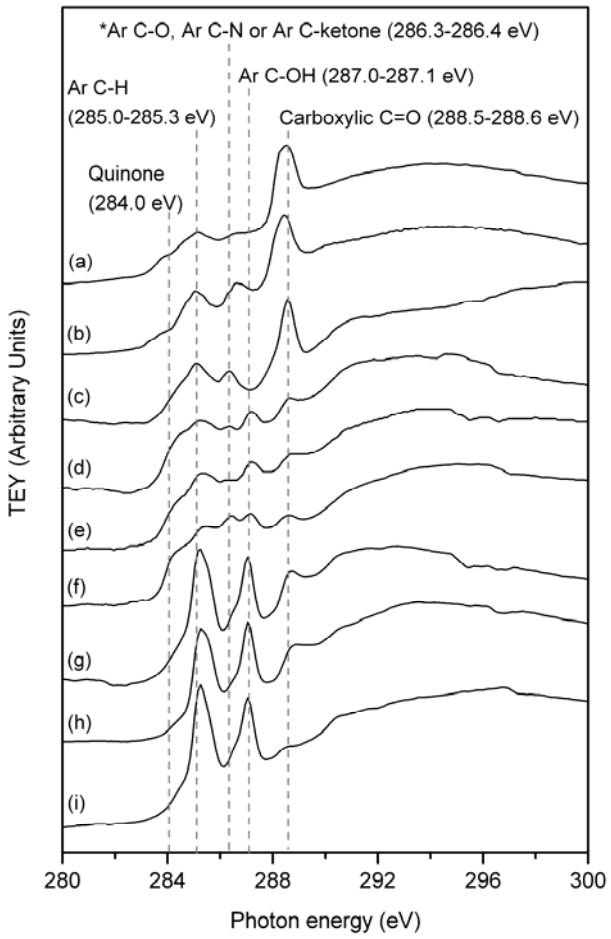

Figure 2.12 Carbon K-edge NEXAFS spectra of the IHSS (a) soil and (b) peat humic acids, and the humic acids extracted from the supernatants of the reaction systems catalyzed by birnessite: (c) Maillard reaction (50 mmole glucose + 50 mmole glycine); pyrogallol-Maillard reaction with (d) 50 mmole pyrogallol, (e) 100 mmole pyrogallol; (f) 50 mmole pyrogallol only; resorcinol-Maillard reaction with: (g) 50 mmole resorcinol and (h) 100 mmole resorcinol; and (i) 50 mmole resorcinol only system. *Ar = aromatic (Hardie et al. 2007). The y-axis is the normalized absorbance.

Hardie et al. (2007) studied the birnessite-catalyzed polyphenol-Maillard reaction pathway using two structurally different polyphenols, namely pyrogallol and resorcinol, and the Maillard reagents, glucose and glycine. They characterized the resultant reaction products using C K-edge and Mn L-edge NEXAFS spectroscopy. Their results clearly demonstrated that the structure of pyrogallol and resorcinol and their molar ratio to Maillard reagents in the polyphenol-Maillard

reaction system not only significantly affect the humification processes but also the biomolecule-induced formation of inorganic C, namely rhodochrosite ($MnCO_3$). The integrated pyrogallol-Maillard reaction systems form the least $MnCO_3$ and are more enriched in Mn(II)-coprecipitated organic components in the solid phase than the integrated resorcinol-Maillard reaction system. They concluded that polyphenols with *ortho*-OH groups (pyrogallol) participate in direct electron transfer reactions more readily than polyphenols with *meta*-OH groups (resorcinol) and subsequently undergo oxidative polymerization and ring cleavage reactions to a greater extent, which results in the formation of polymers with a greater aliphatic character (Figure 2.12) and the suppression of $MnCO_3$ formation. They also compared the humic acid fraction formed in the presence of birnessite from the Maillard reaction, and two polyphenol-Maillard reaction systems with natural soil and peat humic acid using C K-edge NEXAFS (Figure 2.12), and found that these humic acids are basically similar, especially the humic acid from the Maillard reaction and pyrogallol-Maillard systems.

2.5 Biotic Catalysis of Synthetic Humification Pathways

2.5.1 Enzymes

Common extracellular oxidoreductase enzymes in soils, which catalyze the oxidative coupling of phenolic compounds derived from lignins, tannins, and plant and microbial metabolites, include the phenoloxidases, tyrosinase (*o*-diphenoloxidase) and laccase (*p*-diphenoloxidase), and peroxidases (Sjoblad and Bollag 1981). Phenoloxidase enzymes catalyze phenol oxidative coupling reactions in the presence of O_2 by radical formation. Peroxidases catalyze oxidative reactions in the presence of hydrogen peroxide. The oxidized products (quinones) can undergo nucleophilic addition with other quinones or free-NH_2 groups with the eventual production of humic acid-like polymers (Martin and Haider 1980). Many researchers have studied the formation of humic-like substances from the enzymatic polymerization of phenolic compounds, such as catechol, pyrogallol or ferulic acid (Martin and Haider 1971; Ladd and Butler 1975; Marthur and Schnitzer 1978; Martin and Haider 1980; Dec et al. 2001, 2003; Ahn et al. 2006). There has been a lot of recent interest in developing techniques for using these oxidoreductase enzymes as biocatalysts to aid in the breakdown of toxic anthropogenic phenolic compounds and incorporation of the reaction products into existing humus fractions of the soil,

thus rendering them harmless (Durán and Esposito 2000; Burton 2003; Torres et al. 2003; Gianfreda and Rao 2004).

Laccases (EC 1.10.3.2)

Laccases are cuproproteins belonging to the small group of enzymes named blue oxidase enzymes. They possess four neighbour Cu atoms, which are distributed among different binding sites and are involved either in electron capture or binding with oxygen (Burton 2003). They catalyze the oxidation of many organic substances, including phenols, diphenols, aminophenols, polyphenols, polyamines and lignin related molecules, with concomitant reduction of oxygen to water. They also catalyze the demethylation of lignin, methoxyphenol acids and methoxyaromatics, the polymerization of lignin monomers and the co-polymerization of lignin with phenols and acrylamide (Claus 2004). It is produced by both plants and microorganisms, in particular by fungi. Their molecular masses typically vary between 40 000 – 140 000 Da, with laccases of fungal origin often being lower in molecular mass than those from plants. Laccases are capable of catalyzing the oxidation of *p*-diphenols as well as *o*-diphenols, this distinguishes them from tyrosinase, which can only react with *o*-diphenols (Burton 2003; Claus 2004; Baldrian 2006). Chefetz et al. (1998) studied the interaction of laccase produced by thermophilic fungi (*C. thermophilium*) with a wide range of phenolic substrates and concluded it could be involved in polymerization reactions that yield humic macromolecules. They hypothesized that during composting reactions, natural and xenobiotic phenols are oxidized by laccase present in the compost environment, resulting in the formation of free radicals which could be spontaneously bound to soluble high-molecular-weight compounds and results in the formation of humic macromolecules.

Tyrosinases (EC1.10.3.1)

Tyrosinases are also known as polyphenol oxidases or catecholases. They have a coupled binuclear copper active site. They can catalyze the hydroxylation of monophenols with molecular oxygen to form *o*-biphenols (cresolase activity), as well as the oxidation of *o*-diphenols to *o*-quinones (catecholase activity) (Figure 2.13). These reactions may be separate or sequential. The highly reactive quinones generally undergo further, non-enzymatic reactions resulting in the polymerization, and the subsequent formation of melanins. Tyrosinase is

produced by plants, animals and microorganisms, in particular by fungi and bacteria (Durán and Esposito 2000; Burton 2003; Claus and Decker 2006).

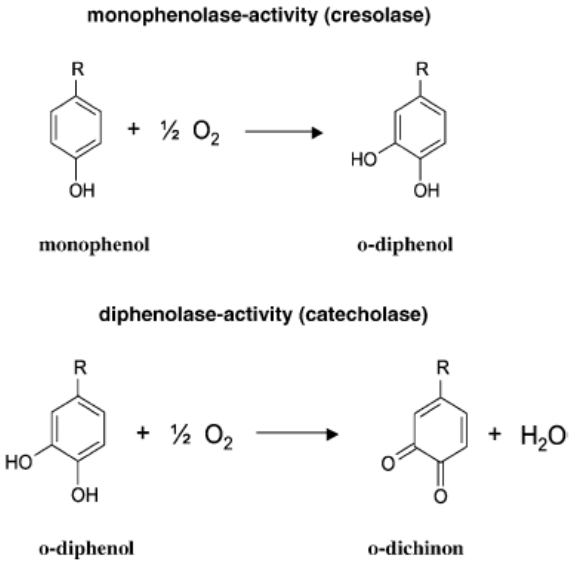

Figure 2.13 Enzymatic activities of tyrosinases (Claus and Decker 2006).

Peroxidases (EC 1.11.1.7)

Peroxidases are hemoproteins, produced mainly by microorganisms and plants, which catalyze oxidation of the recalcitrant non-phenolic lignin units in the presence of hydrogen peroxide (Durán and Esposito 2000). This is possible because of the formation of a high redox potential oxo-ferryl intermediate during the reaction of the heme cofactor with H_2O_2 (Martínez et al. 2005). Dubey et al. (1998) studied the polymerization of catechol by plant peroxidases, and found that the resultant polymers consisted of phenylene and oxyphenylene units (Figure 2.14).

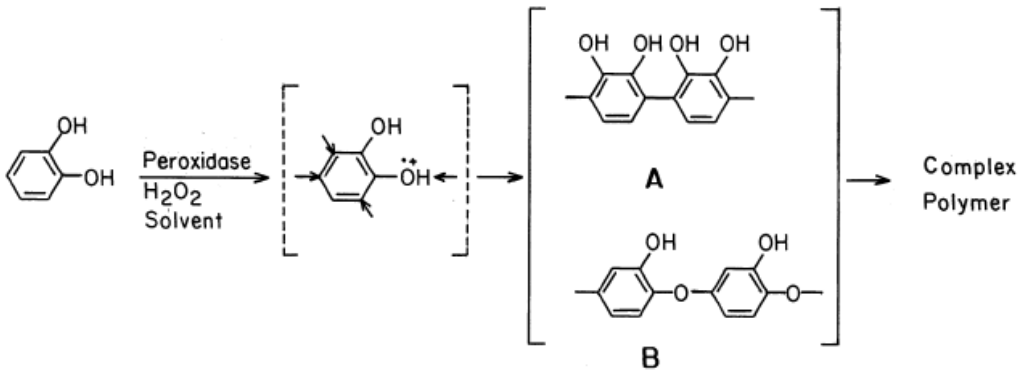

Figure 2.14 Possible reaction sequence of polymer formation from catechol by peroxidase (Dubey et al. 1998).

2.5.2 Microorganisms

The production of humic substances by microorganisms is an extracellular process, as the enzymes are secreted into the external solution which contains the phenolic compounds derived from lignin and tannic acid degradation and microbial and plant metabolites. These phenolic compounds can then be enzymatically oxidized to quinones, which can undergo further polymerization or polycondensation reactions with other biomolecules (e.g., amino acids) to form humic polymers (Stevenson 1994; Bollag et al. 1998; Burton 2003).

Fungi are the most important group of organisms responsible for the cleavage of lignin. The majority of studies have focused on the basidiomycetes known as "white-rot fungi". White-rot fungi such as *Phanerochaete chrysosporium* and *Coriolus versicolor* are the most efficient ligninolytic organisms that have been found to date. Their ability to degrade lignin and a wide variety of aromatic compounds is due to a nonspecific extracellular enzyme system, which involves lignin peroxidases, laccases and manganese-dependent peroxidases, as well as, hydrogen-producing oxidases which are also able to catalyze the oxidative polymerization of phenolic compounds (Sjoblad and Bollag 1981; Lopez et al. 2006) and the polycondensation of phenolic compounds and amino acids (Martin and Haider 1980). Yavmetidinov et al. (2003) studied the formation of humic-like substances produced by the white-rot fungi, Cor*iolus hirsutus* and *Cerrena maxima*, grown on oat straw. They analyzed the humic substances formed using liquid state ^{13}C NMR and FTIR, and found that these humic substances closely resembled the spectra obtained from soil humic acids (Figure 2.15). Both these strains of fungi produce high quantities of the enzyme laccase; therefore, they concluded that these fungi play an important role in not only the degradation of lignin but also the formation of high-molecular weight humic substances.

Martin and Haider (1971) concluded that microscopic fungi of the *Imperfecti* group play a significant role in the synthesis of humic substances in soil. Their studies showed that fungi such as *Hendersonula toruloidea, Epicoccum nigrum, Stachybotrys atra, Stachysbotrys chartarum* and *aspergillus sydowi* degrade lignin, as well as, cellulose and other organic plant constituents and in the process synthesize humic-acid like polymers. The initial degradation of lignin by fungi involves the release of the primary phenylpropane lignin structural units, such as

coniferaldehyde, *p*-hydroxybenzaldehyde and synapylaldehyde. These phenylpropane units are then further degraded into polyphenols by the fungal enzymes (Stevenson 1994).

Phenoloxidase activity has recently been found in lichenized ascomycetes belonging to a variety of taxonomic groups (Zavarzina and Zavarzin 2006). The researchers concluded that the oxidases discovered may play an important role in the phenolic metabolism of lichens and be involved in the formation of humus during primary soil formation processes, which may be a previously unknown geochemical function of lichens.

Microorganisms can also synthesize polyphenols which can contribute to humus formation in natural environments, as lignin is not present in all environments. Numerous phenolic and hydroxyl aromatic acids are synthesized by microorganisms from non-aromatic C sources, in particular by actinomycetes and fungi (Stevenson 1994). Martin and Haider (1971) reviewed the studies which investigated the synthesis of humic acid-like substances by fungi of the *Imperfecti* group. These microscopic fungi can degrade cellulose and other organic constituents besides lignin and in the process synthesize dark-coloured melanins from the phenols synthesized by these fungi. One interesting feature is the occurrence of resorcinol and resorcinol-type constituents which are not found in lignin transformation products.

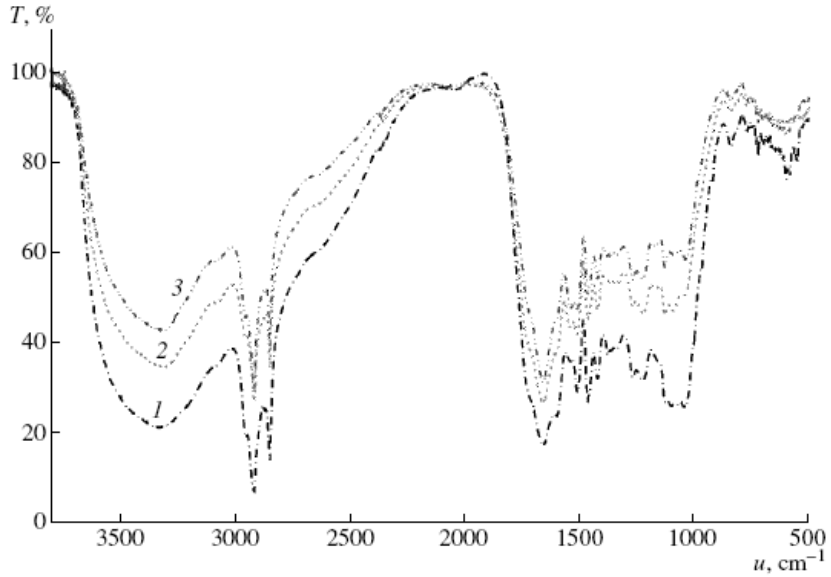

Figure 2.15 FTIR spectra of the humic-like substances produced by (1) *C. maxima*, (2) *C.* maxima + *C. hirsutus* and (3) *C. hirsutus* (Yavmetidinov et al. 2003).

2.6 Abiotic Catalysis of Synthetic Humification Pathways

The classical definition of a catalyst, according to Oswald, is a substance that increases the rate of a chemical reaction without undergoing any permanent chemical alteration itself. In reality the properties of catalysts do change with use (Twigg 1989). Actually many substances are destroyed either as a result of the process that gives them their catalytic activity or because of subsequent combination with the products (Moore and Pearson 1981). From a practical point of view, a catalyst is a substance that changes the rate of the desired reaction, regardless of the fate of the catalyst itself.

Metal oxides, clay minerals and dissolved metals have been shown to catalyze the transformations of natural and synthetic organic compounds, and inorganic substances (Huang 2000). Many metal ions, especially transition metals, have several oxidation states which enables them to act as catalysts in certain redox reactions. Iron oxides and especially Mn oxides are the most reactive in facilitating transformations of organic compounds. This includes catalysis of the ring cleavage of polyphenols, the deamination, decarboxylation, and dealkylation of amino acids, the polymerization of phenolic compounds and their polycondensation with amino acids, and the Maillard reaction (Shindo and Huang 1982, 1984a, 1984b; Huang 2000; Wang and Huang 2000b; 2003, 2005; Jokic et al. 2004b). Table 2.5 provides a complete summary of all the work that has been conducted on mineral catalysis of humification reactions.

Table 2.5 Summary of research conducted on mineral catalysis of abiotic humification reactions (updated from Wang et al. 1986).

Inorganic components as catalysts	Observations	References
	Abiotic Polymerization of Polyphenols	
Oxides, oxyhydroxides and short-range ordered minerals		
Hydrohematite, goethite, hematite and lepidocrocite	Polymerization of hydroquinone (measurement of optical density)	Scheffer et al. (1959)
Silica gel and disturbed quartz surface	Polymerization of hydroquinone, catechol and pyrogallol (measurement of optical density)	Ziechmann (1959)

Allophane	IR spectra of humified polyphenols; measurement of O_2 uptake of pyrogallol solution	Kyuma and Kawaguchi (1964)
SiO_2, Al_2O_3 and silicoalumina	IR spectra resembling natural humic substances; measurement of O_2 uptake	Wang et al. (1983b)
Short-range ordered Fe(III) oxides	Polymerization of phenolic compounds (measurement of optical density); yields of humic polymers	Shindo and Huang (1984a)
Birnessite (δ-MnO_2)	Polymerization of phenolic compounds (measurement of optical density); Δ log K and RF values; yields of humic polymers	Shindo and Huang (1982, 1984a)
Birnessite (δ-MnO_2) and Fe(III) oxides	Measurement of O_2 uptake; ESR determination of free radical content; FTIR study of mineral/organic polymer complexes	McBride (1987)
Birnessite (δ-MnO_2)	Polymerization of pyrogallol (measurement of optical density); ring cleavage of pyrogallol & catechol (measurement of CO_2 release); yields of humic polymers; IR and ^{13}C CPMAS NMR spectra resembling natural HAs	Wang and Huang (1992); Majecher et al. (2000)
Birnessite (δ-MnO_2)	Comparison of reaction mechanisms and products of transformation of catechol by biotic (tyrosinase) and abiotic (birnessite) catalysts	Pal et al. (1994); Nadja et al. (1998, 1999)
Birnessite (δ-MnO_2)	Investigation of the effect of light on ring cleavage of phenolics (measurement of CO_2 release) and abiotic humification	Lee and Huang (1995)
Short-range ordered Mn(IV), Fe(III), Al and Si oxides	Polymerization of pyrogallol (measurement of optical density); ring cleavage of pyrogallol (measurement of CO_2 release); yields of humic polymers; X-ray powder diffractograms, IR and ^{13}C CPMAS NMR spectra resembling natural HAs	Shindo (1992); Wang and Huang (2000a, 2000b)
Silicic acid, hydroxy-Al ions and hydroxy-aluminosilicate ions	Polymerization of catechol (measurement of optical density); X-ray powder diffractograms, electron micrographs and FTIR and ^{13}C CPMAS NMR spectra resembling natural HAs	Liu and Huang (2000, 2002)
Clay-size layer silicates		
Halloysite, Al-vermiculite, montmorillonite, illite and kaolinite	Polymerization of pyrogallol (measurement of optical density)	Kumada and Kato (1970)
Smectites	Polymerization of hydroquinone	Thompson and Moll (1973)

Montmorillonite, illite and kaolinite	Polymerization of phenolic compounds (measurement of optical density); IR spectra resembling natural humic substances; yields of humic polymers; measurement of O_2 uptake	Filip et al. (1977); Wang and Li (1977); Wang et al. (1978a, 1978b)
Nontronite, bentonite, kaolinite and quartz	Polymerization of hydroquinone and pyrogallol (measurement of optical density); intercalation of humic macromolecules in nontronite (XRD investigation into change in basal d-spacings); IR, ESR and ^{13}C CPMAS NMR spectra resembling natural humic substances	Wang and Huang (1986, 1989b, 1989c)
Montmorillonite	Oxidation and polymerization of catechol, pyrogallol and 2,6-dimethylphenol (FTIR spectra); SEM coupled with energy dispersive X-ray spectrometry investigation of reaction products on surface of clay minerals, ^{13}C NMR, MALDI MS study of reaction products	Birkel et al. (2002)
Primary minerals		
Olivines, pyroxenes, amphiboles, micas and feldspars	Polymerization of phenolic compounds (measurement of optical density); SEM micrographs and IR spectra resembling natural HAs; yields of humic acids; measurement of O_2 uptake	Shindo and Huang (1985a)
Natural soils		
Oxisol, Inceptisol and silt fraction of Mollisol	IR spectra resembling natural humic substances; yields of humic polymers; ESR spectra which indicate presence of stabilized free radicals (semiquinones) and resemble those of natural HAs; measurement of O_2 uptake	Wang et al. (1978b, 1978c, 1983a)
Forest soils (Alfisol and Inceptisol)	Polymerization of phenolic acids (measurement of optical density); investigated rate of Mn(II) and Al dissolution	Pohlman and McColl (1989)
Mollisol	Polymerization of pyrogallol (measurement of optical density); IR and ESR spectra of humic macromolecules resembling natural substances; measurement of CO_2 release	Wang and Huang (1989a)
<u>Abiotic Copolymerization of Amino Acids and Polyphenols</u>		
Birnessite (δ-MnO_2)	Polycondensation of glycine and pyrogallol/hydroquinone (measurement of optical density); IR and ESR spectra of N-polymers resembling natural humic substances; yields of humic substances; measurement of O_2 uptake; decarboxylation and dealkylation of glycine	Shindo and Huang (1984b); Wang and Huang (1987, 2005); Wang and Lin (1993)

Nontronite	Polycondensation of glycine and pyrogallol (measurement of optical density); IR and ESR spectra of N-polymers resembling natural humic substances; yields of humic substances	Wang and Huang (1991)
Oxisol and Mollisol clay fractions	Polycondensation of glycine and pyrogallol (measurement of optical density); IR and ESR spectra of N-polymers resembling natural humic substances; yields of humic substances; measurement of CO_2 and NH_3 released	Wang and Huang (2003)
	Maillard Reaction	
Absence of catalysis	Pioneering work on condensation reactions between sugars and amino acids to form melanoidins in the absence of catalysts	Maillard (1913)
Absence of catalysis	Condensation reaction between basic amino acids and sugars in the absence of catalysts results in N-rich polymers similar to humic substances in marine environments	Hedges (1978)
Oxides, oxyhydroxides and short-range ordered minerals		
Birnessite (δ-MnO_2)	Condensation of glucose and glycine under soil ambient conditions (measurement of optical density); yields of humic substances; XANES study of change in speciation of Mn; ESR study of Mn speciation in solution; ^{13}C CPMAS NMR spectra of FA fraction resembling spectra of natural FAs	Jokic et al. (2001b)
Birnessite (δ-MnO_2)	Investigation of the effect of light on Maillard reaction - condensation of glucose and glycine (measurement of optical density); yields of humic substances; EPR and XANES study of change in speciation of Mn; FTIR study of solid residues	Jokic et al. (2001a)
Birnessite (δ-MnO_2)	Condensation of glucose and glycine (measurement of optical density); yields of humic substances; XANES, Py-FIMS and Curie-point Py-GC/MS studies of solid residue – show that amide and heterocyclic N compounds are formed (dominant N forms in natural humic substances)	Jokic et al. (2004a)
Goethites	Condensation of arginine and glucose at 37° C; C and N fractions yields; FTIR spectra of solid residue and supernatant humic substances	Gonzalez and Laird (2004)

Clay-size layer silicates		
Montmorillonite, nontronite, kaolinite and quartz (saturated with Cu^{2+} , Ca^{2+}, Al^{3+})	Condensation of glucose and tyrosine / glycine / tryptophan at 70° C: FTIR spectra resembling natural humic substances; yields of humic substances; XRD investigation into change in d-spacings	Arafaioli et al. (1997, 1999); Bosetto et al. (1995, 1997, 2002)
Smectites	Condensation of arginine & glucose at 37° C; C and N fractions yields; FTIR spectra of solid residue and supernatant humic substances; XRD investigation into change in d-spacings	Gonzalez and Laird (2004)
	Integrated Abiotic Humification Pathway	
Birnessite (δ-MnO_2)	Integration of abiotic polyphenol and Maillard reaction pathways – polycondensation of catechol/pyrogallol/resorcinol-glucose-glycine (measurement of optical density); yields of HA; XANES study of change in speciation of Mn; ^{1}H NMR & ^{13}C CPMAS NMR spectra of HA fraction; atomic force micrographs resembling natural HAs; C K-edge NEXAFS study of HA	Jokic et al. (2004b); Hardie et al. (2007)

2.6.1 Oxides, Oxyhydroxides and Short-Range Ordered Minerals

The surfaces of metal oxides are very reactive in promoting the polymerization of phenolic compounds. They can act as Lewis acids by accepting electrons from hydroxyphenolics, leading to the formation of highly reactive semiquinone radicals which readily undergo coupling reactions with other semiquinones, phenolics or existing humus (Dec and Bollag 2000; Huang 2000). Shindo and Huang (1984a) investigated the catalytic ability of short-ranged ordered Mn, Fe, Al and Si oxides in the oxidative polymerization of catechol, resorcinol and hydroquinone. They determined the degree of polymerization (browning) by measuring the visible absorbances (at 600 nm) of the supernatants from the various reactions systems. They showed that the visible absorbance was directly correlated with the yield of humic polymers. They found that Mn oxides (birnessite, cryptomelane, pyrolusite) were the most powerful catalysts of oxidative polymerization reactions, compared to Fe, Al and Si oxides (Figure 2.16). Wang and Huang (2000a) characterized the pyrogallol-derived polymers formed by the catalysis of short-ranged ordered Mn, Fe, Al and Si oxides. They showed that the infra-red spectra of the FA fraction from the Mn oxide-pyrogallol system closely resembled that of the FA fraction extracted from a natural Borosaprist soil (Figure 2.17).

The catalytic effectiveness of a metal ion depends on its ability to complex with ligands and shift electron density and molecular conformation in ways favourable for the reaction (Hoffmann 1980; Huang 2000). The Mn oxide has the highest catalytic power in promoting catechol humification compared with Fe and Al oxides (Liu and Huang 2001). This is, in part, attributable to the lower electronegativity of Mn. The electronegativity values of Mn, Fe, Al, H, and O are, respectively, 1.55, 1.83, 1.61, 2.20, and 3.44 (Porterfield 1983). Catechol acts as a hard Lewis base and Al, Fe, and Mn are hard Lewis acids. When Al, Fe, or Mn replaces H in catechol to form metal-catechol complexes, the electron cloud delocalizes from phenolic oxygen into the π-orbital formed from overlap of the 2p orbitals of the aromatic C atoms, thus accelerating the formation of semiquinone free radicals and their coupling to polycondensates. The electron cloud around the Mn-O bond in the Mn oxide-phenolic complex should be more delocalized than that around the Al-O bond in the Al-catechol complex and especially the Fe-O bond in the Fe oxide-phenolic complex due to the lower electronegativity of Mn than those of Al and Fe. This partially explains the greater accelerating effect of Mn oxide on the humification of catechol than Fe and Al oxides. Redox reactions also play an important role in many abiotic catalyses (Huang 2000). Aluminum oxide is not subject to redox reaction. The standard electrode potential (E°) values of the overall redox reaction of the Fe(III) oxide-catechol and Mn(IV) oxide-catechol systems are +0.071 V and +0.509 V, respectively, as indicated by the following reactions (Shindo and Huang 1984a):

$$Fe^{3+} + e^- = Fe^{2+} \qquad E° = 0.770\ V \qquad (2.2)$$

$$MnO_2 + 4H^+ + 2e^- = Mn^{2+} + 2H_2O \qquad E° = 1.208\ V \qquad (2.3)$$

$$C_6H_4(OH)_2 = C_6H_4O_2 + 2H^+ + 2e^- \qquad E° = -0.6992 \qquad (2.4)$$

The positive E° values of the overall redox reactions indicate that the reactions are thermodynamically feasible and catechol oxidation can thus be accelerated by Fe oxide and especially Mn oxide. This also explains the stronger catalytic ability of the Mn oxide than Fe and Al oxides in accelerating catechol oxidation. In addition, the lower point of zero salt effect (PZSE) and more negative charges of the Mn oxide than the Fe and Al oxides could also enhance

the oxidation of catechol (Liu and Huang 2001). More negative charges of the Mn oxide may favour the binding of protons released from catechol (Eq. 2.4) and subsequently increase the catalytic reaction rate. Therefore, the catalytic ability of a metal oxide in polyphenol transformation depends on the E° value of the overall redox reaction and the ability of the metal ions to complex with ligands, to shift electron density and molecular confrontation in the way conducive to the reaction, and to favour the binding of protons to the metal oxide.

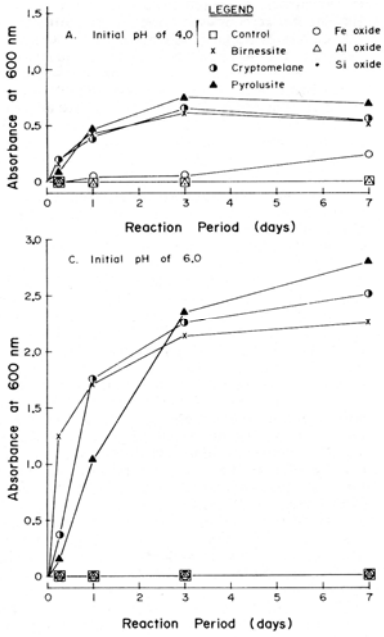

Figure 2.16 Changes in the degree of darkening of hydroquinone solution at pH 4.0 and 6.0 as influenced by various oxides as a function of time (Shindo and Huang 1984a).

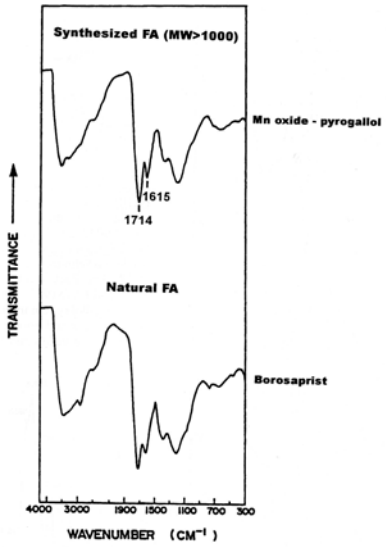

Figure 2.17 Infra-red spectra of the synthesized FA in the Mn(IV) oxide-pyrogallol system and the FA extracted from a Borosaprist (Terric Humisol) (Wang and Huang 2000a).

It has also been shown that there is a concomitant mechanism resulting in aromatic ring cleavage and the release of CO_2 during metal oxide catalysis of polyphenol polymerization reactions (Wang and Huang 1994; Lee and Huang 1995; Majecher et al. 2000; Wang and Huang 2000b). Wang & Huang (2000b) studied the ring cleavage and oxidative polymerization of pyrogallol by short-ranged ordered Mn, Fe, Al and Si oxides under aerobic and anaerobic conditions. They found that the presence of oxygen significantly enhanced oxide-catalyzed ring cleavage of pyrogallol and the resultant release of CO_2 (Table 2.6). The semiquinone free radicals formed appear to be partially transformed, through ring cleavage, to aliphatic fragments, resulting in the development of carboxyl groups and subsequent decarboxylation and CO_2 release (Liu and Huang 2001). The ability of short-range ordered oxides of Al and Si, and especially Fe and Mn in enhancing the formation of aliphatic and carboxylic groups in humic polymers derived from polyphenol humification may, in part, contribute to the high aliphaticity of humic substances in soils (Schnitzer 1977; Wilson and Goh 1977; Hatcher et al. 1981; Preston et al. 1982) and the variation in their characteristics, including carboxyl group content, with soils from different climatic zones (Schnitzer 1977).

Table 2.6 Release of CO_2 in oxide-pyrogallol systems in air or N_2 atmosphere at the end of 90-h reaction period (Wang and Huang 2000b).

	CO_2 release (μmol)[†]		
Oxide	**Air**	**N_2**	**$LSD_{0.05}$**
Manganese	463.8 ± 0.3[‡]	13.7 ± 0.1	1.4
Iron	124 ± 2	21.4 ± 0.1	8.6
Aluminum	52.7 ± 0.4	18.4 ± 0.3	2.2
Silicon	28.4 ± 0.0	2.7 ± 0.0	4.3
No catalyst	24.5 ± 0.3	0	1.3
$LSD_{0.05}$	3.4	0.5	

[†]The amounts of CO_2 released in the systems, which contained 100 mg of oxide (0.2-2 μm) and 0.5 mmol of pyrogallol in 30 mL of sterilized aqueous solution, adjusted to pH 6.00.
[‡]The average deviation from the mean.

Liu and Huang (2000) reported that silicic acid and especially hydroxyl-Al ions substantially enhance oxidative polymerization of catechol. Liu and Huang (2002) showed that

hydroxyl-aluminosilicate ions, which are precursors to noncrystalline aluminosilicates, are also effective in promoting the oxidative polymerization of catechol. A proposed mechanism for the catalytic effect of hydroxy-aluminosilicate ion on the humification of catechol is depicted in Figure 2.18. Catechol acts as a hard Lewis base and Al and Si of hydroxy-aluminosilicate ions are hard Lewis acids. Hydroxy-aluminosilicate ions can complex with catechol through Al-O and Si-O bond formation. The electronegativity values of Al, Si, H, and O are respectively, 1.61, 1.90, 2.20, and 3.44 (Hueey 1983). Therefore, when Al or Si replaces H in catechol, the electron cloud delocalizes around the Al-O and Si-O bonds from phenolic oxygen into the π-orbital bonding formed from the overlaps between the 2p orbitals of the carbon atoms of the aromatic ring, thus apparently accelerating the formation of semiquinone free radicals and their coupling to form polycondensates. The semiquinone free radicals formed appear to be partially transformed, through ring cleavage, to aliphatic fragments, resulting in the development of carboxyl groups and subsequent decarboxylation and CO_2 release.

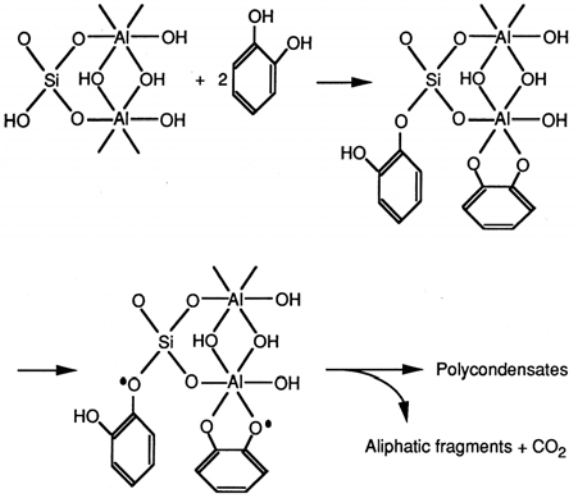

Figure 2.18 Proposed mechanism for the catalysis of hydroxyl-aluminosilicate ions in catechol humification (Liu and Huang 2002).

The structure and functionality of polyphenolics also affect the oxidative polymerization catalytic ability of soil mineral oxides. Pohlman and McColl (1989) demonstrated that polyhydroxyphenolic acids with *p*- or *o*-OH groups are more readily oxidized to polymeric humic products by Mn oxides than *m*-polyhydroxyphenolic acids. Similarly, Shindo and Huang (1992) investigated the oxidative polymerization of various diphenols by Mn oxide and found that HA yields increase in the following order: hydroquinone (*p*-OH group) > catechol (*o*-OH

group) > resorcinol (*m*-OH group). Birnessite (δ-MnO_2) has been shown to catalyze polycondensation reactions between amino acids and phenolic compounds in the abiotic formation of organic N complexes (Shindo and Huang 1984b). Birnessite is able to promote the deamination and decarboxylation (Wang and Huang 1987), and dealkylation (Wang and Huang 1997) of glycine. Wang and Huang (2005) showed that birnessite promotes the incorporation of carboxyl and especially alkyl C of glycine into the polycondensates formed with pyrogallol.

Commonly found soil metal oxides, birnessite (Jokic et al. 2001b) and goethite (Gonzalez and Laird 2004), have also been shown to catalyze the Maillard reaction, under typical pH and temperature ranges found in the natural environment. Jokic et al. (2001b) were the first to report that birnessite catalyzes the Maillard reaction between glucose and glycine. This reaction is kinetically sluggish under ambient temperatures (Jokic et al. 2001c), but the presence of birnessite significantly catalyzes the reaction by decreasing the activation energy required. Jokic et al. (2001a) investigated the effect of light on birnessite catalysis of the Maillard reaction, and showed that the reaction is promoted by light but also readily occurs in the absence of light. This means that the reaction could readily occur in the subsoil in the presence of a mineral catalyst such as birnessite. Jokic et al. (2004a) showed that birnessite catalyzes the Maillard reaction between glucose and glycine resulting in the formation of humic substances that contain significant amounts of heterocyclic and amide N, which provides an explanation for one of the pathways for the formation of heterocyclic and amide N found in humic substances in the environment. Jokic et al. (2004b) were the first to investigate an integrated polyphenol-Maillard reaction humification pathway as catalyzed by birnessite, by studying the reaction between glucose, glycine and catechol. They found that the presence of birnessite significantly accelerates this integrated humification pathway under temperatures and a neutral pH typical of natural environments.

2.6.2 Clay Size Layer Silicates

Besides metal oxides, clay size layer silicates have the ability to catalyze the oxidative transformation of biomolecules (Wang et al. 1978a; Wang et al. 1986; Bollag et al. 1998; Huang 2000, 2004). Before the pioneering work on the catalytic role of clay size layer silicates in oxidative polymerization of phenolic compounds and the subsequent formation of humic substances (Kumada and Kato 1970; Filip et al. 1977; Wang and Li 1977), the conversion of

many aromatic amines into their coloured derivatives by clay minerals had been investigated (Faust 1940; Hauser and Legget 1940). Solomon (1968) reported that, except for talc, a large number of representative clay minerals produce a blue colour of varying intensity when brought in contact with a saturated solution of benzidine hydrochloride. The active sites for the oxidation of benzidine are located on the crystal edges and on transition metal atoms in the higher oxidation state that occupy octahedral sites in the silicate layers. Thompson and Moll (1973) measured the oxidative power of smectites by oxidation of hydroquinone to *p*-benzoquinone in a clay slurry. Oxidation occurs in the presence of O_2 (air), but not of N_2 unless Fe^{3+} or Cu^{2+} are the exchangeable cations. Adsorbed O_2 molecules or radicals on the clay surface are apparently responsible for the oxidation.

Montmorillonite, vermiculite, illite, and kaolinite accelerate the formation of HAs to varying degrees (Table 2.7) (Shindo and Huang 1985b). The promoting effect of 2:1 layer silicates is higher than that of 1:1 layer silicates because of the larger specific surface area and lattice imperfection which favour the adsorption of O_2 molecules or radicals. Many studies focused on the oxidative catalytic ability of transition metal-saturated smectites on aromatic molecules (Pinnavais et al. 1974; Mortland and Halloran 1976). However, the most common exchangeable cations found on smectites in soils are alkaline earth metals such as Ca. One of the well-identified precursors (Flaig et al. 1975; Hayes 1991) for the formation of humic substances, hydroquinone, can be transformed in aqueous solution at near neutral pH (6.5) to humic macromolecules and deposited in the interlayers of nontronite saturated with Ca which is the most common and most abundant exchangeable cation in soils and sediments (Wang and Huang 1986). Most of the interlayer humic macromolecules are highly resistant to alkaline extraction and is, thus, humin type materials. Therefore, besides Al interlayering of clays (Barnhisel and Bertsch 1989), the formation of humic substance interlayers in 2:1 layer silicate, through polymerization of phenol monomers and the associated reactions in soils and sediments, merits attention. The catalytic sequence of selected minerals in the smectite group is: nontronite > montmorillonite > hectorite, which can be related to the dominant structural metals of each mineral. Nontronite contains Fe(III) as the major structural cation in the octahedral sheet, while montmorillonite contains predominantly Al and hectorite Mg and Al (Wang and Huang 1986).

Wang and Huang (1989b) showed that the edge-sites of kaolinite provided all of its catalytic power whereas, in the case of nontronite its edge-sites only partially accounted for its

catalytic power. They also found that edge-site adsorption of humic polymers only accounted for a small fraction of the total amount of humic substances sorbed by the minerals. Nontronite also has the ability to cleave the aromatic ring of pyrogallol, catechol and hydroquinone. The ability of nontronite to promote ring cleavage of polyphenols is related to the structure and functionality of the polyphenols (Wang and Huang 1994). Catechol with two hydroxyl groups in the *ortho* positions, is more easily cleaved than hydroquinone, which has two hydroxyl groups in the *para* positions (Table 2.8). Pyrogallol, which has three hydroxyls all *ortho* to one another, is by far the most easily cleaved of the three polyphenols.

Table 2.7 Effects of clay minerals on the synthesis of humic acids (HA) at an initial pH of 5.5 at the end of 7 days (Shindo and Huang 1985b).

	Yield of HA (g HA-carbon kg^{-1} inorganic material)*		
System	Soluble fraction	Precipitated fraction	Total
Control†	0.68 (100)‡	0.30 (100)	0.98 (100)
Montmorillonite	1.25 (184)	0.31 (103)	1.56 (159)
Vermiculite	0.98 (144)	0.31 (103)	1.29 (132)
Illite	0.77 (113)	0.32 (107)	1.09 (111)
Kaolinite	0.68 (100)	0.31 (103)	0.99 (101)

*1 mL of 0.02 M $KMnO_4$ consumed was calculated as corresponding to 0.45 mg carbon.
†In the absence of inorganic material.
‡The index of the yield of HA in the control system is assigned 100 as the basis for comparison.

Clay size layer silicates also have the ability to catalyze the polycondensation of phenolic compounds and amino acids. Wang et al. (1985) examined the catalytic effect of Ca-illite on the formation of N-containing humic polymers in systems containing various phenolic compounds and amino acids. The yields and N contents of the resultant HAs were dependant on the nature of the amino acids. Nontronite can also catalyze the polycondensation of glycine and pyrogallol (Wang and Huang 1991). Molecular O_2 chemisorbed on silicates, such as nontronite, has a strong oxidative power (Solomon and Hawthorne 1983), and seems to be responsible for the ring cleavage of pyrogallol, and the decarboxylation and deamination of glycine (Wang and Huang 1991). Gonzalez and Laird (2004) showed that four different smectites saturated with various metal cations could catalyze the Maillard reaction between arginine and glucose at an environmentally relevant temperature (37° C). Of the saturating cations investigated (Ca, Na,

Cu(II) and Al), only Cu (II) significantly altered the amount of humic substance produced. They also observed that some of the adsorbed humic substances were intercalated into the smectites.

Table 2.8 Release of carbon dioxide in the nontronite-polyphenol systems at the end of a 90-h reaction period (Wang and Huang 1994).

Reaction condition		
Nontronite	Polyphenol	CO_2 release (μmol*)
+[†]	Pyrogallol	263
-[‡]	Pyrogallol	54
+	Catechol	88
-	Catechol	34
+	Hydroquinone	49
-	Hydroquinone	21

*Amount of CO_2 released in the systems containing 1 g of Ca-nontronite (0.2-2 μm), 5 mmol of pyrogallol, catechol or hydroquinone in 30 mL of aqueous solution adjusted to pH 6.00.
[†]In the presence.
[‡]In the absence.

2.6.3 Primary Minerals

Primary minerals are the rock-forming minerals in the earth's crust and are present in soils and aquatic sediments (Dixon and Weed 1989; Dixon and Schulze 2002). These minerals differ in their abilities to accelerate the abiotic polymerization of hydroquinone (Table 2.9). The sequence of the catalytic power of the primary minerals is: tephroite > actinolite > hornblende, fayalite > augite > biotite > muscovite ≅ albite ≅ orthoclase ≅ microcline ≅ quartz (Shindo and Huang 1985a). The degree of acceleration of the oxidative polymerization of hydroquinone is greatest in the tephroite system which increases the total HA yield more than nine-fold. This is attributable to: (1) tephroite (ideal chemical formula, $MnSiO_4$) is a Mn-bearing silicate, (2) part of the Mn in tephroite is present in the higher valence states, and (3) the oxidation of diphenols [$C_6H_4(OH)_2$] by Mn(III) and Mn(IV) is thermodynamically favourable (Weast 1978).

The hydroquinone-derived polymers formed in the presence of the tephroite system (Shindo and Huang 1985a) have similar IR absorption bands to those of soil humic substances (Schnitzer 1978). The surface features of these polymers (Figure 2.19) are similar to those of soil HA and FA (Stevenson and Schnitzer 1982) with the smallest discrete particles being

spheroids with diameters of 0.1 to 0.2 μm (Figure 2.19a) and some aggregation of individual spheroids (Figure 2.19b and c). Small aggregates resemble moss while the large aggregates are nodule like (1-5 μm diameter) and doughnut like (6-8 μm diameter) (Figure 2.19a and b). The polymers do not appear to be associated with the surfaces of tephroite particles (Figure 2.19d). The role of primary minerals in the oxidative polymerization of polyphenols and the subsequent formation of humic substances in soils and sediments should not be overlooked.

Table 2.9 Effects of primary minerals on the synthesis of HA at an initial pH of 5.5 at the end of 7 days (Shindo and Huang 1985a).

	Yield of HA (g HA-carbon kg^{-1} inorganic material)*		
System	Soluble fraction	Precipitated fraction	Total
Control†	0.68 (100)‡	0.30 (100)	0.98 (100)
Tephroite	6.60 (971)	1.90 (633)	8.50 (867)
Hornblende	3.24 (476)	1.05 (350)	4.29 (438)
Augite	2.90 (426)	0.67 (223)	3.57 (364)
Biotite	2.03 (299)	0.55 (183)	2.58 (263)
Quartz	1.15 (169)	0.32 (107)	1.47 (150)
Microcline	0.98 (144)	0.32 (107)	1.30 (133)

*1 mL of 0.02 M $KMnO_4$ consumed was calculated as corresponding to 0.45 mg carbon.
†In the absence of inorganic material.
‡The index of the yield of HA in the control system is assigned 100 as the basis for comparison.

2.6.4 Natural Soils

A number of studies have investigated the abiotic catalytic ability of natural soils (whole soils and clay fractions) as catalysts for the polymerization of polyphenols (Wang et al. 1978b, 1978c, 1983a; Wang and Huang 1989a), phenolic acids (Pohlman and McColl 1989) and the polycondensation of polyphenols and amino acids (Wang and Huang 2003). Wang and Huang (1989a) examined the catalytic ability of the sterilized Ap horizon from a Mollisol from Saskatchewan, Canada, on the ring cleavage and polymerization of pyrogallol. They reported that abiotic processes evidently cause the polymerization of pyrogallol as well as its ring cleavage and the formation of its fragments. The IR and ESR spectra of the HS formed closely resemble those of naturally occurring HS. Wang and Huang (2003) showed that the clay

fractions from a tropical Oxisol and temperate Mollisol catalyze the abiotic polycondensation of pyrogallol and glycine and the subsequent formation of humic substances. The polymerization of pyrogallol and glycine, the abiotic ring cleavage of pyrogallol, and the deamination of glycine are greatly enhanced by the presence of the sterilized soil clays, all of which increased with increasing temperature (Wang and Huang 2003). The abiotic catalytic ability of soils in the formation of humic substances is due to the reactive components, namely Mn, Fe, and Al oxides, (oxy)hydroxides, and SRO mineral colloids, clay-size layer silicates, and some reactive primary minerals which have been extensively investigated as discussed in sections 2.6.1 to 2.6.3 .

Little is known on the catalysis of the Maillard reaction and especially the integrated polyphenol-Maillard reaction by natural soils and sediments. Further work is warranted on this subject matter to advance our understanding of the role of abiotic catalysis in the formation of humic substances and related C turnover and N transformations in the environment.

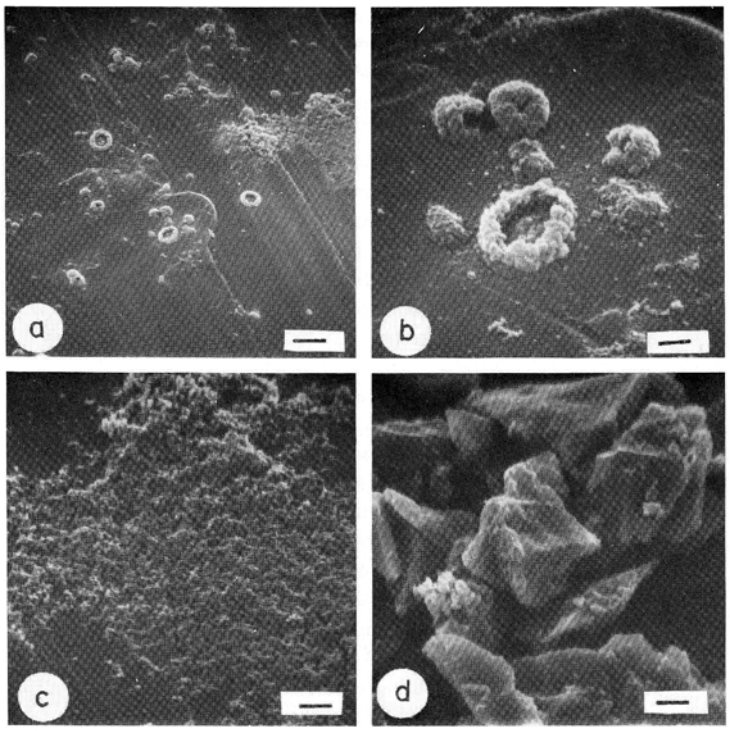

Figure 2.19 SEM micrographs of hydroquinone polymers in the supernatant and mineral particles settled in the tephroite system at the ratio of mineral to hydroquinone solution of 0.01 at the initial pH of 6.0 at the end of 7 days. (a), (b), (c): hydroquinone polymers; (d): tephroite particles after reaction with hydroquinone. Bar in Fig. 2.19a = 10 μm; bars in Fig. 2.19b-d = 2 μm (Shindo and Huang 1985a).

2.7 Comparison of the Mechanisms and Significance of Biotic and Abiotic Catalyses of Humification Reactions in Natural Environments

2.7.1 Comparison of the Mechanisms of Biotic and Abiotic Catalyses of Synthetic Humification Reactions

There have been numerous studies in recent years investigating the differences in oxidative coupling reactions of phenols catalyzed by enzymes or mineral colloids. Both mineral colloids and oxidoreductive enzymes contain metals which can act as electron acceptors to catalyze the oxidative transformation of organics, hence there are similarities in their reaction products. However, there are differences in the mechanisms by which these catalysts operate.

Pal et al. (1994) compared the catalysis of oxidative coupling reactions of various phenolic compounds by the enzymes, laccase and tyrosinase, and mineral catalyst, birnessite. Birnessite acts as a heterogeneous catalyst whereas laccase and tyrosinase function as homogenous catalysts. Laccase and tyrosinase continue to oxidize catechol after repeated additions of the chemical, while birnessite lost its oxidizing activity after the first addition of catechol (Figure 2.20). In the case of birnessite, Mn serves as a terminal electron acceptor during the oxidative coupling reactions and thus is altered or consumed. The enzymes on the other hand are able to successfully mediate the transfer of an electron to an electron acceptor (O_2) in a cyclic manner. They concluded that enzymes as homogenous catalysts appeared to be more effective oxidative agents compared to abiotic agents as heterogeneous catalysts. In the natural environment, however, the Mn^{2+} that is released during birnessite-induced oxidation of phenolic compounds such as catechol, could be reoxidised to higher valency oxides depending on the redox potential of the environment, and could thus regain its catalytic potential. This has been observed for Fe oxides (McBride 1987). Furthermore, redox transformations between reduced and oxidized Mn forms are strongly catalyzed by bacteria. Microbial Mn(II) oxidation is a major process that can produce Mn oxide coatings in soils and marine sediments (McLean et al. 2002).

Based on electron spin resonance studies, the oxidative polymerization of polyphenols (such as catechol) by birnessite (δ-MnO_2) proceeds through the formation of semiquinone radicals (McBride 1989), whereas with tyrosinase, it proceeds without the semiquinone radical formation as electron transfer is controlled by the binuclear copper active site (Himmelwright et al. 1980). Thus, the formation of humic polymers (melanins) as mediated by tyrosinase or

birnessite has been reported to be controlled by different mechanisms (Figure 2.21). Park et al. (1999) investigated the effect of a variety of humic constituents on the transformation of chlorinated phenols and anilines in the presence of peroxidase, tyrosinase, laccase and birnessite. They found that the addition of catechol resulted in a significant reduction of transformation in the peroxidase, laccase and birnessite systems, whereas it enhanced transformation in the tyrosinase systems. They suggested that the varying effect of catechol could be explained by different transformation mechanisms involving either *o*-quinone coupling (with tyrosinase) or free radical coupling (with peroxidase, laccase or birnessite).

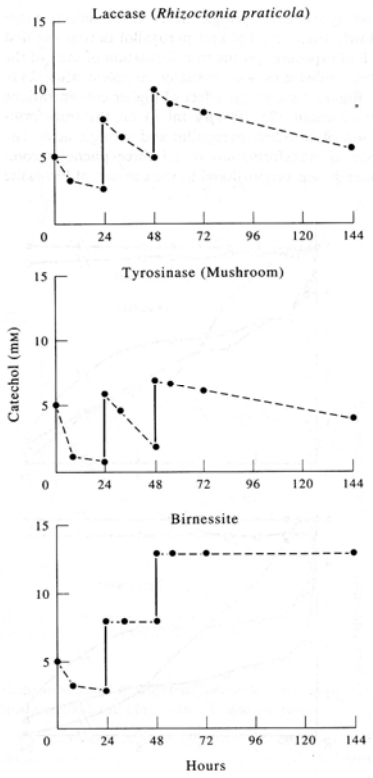

Figure 2.20 Transformation of catechol by laccase (0.4 units.ml^{-1}), tyrosinase (0.4 units.ml^{-1}) and birnessite (600ug.ml^{-1}) after repeated addition of substrate (Pal et al. 1994).

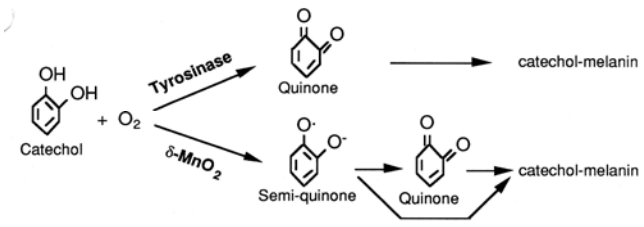

Figure 2.21 Mechanisms of the oxidative polymerization of catechol to melanins (humic polymers) in the presence of tyrosinase or birnessite (Naidja et al. 1999).

Naidja and Huang (2002) showed that the Henri-Michaelis-Menten theory, which is usually applied to the kinetics of homogenous enzymatic catalysis reactions, can also be applied to the abiotic catalysis of catechol oxidation by birnessite (Figure 2.22). Naidja et al. (1999) compared the kinetics of catechol oxidation by birnessite and tyrosinase. They found that tyrosinase has a slightly lower activation energy which causes the reaction rate to proceed at a rate three times faster than that of birnessite. However, unlike birnessite, tyrosinase is inactivated at temperatures above 30° C because of denaturation of the protein molecules; birnessite oxidation activity continues to increase with increasing temperature (Figure 2.23). Therefore, the data suggest that, compared with enzymes such as tyrosinase, metal oxides such as birnessite would play a more important role in the transformation of phenolic compounds in warmer regions.

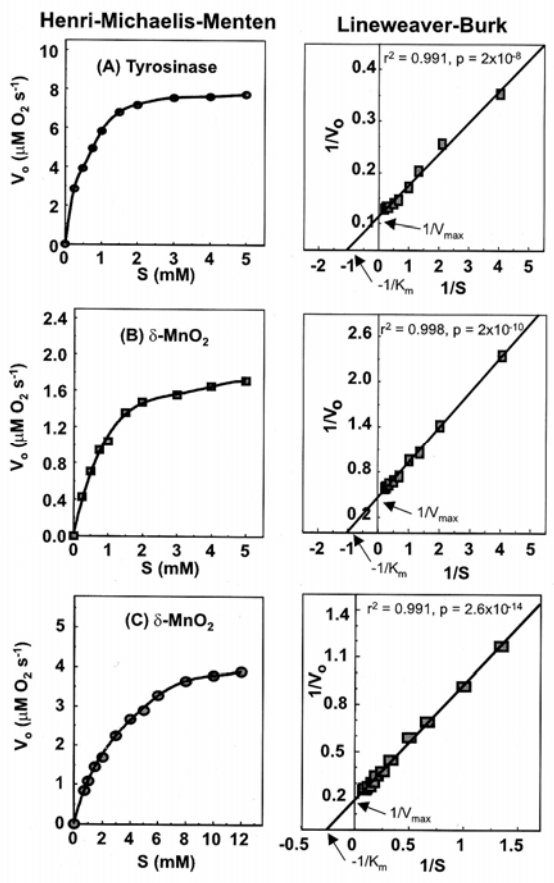

Figure 2.22 Initial velocity of oxygen consumption as a function of the substrate (catechol) concentration in the presence of 0.074 mg (7.11 x 10^{-9} M) tyrosinase (A), 2.0 mg (2.8 x 10^{-4} M with a corresponding concentration of the mineral active sites, $[M_0^+]$1.71 x 10^{-6}) of δ-MnO_2 (B) and 10.0 mg (1.40 x 10^{-3} M with a corresponding concentration of the mineral active sites, $[M_0^+]$8.54 x 10^{-6}) of δ-MnO_2 (C) (Naidja and Huang 2002).

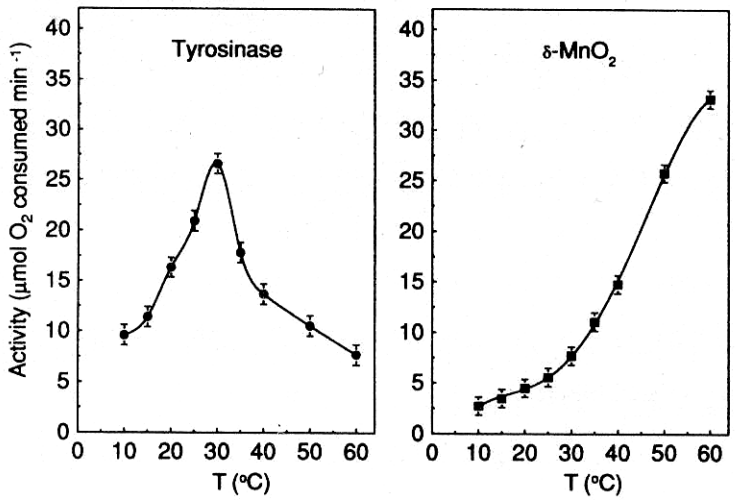

Figure 2.23 Effect of temperature on the activity of tyrosinase (0.148 mg) and δ-MnO_2 (2.0 mg) at an initial pH of 6.0 (Naidja et al. 1999).

2.7.2 Comparison of the Products of Biotic and Abiotic Catalyses of Synthetic Humification Reactions

Shindo and Huang (1992) compared the catalytic effects of Mn(IV) oxide and tyrosinase on the oxidative polymerization of diphenols (hydroquinone, catechol, and resorcinol) in the pH range of 4-8. Mn oxide influences the darkening of hydroquinone and resorcinol to a larger extent than does tyrosinase, while the reverse is true for catechol. The yields of humic acids are also significantly influenced by the kind of catalyst and diphenol used. Their findings indicated that the relative catalytic effects of Mn(IV) oxides and tyrosinase in promoting the formation of diphenol-derived humic substances would vary with the type of diphenols in natural systems. Naidja et al. (1998) studied the difference in the reaction products from the transformation of catechol catalyzed by birnessite or tyrosinase. They found that the polymers formed in the tyrosinase-catechol system have a higher degree of aromatic ring condensation than in the birnessite-catechol system. In addition, they found that the products derived from birnessite catalysis contain a greater fraction of lower molecular weight fragments and aliphatic components than that of tyrosinase catalysis. Dec et al. (2001) investigated oxidative coupling, decarboxylation and demethylation of a number of natural phenolic compounds by the phenoloxidase enzymes, peroxidase, laccase and tyrosinase, and mineral catalyst, birnessite. They observed that birnessite is able to catalyze the ring cleavage of catechol and the

decarboxylation of *p*-hydroxybenzoic acid, vanillic acid, *p*-coumaric acid and ferulic acid to a much greater extent than the enzymes.

2.7.3 The Effect of Environmental Particles on Activity of Biotic Catalysts

A number of environmental particles have been shown to alter the activity of phenoloxidase and other extracellular enzymes associated with the decomposition of organic residues. Mineral colloids not only influence the activity, but also the long-term stability of extracellular enzymes in soils (Naidja et al. 2002) and aquatic environments (Tietjen and Wetzel 2003).

Ruggiero et al. (1989) investigated the ability of a natural silt loam soil and the clay minerals, montmorillonite (Mte) and kaolinite (Kte), to immobilize laccase. They compared the catalytic abilities of the soil-enzyme and clay-enzyme complexes to degrade 2,4-dichlorophenol. They found that the immobilized laccase remains active in removing the substrate even after 15 repeated cycles of substrate addition (Figure 2.24). However, Claus and Filip (1988) found that the activity of tyrosinase, laccase and peroxidase is inhibited by immobilization on bentonite. The type of saturating cations on clay surfaces also substantially influences enzymatic activity (Claus and Filip 1990).

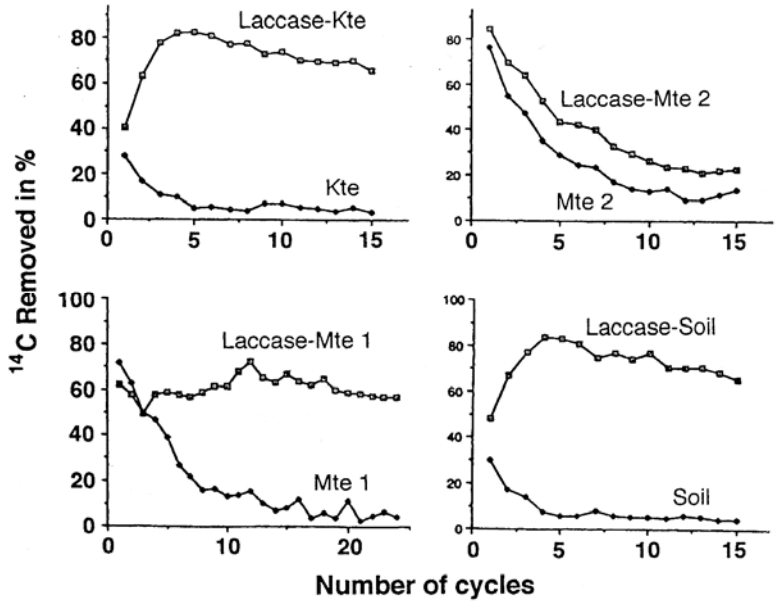

Figure 2.24 Removal of ^{14}C-2,4-dichlorophenol by laccase immobilized on clays and soil (Ruggiero et al. 1989).

Gianfreda and Bollag (1994) investigated the behaviour of laccase and peroxidase in the presence of a montmorillonite, a kaolinite and a silt loam soil. They observed considerable variation in the retained activities of the two enzymes immobilized on the different supports as well as variation in the amount of each enzyme sorbed (Table 2.10). Interestingly enough, laccase immobilized on montmorillonite showed a higher specific activity (118%) than that of the free enzyme. This may be attributed to the steric modification of the immobilized enzyme or possibly due to the catalytic ability of montmorillonite itself. Their studies showed that the performance of these enzymes is significantly affected by soil mineral colloids.

Table 2.10 Immobilization of laccase and horseradish peroxidase on different supports (Gianfreda and Bollag 1994).

Enzyme and support	Enzymatic activity		
	Units adsorbed*	Specific activity†	Residual specific activity‡ (%)
Laccase			
Glass beads	28.8	63.7	236.0
Montmorillonite	19.8	31.8	118.0
Kaolinite	13.1	23.1	85.5
Soil	15.7	24.4	90.4
Peroxidase			
Glass beads	8.4	91.6	93.8
Montmorillonite	23.0	102.8	105.2
Kaolinite	9.5	78.9	80.7
Soil	15.0	92.6	94.8

*Expressed as umol O_2 consumed min^{-1} for laccase and umol guaiacol transformed min^{-1} for peroxidase.
†Units adsorbed/protein adsorbed.
‡Calculated as percentage of the specific activity of the free enzyme (laccase = 27 $umol.min^{-1}$; peroxidase = 97.7 $umol.min^{-1}$).

Naidja et al. (1997) showed that tyrosinase immobilized on montmorillonite coated with Al hydroxide polymers retains a higher specific activity than the free enzyme after 30 days at 25° C. Naidja et al. (2002) investigated the immobilization of tyrosinase by birnessite. Birnessite was found to have a high affinity for adsorbing tyrosinase and significantly altered its molecular conformation. Ahn et al. (2006) investigated the effect of the presence of birnessite on the catechol oxidative coupling activity of laccase. Birnessite was shown to have an inhibitory effect on catechol oxidation by laccase (Figure 2.25), which was attributed to the formation of humic polymers by catalysis of birnessite and the Mn^{2+} ions released from the mineral.

Humic acids have been shown to slightly inhibit tyrosinase activity by complexing the enzyme (Ruggiero and Radogna 1988). Allison (2006b) also demonstrated that the addition of humic acid to a soil significantly decreased the polyphenoloxidase activity of the soil.

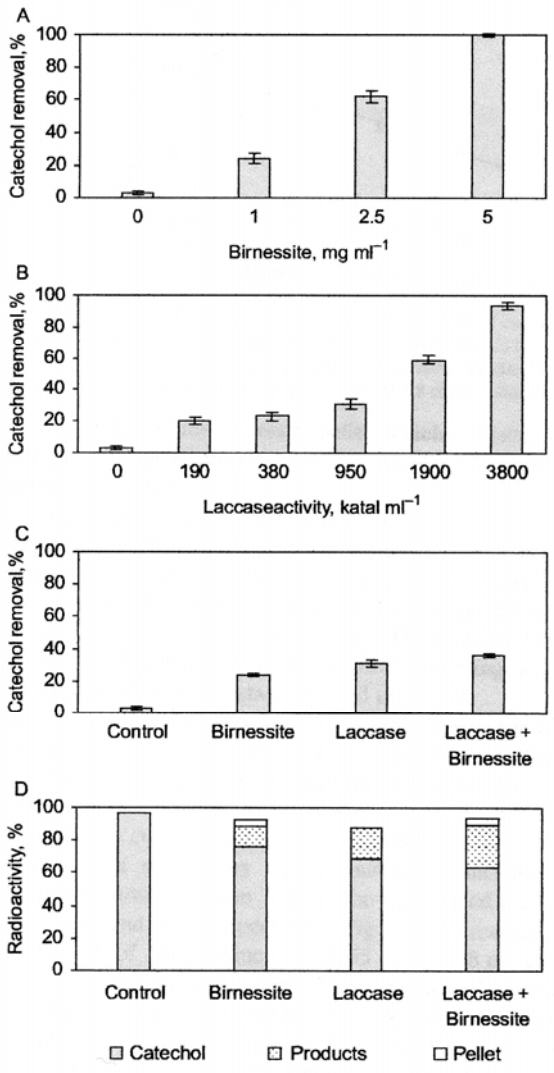

Figure 2.25 Transformation of catechol (0.1 M) in binary and ternary systems: (A) Catechol removal by increasing concentrations of birnessite; (B) Catechol removal by increasing activities of *Trametes villosa* laccase; (C) Catechol removal by *T. villosa* laccase (950 katal ml^{-1}) and birnessite (1 mg ml^{-1}) applied together; (D) Distribution of radioactivity after the incubation of ^{14}C labeled catechol with *T. villosa* laccase (950 katal ml^{-1}) and birnessite (1 mg ml^{-1}). The reactions were carried out in 0.5% NaCl for 24 h at 25° C (Ahn et al. 2006).

2.7.4 The Significance of Biotic and Abiotic Catalysts in Synthetic Humification Reactions in Natural Environments

In the past the mineral matrix was considered as inert, only providing stabilization support for enzymes and humic substances; however, due to the overwhelming amount of evidence at the molecular level, there is no doubt that minerals participate in abiotic catalysis of humification reactions in soils. Naidja et al. (2000) referred to mineral particles as the *Hidden Half* of enzyme-clay complexes, which not only prolong the activity of immobilized enzymes but are also readily able to participate in electron transfer reactions. Many environmental factors can negatively affect the activity of biotic catalysts, such as temperature (Naidja et al. 1999), presence of humic substances (Allison 2006b), or presence of certain mineral particles (Claus and Filip 1988, 1990; Ahn et al. 2006). The problem with abiotic catalysts is degeneration of the catalyst which might be slow depending on the redox conditions in the environment as well as the nature of the mineral catalyst (McBride 1987). However, minerals are highly abundant in soils and sediments, and typically make up about 45% of the total soil volume in a loam soil, whereas, organic matter contributes to about 5% (Sparks 2003). Microorganisms which are the major source of extracellular enzymes in soils make up about 1-4% of the total organic matter in a soil (Stevenson 1994). Therefore, besides enzymes, mineral particles should play a significant role in the humification process in the environment, especially under warmer conditions.

Another important consideration is the relative size of enzymes versus that of micropores (less than 2 nm) in environmental particles which are especially abundant in non-crystalline mineral phases. Simple biomolecules (e.g., glucose, MW = 180 Da) can readily enter into micropores and can become stabilized by reacting with the mineral surface, whereas large macromolecules such as enzymes (e.g. laccase, MW = 60 000 Da and diameter = 5 nm (Andersen et al. 1996) cannot enter and react with the trapped biomolecules.

2.8 Conclusions and Future Research Prospects

Environmental organic matter is a composite of humic and non-humic substances, which is formed through operation and interactions of various biotic and abiotic processes. Humic substances are formed through both selected preservation (residue) and catalytic synthesis mechanisms. Both enzymatic and mineral catalyses contribute to the formation of humic substances in the environment. The relative importance of these catalytic reactions would depend

on vegetation, microbial population and activity, enzymatic activity, mineralogical composition and surface chemistry of environmental particles, management practices, and environmental conditions. Selective preservation pathways would play a more important role in humification processes in poorly drained soils and lake sediments, compared with more aerated environmental conditions.

The existing research data indicate that humic substances have both macromolecular as well as supramolecular characteristics. The origin of environmental macromolecules (polymers) may include biomolecules from the selective preservation pathway and humification products from catalytic synthesis mechanisms. A supramolecule is a system of two or more molecular entities held together and organized by means of intermolecular (noncovalent) binding interactions. Macromolecules as well as small molecules may form supramolecular structures, the properties of which largely determine the reactivity of the material. Humic polymers may encapsulate or anchor unstable biological constituents by hydrophobic and hydrogen bonding forces and/or chemical binding. Any biomolecules intimately associated with humic polymers may, thus, not be separated effectively by chemical and physical methods and are by operational definition humic components. Therefore, many relatively unstable biological constituents may survive in environmental humus for a significant length of time in the humification process. Furthermore chemical protection of organic materials by mineral colloids, especially short-range ordered Al and Fe (oxy)hydroxides, and physical protection of plant-like materials within aggregates deserve close attention in understanding the degradation of biological residues, the formation of humic substances, and global C cycling and climate change.

Our knowledge on the intrinsic mechanisms of environmental processes pertaining to the genesis of humic substances in nature remains to be advanced. Previous studies on abiotic and biotic catalyses have focused on polyphenols, amino acids and sugars, while no work has been done on lipids, one of the most refractory components of plant materials and a significant contributor to the humin fraction of soil organic matter. The interactions of lipids, proteins and polyphenols in the presence of these catalysts remains to be studied. Our understanding of the influence of pedogenic factors and anthropogenic activities on the transformation of biological constituents to humic substances and the nature and properties of the resultant mineral-humus complexes are still very limited. A vast majority of environmental organic matter is associated with mineral particles. More research should be conducted to uncover the impact of physical-

chemical-biological interfacial reactions on biogeochemical reactions, which, in turn, govern the humification processes and the formation of mineral-humus complexes. Also additional research about the type of organisms responding to the transformation of humic substances as well as their role is needed.

Use of advanced analytical instrumentation, i.e., synchrotron-based X-ray absorption spectroscopy, spectromicroscopy and infrared spectroscopy (Myneni 2002; Lehmann et al. 2007; Wan et al. 2007), atomic force microscopy (Maurice 1998), multi-dimensional nuclear magnetic resonance spectroscopy (Simpson et al. 2001; Simpson 2002), and the like should shed light on the mystery of environmental humic substances and their complexes with mineral particles. Fundamental understanding of this subject matter at the molecular level and the impacts on the ecosystem would facilitate our development of innovative management strategies to regulate the behaviour of the ecosystem on a global scale. Future research on this extremely important and exciting area of science should be stimulated to restore as well as sustain ecosystem integrity.

3 EXPERIMENTS, RESULTS AND DISCUSSION

3.1 Research Unit 1: *The effect of catechol interaction with the Maillard reaction on abiotic humification as catalyzed by birnessite*

3.1.1 Introduction

In the environment, humification is pivotal in transforming biomolecules originating from organized structures typical of organisms to randomly polymerized, heterogeneous humic substances characteristic of biogeochemical systems. Humic substances are formed through selective preservation processes and biotic (enzymatic) and abiotic (mineral) catalytic mechanisms (Stevenson 1994; Bollag et al. 1998; Huang 2004; Clapp et al. 2005). The dark colour of humic substances can be attributed to oxidative browning reactions between biomolecules such as sugars, polyphenols, lipids, amino acids and proteins (Rouet-Mayer et al. 1990; Hidalgo and Zamora 2000; Zamora and Hidalgo 2005; Bittner 2006). These browning reactions mostly involve carbonyl-amine reactions and result in the generation of highly coloured, high and low molecular weight polymers (Hidalgo and Zamora 2000). Abundant research evidence at the molecular level shows that enzymes and mineral colloids can enhance the polymerization and/or polycondensation of biomolecules such as amino acids, sugars, and polyphenols, derived from the breakdown of biological residues and from biological metabolites (Stevenson 1994; Bollag et al. 1998; Huang 2000, 2004).

The abiotic catalysis of the polyphenol pathway of humification (polymerization reactions of polyphenolics and polycondensation reactions between polyphenolics and amino acids) has been studied using a host of soil mineral colloids (Wang et al. 1986; Bollag et al. 1998; Wang and Huang 2003; Huang 2004). The Maillard reaction (condensation reactions between sugars and amino acids) is also regarded as an important pathway in natural humification processes (Maillard 1913; Ikan et al. 1996; Arafaioli et al. 1999; Jokic et al. 2001a, 2001b; Bosetto et al. 2002; Gonzalez and Laird 2004). However, in nature it is likely that the polyphenol and Maillard reaction pathways interact with each other since sugars, amino acids and polyphenols all coexist in soil solutions and aquatic environments. The integrated polyphenol-Maillard humification pathway was first studied by Jokic et al. (2004b) using birnessite (δ-MnO_2) as catalyst and using equimolar concentrations of glucose, glycine and catechol. They reported that birnessite significantly accelerated humification processes at temperatures and a pH typical of natural

environments. They found that the isolated humic materials had complex spectral and physical characteristics similar to naturally occurring soil humic materials.

The relative abundance of biomolecules varies with vegetation, microbial community and the environment (Stevenson 1994; Kögel-Knabner 2002). Sugars and amino acids are among the most abundant biomolecules of terrestrial and aquatic environments (Anderson et al. 1989). The concentration of phenolics in soil solutions is typically low, however, they are the most reactive forms of carbon in soils (Fox 1995). Simple phenols would not persist in soils for long due to their rapid transformation and thus would not be detected in great concentrations. The concentration of water-extractable catechol from forest soils has been reported at between 2-8 mg kg^{-1} dry weight, while the concentration of phenolic acids such as benzoic acid is found at higher concentrations ranging from 2-188 mg kg^{-1} dry weight (Muscolo and Sidari 2006). As polyphenols, amino acids and sugars differ significantly in their chemical reactivity it is expected that the relative amount of these biomolecules will strongly affect humification processes and products. Therefore, the objective of the present experiment was to examine the effect of the molar ratio of catechol to Maillard reagents on the humification process in the integrated catechol-Maillard system as catalyzed by birnessite. The degree of humification and the nature of the humic products formed in the integrated catechol-Maillard system (glucose, glycine and catechol), with an increasing concentration of catechol to a fixed concentration of Maillard reagents, was compared with the Maillard reaction (glucose and glycine) and catechol only systems. Our ultimate goal was to elucidate the role of polyphenols, such as catechol, in influencing the abiotic mineral-catalyzed polyphenol-Maillard humification pathway.

3.1.2 Materials and Methods

3.1.2.1 Materials

Birnessite has been found to be one of the most powerful catalysts of abiotic humification reactions (Huang 2000) and was thus selected as the mineral catalyst in this study. Birnessite (δ-MnO_2) was synthesized according to one of the methods described by McKenzie (1971), which involves slowly adding concentrated HCl to boiling $KMnO_4$. The precipitate was washed by means of repeated filtration using distilled deionized water (henceforth referred to as water) on a 0.1 μm pore Millipore membrane filter, until the wash water was tested free from chloride ($AgNO_3$ test). It was then freeze-dried, and finally lightly ground using a mortar and pestle. The

synthesized birnessite was characterized by means of X-ray diffraction (XRD) (Rigaku Rotaflex 200SU, Tokyo, Japan), Fourier transform infrared (FTIR) spectroscopy (Bruker Equinox 55, Ettlingen, Germany), Mn L-edge near edge X-ray absorption fine structure (NEXAFS) spectroscopy on SGM (Spherical Grating Monochromator) beamline at the Canadian Light Source (Saskatoon, SK, Canada) and BET specific surface area analysis (Quantachrome Autosorb-1, Syosset, NY, USA) using N_2 gas. Catechol, D-glucose (Sigma-Aldrich ACS reagent grade >99%) and glycine (Sigma Ultra pure grade >99%) were obtained from Sigma Aldrich Canada Ltd (Oakville, ON, Canada). Pure manganese carbonate and oxides, $MnCO_3$ (99.99%) and MnO_2 (>99%), were obtained from Sigma Aldrich (Oakville, ON, Canada), and MnO (>99%) and Mn_2O_3 (>98%), were obtained from Alfa Aesar, Johnson Matthey Catalog Company, Inc. (Ward Hill, MA, USA), to use as reference compounds in the Mn L-edge NEXAFS studies. Elliot soil (1S102H) and Suwannee River (1S101H) humic acid standards were purchased from the International Humic Substances Society (IHSS), St. Paul, MN, USA, and used in the C K-edge NEXAFS study.

3.1.2.2 Incubation experiment.

Sterile conditions were maintained throughout the experiment in order to establish the role of abiotic processes. All glassware, birnessite, water and apparatus were autoclaved prior to the experiments. In addition to this, thimerasol, an antiseptic agent, was added to each flask (0.02 %, w/v) before any of the reagents were added. Thimerasol does not affect the oxidation process of phenolic compounds (Wang et al. 1983a). In order to investigate the effect of the molar ratio of catechol to Maillard reagents, a number of treatments were employed with increasing amounts (0, 0.00125, 0.0025, 0.0125, 0.0250, 0.0500, 0.1000 moles) of catechol added to a fixed molar ratio of Maillard reagents (0.05 mole glucose + 0.05 mole glycine) using birnessite as catalyst. There was also a set of treatments containing only catechol in increasing amounts (0, 0.00125, 0.0025, 0.0125, 0.0250, 0.0500, 0.1000 moles) and birnessite. Two and a half grams of birnessite were suspended in each of the reaction solutions in a 250 mL flask. There were selected control treatments in which birnessite was absent, i.e., the catechol only system (0.05 mole catechol), the Maillard reaction system (0.05 mole glucose + 0.05 mole glycine), and the integrated equimolar catechol-Maillard system (0.05 mole glucose + 0.05 mole glycine + 0.05 mole catechol). All the reaction systems were adjusted to an environmentally relevant pH 7.0 using 0.1 M HCl or 0.1 M

NaOH. The final volume of the flasks was made up to 100 mL using autoclaved water. The flasks were then tightly sealed and placed in a constant temperature water bath at 45° C for a period of 15 days while gently shaking. Forty-five degrees centrigrade is an environmentally relevant temperature as it is common in tropical and subtropical areas, and has also been reported in temperate areas as the approximate temperature of an exposed sunlit soil surface on a day when the ambient air temperature is 25° C (Jury et al. 1991). All treatments were performed in triplicate. The absence of microbial growth was verified by culturing aliquots of selected samples at the end of the incubation period. Aerobic microbial growth was tested for by culturing on Tryptocase Soy Agar (TSA) plates, while anaerobic microbial growth was tested for on TSA plates in a BBL GasPak 150 Large Anaerobic System. All cultures were incubated for a period of 5 and 9 days at 28° C (Jokic et al. 2004b).

3.1.2.3 Characterization of reaction systems at the end of the incubation period and isolation of humic acids.

At the end of the reaction period, the final pH and Eh of the suspensions were measured. The samples were then centrifuged at 25,000 g for 40 min to separate the solid residue from the solution. The absorbance of the supernatant was measured between 400 and 600 nm on a UV-visible spectrophotometer (Beckman DU 650 microprocessor controlled spectrophotometer, Fullerton, CA, USA). The visible absorbance at 400 and 600 nm provides an indication of the extent of polymerization which has taken place in the reaction systems (Shindo and Huang 1982, 1984a, 1984b). Shindo and Huang (1984a) studied the polymerization of polyphenols by short-range ordered Mn, Fe, Al and Si oxides, and showed that the yield of humic polymers was directly related to the visible absorbance. Likewise, with natural humic substances, Gan et al. (2007) showed that visible absorbance can be used to determine the concentration of fulvic acid in solution. The supernatant was diluted with water prior to absorbance determination and the values obtained were subsequently multiplied by the dilution factor. The Mn content of the supernatant was determined using atomic absorption spectroscopy at 279.5 nm (Varian Spectra AA 220, Walnut Creek, CA, USA). The solid residue was repeatedly washed with water using centrifugation at 25,000 g for 40 min until the wash water was clear. These water extracts were collected and added to the supernatant. The washed residue was then freeze-dried. The combined water extracts and supernatant was then acidified to pH 1.0 using 6 M HCl and allowed to stand

for 24 h to precipitate the humic acid (HA) fraction out of the solution (Swift 1996). The acidified suspensions were then centrifuged at 25,000 g for 45 min to separate the HA fraction from the rest of the solution containing the fulvic acid (FA) fraction and non-humic substance fraction. The HA residue was then resuspended in a 0.1 M HCl and 0.3 M HF solution and shaken for 48 h. The suspension was then centrifuged again as described before and the sedimented HA was dialyzed in 1000 molecular weight cut off dialysis tubing for 5 days in distilled deionized water until the water tested free from chloride ($AgNO_3$ test). The purified HA was then freeze-dried. Selected HA samples which were used in the NEXAFS study were not purified using the HCl/HF treatment but were instead dialyzed immediately after being separated by acidification and centrifugation; it was not necessary to remove all the Mn, as its presence does not interfere with XAS studies. Furthermore, the HA samples without the HCl/HF treatment were used in the Mn L-edge NEXAFS studies to investigate the nature of Mn bonding in the samples.

3.1.2.4 Characterization of reaction products

Near edge X-ray absorption fine structure (NEXAFS) spectroscopy. The speciation of C, N and Mn was investigated in selected solid residue and supernatant HA fractions using C and N K-edge and Mn L-edge NEXAFS on the SGM (Spherical grating monochromator) beamline (Regier et al. 2007) at the Canadian Light Source (Saskatoon, SK, Canada). A number of pure reference compounds (glucose, glycine, pyrogallol, $MnCO_3$, MnO, Mn_2O_3, MnO_2) and IHSS soil and river HA standards, were also examined. Samples which were investigated for Mn were lightly ground and mounted on carbon tape. Samples which were investigated for C and N were mounted on gold (Au)-coated (~400 Å) silicon (Si) wafers by making dilute suspensions of the samples in distilled deionized water and then placing a drop of the suspension on the wafer and allowing it to dry. An exit slit width of 20 μm and a dwell time of 0.1s were used to minimize damage due to exposure to radiation. These spectra were recorded by total electron yield (TEY) at an energy step size of 0.1 eV. The Mn and N spectra were normalized to the TEY of a gold I_0 mesh which was placed in front of the sample in the path of the beam. The C spectra were normalized to a clean Au-coated Si wafer, so that the signals from C in the beamline and C contamination on the gold I_0 mesh would not interfere with the signal from our samples (Watts et al. 2006). Spectra obtained were analyzed using aXis2000 software (Hitchcock et al. 2005). The

energy scale of the C and Mn spectra were internally calibrated using glycine and MnO, respectively, based on calibrated values reported from previous studies (Garvie and Craven 1994; Boese et al. 1997). All the spectra were normalized to each other, with the maximum intensity of each spectrum fixed at 1.

Fourier transform infrared (FTIR) spectroscopy. FTIR spectra were obtained from the washed and freeze-dried solid residues and purified HA fractions. This was done by preparing KBr disks containing 1% w/w sample and running it on a Bruker Equinox 55 FTIR (Ettlingen, Germany) connected with a purge gas generator.

Total carbon analysis. Total carbon analysis of the solid residues was performed using a dry combustion method on a Leco CR-12 Carbon Analyzer (Leco Corporation, St. Joseph, MI, U.S.A.) as described by Wang and Anderson (1998).

Pyrolysis field ionization mass spectrometry (Py-FIMS). Pyrolysis soft ionization combined with in-source mass spectrometry (Py-FIMS) was used to analyze the solid residues of the Maillard reaction system, the equimolar catechol-Maillard system and the catechol only system, as described by Schulten (2002).

Pyrolysis-gas chromatography/mass spectrometry (Py-GC/MS). The solid residue from the equimolar catechol-Maillard system was analyzed using the Py-GC/MS technique as described by Schulten (2002).

3.1.3 Results and Discussion

In all the reaction systems studied, no aerobic or anaerobic microbial growth was observed. Thus, all the processes studied were abiotic in nature. The X-ray diffractogram of the synthesized birnessite had characteristic d-values of 7.21, 3.61 and 2.45 Å as reported by McKenzie (1989). The FTIR spectrum of the synthesized birnessite showed typical birnessite absorption bands at 3400, 1621, 509 and 466 cm^{-1} (Potter and Rossman 1979). The Mn L-edge NEXAFS spectrum showed that the synthesized birnessite contained predominantly Mn(IV) with some Mn(III), which was also previously reported using Mn K-edge X-ray absorption spectroscopy (Jokic et al. 2001b). The BET specific surface area of the synthesized birnessite was 63 m^2 g^{-1}, which is characteristic for synthetic birnessite (McKenzie 1971).

3.1.3.1 The effect of the presence of birnessite on the reaction systems

The presence of birnessite significantly enhanced humification in the Maillard reaction, catechol only and integrated catechol-Maillard reaction systems, as the absorbances (degree of browning/polymerization) were much greater in the presence than in the absence of birnessite (Figure 3.1.1). The most dramatic enhancement of browning by birnessite was observed in the integrated catechol-Maillard system (Fig. 3.1.1c). The pH and pH + pE (redox status) values obtained from selected systems reacted in the presence or absence of birnessite are shown in Table 3.1.1. The pH + pE value is a function of the dissolved oxygen concentration in solution, and is thus an indication of the redox status of a system (Lindsay 1979). The systems reacted in the presence of birnessite had higher final pH values than the control systems (Table 3.1.1). The reduction of birnessite by reaction with the biomolecules results in the consumption of protons (Eq. 3.1.1), therefore the birnessite-containing systems had higher pH values.

$$MnO_2 + 4H^+ + 2e^- \rightarrow Mn^{2+} + 2H_2O \qquad (3.1.1)$$

The final pH + pE value (redox status) of the birnessite systems was much lower than that of the control systems, indicating that more dissolved oxygen was consumed in the birnessite systems and thus more oxidative polymerization took place. This is in accord with the enhanced degree of browning observed in the birnessite-containing systems (Fig. 3.1.1).

Table 3.1.1 Effect of birnessite on the final pH and redox status (pH + pE) of the Maillard reaction, catechol only and equimolar catechol-Maillard systems.

Treatment	pH	pH + pE
Birnessite present		
Maillard (0.05 mol glucose + 0.05 mol glycine)	8.08 ± 0.06	7.37 ± 0.31
Catechol (0.05 mol catechol)	7.27 ± 0.04	8.59 ± 0.12
Catechol-Maillard (0.05 mol glucose + 0.05 mol glycine + 0.05 mol catechol)	6.85 ± 0.01	6.74 ± 0.19
Birnessite absent		
Maillard (0.05 mol glucose + 0.05 mol glycine)	6.26 ± 0.07	10.93 ± 0.44
Catechol (0.05 mol catechol)	4.17 ± 0.29	10.45 ± 0.72
Catechol-Maillard (0.05 mol glucose + 0.05 mol glycine + 0.05 mol catechol)	5.49 ± 0.07	8.78 ± 0.52

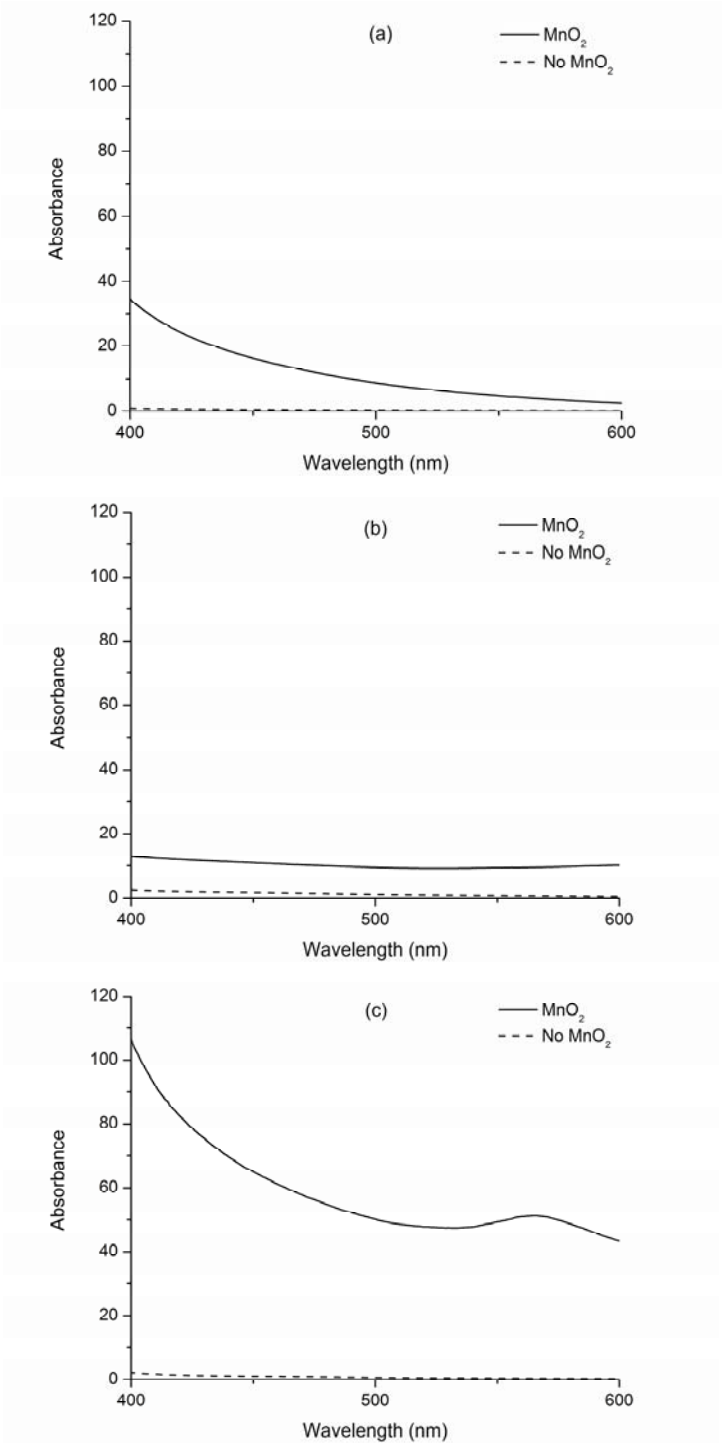

Figure 3.1.1 Comparison of the effect of birnessite on the absorbances of the supernatants of (a) the Maillard system (0.05 mole glucose + 0.05 mole glycine), (b) the 0.05 mole catechol system and (c) the equimolar integrated catechol-Maillard system (0.05 mole glucose + 0.05 mole glycine + 0.05 mole catechol). The absorbances are scaled by the dilution factor.

3.1.3.2 Influence of the molar ratio of catechol to Maillard reagents on reactions systems incubated in the presence of birnessite

The visible absorbance (at 400 and 600 nm) of the supernatants of the Maillard, catechol only and integrated catechol-Maillard reaction systems with increasing amount of catechol added are shown in Fig. 3.1.2. The visible absorbance units are arbitrary absorbance units, as they are the absorbance obtained from the diluted samples multiplied by the dilution factor. As the amount of catechol was increased above 0.0025 mole in the integrated catechol-Maillard system, the increase in absorbance was substantially higher than the sum of the absorbance of the Maillard only and catechol only systems, indicating the interactions of catechol with glucose and glycine (Fig. 3.1.2). The absorbance results indicate that the integrated catechol-Maillard pathway is not merely an additive pathway but a synergistic reaction between catechol and glucose and glycine. The results also show that a relatively small amount of catechol to Maillard reagents (molar ratio of 1:20) results in a substantial increase in the extent of humification.

The pH and redox status (pH + pE) of the birnessite-catalyzed integrated catechol-Maillard reaction and catechol only systems with increasing amount of catechol added are shown in Fig. 3.1.3. The pH of the reaction systems is controlled by two processes, namely the proton-consuming reduction of birnessite, and the proton-generating oxidative polymerization reactions. The integrated catechol-Maillard reaction system had substantially lower pH (Fig. 3.1.3a) and pH + pE (Fig. 3.1.3b) values than the catechol only system. Therefore, compared with the catechol only system, the integrated system generated more protons and consumed more dissolved oxygen, which is in accord with the greater degree of browning (oxidative polymerization) observed in the integrated catechol-Maillard system compared with the catechol only system (Fig. 3.1.2).

There was a substantial drop in the pH of the catechol-Maillard systems when the amount of catechol in the system was higher than 0.0025 mole (Fig. 3.1.3a), indicating that humification was substantially enhanced above this threshold value. This is also reflected in the absorbance results (Fig. 3.1.2); the integrated catechol-Maillard treatments containing more than 0.0025 mole catechol exhibited a significant increase in the degree of browning, and the deviation from the extrapolated curve representing the sum of the absorbances of the Maillard reaction only and the catechol only systems increased with increasing amount of catechol in the system.

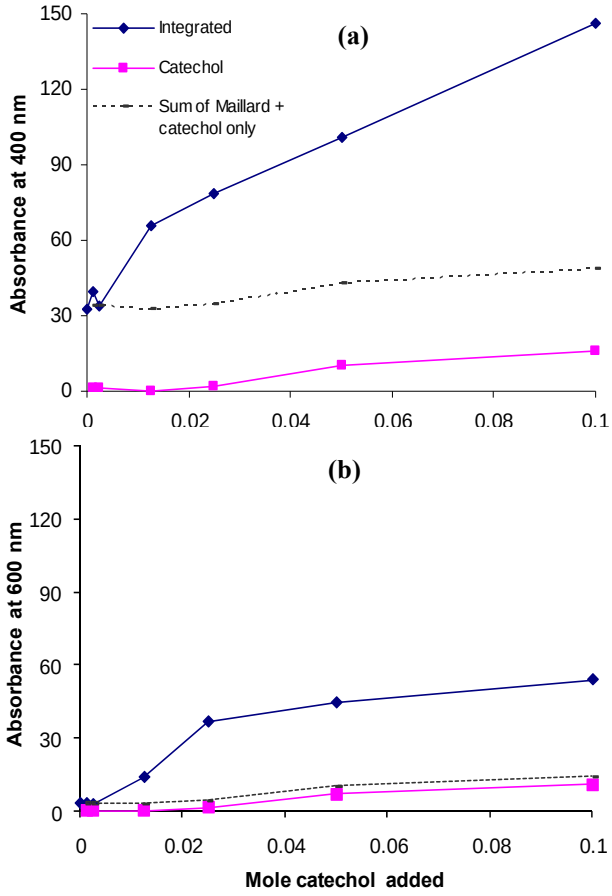

Figure 3.1.2 Comparison of the absorbances of the supernatants of the integrated catechol-Maillard and catechol reaction systems at (a) 400 nm and (b) 600 nm, in the presence of birnessite, with increasing amount of catechol added. The absorbance of the supernatant in the Maillard reaction system (0.05 mole glucose + 0.05 mole glycine) is the first point in the integrated system, i.e., 0 mole of catechol added. The dotted line represents the sum of the absorbances of the Maillard only and catechol only systems. The absorbances are scaled by the dilution factor.

The concentration of Mn in the supernatant of the integrated catechol-Maillard and catechol only systems with increasing amount of catechol added is shown in Figure 3.1.4. As the degree of humification in the catechol-Maillard system increased due to increased catechol present in the reaction system (Fig. 3.1.2), the concentration of Mn in solution decreased (Fig. 3.1.4). This indicates that the Mn in solution was increasingly sorbed to the humic polymers formed with increasing catechol added to the system. The catechol only system showed significant browning after 0.025 mole catechol added (Fig. 3.1.2) and this corresponded with a

marked decrease in the Mn concentration in solution (Fig. 3.1.4). The Mn concentration was substantially lower in the catechol only system than in the integrated catechol-Maillard system (Fig. 3.1.4). This indicates that more Mn(II) was sorbed in the residue of the catechol only system and/or less Mn(II) was released.

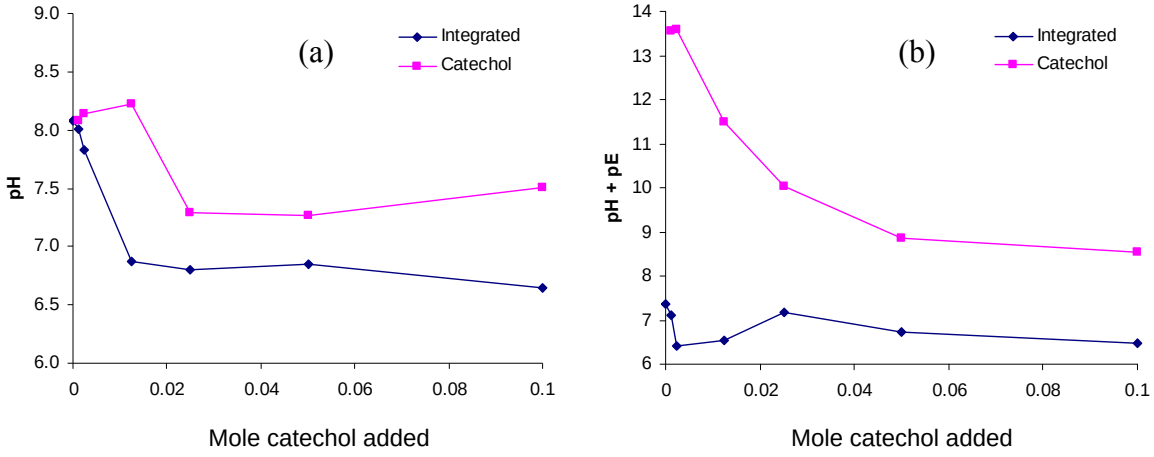

Figure 3.1.3 Comparison of (a) the pH and (b) redox status (pH + pE) of the catechol only and integrated catechol-Maillard systems in the presence of birnessite, with increasing amount of catechol added. The pH and pH + pE values of the Maillard reaction system (0.05 mole glucose + 0.05 mole glycine) are the first points in the integrated system, i.e., 0 mole catechol added.

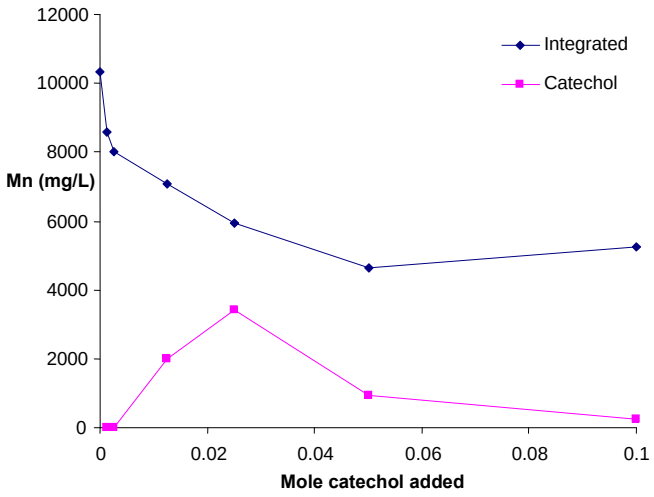

Figure 3.1.4 Comparison of the Mn concentration in the supernatant of the catechol-only and integrated catechol-Maillard systems reacted in the presence of birnessite, with increasing amount of catechol added. The Mn concentration in the supernatant of the Maillard reaction system (0.05 mole glucose + 0.05 mole glycine) is the first point in the integrated system, i.e., 0 mole catechol added.

3.1.3.3 Characterization of reaction products from reaction systems catalyzed by birnessite

3.1.3.3.1 Humic acid isolated from the supernatant of the reaction systems

Near edge X-ray absorption fine structure (NEXAFS) spectroscopy

The C K-edge NEXAFS spectra of IHSS Elliot soil and Suwannee River HA samples and the HA extracted from the supernatant of selected reaction systems catalyzed by birnessite are shown in Fig. 3.1.5. Spectroscopic assignments are based on the absorption maxima of the reference compounds (glucose, glycine and pyrogallol) and on values reported by previous C NEXAFS studies (Myneni 2002; Urquhart and Ade 2002; Dhez et al. 2003; Cooney and Urquhart 2004; Hitchcock and Mancini 2004). The NEXAFS narrower and sharper core (C 1s) $\rightarrow \pi^*$ transitions have been found to be the most useful for chemical analyses and identification of organic compounds due to their chemical sensitivity based on the chemical energy shifts (Urquhart and Ade 2002).

The lowest absorption bands at around 284.0 eV usually correspond to molecules with low energy π^* states, such as quinones (Francis and Hitchcock 1992). Absorption bands near 285 eV are generally ascribed to C 1s (C-H) $\rightarrow 1\pi^*_{C=C}$ transitions (Urquhart and Ade 2002; Cooney and Urquhart 2004), which are characteristic of C=C unsaturation. The transitions of aromatic C bound to carbonyl (e.g., terephthalate species) tend to overlap with unsaturated aromatic C-H transitions due to the strong electronic interactions between the benzene π^* density and carbonyl π^* density, and are generally found in the 284.4-285.0 eV range (Cooney and Urquhart 2004).

The absorption bands near 286-288 eV are characteristic of functionalized aromatic groups C 1s (C-R) $\rightarrow 1\pi^*_{C=C}$ transitions (R = functional group), such as aromatic C bound to aldehyde (286.0 eV), ketone (286.4 eV), urea (286.4 eV), carbamate (286.6-286.8 eV), amine (286.8-286.9 eV), phenol (287.0-287.3 eV) and ester (287.1 eV) groups (Urquhart and Ade 2002; Dhez et al. 2003; Cooney and Urquhart 2004; Hitchcock and Mancini 2004). Heterocyclic N compounds C 1s (C-N) $\rightarrow 1\pi^*_{C=C}$ transitions also occur in the ~286-287 eV range, e.g., pyridine (285.7 eV) and pyrrole (286.3 eV) (Dhez et al. 2003; Hitchcock and Mancini 2004). The C=N and C≡N π^* transitions usually occur around 286.3 eV (Myneni 2002). Generally speaking, a stronger electron withdrawing substituent on the aromatic ring, will result in a higher energy shift of the C 1s (C-R) $\rightarrow 1\pi^*_{C=C}$ transition.

The carbonyl C 1s (C-R) → $1\pi^*_{C=O}$ transitions usually occur between 286-291 eV, and can be used to distinguish between groups such as aldehydes (286.2-286.4 eV), ketones (286.6-286.8 eV), amide (287.8-288.2 eV), acetic/acetate (288.1-288.6 eV), urea (289.2-289.8 eV), carbamate (289.9.0-290.1 eV) and carbonate (290.2-290.6 eV) (Urquhart and Ade 2002). The main cause of the shifts observed in C 1s (C-R) → $1\pi^*_{C=O}$ transitions is the inductive effect of the neighbouring atoms on the carbonyl C 1s binding energy (Urquhart and Ade 2002). Low lying σ* orbitals also provide valuable information in identifying aliphatic functionalities. Saturated aliphatic C exhibits C 1s (C-H) → σ^*_{C-H} transitions in the 287.1-287.9 eV range, while aliphatic alcohol C 1s (C-H) → σ^*_{C-O} transitions are found shifted to a higher energy in the 289.2-289.5 eV range (Dhez et al. 2003).

The spectra of the IHSS Elliot soil and Suwannee River HA samples (Fig 3.1.5a and b) were dominated by aliphatic carboxylic groups (288.6 eV) and also contained aromatic C-H (285.0-285.3 eV) and functionalized aromatic groups (286.4-287.1 eV). Similar to the natural HAs, the HA isolated from the supernatant of the Maillard reaction was dominated by carboxylic type C (288.6 eV), with evidence of aromatic C-H and aromatic C bound to ketone or N (286.4 eV). The relative intensity of the aromatic functionalities (285.0-287.0 eV) increased in the integrated catechol-Maillard (Fig. 3.1.5d and e) systems with increasing amount of catechol added to the system.

The HA from the catechol only system was dominated by aromatic C-H (285.0-285.3 eV) and phenolic functional groups (287.0-287.1 eV) (Fig. 3.1.5f). There was also evidence of aliphatic carboxylic groups (288.6 eV) in the catechol only system, which is attributed to the ring cleavage of catechol by birnessite which results in the formation of aliphatic fragments. These aliphatic fragments can undergo further polymerization and be incorporated into the humic polymers (Wang and Huang 1992; Majecher et al. 2000). The spectra of the natural HAs (Fig. 3.1.5a and b) show the presence of similar functional groups to that of the HA from the Maillard reaction (Fig. 3.1.5c) and equimolar integrated catechol-Maillard system (Fig. 3.1.5d).

FTIR spectroscopy

The FTIR spectra of the purified HA fractions from the supernatants of selected reaction systems catalyzed by birnessite are shown in Figure 3.1.6. Comprehensive assignments of the absorption bands in Figure 3.1.6 are given in Table 3.1.2.

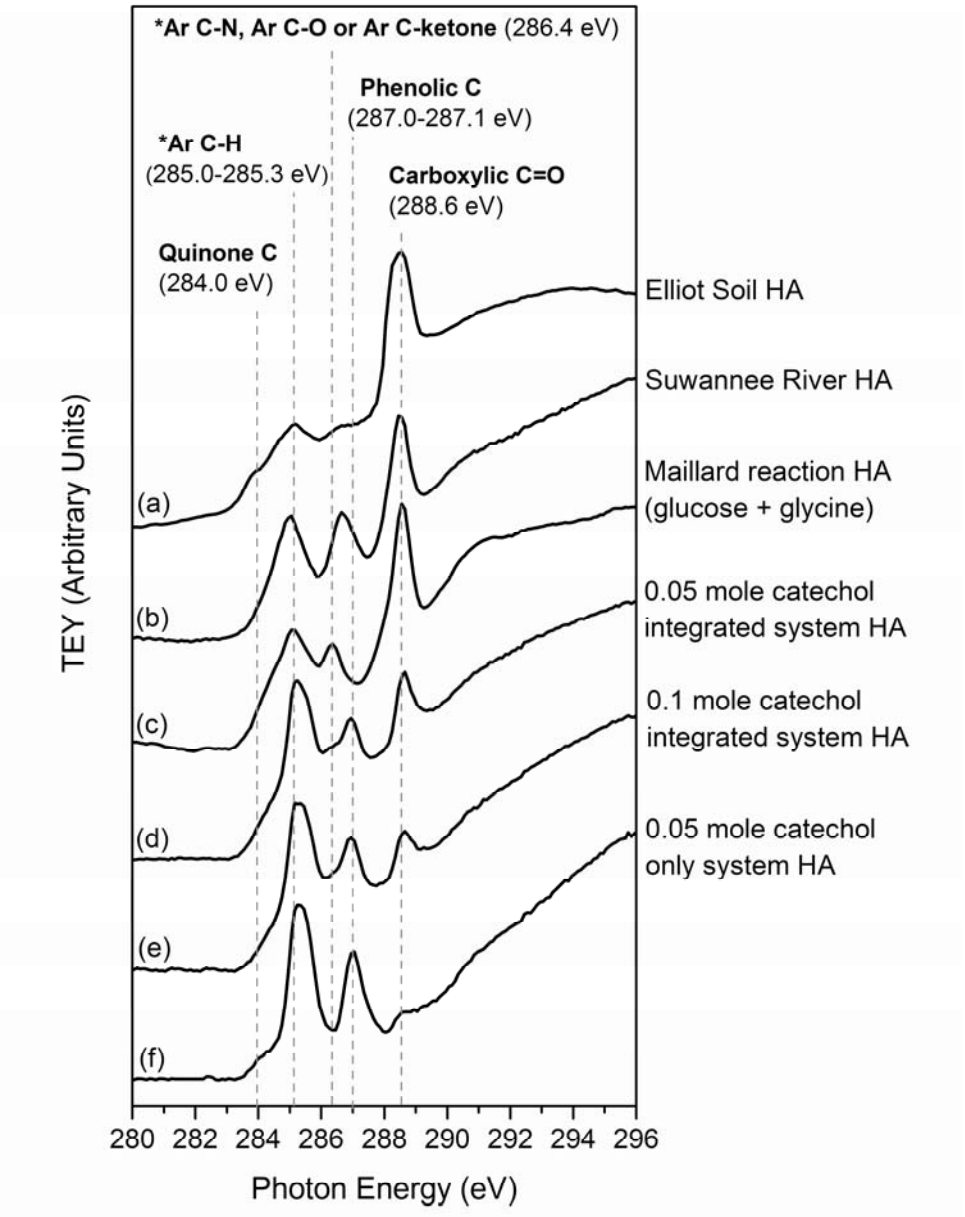

Figure 3.1.5 Carbon K-edge NEXAFS spectra of IHSS (a) Elliot soil HA and (b) Suwannee River HA and the HA isolated from the supernatants of systems reacted in the presence of birnessite: (c) the Maillard reaction (0.05 mole glucose + 0.05 mole glycine); the catechol-Maillard system with: (d) 0.05 mole catechol, and (e) 0.1 mole catechol; and (f) the 0.05 mole catechol only system. *Ar = aromatic.

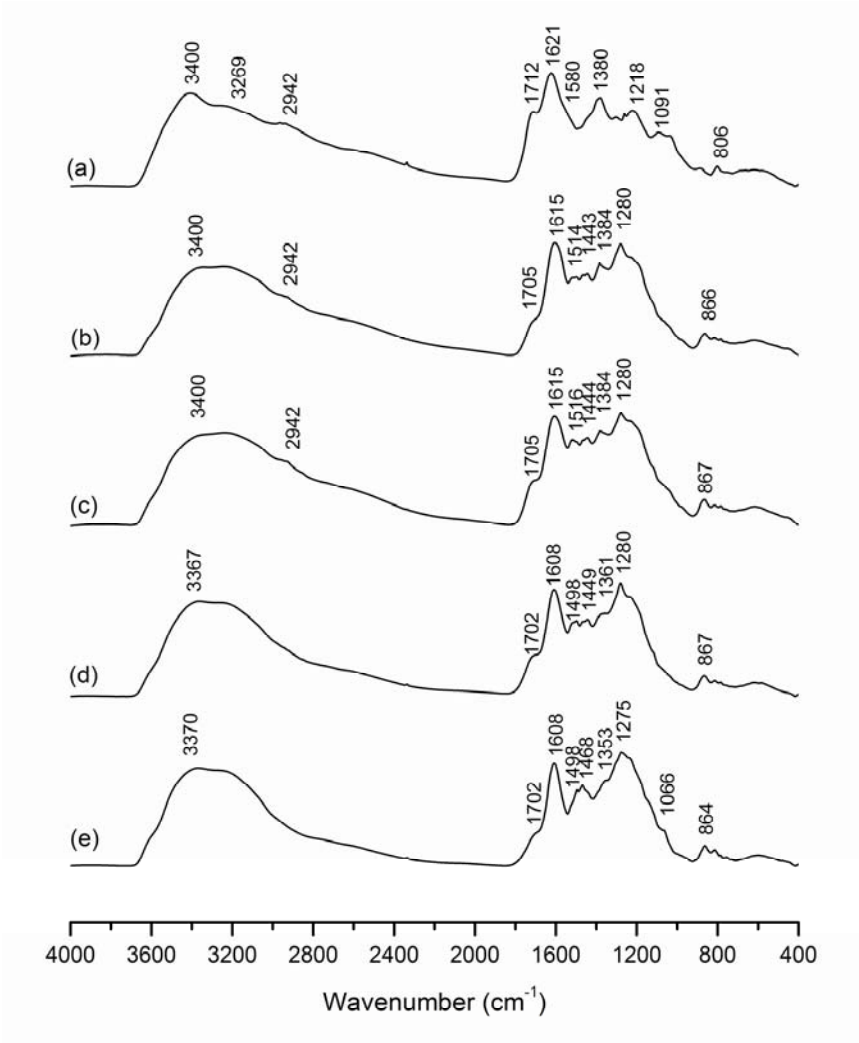

Figure 3.1.6 FTIR spectra of the purified HA fractions from the supernatant of systems catalyzed by birnessite: (a) the Maillard reaction (0.05 mole glucose + 0.05 mole glycine); the integrated catechol-Maillard reaction system with (b) 0.025 mole catechol, (c) 0.05 mole catechol, and (d) 0.1 mole catechol; and (e) 0.05 mole catechol only.

Interpretation of the absorption bands was based on the spectra of the unreacted catechol, glucose and glycine and previous works (van der Merel and Beutelspacher 1976; Stevenson 1994; Aktas et al. 2003; Silverstein et al. 2004). The broad OH stretch absorption band at around 3370-3400 cm^{-1} observed in all the spectra (Fig. 3.1.6) is also attributed to intramolecular H-bonding between polymers (Aktas et al. 2003). The HA isolated from the Maillard system (Fig. 3.1.6a) was dominated by strong absorption bands at 1380 cm^{-1}, which may be attributed to OH and C-O stretch of phenols, C-H deformation of CH_2 and CH_3, or asymmetrical stretch of COO^-, 1621 cm^{-1} which is attributed to aromatic C=C stretches, and 1712 cm^{-1} which is ascribed to the symmetric C=O stretch of COOH. The HAs isolated from the supernatant of the catechol-

Maillard and catechol only systems (Fig. 3.1.6b-e) were dominated by strong absorption bands at 1275-1280 cm^{-1}, which may be attributed to the C-O stretch of phenols or phenyl ethers, and 1608-1615 cm^{-1} which may be ascribed to aromatic C=C ring stretch. The absorption bands at 1066 and 1275 cm^{-1} in HA of the catechol only system (Fig. 3.1.6e) are characteristic of phenyl ethers (Aktas et al. 2003) which indicated that the HA polymers contain phenolic units linked by ether bonds and that they still contain a high amount of phenolic –OH groups. Thus, it can be concluded that the HAs from the catechol-Maillard and catechol only systems were more aromatic in nature than the HA from the Maillard system. These observations are in accord with the C K-edge NEXAFS spectroscopic data (Fig. 3.1.5).

Table 3.1.2 Assignment of the FTIR absorption bands of the purified HA fractions from the supernatants of the Maillard, integrated catechol-Maillard and catechol only systems reacted in the presence of birnessite.

(a) Maillard reaction system		**(b) to (d) Integrated catechol-Maillard systems**		**(e) Catechol only system**	
Wavenumber (cm^{-1})		**Wavenumber (cm^{-1})**		**Wavenumber (cm^{-1})**	
806	Out of plane aromatic =C-H bend	866-867	Aliphatic C-O stretch, out of plane aromatic =C-H bend	864	Aliphatic C-O stretch, out of plane aromatic =C-H bend
1091	Aliphatic C-O stretch	1280	C-O stretch of phenols or phenyl ethers	1066	C-O stretch of phenols or phenyl ethers
1218	C-O stretch of phenols or phenyl ethers	1361-1384	OH deformation and C-O stretch of phenols, C-H deformation of CH_2 & CH_3, asymmetrical stretch of COO^-	1275	C-O stretch of phenols or phenyl ethers
1380	OH deformation and C-O stretch of phenols, C-H deformation of CH_2 & CH_3, asymmetrical stretch of COO^-	1443-1449	Assymetrical bending of CH_2 & CH_3 deformation band, C=C aromatic ring stretch	1353	OH deformation and C-O stretch of phenols, C-H deformation of CH_2 & CH_3, asymmetrical stretch of COO^-
1580	Symmetric C-O stretch of COO^-, N-H deformation + C=N amide II band	1498-1516	Symmetric C-O stretch of COO^-, N-H deformation + C=N amide II band	1468	Assymetrical bending of CH_2 & CH_3 deformation band, C=C aromatic ring stretch
1621	Aromatic C=C ring stretch	1608-1615	Aromatic C=C ring stretch	1498	Symmetric C-O stretch of COO^-
1712	Symmetric C=O stretch of COOH	1702-1705	Symmetric C=O stretch of COOH	1608	Aromatic C=C ring stretch
2942	Aliphatic C-H stretch	2942	Aliphatic C-H stretch	1702	Symmetric C=O stretch of COOH
3269	OH or N-H stretch	3400-3367	OH stretch	3370	OH stretch
3400	OH stretch				

The FTIR spectra of the unreacted biomolecules, glucose, glycine and catechol, are shown in Fig. 3.1.7. Comprehensive assignment and interpretation of the FTIR absorbance bands of glucose, glycine and catechol can be found in previous works (Aktas et al. 2003; Fischer et al. 2005; Ibrahim et al. 2006). The HA fractions isolated from the reaction systems catalyzed by birnessite (Fig. 3.1.6) were distinctly different and more poorly ordered and heterogeneous compared with the unreacted biomolecules (Fig. 3.1.7).

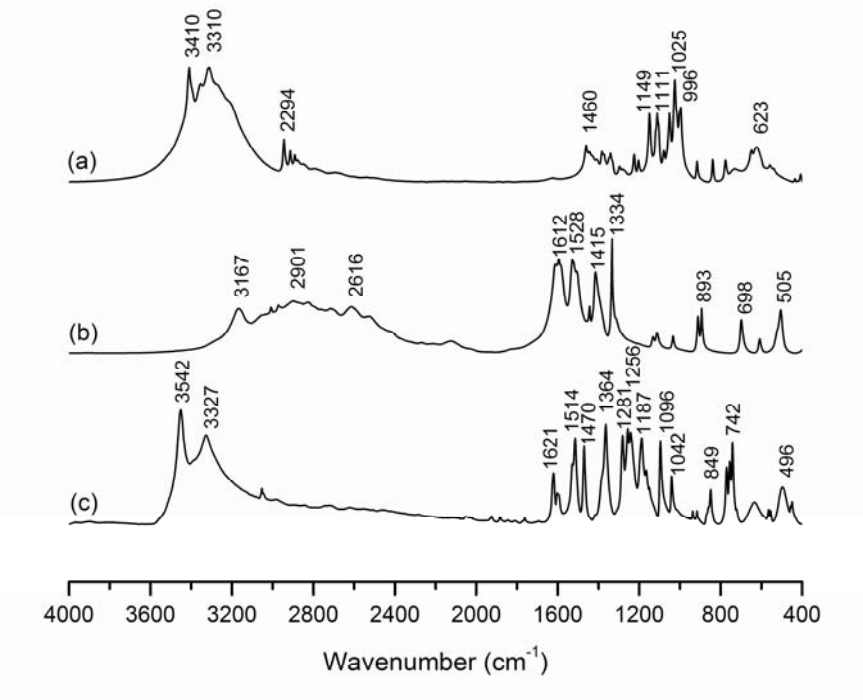

Figure 3.1.7 FTIR spectra of the unreacted biomolecules: (a) glucose, (b) glycine and (c) catechol.

3.1.3.3.2 Solid phase

Total carbon analysis

Table 3.1.3 shows the results of the total C contents on the solid residues from selected reaction systems. Rhodochrosite ($MnCO_3$) was identified as the primary product in the solid residue of the Maillard reaction system using X-ray diffraction (data not shown). The total carbon content of the solid residue of the Maillard reaction system (13.1 %) was relatively close to that of pure $MnCO_3$ (10.4%), whereas the solid residues of catechol containing systems contained much higher total C percentages. It was also apparent from visible inspection of the

solid residues that the Maillard reaction system contained less humified material, as it was yellowish-white in colour (similar to pure $MnCO_3$), whereas, the colour of the residues in the catechol containing systems ranged from light brown to deep black, becoming progressively darker with increasing amounts of catechol in the system.

It was not possible to differentiate between organic and inorganic C using the LECO analyzer as it is based on a dry combustion method and measures the CO_2 released at 841 °C and 1100 °C to distinguish between CO_2 released from organic C (841° C) and total C , i.e., inorganic C + organic C (1100° C). Manganese carbonate decomposes at temperatures above 200°C, which is substantially lower than the melting point of $CaCO_3$ (825° C) (Perry and Phillips 1995). Calcium carbonate is considered the most common form of inorganic C in soils and sediments. Thus, the C from $MnCO_3$ would be included in the "organic C" fraction using the conventional dry combustion method.

Table 3.1.3 Total carbon contents of the solid residues from selected reaction systems

Reaction system	% Carbon
Maillard reaction (0.05 mole glucose + 0.05 mole glycine)	13.1
Catechol-Maillard system with 0.0025 mole catechol	21.4
Catechol-Maillard system with 0.025 mole catechol	33.9
Catechol-Maillard system with 0.05 mole catechol	34.7
Catechol-Maillard system with 0.10 mole catechol	36.7
Catechol only system (0.05 mole catechol)	39.2

Manganese L-edge NEXAFS spectroscopy

The Mn $L_{2,3}$-edges NEXAFS spectra of the solid residues from the Maillard reaction, integrated catechol-Maillard and catechol only systems catalyzed by birnessite, as well as, reference di-, tri- and tetra-valent Mn oxide and carbonate compounds are shown in Figure 3.1.8. The Mn $L_{2,3}$-edges provide a sensitive fingerprint of the valence of Mn based on the absorption maxima and shape of the spectra, and in some cases the site symmetry and ligands can also be identified (Garvie and Craven 1994; Grush et al. 1996). The maximum absorption peak (white line) of Mn(II) was observed at 640.3 eV, Mn(III) at 641.7 eV, and Mn(IV) at 644.0 eV, at the Mn L_3 edge (Fig. 3.1.8). The shapes and photon energy values of the spectra of Mn species

obtained in this study are in agreement with those of previous Mn $L_{2,3}$-edges NEXAFS studies (Cramer et al. 1991; Garvie and Craven 1994; Grush et al. 1996; Gilbert et al. 2003).

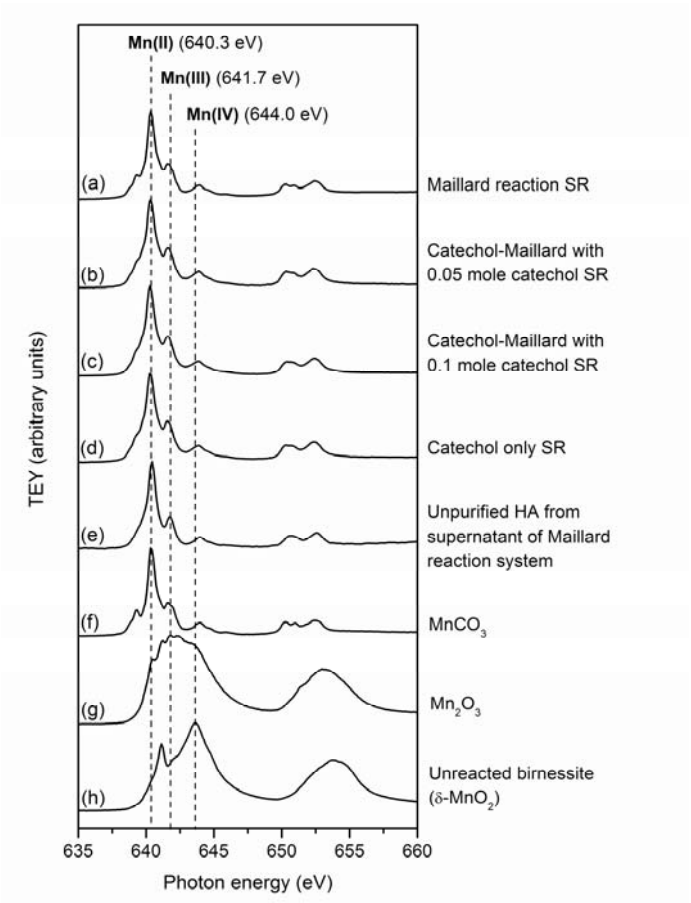

Figure 3.1.8 Manganese L-edge NEXAFS spectra of the solid residues (SR) of systems reacted in the presence of birnessite: (a) the Maillard reaction system (0.05 mole glucose + 0.05 mole glycine); the catechol-Maillard system with (b) 0.05 mole catechol, and (c) 0.1 mole catechol; (d) the catechol only system; (e) unpurified HA extracted from the supernatant of the Maillard reaction system; (f) $MnCO_3$, (g) Mn_2O_3 and (h) unreacted birnessite (δ-MnO_2). The dotted lines indicate the photon energy of the maximum absorption peak of Mn in divalent, trivalent or tetravalent states on the Mn L_3-edge.

The Mn $L_{2,3}$-edges spectra of the solid residues from the Maillard reaction (Fig. 3.1.8a), catechol-Maillard (Fig. 3.1.8b-c) and catechol only (Fig. 3.1.8d) systems show that Mn was predominantly in the divalent form in these systems. This indicates that the birnessite [mostly Mn(IV) oxide with some Mn(III)] was reduced to Mn(II) during the reaction period. This was also confirmed by FTIR analysis of the solid residues which showed the absence of birnessite (data not shown). The Mn L_3-edge of the unpurified HA isolated from the Maillard reaction system (Fig. 3.1.8e) differs from that of pure $MnCO_3$ (Fig 3.1.8f) in that the minor absorption

peak (~639.1 eV) to the left of the maximum Mn(II) absorption peak (640.3 eV) is not resolved. The Mn L-edge spectrum of Mn(II) acetate (data not shown) looks identical to that of the the Mn(II) bound to HA (Fig. 3.1.8e). The shape of the spectra correspond to Mn(II) that is covalently bonded to either O or N and in octahedral conformation (Grush et al. 1996). The spectra of the Maillard reaction residue (Fig. 3.1.8a) looks most similar to that of pure $MnCO_3$ (Fig. 3.1.8f), whereas the patterns of the residues from the catechol containing systems (Fig. 3.1.8b-d) appear more like the extracted HA (Fig. 3.1.8e). This indicates that the Mn(II) in the solid residues from the integrated catechol-Maillard and catechol only systems was bound to humic polymers. This also confirms the trend observed in the total C data (Table 3.1.3), which indicates that with increasing amounts of catechol added in the systems, there was increasing C content in the solid phase. This is attributable to increased humification (Fig. 3.1.2) and, ultimately, co-precipitation with Mn(II) (Fig. 3.1.4).

Carbon K-edge NEXAFS spectroscopy

The C K-edge NEXAFS spectra of the solid residue of selected reaction systems are shown in Figure 3.1.9. The C K-edge NEXAFS spectrum of the solid residue from the Maillard reaction system (Fig. 3.1.9a) clearly shows that carbonate C=O (290.2 eV) and aliphatic carboxylic C=O (288.6 eV) were the dominant functional groups present. The formation of $MnCO_3$ in the solid residues was suppressed with increasing amount of catechol added to the reaction systems (Fig. 3.1.9a-d), as indicated by the total C contents (Table 3.1.3) and Mn L-edge NEXAFS spectra (Figure 3.1.8). The C K-edge NEXAFS spectroscopic data indicate that the humified organic substances in solid residues were rich in carboxylic groups (Fig. 3.1.9) whereas the HA from the supernatant of the reaction systems was more aromatic in nature (Fig. 3.1.5). The chemical partitioning of humic substances in the solid and solution phases occurred due to coprecipitation with Mn(II), similar to what was observed with natural HA (Christl and Kretzchmar 2007). Aliphatic carboxylic groups have a much higher affinity for binding divalent cations, such as dissolved Mn(II), than phenolic OH groups; and it is well known that COOH functionalities give humic substances most of their cation complexing capacity (Stevenson 1994). The logarithm of the stability constant (K) (μ = 0.1, 25° C) of the complex of glycine and Mn(II) is +2.80, whereas for catechol and Mn(II) its log K is -14.70 (Martell and Smith 2004). This indicates that the humic substances which posses aliphatic carboxylic functionalities would

be able to sorb Mn(II) to a much greater extent than the polymers with more aromatic or phenolic character. Increased metal complexation would eventually result in the coprecipitation of metal with humic substances out of solution due to decreased solubility as a result of increase in molecular size and charge neutrality (McBride 1994).

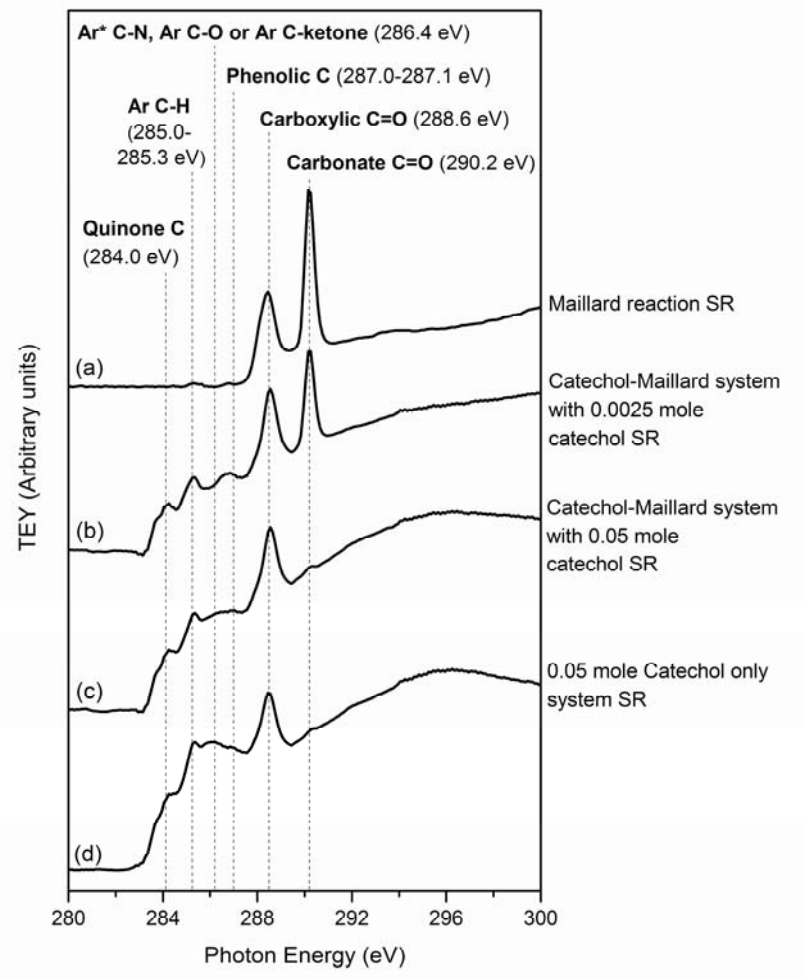

Figure 3.1.9 Carbon K-edge NEXAFS spectra of the solid residues (SR) from systems reacted in the presence of birnessite: (a) the Maillard reaction (0.05 mole glucose + 0.05 mole glycine); the integrated catechol-Maillard systems with (b) 0.0025 mole catechol, and (c) 0.05 mole catechol; and (d) the 0.05 mole catechol only system.

Nitrogen K-edge NEXAFS spectroscopy

The N K-edge NEXAFS spectra of the natural IHSS soil and river HA and the solid residues from the Maillard and equimolar integrated catechol-Maillard system are shown in Figure 3.1.10. Spectroscopic assignments are based on values reported by previous N NEXAFS studies (Vairavamurthy and Wang 2002; Leinweber et al. 2007). Amide is the dominant

functional group of the natural HA, while there is evidence of some heterocyclic N functionalities (Fig. 3.1.10a and b). The formation of amide and heterocyclic N compounds is evident in the Maillard reaction and integrated catechol-Maillard systems reacted in the presence of birnessite (Fig. 3.1.10c and d). The solid residue of the Maillard reaction system (Fig. 3.1.10c) was dominated by amide N compared with that of the equimolar integrated catechol-Maillard system (Fig. 3.1.10d). It would appear that addition of catechol to the Maillard system has promoted the formation of heterocyclic N (Fig. 3.1.10c and d).

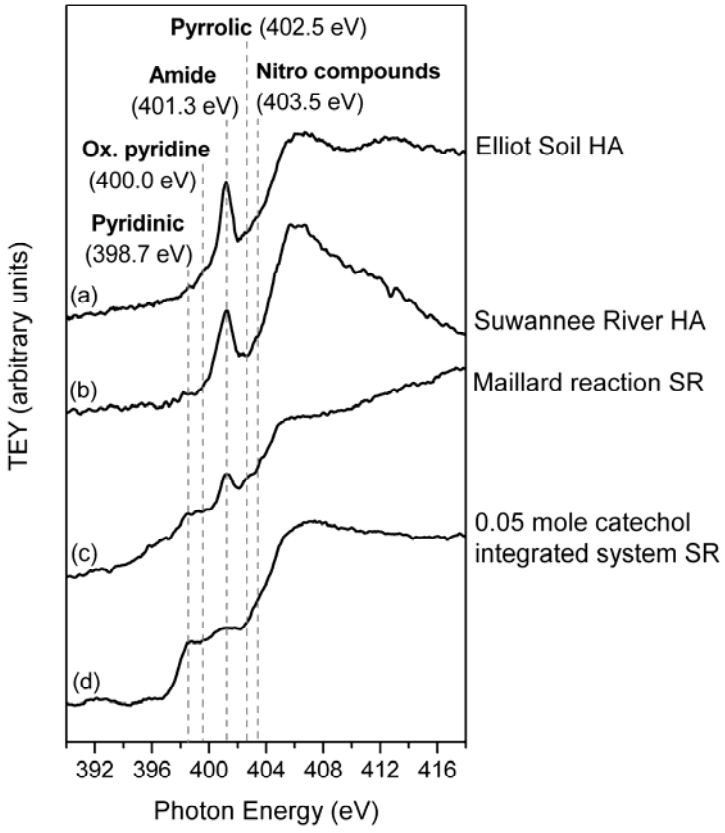

Figure 3.1.10 Nitrogen K-edge NEXAFS spectra of IHSS (a) Elliot soil HA and (b) Suwannee River HA and the solid residues (SR) from systems reacted in the presence of birnessite: (c) the Maillard reaction (0.05 mole glucose + 0.05 mole glycine), and (d) the equimolar integrated catechol-Maillard system (0.05 mole catechol + 0.05 mole glucose + 0.05 mole glycine).

Pyrolysis field ionization mass spectrometry (Py-FIMS)

Figure 3.1.11 shows the Py-FIMS spectra of the solid residues (SR) from the Maillard reaction, equimolar catechol-Maillard and catechol only reaction systems. Broad categorization of the volatile organic compounds occurring in the Py-FIMS results, by means of identification of typical biochemical marker signals, is shown in Table 3.1.4.

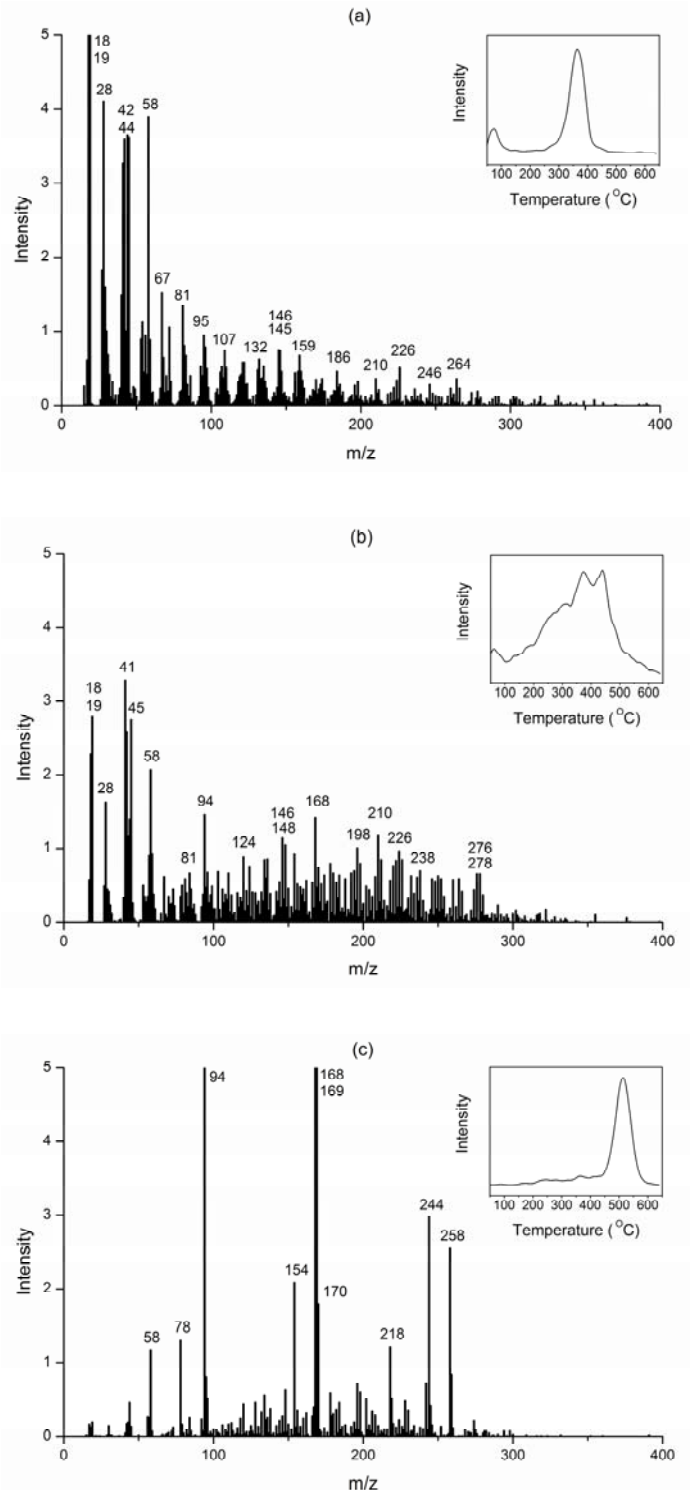

Figure 3.1.11 Py-FIMS spectra of the solid residues from selected systems catalyzed by birnessite: (a) the Maillard reaction system (0.05 mole glucose + 0.05 mole glycine), (b) the equimolar catechol-Maillard system, and (c) the 0.05 mole catechol only system.

It was found that 48.0% of the organic products in the Maillard reaction system SR were of a molecular mass between 15 and 56, whereas 22.4% of the equimolar catechol-Maillard reaction system SR and only 2.1% of the catechol only system SR fell into this low molecular mass category (Table 3.1.4). This implies that the catechol containing systems produced organic compounds that are of a larger molecular weight and thus more humified. It can also be seen from the thermograms, inset in the right hand corner of each mass spectrum, that systems containing catechol (Fig. 3.1.11b and c) resulted in organic products with a higher thermal stability compared with the Maillard reaction system (Fig. 3.1.11a). The Py-FIMS spectrum of the catechol-Maillard system appears the most heterogeneous of the three systems (Fig. 3.1.11b).

Table 3.1.4 Interpretation of the Py-FIMS results of the solid residues from the Maillard (0.05 mole glucose + 0.05 mole glycine), equimolar catechol-Maillard (0.05 mole catechol + 0.05 mole glucose + 0.05 mole glycine) and catechol only (0.05 mole catechol) systems catalyzed by birnessite.

Reaction system	EX 1	EX 2	EX 3	EX 4	EX 5	EX 6	EX 7	EX 8	EX 9	EX 10	Σ EX 1-10
	% of volatile compounds										
Maillard reaction	5.3	4.5	0.7	0.7	5.7	7.8	3.2	0.1	48.0	11.7	87.7
Integrated catechol-Maillard	5.8	14.2	1.1	2.1	13.3	6.4	5.3	0.1	22.4	12.1	82.8
Catechol only	2.3	56.1	0.5	6.8	8.6	0	0	0	2.1	14.3	90.7

EX 1: Carbohydrates	EX 2: Phenols + lignin monomers	EX 3: Lignin dimers	EX 4: Lipids, alkanes, alkenes, fatty acids, n-alkyl esters
EX 5: Alkyl aromatics	EX 6: N-containing compounds	EX 7: Peptides	EX 8: Fatty acids n-C16 to n C34
EX 9: M/z of 15 - 56 (low molecular weight components)	EX 10: (M+1)-signals (ionized fragments)		

Pyrolysis-gas chromatography/mass spectrometry (Py-GC/MS)

The interpretation of the results of the Py-GC/MS analysis of the solid residue from the integrated equimolar catechol-Maillard system reacted in the presence of birnessite is shown in Table 3.1.5. Less than 25% of the organic compounds in the residue could be identified as this technique identifies only the volatile components. The results indicate that the residue contained significant amounts of aliphatic (9.53%), heterocyclic N and aromatic C bound to N compounds

(8.71%), cyclic (3.29%) and substituted benzene (2.42%) compounds. The heterocyclic N and aromatic C bound to N compounds included a variety of pyrazine, pyridine, pyrrole and benzoxazole compounds. The highest contributor compounds were methylated benzoxazole compounds (1.43%) and benzene isocyanato compounds (1.17%). Both these compounds contain aromatic C bound directly to nitrogen. These types of functionalities were also identified in C K-edge NEXAFS spectra of the HA fraction isolated from the supernatant, and solid residues from the catechol-Maillard system (photon energy value at 286.4 eV) (Fig. 3.1.5d and 3.1.9c, respectively). Heterocyclic N functional groups were also identified in the N K-edge NEXAFS spectra of the solid residues from the integrated catechol-Maillard system solid residue (photon energy value 398.7, 400.0 and 402.5 eV) (Fig. 3.1.10d).

Table 3.1.5 Interpretation of the Py-GC/MS results of the solid residue from the integrated equimolar catechol-Maillard system reacted in the presence of birnessite.

Peak Area %	MW	Compounds
		N-containing compounds
0.19	80	Pyrazine
0.43	106	Pyrazine, ethenyl-
0.65	110	Pyrazine, methoxy-
0.11	67	1H-Pyrrole
0.14	81	1H-Pyrrole, 1-methyl-
0.31	95	1H-Pyrrole, 2,5-dimethyl-
0.52	79	Pyridine
0.23	93	Pyridine, 2-methyl-
0.66	93	Pyridine, 3-methyl-
0.07	93	Pyridine, 4-methyl-
0.22	107	Pyridine, 2,3-dimethyl-
0.29	109	2-Pyridinemethanol
0.11	109	Pyridine, 3-methyl-, 1-oxide
0.65	123	Pyridine, 3-ethyl-, 1-oxide
0.22	133	s-Triazolo[4,3-a]pyridine, 7-methyl-
0.42	80	Pyridazine
0.27	94	Pyrimidine, 4-methyl-
0.17	124	Ethanone, 1-(4-methyl-1H-imidazol-2-yl)-
0.44	136	6H-Purin-6-one, 1,7-dihydro-
0.99	133	Benzoxazole, 2-methyl
0.44	133	Benzoxazole, 2-methyl-
1.17	119	Benzene, isocyanato-
8.71		**Sum of N-containing compounds**
		Substituted furans
0.10	96	Furan, 2,5-dimethyl-
0.10		**Sum of substituted furans**
		Substituted benzenes

0.23	78	Benzene
0.41	104	Styrene
0.29	122	Benzaldehyde, 2-hydroxy-
0.44	152	Benzaldehyde, 3-hydroxy-4-methoxy-
0.19	122	1,3-Benzodioxole
0.54	278	1, 2-Benzenedicarboxylic acid, dibutyl ester
0.31	390	1, 2-Benzenedicarboxylic acid, dioctyl ester
2.42		**Sum of substituted benzenes**
		Substituted phenols
0.39	94	Phenol
0.39		**Sum of substituted phenols**
		Aliphatic compounds
0.96	184	Tridecane
0.19	198	Tetradecane
0.27	212	Pentadecane
0.27	226	Hexadecane
0.39	240	Heptadecane
0.72	254	Octadecane
1.39	268	Nonadecane
1.35	282	Eicosane
1.04	296	Heneicosane
0.76	310	Docosane
0.37	324	Tricosane
0.77	96	1,2-Heptadiene
0.29	96	2,4-Hexadienal
0.78	270	Hexadecanoic acid, methyl ester
9.53		**Sum of aliphatic compounds**
		Cyclic compounds
0.63	82	2-Cyclopenten-1-one
0.15	96	2-Cyclopenten-1-one, 2-methyl-
0.21	96	2-Cyclopenten-1-one, 3-methyl-
0.25	80	1,3-Cyclopentadiene, 5-methyl-
0.45	80	1,3-Cyclohexadiene
0.33	80	1,4-Cyclohexadiene
1.26	98	Cyclopentane, ethyl-
3.29		**Sum of cyclic compounds**
75.56		**Unidentified compounds**
100.00		**Sum of area of whole chromatogram**

3.1.4 Conclusions

The significance of linking the polyphenol and Maillard reactions as promoted by birnessite (δ-MnO_2) into an integrated humification pathway has been demonstrated by Jokic et al. (2004b) using a system containing catechol, glucose and glycine. However, the effect of the molar ratio of catechol to Maillard reagents in influencing the integrated polyphenol-Maillard reaction humification pathway remained to be uncovered.

The results of this study show that the increasing molar ratio of catechol to Maillard reagents resulted in significant enhancement in the degree of humification in the integrated catechol-Maillard pathway. This increase in humification was substantially higher than the sum of the humification in the Maillard reaction system and that in the catechol alone systems. The visible spectroscopic data indicate that the threshold value in our system to observe significant increases in the degree of humification was a molar ratio of catechol to Maillard reagents greater than 0.05 (i.e., 0.0025 mole catechol to 0.05 mole glucose + 0.05 mole glycine). This synergistic effect was attributed to the multiple processes which can occur in the integrated reaction system, namely, the Maillard reaction, the polymerization of catechol and polycondensation of catechol and glycine, and the interaction of oxidation products of glucose and Maillard reaction products with catechol.

The molar ratio of polyphenol (catechol) to Maillard reagents (glucose + glycine) significantly influenced the nature of the humic substances formed. Increasing the molar ratio of catechol to Maillard reagents to greater than 0.05 in the integrated catechol-Maillard system resulted in the formation of humic substances with an increasingly aromatic character. The C K-edge NEXAFS spectra indicate that the Suwannee River HA standard from the IHSS was basically similar to the HA from the Maillard reaction system and the integrated system at equimolar ratio of catechol to Maillard reagents. Amide and heterocyclic N functionalities were formed in Maillard and integrated catechol-Maillard systems, similar to those found in natural HAs. The chemical partitioning of humic substances in the solid and solution phases occurred in the systems studied due to coprecipitation with Mn(II), similar to previous observations of natural HA in the literature.

The findings obtained in the this study show the significance of the relative abundance of biomolecules, such as polyphenols, sugars and amino acids, in influencing mineral-catalyzed abiotic humification pathways and products in natural environments.

3.2 Research Unit 2: *Biomolecule-induced formation of rhodochrosite in the birnessite-polyphenol-Maillard humification pathway*

3.2.1 Introduction

Humic substances are formed through both selective preservation processes and biotic (enzymatic) and abiotic (mineral) catalytic mechanisms (Bollag et al. 1998; Huang 2004). Abundant research evidence at the molecular level shows that mineral colloids can enhance the abiotic polymerization and/or polycondensation of biomolecules such as amino acids, sugars, and polyphenols, derived from the breakdown of biological residues and from biological metabolites (Stevenson 1994; Bollag et al. 1998; Huang 2000, 2004; Clapp et al. 2005).

The polyphenol pathway of humification (polymerization reactions of polyphenolics and polycondensation reactions between polyphenolics and amino acids) has been intensely studied using various soil mineral colloids, such as Al, Fe and Mn oxides, clay size layer silicates and primary minerals, as catalysts (Wang et al. 1986; Bollag et al. 1998; Wang and Huang 2000b, 2003, 2005; Huang 2004). The Maillard reaction (condensation reactions between sugars and amino acids) is also regarded as an important pathway in natural humification processes (Ikan et al. 1996), and the abiotic catalysis of the Maillard reaction under environmentally relevant conditions has been investigated using birnessite (Jokic et al. 2001b), goethite and smectites (Gonzalez and Laird 2004). However, in nature it is likely that the polyphenol and Maillard reaction pathways interact with each other since sugars, amino acids and polyphenols all coexist in soil solutions and aquatic environments. The integrated polyphenol-Maillard humification pathway was first studied by Jokic et al. (2004b) using birnessite as catalyst and using equimolar concentrations of glucose, glycine and catechol.

Birnessite has been found to be one of the most powerful catalysts of abiotic humification reactions (Huang 2000). It has been previously shown that during birnessite-catalyzed abiotic humification reactions CO_2 is produced due to the oxidation of glycine (Wang and Huang 1987, 2005), catechol (Majecher et al. 2000), pyrogallol (Wang and Huang 2000b) and glucose (Jokic et al. 2004b) by birnessite. Carbon dioxide can dissolve in solution to from carbonic acid which can dissociate to form bicarbonate and carbonate (Lindsay 1979). However, the abiotic biomolecule-induced formation of carbonate remains to be uncovered. The relative abundance of biomolecules varies with vegetation, microbial community and the environment (Stevenson

1994; Kögel-Knabner 2002). Sugars and amino acids are among the most abundant biomolecules of terrestrial and aquatic environments (Anderson et al. 1989). The concentration of phenolics in soil solutions is typically low; however, they are the most reactive forms of carbon in soils (Fox 1995). The effect of the relative abundance of biomolecules, such as, polyphenols, amino acids and sugars, on carbonate formation is even less understood.

Therefore, the objective of the present study was to examine the effect of the molar ratio of catechol to Maillard reagents in the integrated polyphenol-Maillard reaction humification pathway on carbonate formation processes under the influence of birnessite. Rhodochrosite ($MnCO_3$) is typically formed in environments with high concentrations of Mn(II) and alkalinity, and has been found in lacustrine, brackish and marine sediments (Sternbeck 1997). It has been hypothesized that in these environments, rhodochrosite is commonly formed as a result of diagenesis in rapidly accumulating, fine-grained organic rich sediments, where CO_2 is supplied by the oxidation of organic matter in part by Mn oxides (Okita et al. 1988; van Cappellen and Wang 1996; Glasby and Schultz 1999). Rhodochrosite has also been identified as the dominant Mn-bearing phase in a palustrine emergent wetland using Mn K-edge XANES and EXAFS (La Force et al. 2002).

3.2.2 Materials and Methods

3.2.2.1 Materials

Birnessite (δ-MnO_2) was synthesized according to one of the methods described by McKenzie (1971), which involves slowly adding concentrated HCl to boiling $KMnO_4$. The precipitate was washed by means of repeated filtration using distilled deionized water (henceforth referred to as water) on a 0.1 μm pore Millipore membrane filter, until the wash water was tested free from chloride ($AgNO_3$ test). It was then freeze-dried, and finally lightly ground using a mortar and pestle. The synthesized birnessite was characterized by means of X-ray diffraction (XRD) (Rigaku Rotaflex 200SU, Tokyo, Japan), Fourier transform infrared (FTIR) spectroscopy (Bruker Equinox 55, Ettlingen, Germany), and Mn L-edge near edge X-ray absorption fine structure (NEXAFS) spectroscopy on the SGM (Spherical Grating Monochromator) beamline at the Canadian Light Source (Saskatoon, SK, Canada). Catechol (Sigma-Aldrich ACS reagent grade >99%), D-glucose (Sigma-Aldrich ACS reagent grade >99%) and glycine (Sigma Ultra pure grade >99%) were obtained from Sigma Aldrich Canada

Ltd. (Oakville, ON, Canada). The Mn reference compounds, $MnCO_3$ (99.99%) and MnO_2 (>99%), were obtained from Sigma Aldrich Canada Ltd. (Oakville, ON, Canada), and MnO (>99.9%) and Mn_2O_3 (>98%) were obtained from Alfa Aesar, Johnson Matthey Catalog Company, Inc. (Ward Hill, MA, USA), and were used as reference compounds in the NEXAFS studies.

3.2.2.2 Incubation experiment

Sterile conditions were maintained throughout the experiment in order to establish the role of abiotic processes. All glassware, birnessite, water and apparatus were autoclaved prior to the experiments. In addition to this, thimerasol, an antiseptic agent, was added to each flask (0.02 %, w/v) before any of the reagents were added. Thimerasol does not affect the oxidation process of phenolic compounds (Wang et al. 1983a). In order to investigate the effect of the molar ratio of catechol to Maillard reagents, a number of treatments were employed with increasing amounts (0, 0.00125, 0.0025, 0.0125, 0.0250, 0.0500, 0.1000 moles) of catechol added to a fixed molar ratio of Maillard reagents (0.05 mole glucose + 0.05 mole glycine) using birnessite as catalyst. There was also a treatment containing 0.05 mole catechol and birnessite. Two and a half grams of birnessite were suspended in each of the reaction solutions in a 250 mL flask. There were selected control treatments in which birnessite was absent, i.e., the catechol only system (0.05 mole catechol), the Maillard reaction system (0.05 mole glucose + 0.05 mole glycine), and the integrated equimolar catechol-Maillard system (0.05 mole glucose + 0.05 mole glycine + 0.05 mole catechol). All the reaction systems were adjusted to an environmentally relevant pH 7.0 using 0.1 M HCl or 0.1 M NaOH. The final volume of the flasks was made up to 100 mL using autoclaved water. The flasks were then tightly sealed and placed in a constant temperature water bath at 45° C for a period of 15 days while gently shaking. Forty-five degrees centigrade is an environmentally relevant temperature as it is common in tropical and subtropical areas, and is the approximate temperature of an exposed sunlit soil surface on a day when the ambient air temperature is 25° C (Jury et al. 1991). All treatments were performed in triplicate. The absence of microbial growth was verified by culturing aliquots of selected samples at the end of the incubation period. Aerobic microbial growth was tested for by culturing on Tryptocase Soy Agar (TSA) plates, while anaerobic microbial growth was tested for on TSA plates in a BBL GasPak

150 Large Anaerobic System. All cultures were incubated for a period of 5 and 9 days at 28° C (Jokic et al. 2004b).

3.2.2.3 Characterization of reaction systems at the end of the incubation period and isolation of the solid residue

At the end of the reaction period, the final pH and Eh of the suspensions were measured. The samples were then centrifuged at 25,000 g for 40 min to separate the solid residue from the solution. The absorbance of the supernatant was measured between 400 and 600 nm on a UV-visible spectrophotometer (Beckman DU 650 microprocessor controlled spectrophotometer, Fullerton, CA, USA). The visible absorbance provides an indication of the extent of polymerization which has taken place in the reaction systems (Shindo and Huang 1982, 1984a, 1984b). Shindo and Huang (1984a) studied the polymerization of polyphenols by short-range ordered Mn, Fe, Al and Si oxides, and showed that the yield of humic polymers was directly related to the visible absorbance. Likewise, with natural humic substances, Gan et al. (2007) showed that visible absorbance can be used to determine the concentration of fulvic acid in solution. The Mn content of the supernatant was determined using atomic absorption spectroscopy at 279.5 nm (Varian Spectra AA 220, Walnut Creek, CA, USA). Electron paramagnetic resonance (EPR) was used to characterize the supernatants from selected reaction systems on a Bruker EMX EPR spectrometer (Ettlingen, Germany). The analysis was performed at room temperature in the field modulation mode of 100 KHz and modular amplitude of 2 G, and at a microwave frequency of 9 – 10 GHz. The solid residue was repeatedly washed with water using centrifugation at 25,000 g for 40 min until the wash water was clear. The washed residue was then freeze-dried.

3.2.2.4 Characterization of solid residues

X-ray diffraction (XRD). The solid residues and unreacted birnessite were examined using X-ray diffractometry on a Rigaku Rotaflex 200SU (Tokyo, Japan) with a rotating Fe anode and graphite monochromator. The samples were lightly ground and then mounted on glass slides by making a slurry of the ground sample with acetone and allowing it to dry. The scans were performed at 40 kV and 160 mA, from 4 to 80 °2θ, at a step size of 0.02 °2θ at a scanning rate of 0.1 °2θ sec^{-1}.

Fourier transform infrared (FTIR) spectroscopy. FTIR spectra were obtained from the washed and freeze-dried solid residues and unreacted birnessite. This was done by preparing KBr disks containing 1% w/w sample and running it on a Bruker Equinox 55 FTIR (Ettlingen, Germany) connected with a purge gas generator.

Near edge X-ray absorption fine structure (NEXAFS) spectroscopy. Manganese speciation of selected solid residues was investigated using Mn L-edge NEXAFS on the SGM (Spherical grating monochromator) beamline at the Canadian Light Source (Saskatoon, SK, Canada). A number of pure reference compounds ($MnCO_3$, MnO, Mn_2O_3, MnO_2) were also examined. Samples were lightly ground and mounted on carbon tape. An exit slit width of 50 μm and a dwell time of 0.3 s were used to minimize damage due to exposure to radiation. These spectra were recorded by total electron yield (TEY) at an energy step size of 0.1 eV. The Mn spectra were normalized to the TEY of a gold I_0 mesh which was placed in front of the sample in the path of the beam. Spectra obtained were analyzed using aXis2000 software program (Hitchcock et al. 2005). The energy scale of the Mn spectra were internally calibrated using MnO, based on calibrated values reported from previous studies (Garvie and Craven 1994). All the spectra were normalized to each other, with the maximum intensity of each spectrum fixed at 1.

Atomic force microscopy (AFM). The surface features of selected solid residues were investigated using atomic force microscopy. Five milligrams of each sample was dispersed in 25 ml distilled deionized water using ultrasonification (Branson Sonifier Model 350, Danbury, CT, USA) at 40 kHz and 150 watts for 2 min in an ice bath. One drop of the suspension was placed on a glass slide cover slip and allowed to dry overnight at room temperature. The glass cover slip was then mounted on a magnetized stainless steel disk with double sided tape. The AFM images were obtained under ambient conditions using an etched silicon cantilever in tapping mode with a NanoScope III atomic force microscope (Digital Instruments, Inc., Santa Barbara, CA, USA).

3.2.3 Results and Discussion

3.2.3.1 Characterization of the reaction systems at the end of the incubation period

In all the reaction systems, no aerobic or anaerobic microbial growth was observed. Thus all the processes studied were abiotic in nature. The suspension pH and redox status, and the visible absorbance (400 and 600 nm) and Mn concentration values of the supernatant of the

Maillard reaction, catechol only and integrated catechol-Maillard systems, reacted in the presence or absence of birnessite are shown in Table 3.2.1.

Table 3.2.1 The solution pH, visible absorbance (400 and 600 nm) and Mn concentration of the Maillard reaction, catechol-only and selected integrated catechol-Maillard systems in the presence or absence of birnessite.

Treatment	pH	Visible absorbance (400 nm)	Visible absorbance (600 nm)	[Mn] (mmol L^{-1})
Birnessite present				
Maillard reaction (0.05 mole glucose + 0.05 mol glycine)	8.08 ±0.06	32.61 ±0.93	3.00 ±0.37	193.1 ±3.3
Catechol-Maillard system with 0.0025 mole catechol	7.83 ±0.05	34.14 ±0.32	2.52 ±0.25	144.4 ±2.6
Catechol-Maillard system with 0.025 mole catechol	6.81 ±0.03	78.58 ±4.99	36.41 ±2.25	116.2 ±3.9
Catechol-Maillard system with 0.05 mole catechol	6.85 ±0.01	100.00 ±6.37	44.21 ±5.34	92.0 ±4.9
Catechol-Maillard system with 0.1 mole catechol	6.65 ±0.02	146.04 ±2.36	53.67 ±1.99	103.4 ±4.3
Catechol only (0.05 mole catechol)	7.27 ±0.04	10.29 ±4.21	6.97±4.06	17.3 ±0.2
Birnessite absent				
Maillard reaction (0.05 mol glucose + 0.05 mol glycine)	6.26 ±0.07	0.74 ±0.08	0.12 ±0.02	-
Catechol-Maillard system with 0.05 mole catechol	5.49 ±0.07	2.84 ±0.57	0.42 ±0.09	-
Catechol only (0.05 mol catechol)	4.17 ±0.29	2.04 ±0.33	0.62 ±0.26	-

The two concurrent processes which affect the pH of the reaction systems were apparently: (i) the polymerization reactions of the biomolecules, which resulted in the generation of protons, and (ii) the reduction of birnessite which resulted in the consumption of protons. Therefore, the control systems had lower pH values than birnessite-containing systems. All these systems also showed a dramatically higher degree of humification in the presence of birnessite, most notably the integrated reaction system (Visible absorbance values – Table 3.2.1). Increasing the molar ratio of catechol to Maillard reagents in the birnessite-catechol-Maillard system

promoted browning (humification) and consequently decreased the pH of the systems (Table 3.2.1 – visible absorbance and pH values). There was also a subsequent decrease in the Mn concentration in solution due to the enhanced sorption of dissolved Mn by the humic polymers.

The EPR spectra of the supernatants of the Maillard reaction, catechol only and equimolar catechol-Maillard systems are shown in Figure 3.2.1. The EPR results of the supernatant analyses confirm the presence of aqueous Mn^{2+} in all of the reaction systems studied (Dasgupta et al. 2006). Aqueous manganese (II) has a typical g-value of around 2.0 and shows the typical six-lined pattern with a hyperfine splitting value of about 95 Gauss. This indicates that the reactions were catalyzed by birnessite, which acts as oxidant in the system. The most intense pattern was obtained in the case of the Maillard system (Fig. 3.2.1a) which is in accord with the concentrations of Mn in the supernatants determined by AAS (Table 3.2.1).

3.2.3.2 Characterization of the solid residue

X-ray diffraction. Figure 3.2.2 shows the X-ray diffractograms of the solid residues from the Maillard, integrated catechol-Maillard and catechol only reaction systems. The unreacted birnessite shows the characteristic d-values of synthetic K-birnessite at 7.21, 3.61 and 2.45 Å (Fig. 3.2.2f) as reported by McKenzie (1989). The solid residue from the Maillard reaction system (Fig. 3.2.2a) clearly shows the formation of crystalline rhodochrosite ($MnCO_3$) with typical d-values of 3.67, 2.84. 2.18 and 1.76 Å (Joint Committee on Powder Diffraction Standards 1974). As the amount of catechol in the integrated reaction systems was increased, there was a subsequent decrease in the amount and crystallinity of the $MnCO_3$ formed (Fig. 3.2.2b – d). The diffractogram of the solid residue from the catechol only reaction system (Fig. 3.2.2e) also shows some poorly crystalline $MnCO_3$ (2.84 Å), as well as, some unidentified crystalline reaction products (sharp peaks at d-values of 13.2 and 9.49 Å). The d-values do not match that of any known Mn oxide, organometallic or organic compound (Joint Committee on Powder Diffraction Standards 1974; International Centre for Diffraction Data 2006).

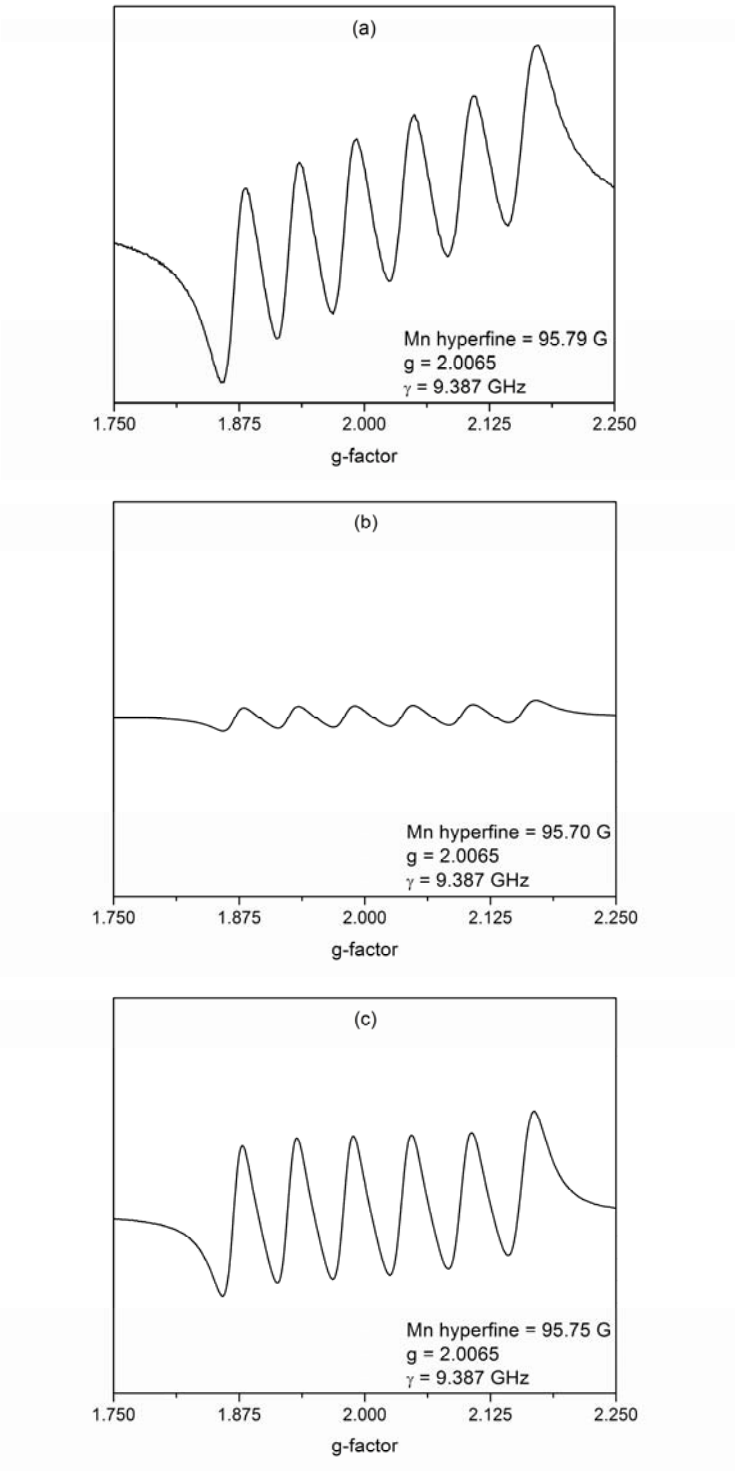

Figure 3.2.1 EPR spectra showing the relative Mn(II) intensities of the supernatants from (a) the Maillard system, (b) the 0.05 mole catechol only system, and (c) the equimolar catechol-Maillard system (0.05 mole catechol + 0.05 mole glucose + 0.05 mole glycine).

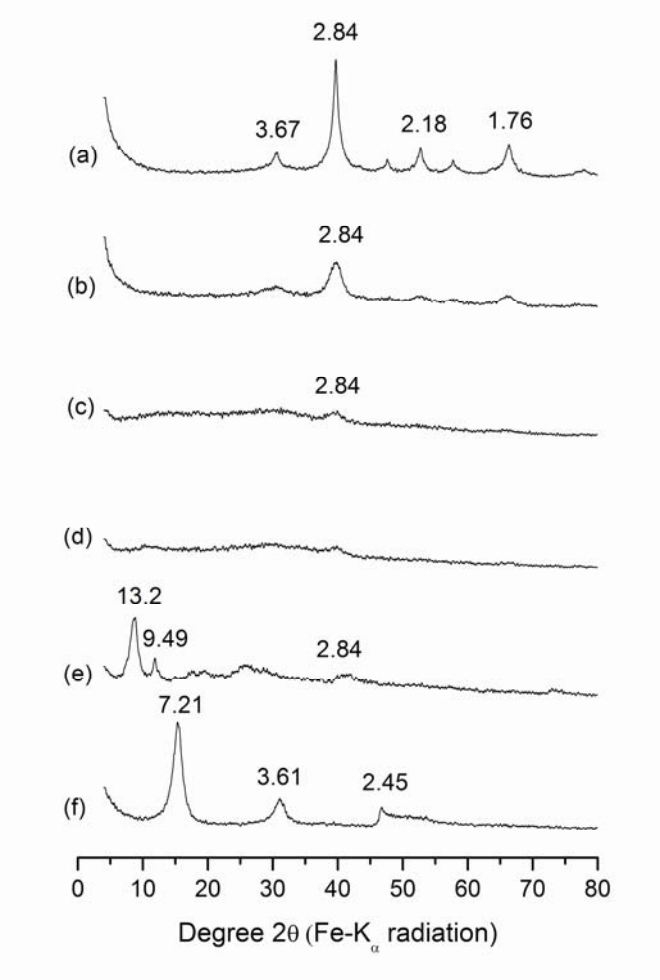

Figure 3.2.2 X-ray diffractograms of the solid residues from systems reacted in the presence of birnessite: (a) the Maillard system; the catechol-Maillard systems with: (b) 0.0025 mole catechol, (c) 0.025 mole catechol, and (d) 0.05 mole catechol; (e) 0.05 mole catechol-only; and (f) unreacted birnessite. The d-values are indicated in Angstrom.

FTIR spectroscopy. The FTIR spectra of pure $MnCO_3$, unreacted birnessite and the solid residues from the Maillard reaction, integrated catechol-Maillard and catechol only systems catalyzed by birnessite are shown in Figure 3.2.3. Comprehensive assignments of the absorption bands in Figure 3.2.3 are given in Table 3.2.2. Interpretation of the absorption bands was based on spectra in the literature (van der Merel and Beutelspacher 1976; Stevenson 1994; Aktas et al. 2003; Silverstein et al. 2004). The unreacted birnessite (Fig. 3.2.3h) shows typical absorption bands at 3400, 1621, 509 and 466 cm^{-1} (Potter and Rossman 1979). The dominant absorption bands of $MnCO_3$ occur at 1460, 1076, 860 and 725 cm^{-1} (Fig. 3.2.3a) which is in agreement with the spectrum published by Nyquist and Kagel (1971).

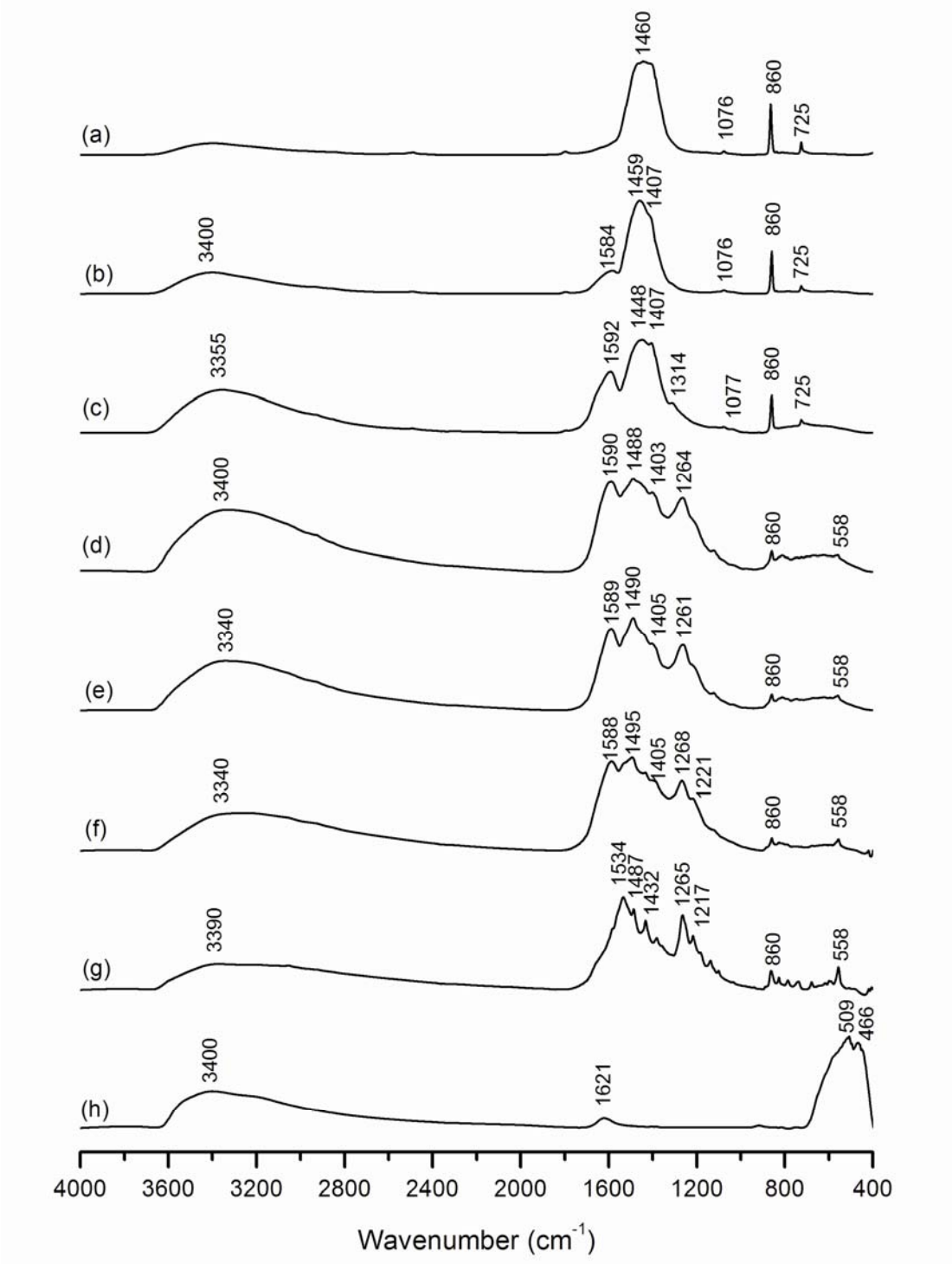

Figure 3.2.3 FTIR spectra of (a) pure $MnCO_3$; the solid residues from systems reacted in the presence of birnessite: (b) the Maillard reaction (0.05 mole glucose + 0.05 mole glycine); the integrated catechol-Maillard system with (c) 0.0025 mole catechol, (d) 0.025 mole catechol, (e) 0.05 mole catechol, and (f) 0.1 mol catechol; (g) 0.05 mole catechol only; and (h) unreacted birnessite.

Table 3.2.2 Assignments of FTIR absorption bands of the solid residues of the Maillard reaction, catechol-Maillard and catechol only systems shown in Fig. 3.2.3.

(a) Pure $MnCO_3$		**(b) Maillard reaction system**		**(c) Integrated catechol-Maillard system with 0.0025 mole catechol**	
Wavenumber (cm^{-1})		**Wavenumber (cm^{-1})**		**Wavenumber (cm^{-1})**	
725	Carbonate C-O out of plane bend	725	Carbonate C-O out of plane bend	725	Carbonate C-O out of plane bend
860	Carbonate C-O stretch	860	Carbonate C-O stretch	860	Carbonate C-O stretch
1076	Carbonate C-O stretch	1076	Carbonate C-O stretch	1077	Carbonate C-O stretch
1460	Carbonate symmetric C-O stretch	1407	OH deformation of phenols, C-H deformation of CH_2 & CH_3, symmetrical stretch of COO^-	1314	Symmetrical stretch of COO^-
		1459	Carbonate symmetric C-O stretch, asymmetrical bending of CH_2 & CH_3 deformation band	1407	OH deformation of phenols, C-H deformation of CH_2 & CH_3, symmetrical stretch of COO^-
		1584	Aromatic C=C stretch, Symmetric C-O stretch of COO^-, N-H deformation + C=N amide II band	1448	Carbonate symmetric C-O stretch, asymmetrical bending of CH_2 & CH_3 deformation band
		3400	OH stretch	1592	Aromatic C=C stretch, Symmetric C-O stretch of COO^-, N-H deformation + C=N amide II band
				3355	OH stretch
(d), (e) and (f) Integrated catechol-Maillard system with 0.025, 0.05 and 0.1 mole catechol, respectively.		**(g) 0.05 mol catechol only system**		**(h) Unreacted birnessite**	
558	Mn-O vibrations, aliphatic C-O stretches	558	Mn-O vibrations	466	Mn-O vibrations in birnessite
860	Carbonate C-O stretch	860	Carbonate C-O stretch	509	Mn-O vibrations in birnessite
1221	C-O stretch of phenols or phenyl ethers	1217	C-O stretch of phenols or phenyl ethers	1621	O-H stretch from water in birnessite crystal structure
1261-1268	C-O stretch of phenols and phenyl ethers	1265	C-O stretch of phenols or phenyl ethers	3400	OH stretch
1403-1405	OH deformation of phenols, C-H deformation of CH_2 & CH_3, symmetrical stretch of COO^-	1432	OH deformation of phenols, C-H deformation of CH_2 & CH_3, symmetrical stretch of COO^-		
1488-1495	Symmetric C-O stretch of COO^-, N-H deformation + C=N amide II band	1487	Symmetric C-O stretch of COO^-		
1588-1590	Aromatic C=C stretch, Symmetric C-O stretch of COO^-, N-H deformation + C=N amide II band	1534	Aromatic C=C stretch, Symmetric C-O stretch of COO^-		
3340-3400	OH stretch	3390	OH stretch		

The solid residue of the Maillard reaction system consisted predomiantly of $MnCO_3$ (Fig. 3.2.3b). Other absorption bands arising from humic substances are also observed, namely a broad O-H stretch band at 3400 cm^{-1}, a weak carboxylic or C=C band at 1584 cm^{-1}, and possibly other signals overlapping with the $MnCO_3$ band (1460 cm^{-1}) from 1400-1500 cm^{-1} possibly due to carboxylic, aliphatic C-H or phenolic stretches. The spectrum of the integrated catechol-Maillard system with 0.0025 mole catechol added (Fig. 3.2.3b) shows a noticeable decrease in the intensity of the carbonate bands at 725, 860 and 1077 cm^{-1}. The spectra of the 0.025 mole catechol integrated system (Fig. 3.2.3c) and subsequent integrated systems with increasing catechol (Fig. 3.2.3d and e) show a more dramatic change from the Maillard and 0.0025 mole catechol integrated systems. There is an increase in the intensity of the aromatic C=C band/carboxylic C-O band (1588-1590 cm^{-1}) and the phenol C-O (1261-1268 cm^{-1}) stretch bands (Fig. 3.2.3b-e). There is also a significant decrease in the intensity of the carbonate band at 860 cm^{-1}, and a complete disappearance of the carbonate stretches at 725 and 1076-1077 cm^{-1}. In the catechol only system (Fig. 3.2.3f), the most prominent peaks are the C=C aromatic/carboxylic stretches (1534 cm^{-1}) and the phenol C-O stretches (1217 and 1265 cm^{-1}). The broad -OH stretch band at 3340-3400 cm^{-1} (Fig 3.2.3) can also be attributed to intramolecular H-bonding between polymers (Aktas et al. 2003). These spectra show that as the amount of catechol in the integrated catechol-Maillard system was increased, there was a shift from the reaction products containing predominantly inorganic $MnCO_3$ to humified organic products that were significantly aromatic. This transition was most visible from the catechol-Maillard system containing 0.025 mole catechol and onwards (Fig. 3.2.3c-e). These results are in agreement with the XRD results (Fig. 3.2.2).

Manganese L-edge NEXAFS spectroscopy. The Mn $L_{2,3}$-edges NEXAFS spectra of the solid residues from the Maillard, equimolar catechol-Maillard and catechol only reaction systems, as well as, reference di-, tri- and tetra-valent Mn oxide and carbonate compounds are shown in Fig. 3.2.4. The Mn $L_{2,3}$-edges provide a sensitive fingerprint of the valence of Mn based on the absorption maxima and shape of the spectra, and in some cases the site symmetry and ligands can also be identified (Garvie and Craven 1994; Grush et al. 1996).

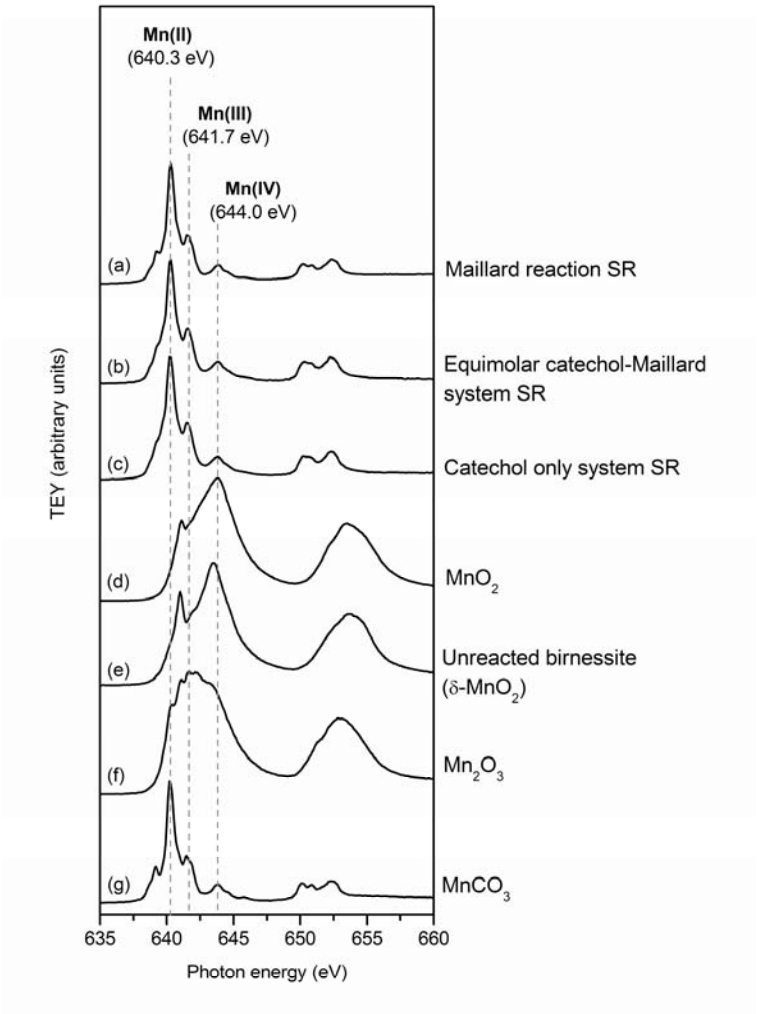

Figure 3.2.4 Manganese $L_{2,3}$-edge NEXAFS spectra of the solid residues from (a) the Maillard reaction (0.05 mole glucose + 0.05 mole glycine), (b) the equimolar catechol-Maillard system (0.05 mole catechol + 0.05 mole glucose + 0.05 mole glycine), (c) 0.05 mole catechol only systems; and reference compounds (d) MnO_2, (e) unreacted birnessite, (f) Mn_2O_3 and (g) $MnCO_3$. The dotted lines indicate the photon energy of the maximum absorption peak of Mn in divalent, trivalent or tetravalent states on the Mn L_3-edge.

The Mn $L_{2,3}$-edge NEXAFS spectra of the unreacted birnessite (Fig. 3.2.4e) shows that the synthesized birnessite contains predominantly Mn(IV) with some Mn(III), which was also previously reported using Mn K-edge X-ray absorption spectroscopy (Jokic et al., 2001a). The Mn $L_{2,3}$-edges spectra of the solid residues from the reaction systems show that Mn was principally in the divalent form in these systems (Fig. 3.2.4a-c).The spectra of the solid residues from the equimolar catechol-Maillard reaction system (Fig. 3.2.4b) and catechol only system (Fig. 3.2.4c) look similar to each other in that the minor absorption peak to the left of the

maximum absorption peak is not resolved, compared with pure $MnCO_3$ (Fig. 3.2.4g). The Mn L-edge spectrum of Mn(II) acetate (data not shown) looks identical to that of the Mn(II) bound to HA (fig. 3.1.8e). The shape of these spectra corresponds to Mn(II) that is covalently bonded to either O or N and in octahedral conformation (Grush et al. 1996), indicating that the Mn(II) in the solid residues from the integrated catechol-Maillard and catechol only systems (Fig. 3.2.4b and c) is covalently bonded to humic polymers. However, the spectrum of the solid residue of the Maillard reaction (Fig. 3.2.4a) looks more similar to that of pure $MnCO_3$ (Fig. 3.2.4g), which is in agreement with the XRD (Fig. 3.2.2a) and FTIR (Fig. 3.2.3a) data, showing that the solid residue consisted predominantly of $MnCO_3$ and some humic substances.

The formation of $MnCO_3$ in the catechol-Maillard reaction system as influenced by the molar ratio of catechol to Maillard reagents is clearly shown by the XRD, FTIR and Mn L-edge NEXAFS data (Fig. 3.2.2, 3.2.3 and 3.2.4). It has been previously shown that CO_2 is produced during the oxidation of glycine (Wang and Huang 1987, 2005), catechol (Majecher et al. 2000), pyrogallol (Wang and Huang 2000b) and glucose (Jokic et al. 2004b) by birnessite. Carbon dioxide released from these biomolecules dissolves in solution to form carbonic acid (Eq. 3.2.1):

$$CO_2 + H_2O \leftrightarrow H_2CO_3 \ldots \text{(Log K = -1.46) (Lindsay 1979)} \quad (3.2.1)$$

Carbonic acid dissociates to form bicarbonate and eventually carbonate depending on the pH of the solution (Eq. 3.2.2 and 3.2.3):

$$H_2CO_3 \leftrightarrow H^+ + HCO_3^- \ldots \text{(Log K = -6.36) (Lindsay 1979)} \quad (3.2.2)$$

$$HCO_3^- \leftrightarrow H^+ + CO_3^{2-} \ldots \text{(Log K = -10.33) (Lindsay 1979)} \quad (3.2.3)$$

The partial pressure of CO_2 in the atmosphere is usually 0.0003 atm, however in a water-logged system the partial pressure can be as high as 0.3 atm, thus resulting in much higher CO_3^{2-} concentrations (Lindsay 1979). The CO_2 released from the oxidation of biomolecules (glucose, glycine, catechol) would enhance the partial pressure of CO_2 and dissolution of CO_2 in water to form H_2CO_3. Reduction of birnessite by the biomolecules resulted in substantial release of Mn (Table 3.2.1). Mn was present as Mn(II) in solution as shown using EPR spectrometry (Fig.

3.2.1). Thus, $MnCO_3$ (rhodochrosite) can form in the system when the activity product of Mn^{2+} and CO_3^{2-} (Eq. 3.2.4) exceeds the Ksp of $MnCO_3$ (1.8×10^{-18}) (Lindsay 1979):

$$Mn^{2+}{}_{(aq)} + CO_3^{2-}{}_{(aq)} \leftrightarrow MnCO_3{}_{(s)} \quad \ldots\ldots\ldots\ldots\ldots\ldots\ldots\ldots\ldots\ldots (3.2.4)$$

Therefore the biomolecule-induced formation of $MnCO_3$ is considered to be a mechanism for the formation of rhodochrosite, as the CO_2 is derived from the oxidation of biomolecules and the XRD (Fig. 3.2.2), FTIR (Fig. 3.2.3), and Mn L-edge NEXAFS (Fig. 3.2.4a) data show the presence of $MnCO_3$ in the reaction systems during humification of the biomolecules. Okita et al. (1988) hypothesized that the $MnCO_3$ deposit at Molango, Mexico, was formed due to the reduction of manganese oxides by organic materials and that the organic-derived CO_2 resulted in negative $\delta^{13}C$ values and manganese carbonate formation. The present experimental findings also provide the first experimental evidence to substantiate the hypothesis of the biogenic formation of $MnCO_3$ deposits in nature. Increasing the catechol concentration in the catechol-Maillard reaction systems resulted in less $MnCO_3$ formation (Fig. 3.2.2a-d and 3.2.3a-e). This is, in part, attributed to the lower solution pH values (Table 3.2.1), due to increased oxidative polymerization reactions, which decreased the CO_3^{2-} concentration in solution. Furthermore, the larger amounts of humic polymers formed with increasing catechol concentration as indicated by the visible absorbance (Table 3.2.1) apparently had an inhibitory effect on $MnCO_3$ formation, due to perturbation of the crystallization of pure $MnCO_3$ (Fig. 3.2.2) and is also attributable to the competing effect of humic polymers for Mn^{2+} through complexation as indicated by the solution Mn concentrations (Table 3.2.1).

Atomic Force Microscopy. The atomic force micrographs of unreacted birnessite, pure $MnCO_3$ and the solid residues from the Maillard and equimolar catechol-Maillard systems are shown in Fig. 3.2.5. $MnCO_3$ has a rhombohedral structure, with cleavage occurring in three directions (Kosterov et al. 2006). It tends to occur in botryoidal (grape-like), columnar and massive-granular habits (Fig. 3.2.5d). Birnessite (Fig. 3.2.5a) shows a typical platy structure. The residue from the Maillard reaction (Fig. 3.2.5b) looks very similar to that of the pure $MnCO_3$ (Fig. 3.2.5d), showing layers of columnar rhombohedral structures and rounded, botryoidal-shaped particles. The residue from the catechol-Maillard system (Fig. 3.2.5c) consisted of relatively flat,

irregularly-shaped particles interdispersed with small, more elevated aggregates (the small white specks). The surface features of the $MnCO_3$ are no longer visible in the solid residue of the catechol-Maillard system (Fig. 3.2.5c). The atomic force micrographs (Fig. 3.2.5) are in accord with the XRD (Fig. 3.2.2), FTIR (3.2.3) and Mn L-edge NEXAFS (Fig. 3.2.4) data, indicating the perturbation of catechol on the formation of $MnCO_3$ in the catechol-Maillard reaction humification pathway.

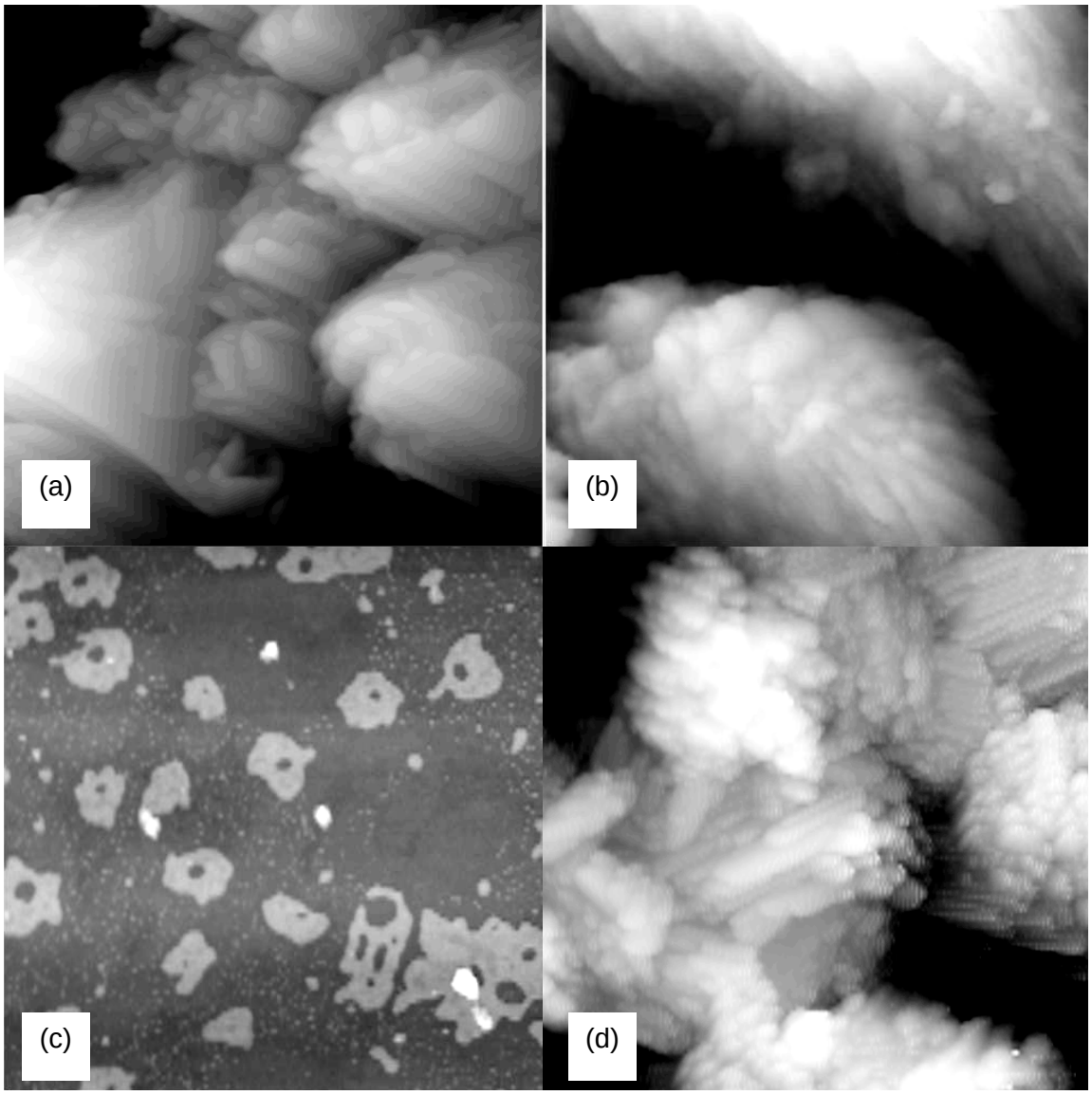

Figure 3.2.5 Atomic force microscopic images of the solid residues from (a) the unreacted birnessite; (b) the Maillard reaction system; (c) the equimolar catechol-Maillard system; and (d) 99.99% pure $MnCO_3$, obtained from Sigma Aldrich. All images are on a 1 μm scale.

3.2.4 Conclusions

It was previously shown that CO_2 evolved during birnessite-catalyzed abiotic humification reactions, as a result of the oxidation of glycine (Wang and Huang 1987, 2005), catechol (Majecher et al. 2000), pyrogallol (Wang and Huang 2000b) and glucose (Jokic et al. 2004b) by birnessite. However, the abiotic biomolecule-induced formation of carbonate remained to be uncovered. The present findings provide the first time evidence for the biomolecule-induced formation of $MnCO_3$ (rhodochrosite) as a result of the abiotic oxidation and cleavage of glucose, glycine or catechol by birnessite in humification pathways.

The molar ratio of catechol to Maillard reagents substantially affected not only the degree of humification but also the extent of $MnCO_3$ formation which was a competing reaction to the genesis of humic substances. The Maillard reaction system showed the greatest amount of rhodochrosite formation. The formation of rhodochrosite steadily decreased with the increase in the amount of catechol in the integrated catechol-Maillard systems. This was attributed to the perturbing effect of the enhanced formation of humic polymers on the crystallization of rhodochrosite, and the lower final pH values of the reaction systems with a greater degree of humification. The present findings also provide experimental evidence at the molecular level for substantiating the hypothesis of the abiotic formation of $MnCO_3$ in aquatic sediments and $MnCO_3$ deposits (Okita et al. 1988; Glasby and Schultz 1999). The findings obtained in the present study elucidate the important influence of the nature and relative abundance of biomolecules (polyphenols, sugars and amino acids) on abiotic humification and associated carbonate formation processes in natural environments.

3.3 Research Unit 3: *The influence of polyphenols on the integrated polyphenol-Maillard humification pathway as catalyzed by birnessite*

3.3.1 Introduction

Humic substances are formed through both selected preservation processes and biotic (enzymatic) and abiotic (mineral) catalytic synthesis mechanisms (Stevenson 1994; Huang 2004; Clapp et al. 2005). The Maillard reaction, involving condensation reactions between sugars and amino acids (Maillard 1913), is regarded as an important pathway in natural humification processes (Ikan et al. 1996). The appeal of the Maillard reaction in understanding humification processes lies in the two proposed precursors (sugars and amino acids) being among the most abundant biomolecules of terrestrial and aquatic environments (Anderson et al. 1989). Further support is lent by the presence of humic substances in marine environments where carbohydrates and proteins, because of their abundance, are more probable precursors of humic substances than lignin or phenolic polymers (Ikan et al. 1996). Although the potential energy barrier of the Maillard reaction is high (Jokic et al. 2001c), Jokic et al. (2001b) reported that birnessite (δ-MnO_2), which is commonly present in the environment, decreases the energy barrier and thus enhances the reaction rates by one to two orders of magnitude under environmentally relevant temperatures (25 and 45° C) and a neutral pH (7.00). Furthermore, Jokic et al. (2004a) clearly showed, using N K-edge NEXAFS, that the Maillard reaction, involving glucose and glycine, catalyzed by birnessite under environmentally relevant conditions not only produces heterocyclic N but also a significant amount of amide N. This provides an explanation for one of the pathways for the formation of heterocyclic N and amide N found in humic substances in the environment. Abundant scientific evidence at the molecular level shows the significance of the polyphenol pathway in humification (Stevenson 1994; Bollag et al. 1998; Huang 2000, 2004). The surfaces of soil metal oxides, particularly redox active oxides such as birnessite, are very reactive in promoting the oxidative polymerization of phenolic compounds. They can act as Lewis acids by accepting electrons from hydroxyphenolics, leading to the formation of highly reactive semiquinone radicals which readily undergo coupling reactions with other semiquinones, phenolics, amino acids or existing humus (Huang 2000).

Sugars, amino acids and polyphenols coexist in soil solutions and natural waters. Therefore, in nature it is most likely that the Maillard reaction and polyphenol pathways do not

occur separately but rather interact with each other. Jokic et al. (2004b) were the first to study an integrated Maillard reaction and polyphenol pathway of humification, using catechol, glucose and glycine as reagents and birnessite as catalyst. Their data showed that the ubiquitous soil mineral, birnessite significantly accelerates humification processes in an integrated polyphenol-Maillard reaction system under pH and temperature conditions typical of natural environments. Haffenden and Yaylayan (2005) showed that adding a mixture of polyphenols (catechol, resorcinol, hydroquinone and pyrogallol) to an equimolar solution of glucose and glycine and then heating, resulted in a significant enhancement of the degree of browning in the system, compared to the heated glucose and glycine reaction system alone. These results support the findings of Jokic et al. (2004b) that the integrated polyphenol-Maillard reaction system is more effective in generating humic polymers than the Maillard reaction alone.

The kinds and relative abundance of biomolecules (i.e., sugars, amino acids and polyphenols) substantially vary with natural vegetation, microbial populations and activity, and the environment (Stevenson 1994; Kögel-Knabner 2002). Sources of phenols include lignin degradation, microbial metabolites, plant root exudates and tannins (Stevenson 1994). The type of phenols produced varies substantially with the organisms involved. For instance, lignin degradation by brown-rot fungi gives rise primarily to catechol-type constituents (Filley et al. 2002), whereas the phenols synthesized by fungi such as *E. Nigrum* differ in that they contain resorcinol and resorcinol-type constituents, which do not occur in lignin degradation products (Martin and Haider 1971). Both lignin degradation and microbial synthesis processes give rise to pyrogallol and pyrogallol-type polyhydroxyphenolic acids (Stevenson 1994). It has been shown that there are significant differences in the reactivity of polyphenols in relation to their structure, most importantly the positions and number of the OH groups on the benzene ring (Stone and Morgan 1984b; McBride 1989; Wang and Huang 1994). Stone and Morgan (1984b) found that the diphenols, catechol (ortho-OH group), resorcinol (meta-OH group) and hydroquinone (para-OH group), are able to reduce and dissolve Mn(III, IV) oxide in the following order catechol > hydroquinone > resorcinol. They concluded that the reducing ability of diphenols is based on their ability to form a surface complex with the Mn oxide prior to electron transfer. Thus ortho- and para-OH groups are readily able to form surface complexes with Mn(III, IV) oxide while the formation of surface complexes with a diphenol containing a meta-OH group is much less favourable. Shindo (1992) studied the polymerization of various

polyphenols by birnessite, and found that pyrogallol yields far more humic acid (1145 mg C/g oxide) than catechol (438 mg C/g oxide) or resorcinol (240 mg C/g oxide). Wang and Huang (1994) reported that pyrogallol, with three OH groups directly next to one another, is far more easily cleaved by nontronite (Fe-bearing smectite) than the diphenols, catechol or hydroquinone. This is directly related to the ability of the polyphenol to form direct surface complexes with the mineral surface, which facilitates electron transfer and subsequent cleavage. They concluded that the greater the ease of ring cleavage of a polyphenol, the more CO_2 is released and the more aliphatic fragments are incorporated into the resultant humic substances. Furthermore, Wang and Huang (2000b, 2005) showed the substantial ring cleavage of pyrogallol by birnessite. It remains yet to be studied what effect the kind of polyphenol has on the integrated polyphenol-Maillard reaction humification processes, as Jokic et al. (2004b) only investigated the catechol-glucose-glycine system.

Therefore, the objective of this study was to investigate the effect of two structurally different polyphenols, namely, resorcinol (1,3-dihydroxybenzene) and pyrogallol (1,2,3-trihydroxybenzene) (Fig. 3.3.1), on the integrated polyphenol-Maillard reaction (glucose and glycine) humification pathway as catalyzed by birnessite. This was carried out by examining and comparing the degree of humification and the nature of the reaction products (humic acid and organo-mineral phase) from the Maillard reaction, resorcinol-Maillard, pyrogallol-Maillard, and resorcinol- and pyrogallol-only systems. The ultimate goal is to elucidate the importance of the nature and relative abundance of biomolecules in influencing abiotic humification pathways and related reaction products in natural environments.

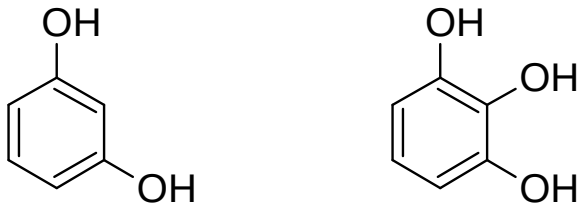

(a) (b)

Figure 3.3.1 Chemical structure of (a) resorcinol and (b) pyrogallol

3.3.2 Materials and Methods

3.3.2.1 Materials

Birnessite (δ-MnO_2) was synthesized according to one of the methods described by McKenzie (1971), which involves slowly adding concentrated HCl to boiling $KMnO_4$. The precipitate was washed by means of repeated filtration using distilled deionized water (henceforth referred to as water) on a 0.1 μm pore Millipore membrane filter, until the wash water tested free from chloride ($AgNO_3$ test). It was then freeze-dried, and finally lightly ground using a mortar and pestle. The synthesized birnessite was characterized by means of X-ray diffraction (XRD) (Rigaku Rotaflex 200SU, Tokyo, Japan), Fourier transform infrared (FTIR) spectroscopy (Bruker Equinox 55, Ettlingen, Germany), C K-edge and Mn L-edge near edge X-ray absorption fine structure (NEXAFS) spectroscopy on SGM (Spherical Grating Monochromator) beamline at the Canadian Light Source (Saskatoon, SK, Canada) and BET specific surface area analysis (Quantachrome Autosorb-1, Syosset, NY, USA) using N_2 gas.

Pyrogallol, resorcinol, D-glucose (Sigma-Aldrich ACS reagent grade >99%) and glycine (Sigma Ultra pure grade >99%) were obtained from Sigma Aldrich Canada Ltd (Oakville, ON, Canada). Pure manganese carbonate and oxides, $MnCO_3$ (99.99%), MnO (>99%), Mn_2O_3 (>99%), MnO_2 (>99%), were obtained from Sigma Aldrich, to use as reference compounds in the XRD and NEXAFS studies. Elliot soil (1S102H) and Florida Peat (1S103H) humic acid standards were purchased from the International Humic Substances Society (IHSS), St. Paul, MN, USA, and used in the C K-edge NEXAFS study.

3.3.2.2 Incubation experiment

Sterile conditions were maintained throughout the experiment in order to establish the role of abiotic processes. All glassware, birnessite, water and apparatus were autoclaved prior to the experiments. In addition to this, thimerasol, an antibacterial agent, was added to each flask (0.02 %, w/v) before any of the reagents were added. Thimerasol does not affect the oxidation process of phenolic compounds (Wang et al. 1983a). In order to investigate the effect of the molar ratio of pyrogallol or resorcinol to Maillard reagents, a number of treatments were employed with increasing amounts (0; 0.00125; 0.0025; 0.0125; 0.0250; 0.0500; 0.1000 moles) of pyrogallol or resorcinol added to a fixed molar ratio of Maillard reagents (0.05 mole glucose + 0.05 mole glycine) using birnessite as catalyst. Two and a half grams of birnessite were

suspended in each of the reaction solutions in a 250 mL flask. There were also selected control treatments in which birnessite was absent, i.e., the pyrogallol or resorcinol only systems (0.05 mole pyrogallol/resorcinol) and the pyrogallol or resorcinol integrated equimolar polyphenol-Maillard system (0.05 mole glucose + 0.05 mole glycine + 0.05 mole pyrogallol/resorcinol). All the reaction systems were adjusted to an environmentally relevant pH 7.0 using 0.1 M HCl or 0.1 M NaOH. The final volume in the flasks was made up to 100 mL using autoclaved water. The flasks were then tightly sealed and placed in a constant temperature water bath at 45° C for a period of 15 days while gently shaking. Forty-five degrees centigrade is an environmentally relevant temperature as it is common in tropical and subtropical areas, and is the approximate temperature of an exposed sunlit soil surface on a day when the ambient air temperature is 25° C (Jury et al. 1991). Therefore, the reaction products formed at 45° C were used for all of the detailed characterization using XRD, FTIR, total C, and C K-edge and Mn L-edge NEXAFS analyses in this study.

To investigate the effect of temperature on humification processes, selected systems (equimolar integrated pyrogallol/resorcinol-Maillard reaction systems with or without birnessite) were also incubated at 25° C for 15 days, and only the pH and pH + pE values of the systems, and Mn concentration and visible absorbance of the supernatants were determined for comparison with the data obtained at 45°C (Table 3.3.1). The rest of the results presented in this study were obtained at 45°C. The absence of microbial growth was verified by culturing aliquots of selected samples at the end of the incubation period. Aerobic microbial growth was tested for by culturing on Tryptocase Soy Agar (TSA) plates, while anaerobic microbial growth was tested for on TSA plates in a BBL GasPak 150 Large Anaerobic System. All cultures were incubated for a period of 5 and 9 days at 28° C (Jokic et al. 2004b). All treatments were performed in triplicate.

3.3.2.3 Characterization of reaction systems at the end of the incubation period and isolation of humic acids

At the end of the reaction period, the final pH and Eh of the suspensions were measured. The samples were then centrifuged at 25,000 g for 40 min to separate the solid residue from the solution. The absorbance of the supernatant was measured between 400 and 600 nm on a UV-visible spectrophotometer (Beckman DU 650 microprocessor controlled spectrophotometer,

Fullerton, CA, USA). The visible absorbance at 400 and 600 nm provides an indication of the extent of polymerization which has taken place in the reaction systems (Shindo and Huang 1982, 1984b). The supernatant was diluted with water prior to absorbance determination and the values obtained were subsequently multiplied by the dilution factor. The Mn content of the supernatant was determined using atomic absorption spectroscopy at 279.5 nm (Varian Spectra AA 220, Walnut Creek, CA, USA).

The solid residue was repeatedly washed with water using centrifugation at 25,000 g for 40 min until the wash water was clear. These water extracts were collected and added to the supernatant. The washed residue was then freeze-dried. The combined washing and supernatant was then acidified to pH 1.0 using 6 M HCl and allowed to stand for 24 h to precipitate the humic acid (HA) fraction out of the solution (Swift 1996). The acidified suspensions were then centrifuged at 25,000 g for 45 min to separate the HA fraction from the rest of the solution containing the fulvic acid (FA) fraction and non-humic substances fraction. The HA residue was then resuspended in a 0.1 M HCl and 0.3 M HF solution and shaken for 48 h. It was then centrifuged again as described before and dialyzed in 1000 molecular weight cut off dialysis tubing for 5 days in distilled deionized water until the water tested free from chloride ($AgNO_3$ test). The purified HA was then freeze-dried. Selected HA samples which were used in the NEXAFS study were not purified using the HCl/HF treatment but were instead dialyzed immediately after being separated by acidification and centrifugation; it was not necessary to remove all the Mn, as its presence does not interfere with XAS studies. Furthermore, the HA samples without the HCl/HF treatment were used in the Mn L-edge NEXAFS studies to investigate the nature of the Mn bonding in the samples.

3.3.2.4 Characterization of the reaction products

Fourier transform infrared (FTIR) spectroscopy. FTIR spectra were obtained from the washed and freeze-dried solid residues and purified HA fractions. This was done by preparing KBr disks containing 1% w/w sample and running it on a Bruker Equinox 55 FTIR (Ettlingen, Germany) connected with a purge gas generator.

X-ray diffraction (XRD). The solid residues, HA and unreacted biomolecules (pyrogallol, resorcinol, glucose and glycine) were examined using X-ray diffractometry on a Rigaku Rotaflex 200SU (Tokyo, Japan) with a rotating Fe anode and graphite monochromator. The samples were

lightly ground and then mounted on glass slides by making a slurry of the ground sample with acetone and allowing it to dry. The scans were performed at 40 kV and 160 mA, from 4 to 80 °2θ, at a step size of 0.02 °2θ at a scanning rate of 0.1 °2θ sec^{-1}.

Total carbon analysis. Total carbon analysis of the solid residues was performed using a dry combustion method on a Leco CR-12 Carbon Analyzer (Leco Corporation, St. Joseph, MI, U.S.A.) as described by Wang and Anderson (1998).

Near edge X-ray absorption fine structure (NEXAFS) spectroscopy. The speciation of C and Mn was investigated in the solid residues and HA fractions from selected reaction systems using C K-edge and Mn L-edge NEXAFS at the Canadian Light Source (Saskatoon, SK, Canada) on the SGM (Spherical grating monochromator) beamline. A number of pure reference compounds (glucose, glycine, pyrogallol, $MnCO_3$, MnO, Mn_2O_3, MnO_2) and IHSS soil and peat HA standards, were also examined. Samples which were investigated for Mn were lightly ground and mounted on carbon tape. Samples which were investigated for C were mounted on 99.99% indium (In) foil or gold (Au)-coated (~400 Å) silicon (Si) wafers. The solid residue samples were mounted on In, by grinding the sample and then pressing the powder into the soft metal, and scraping off the excess. The relatively water soluble samples, i.e., HAs and pure biomolecules, were mounted on the Au-coated Si wafers by making dilute solutions of the samples in distilled deionized water and then placing a droplet on the wafer and allowing it to dry. An exit slit width of 20 μm and a dwell time of 0.1s was used to minimize damage due to exposure to radiation. These spectra were recorded using total electron yield (TEY) at an energy step size of 0.1 eV. The Mn spectra were normalized to the TEY of a gold I_0 mesh which was fixed in front of the sample in the path of the beam. All of the C spectra were normalized to a clean Au-coated Si wafer, so that the signals from C in the beamline and C contamination on the gold I_0 mesh would not interfere with the signal from our samples (Watts et al. 2006). Spectra obtained were analyzed using aXis2000 software (Hitchcock et al. 2005). The energy scale of the C and Mn spectra were internally calibrated using glycine and MnO, respectively, based on calibrated values reported from previous studies (Garvie and Craven 1994; Boese et al. 1997). All the spectra were normalized to each other, with the maximum intensity of each spectrum fixed at 1.

3.3.3 Results

3.3.3.1 Effect of birnessite and incubation temperature on the degree of browning

In all the reaction systems studied, no aerobic or anaerobic microbial growth was observed. Thus, all the processes studied were abiotic in nature. The X-ray diffractogram of the synthesized birnessite (Fig. 3.2.2) had characteristic peaks at 7.21, 3.61 and 2.45 Å (McKenzie 1989). The FTIR spectrum had (Fig. 3.2.3) typical birnessite absorption bands at 3400, 1621, 509 and 466 cm^{-1} (Potter and Rossman 1979). The Mn L-edge NEXAFS spectrum (Fig. 3.2.4) showed that the synthesized birnessite contained predominantly Mn(IV) with some Mn(III), which was also reported by Jokic et al. (2001b), using Mn K-edge X-ray absorption spectroscopy. The BET specific surface area was found to be 63 m^2 g^{-1}, which is characteristic for synthetic birnessite (McKenzie 1971).

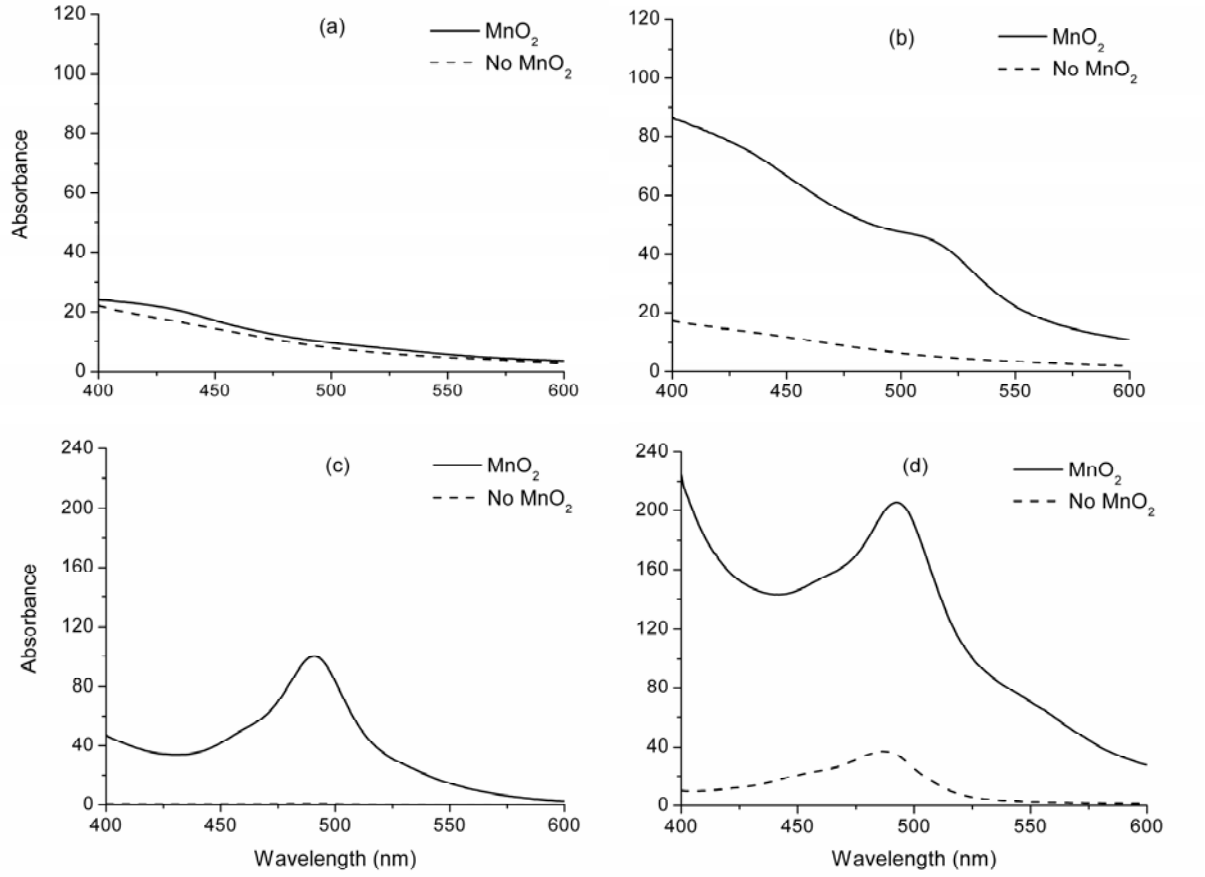

Figure 3.3.2 Comparison of the effect of birnessite on the absorbances of the supernatants of (a) the 0.05 mole pyrogallol only system, (b) the integrated equimolar pyrogallol-Maillard system (0.05 mole glucose + 0.05 mole glycine + 0.05 mole pyrogallol), (c) the 0.05 mole resorcinol only system, (d) the integrated equimolar resorcinol-Maillard system (0.05 mole glucose + 0.05 mole glycine + 0.05 mole resorcinol). The absorbances are scaled by the dilution factor.

The presence of birnessite significantly enhanced humification in the integrated polyphenol-Maillard reaction and resorcinol only systems, as the absorbances (degree of browning) were much greater in the presence than in the absence of birnessite (Figure 3.3.2). The absorbance of the pyrogallol only system (Fig. 3.3.2a) showed the least response to the presence of birnessite. Birnessite had the most dramatic enhancing effect on the degree of browning in the integrated polyphenol-Maillard systems (Fig. 3.3.2b and d) compared to the polyphenol only systems (Fig. 3.3.2a and c). The enhancement of humification in the Maillard reaction system (glucose and glycine) by birnessite at 25° and 45°C was reported by Jokic et al. (2001b).

Temperature also has a substantial influence on browning reactions (Table 3.3.1). The visible absorbances of the pyrogallol- and resorcinol-Maillard reaction systems were much lower in the systems incubated at 25° C than at 45° C, both in the presence and absence of birnessite, indicating that increasing the temperature results in increased abiotic humification reactions. Similarly, Jokic et al. (2004b) studied the equimolar catechol-glucose-glycine system catalyzed by birnessite at 25° and 45° C, and observed enhanced visible absorbance at the higher temperature.

Table 3.3.1 The pH, redox potential (pH + pE), Mn concentration and visible absorbances at 400 and 600 nm of the supernatants of the integrated reaction systems at the equimolar ratio of polyphenol to Maillard reagents incubated at 25° C or 45° C at the end of the 15 day reaction period, in the presence or absence of birnessite.

Reaction system	pH	pH + pE	Mn	Visible absorbance	
			(mmol L^{-1})	400 nm	600 nm
Presence of birnessite					
Pyrogallol-Maillard 25° C	7.04	8.11	16.37	52.63	10.73
Pyrogallol-Maillard 45° C	6.53	7.16	31.83	85.14	12.57
Resorcinol-Maillard 25° C	8.35	10.62	114.49	170.28	18.93
Resorcinol-Maillard 45° C	7.97	7.18	215.67	224.88	26.94
Absence of birnessite					
Pyrogallol-Maillard 25° C	5.08	11.15	*NA	11.60	0.40
Pyrogallol-Maillard 45° C	4.81	10.21	NA	15.89	1.60
Resorcinol-Maillard 25° C	6.45	12.43	NA	0.54	0.03
Resorcinol-Maillard 45° C	6.23	8.60	NA	10.66	3.21

*Not applicable

3.3.3.2 Influence of the molar ratio of polyphenol to Maillard reagents on reactions systems incubated at 45° C in the presence of birnessite

The pyrogallol-Maillard reaction systems had substantially lower final pH values than the resorcinol-Maillard systems (Fig. 3.3.3), which indicated a greater degree of net proton release as a result of oxidative polymerization and the reductive dissolution of birnessite in the pyrogallol systems than in the resorcinol systems. The first three increments of pyrogallol to Maillard reagents (0.00125, 0.0025 and 0.0125 mole of pyrogallol added) resulted in a net final pH that was higher than the starting pH of 7.00 (Fig. 3.3.3). When 0.025 mole pyrogallol was added to the Maillard reagents, there was a net decrease in the final pH of the reaction systems and this trend continued dramatically with increasing amount of pyrogallol present. In contrast, increasing the amount of resorcinol added to Maillard reagents resulted in all the final pH values of the reaction systems being above the starting pH of 7.0 (Fig. 3.3.3), which were within a range of ± 0.5 pH units of the Maillard reaction system's final of pH (8.08). The high final pH of the resorcinol-Maillard systems indicates that the reduction of birnessite, which consumed protons, was the dominant process affecting the pH of the reaction systems.

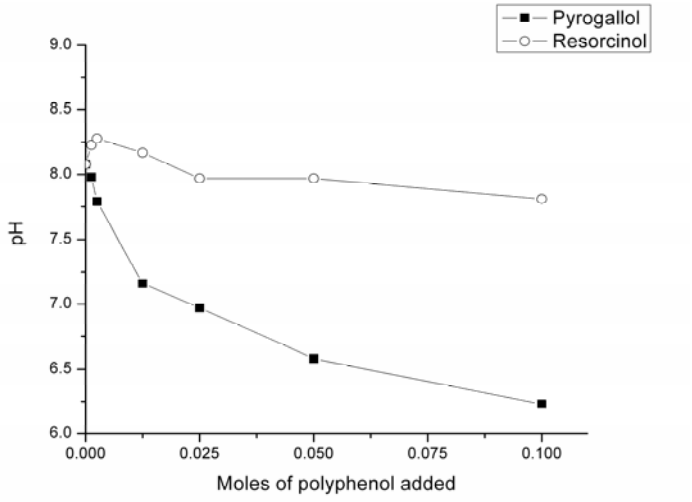

Figure 3.3.3 Comparison of the final pH of the integrated pyrogallol- and resorcinol-Maillard reaction systems, in the presence of birnessite, with increasing amount of polyphenol added. The pH value of the Maillard reaction system was the first point in the reaction system, i.e., 0 mole polyphenol added.

The concentration of Mn in the supernatants of the pyrogallol- and resorcinol-Maillard reaction systems showed significantly different trends (Fig. 3.3.4). Increasing the molar ratio of pyrogallol to Maillard reagents resulted in a dramatic decrease in detectable Mn up until a concentration of 0.025 mole pyrogallol added, and then the Mn concentration flattens out through the 0.05 mole to 0.10 mole pyrogallol treatments. The Mn concentration in the supernatant of the pyrogallol only system (1.6 mmole L^{-1}) was approximately 20 times lower than in the equimolar pyrogallol-Maillard reaction system (31.8 mmole L^{-1}) and approximately 120 times lower than the Maillard reaction system (193.1 mmole L^{-1}). Increasing the molar ratio of resorcinol to Maillard reagents initially resulted in a decrease in the concentration of Mn in the supernatant and then in a dramatic increase in the Mn concentration after the addition of 0.0125 mole or higher amount of resorcinol. The Mn concentration in the supernatant of the resorcinol only system (32.7 mmole L^{-1}) was approximately 7 times lower than in the equimolar resorcinol-Maillard reaction system (215.7 mmole L^{-1}) and 6 times lower than the Maillard reaction system (193.1 mmole L^{-1}).

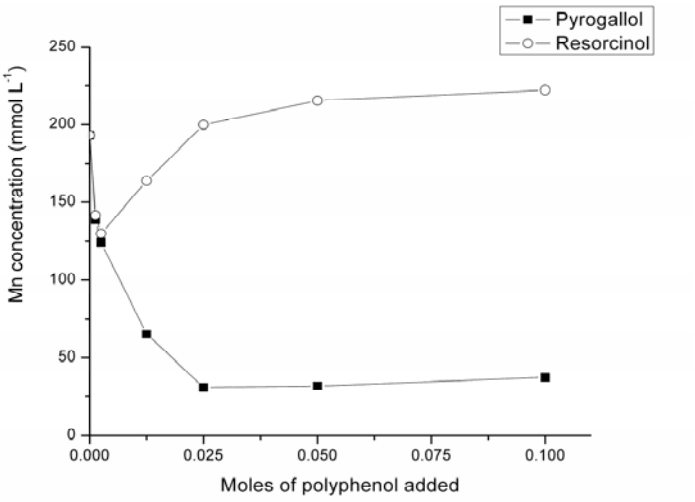

Figure 3.3.4 Comparison of the Mn concentrations in the supernatants of the integrated pyrogallol- and resorcinol-Maillard reaction systems, in the presence of birnessite, with increasing amount of polyphenol added. The Mn concentration of the supernatant in the Maillard reaction system was the first point in the reaction system, i.e., 0 mole of polyphenol added.

Both systems showed the trend of increased visible absorbance with increasing amount of polyphenol added (Fig. 3.3.5). The supernatant of the resorcinol-Maillard reaction systems had a

greater overall visible absorbance than that of the pyrogallol-Maillard reactions systems. These results would appear contrasting to the pH data (Fig. 3.3.3), which indicated that, compared with the resorcinol systems, the pyrogallol systems had a net greater degree of proton release as a result of oxidative polymerization of polyphenol and reduction of birnessite. However, as will be shown later, most of the polymers formed in the resorcinol systems remained suspended in the supernatants of these systems, whereas in the pyrogallol systems substantial amounts of the polymers precipitated and were found in the solid phase complexed with Mn(II).

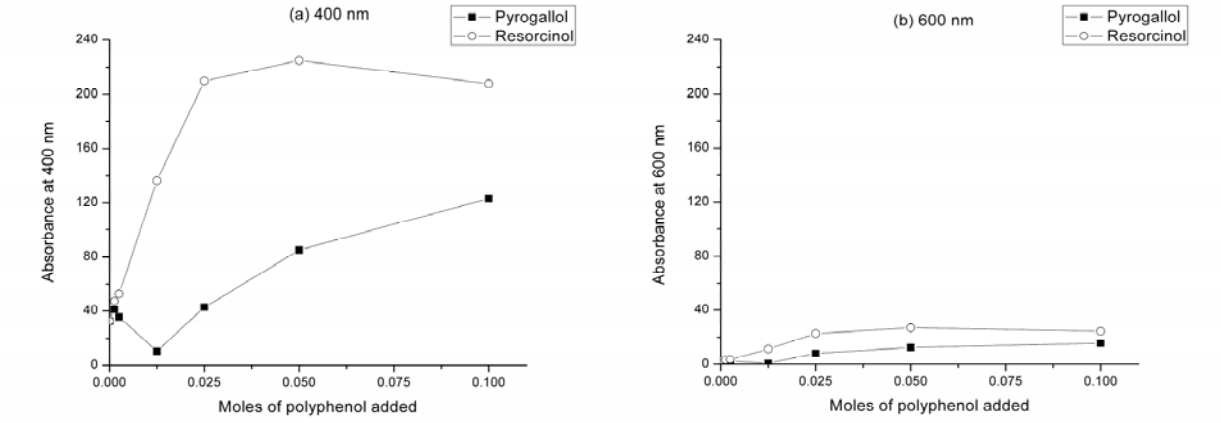

Figure 3.3.5 Comparison of the absorbances at 400 and 600 nm of the integrated pyrogallol- and resorcinol-Maillard reaction systems formed in the presence of birnessite with increasing amount of polyphenol added to the system. The absorbance of the supernatant in the Maillard reaction system was the first point in the reaction systems, i.e., 0 mole of polyphenol added. The absorbances are scaled by the dilution factor.

3.3.3.3 Characterization of reaction products from reaction systems incubated at 45° C in the presence of birnessite

(i) Solid phase

X-ray diffraction

The solid residue from the Maillard reaction system (Fig. 3.3.6a) clearly shows the formation of crystalline $MnCO_3$ (rhodochrosite) with typical d-values of 3.67, 2.84, 2.18 and 1.76 Å (Joint Committee on Powder Diffraction Standards 1974). There was a subsequent decrease in the amount and crystallinity of the $MnCO_3$ formed with the introduction of pyrogallol (Fig. 3.3.6b) into the system. When the amount of pyrogallol in the pyrogallol-Maillard reaction system was increased to 0.025 moles or higher, there was an abrupt

disappearance of a crystalline reaction product (Fig. 3.3.6c-d). The diffractogram of the solid residue from the pyrogallol only reaction system (Fig. 3.3.6e) shows evidence of some poorly crystalline $MnCO_3$ (2.84 Å). The broad band at approximately 3.8 Å seen in the humic substances extracted from the supernatant of the 0.05 mol pyrogallol integrated system (Fig. 3.3.6f), can be clearly seen in the 0.025 and 0.05 mol pyrogallol integrated (Fig. 3.3.6c, d) and 0.05 pyrogallol only systems (Fig. 3.3.6e). This band was also observed by Wang and Huang (2000b) in the pyrogallol-derived humified solid residue as catalyzed by birnessite and other metal oxides, and is mainly attributed to the polyaromatic structure of humic substances (Pollack et al. 1971).

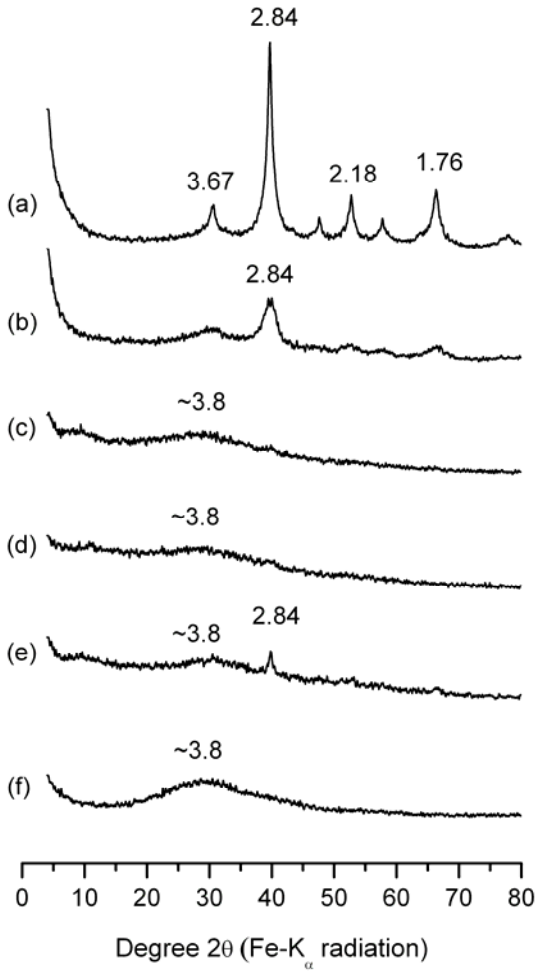

Figure 3.3.6 X-ray diffractograms of the solid residues formed in the presence of birnessite from the (a) Maillard reaction system; the integrated pyrogallol-Maillard reaction systems with: (b) 0.0025 mole pyrogallol, (c) 0.025 mole pyrogallol, (d) 0.05 mole pyrogallol; and (e) 0.05 mole pyrogallol only; and (f) non-purified humic acid from the supernatant of the 0.05 mole pyrogallol integrated system. The d-values are indicated in angstrom.

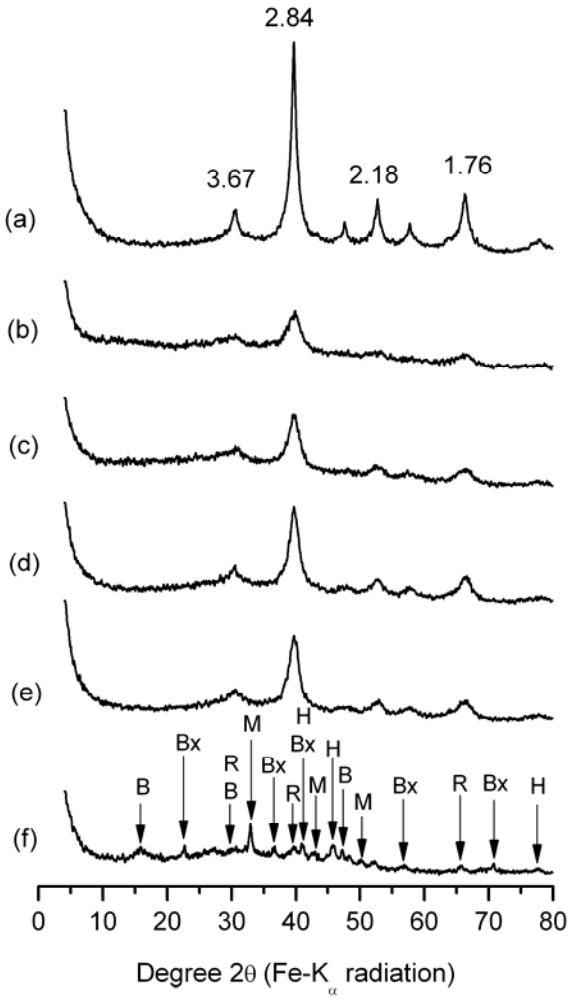

Figure 3.3.7 X-ray diffractograms of the solid residues formed in the presence of birnessite from (a) the Maillard reaction; the integrated resorcinol-Maillard reaction systems with: (b) 0.0025 mole resorcinol, (c) 0.025 mole resorcinol, (d) 0.05 mole resorcinol, (e) 0.10 mole resorcinol; and (f) 0.05 mole resorcinol only system. The d-values are indicated in angstrom. B = birnessite (~7.2, 3.61, 2.45 Å), Bx = bixbyite (4.94, 3.84, 2.72, 1.66 Å), R = rhodochrosite (3.67, 2.84, 1.76 Å), M = manganite (3.41, 2.64, 2.28 Å), and H = hausmannite (2.77, 2.49, 1.54 Å).

The $MnCO_3$ formation trend in the integrated resorcinol-Maillard reaction systems (Fig. 3.3.7) is in contrast to that observed in the pyrogallol-Maillard reaction systems. In the resorcinol-Maillard reaction system, the addition of 0.0025 mole of resorcinol decreased the formation of $MnCO_3$; however, a further increase in the amount of resorcinol added promoted the formation of crystalline $MnCO_3$ as indicated by the intensity of the characteristic peaks of $MnCO_3$ (Fig. 3.3.7b-e). The resorcinol only system (Fig. 3.3.7f) shows evidence of a number of

relatively poorly crystalline Mn(II), Mn(III) and Mn(IV) mineral species: rhodochrosite ($MnCO_3$) at 3.67, 2.84 and 1.76 Å, hausmannite (Mn_3O_4, a mixed Mn(II)/Mn(III) oxide) at 2.77, 2.49 and 1.54 Å, manganite (γ-MnO(OH)) at 3.41, 2.64 and 2.28 Å, synthetic bixbyite (Mn_2O_3) at 4.94, 3.84, 2.72 and 1.66 Å, and birnessite (δ-MnO_2) at ~7.2, 3.61 and 2.45 Å (McKenzie 1989). The XRD results clearly show that resorcinol (Fig. 3.3.7f) was not able to reduce birnessite as strongly as pyrogallol (Fig. 3.3.6e) or the Maillard reagents (Fig. 3.3.7a), and thus birnessite was not completely reduced to Mn(II) as in the pyrogallol and Maillard reaction systems.

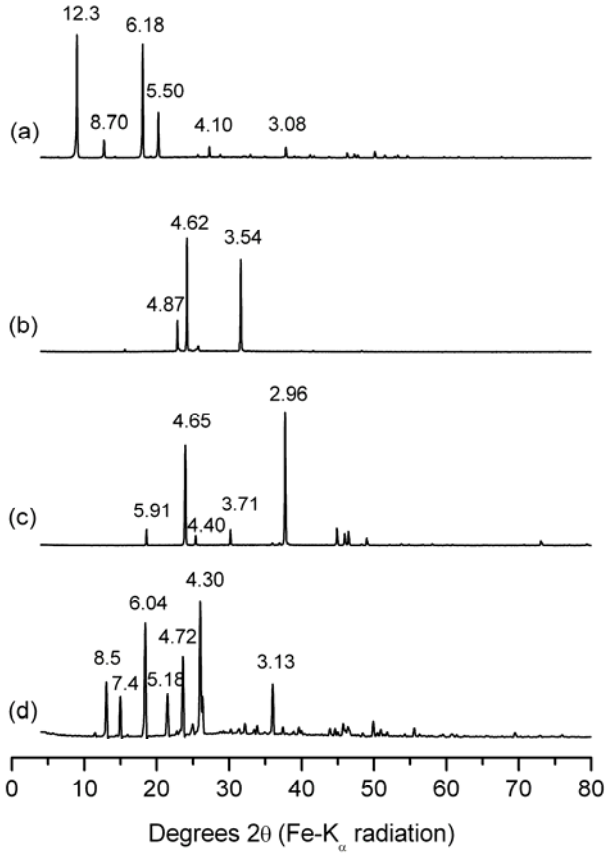

Figure 3.3.8 X-ray diffractograms of unreacted biomolecules: (a) pyrogallol, (b) resorcinol, (c) glycine and (d) glucose. The d-values are indicated in angstrom.

The X-ray diffractograms of the unreacted biomolecules (pyrogallol, resorcinol, glycine and glucose) are shown in Fig. 3.3.8. The XRD spectra of the solid residues from the pyrogallol-Maillard and pyrogallol only systems (Fig. 3.3.6b-e) show that the resultant organic materials are heterogeneous and amorphous in nature, unlike the highly crystalline starting materials (Fig.

3.3.8a-d). The spectrum of the unreacted pyrogallol (Fig. 3.3.8a) shows the typical pyrogallol d-values at 12.3, 8.70 and 5.50 Å (International Centre for Diffraction Data 2006). In addition, there was a crystalline product present which has been identified as poly[(phenyl-p-phenylene)-co-(terephthalate)-co-(p-hydroxy-benzoate)] with d-values of 12.3, 6.18, 4.10 and 3.08 Å (International Centre for Diffraction Data 2006), which was probably formed as a result of pyrogallol transformation in reaction to the heat of the X-rays. Resorcinol (Fig. 3.3.8b), glycine (Fig. 3.3.8c) and glucose (Fig. 3.3.8d) show their respective typical d-values (International Centre for Diffraction Data 2006) and did not appear to be affected by the X-rays.

Total carbon analysis

A comparison of the total C contents of the solid residues from the integrated pyrogallol- and resorcinol-Maillard reaction systems formed in the presence of birnessite is shown in Table 3.3.2. It is important to note that pure $MnCO_3$ has a lower total C content (10.4%) than humic substances, such as fulvic acid (FA) (45.7%) and humic acid (HA) (56.2%) (Schnitzer 1978) or biomolecules such as glycine (31.9%), glucose (40.0%), pyrogallol (57.1%) or resorcinol (65.5%), which helps to explain the trends observed in the total C contents of the solid residues. The solid residues from the Maillard reaction had the lowest total C content (13.1%), which is close to that of pure $MnCO_3$, and this is strongly supported by the XRD data (Fig. 3.3.6a) indicating the presence of crystalline $MnCO_3$. Overall, the solid residues from the resorcinol-Maillard and resorcinol only systems had lower total C contents than the pyrogallol-Maillard and pyrogallol only systems, which again can be related to the extent of $MnCO_3$ formation in the systems, as indicated by XRD (Fig. 3.3.6 and 3.3.7). The pyrogallol systems had an increasing percentage of C in the solid residues with increasing amount of pyrogallol added up to 0.025 mole and thereafter the total C content virtually remained unchanged. This trend is in accord with the XRD (Fig. 3.3.6a-d) data, which indicate an abrupt disappearance of $MnCO_3$ after 0.0025 mole of pyrogallol added in the integrated pyrogallol-Maillard systems and thus higher total C contents are expected due to organic residues. The resorcinol system shows an opposite trend after the 0.025 mole resorcinol treatment, with the percentage of C decreasing in the solid residue. This is also in agreement with the XRD data (Fig. 3.3.7a-e) of the resorcinol solid residues which indicate increasing amounts of $MnCO_3$ formed with increasing amount of resorcinol in the system. The solid residue from the pyrogallol only system was shown to contain

some $MnCO_3$ (Fig. 3.3.6e) and hence has a slightly lower total C content (Table 3.3.2) than the pyrogallol-Maillard systems which contain trace amounts or no $MnCO_3$ (Fig. 3.3.6c-d). The resorcinol only system contained a lower total C content (15.3%) than the resorcinol-Maillard reaction systems (Table 3.3.2) which is probably as a result of the presence of significant amounts of the Mn(II), Mn(III) and Mn(IV) oxides (Fig. 3.3.7f).

Table 3.3.2 Comparison of total carbon contents of solid residues from the Maillard reaction, polyphenol-Maillard, and polyphenol only reaction systems formed in the presence of birnessite

Treatment	Total C content (%)	
	Pyrogallol	Resorcinol
Maillard reaction (0.05 mole glucose + 0.05 mole glycine)	13.1	13.1
Polyphenol-Maillard reaction with 0.0025 mole polyphenol	19.8	22.0
Polyphenol-Maillard reaction with 0.025 mole polyphenol	32.6	27.1
Polyphenol-Maillard reaction with 0.05 mole polyphenol	32.1	20.9
Polyphenol-Maillard reaction with 0.1 mole polyphenol	32.3	17.4
0.05 mole polyphenol	30.8	15.3

FTIR spectroscopy

The FTIR spectra of the solid residues from the Maillard reaction, polyphenol only and selected polyphenol-Maillard reaction systems are shown in Fig. 3.3.9 and 3.3.10. Comprehensive assignments of the absorption peaks are provided in Table 3.3.3. The FTIR spectra of the solid residues from these systems are in agreement with XRD and NEXAFS data of these systems (Fig. 3.3.6, 3.3.7, 3.3.11 and 3.3.12). The FTIR spectra also show that organic substances in the solid residues of the resorcinol-Maillard reaction systems (Fig. 3.3.10b-e) appear to be very similar to those found in the solid residue of the Maillard reaction system (Fig. 3.3.10a). The organic substances found in these systems appear to be dominated by carboxylic functional groups, predominantly in the deprotonated state, as indicated by symmetric (1594 cm^{-1}) and antisymmetric (1408 cm^{-1}) COO^- stretch absorption bands. In contrast to the resorcinol-Maillard reaction systems (Fig. 3.3.10b-e), the resorcinol only system contained humic substances with a significantly aromatic character as indicated by the strong absorption band at 1613 cm^{-1} (Fig. 3.3.10f).

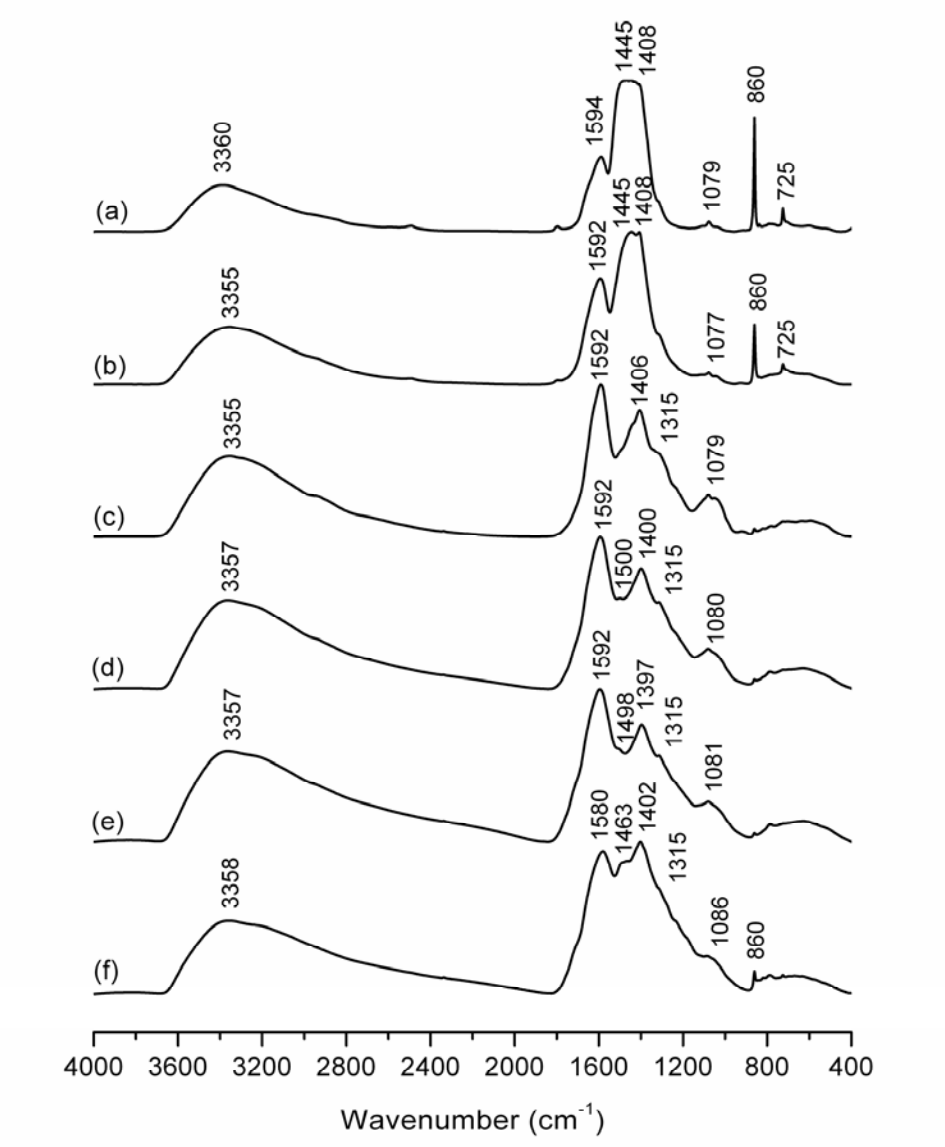

Figure 3.3.9 FTIR spectra of the solid residues formed in the presence of birnessite from (a) the Maillard reaction system (0.05 mole glucose + 0.05 mole glycine); (b-e) the integrated pyrogallol-Maillard reaction systems with: (b) 0.0025 mole pyrogallol, (c) 0.025 mole pyrogallol, (d) 0.05 mole pyrogallol, (e) 0.1 mole pyrogallol; and (f) the 0.05 mole pyrogallol only system.

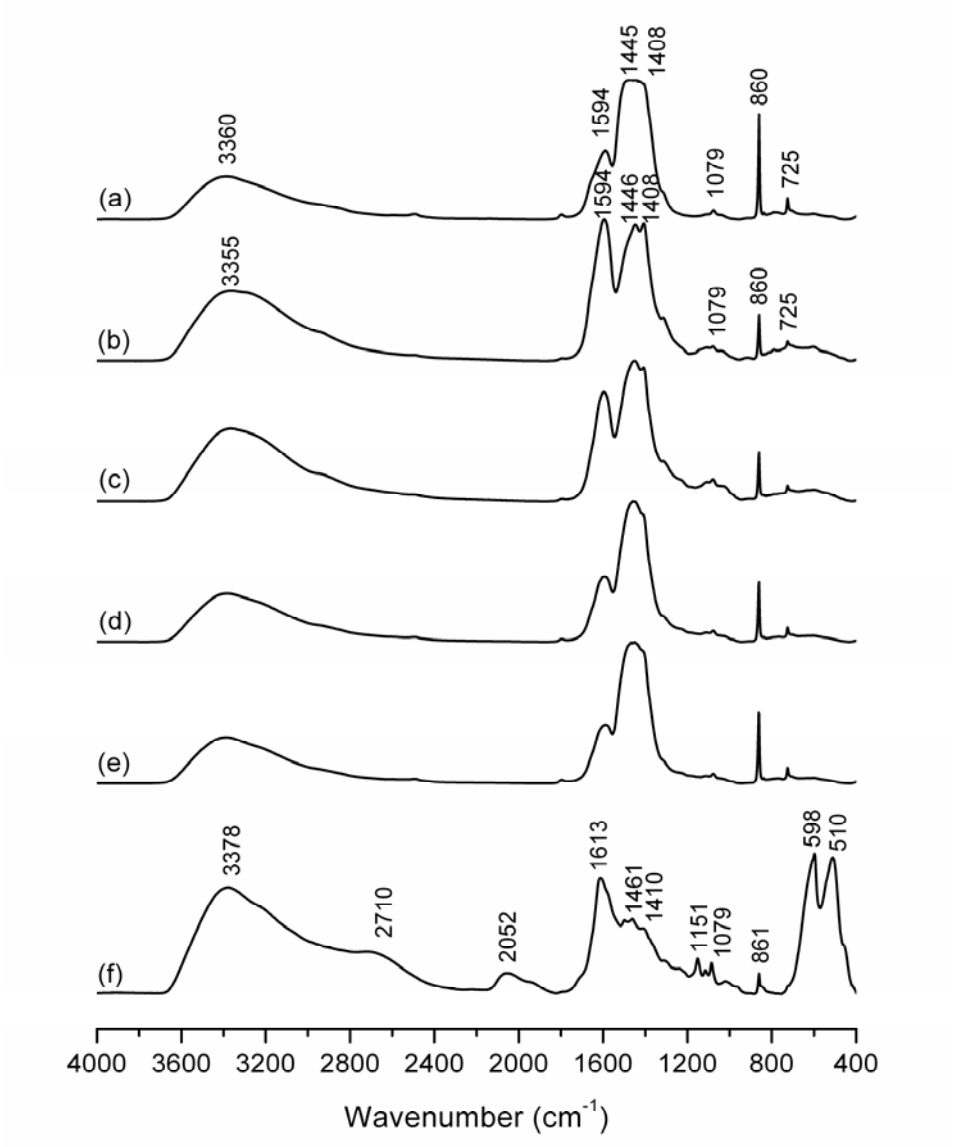

Figure 3.3.10 FTIR spectra of the solid residues formed in the presence of birnessite from (a) the Maillard reaction system (0.05 mole glucose + 0.05 mole glycine); (b-e) the integrated resorcinol-Maillard reaction systems with: (b) 0.0025 mole resorcinol, (c) 0.025 mole resorcinol, (d) 0.05 mole resorcinol, (e) 0.1 mole resorcinol; and (f) the 0.05 mole resorcinol only system.

Table 3.3.3 Assignments of FTIR absorption bands of the solid residues of the Maillard, integrated pyrogallol-Maillard and resorcinol-Maillard reaction, and pyrogallol and resorcinol only systems. Interpretation is based on previous works (van der Merel and Beutelspacher 1976; Stevenson 1994; Silverstein et al. 2004)

Fig. 3.3.9 (a) and (b) Maillard reaction and pyrogallol-Maillard systems with 0.0025 mole pyrogallol		**Fig. 3.3.9 (c), (d) and (e) Pyrogallol-Maillard systems with 0.025, 0.05 and 0.10 mole pyrogallol**		**Fig. 3.3.9 (f) 0.05 mole pyrogallol only system**		**Fig. 3.3.10 (b), (c), (d) and (e) † Resorcinol-Maillard systems with 0.0025, 0.025, 0.05 and 0.10 mole resorcinol**		**Fig. 3.3.10 (f) 0.05 mol resorcinol only system**	
Wavenumber (cm^{-1})		**Wavenumber (cm^{-1})**		**Wavenumber (cm^{-1})**		**Wavenumber (cm^{-1})**		**Wavenumber (cm^{-1})**	
725	Carbonate C-O out of plane bend (rhodochrosite)	1079-1081	Aliphatic C-O stretching	860	Carbonate C-O stretch (rhodochrosite)	725	Carbonate C-O out of plane bend (rhodochrosite)	510, 598	Mn-O vibrations * (manganite, hausmannite)
860	Carbonate C-O stretch (rhodochrosite)	1315	C-O stretch and bending of COOH	1086	Carbonate C-O stretch (rhodochrosite)	860	Carbonate C-O stretch (rhodochrosite)	861, 1079	Carbonate C-O stretch (rhodochrosite)
1077-1079	Carbonate C-O stretch (rhodochrosite)	1397-1406	Asymmetrical COO^- stretch, C-H deformation of CH_2 & CH_3, OH deformation of phenols	1315	C-O stretch and bending of COOH	1077-1079	Carbonate C-O stretch (rhodochrosite)	1151	Mn-O vibrations (manganite, hausmannite)
1408	Asymmetric COO^- stretch, C-H deformation of CH_2 & CH_3, OH deformation of phenols	1498-1500	NH_3^+ symmetrical bending band, aromatic C=C stretch	1402	Asymmetric COO^- stretch, C-H deformation of CH_2 & CH_3, OH deformation of phenols	1408	Asymmetrical COO^- stretch, C-H deformation of CH_2 & CH_3, OH deformation of phenols	1410	Asymmetric COO^- stretch, C-H deformation of CH_2 & CH_3, OH deformation of phenols
1445	Carbonate symmetric C-O stretch (rhodochrosite), asymmetrical bending of CH_2 & CH_3	1592	Symmetric COO^- stretch, N-H deformation + C=N amide II band	1463	Carbonate symmetric C-O stretch (rhodochrosite), Asymmetrical bending of CH_2 & CH_3	1446	Carbonate symmetric C-O stretch (rhodochrosite), asymmetrical bending of CH_2 & CH_3	1461	Carbonate symmetric C-O stretch (rhodochrosite), asymmetrical bending of CH_2 & CH_3
1594	Symmetric COO^- stretch, N-H deformation + C=N amide II band	3355-3358	OH stretch	1580	Symmetric COO^- stretch	1594	Symmetric COO^- stretch, N-H deformation + C=N amide II band	1613	C=C aromatic ring stretch, symmetric COO^- stretch
3360	OH stretch			3358	OH stretch	3355	OH stretch	2052, 2710	Ketone, aldehyde
								3378	OH stretch

*Presence of trace amounts of birnessite

†Fig. 3.3.9 (a) Maillard reaction is the same as Fig. 3.3.10 (a)

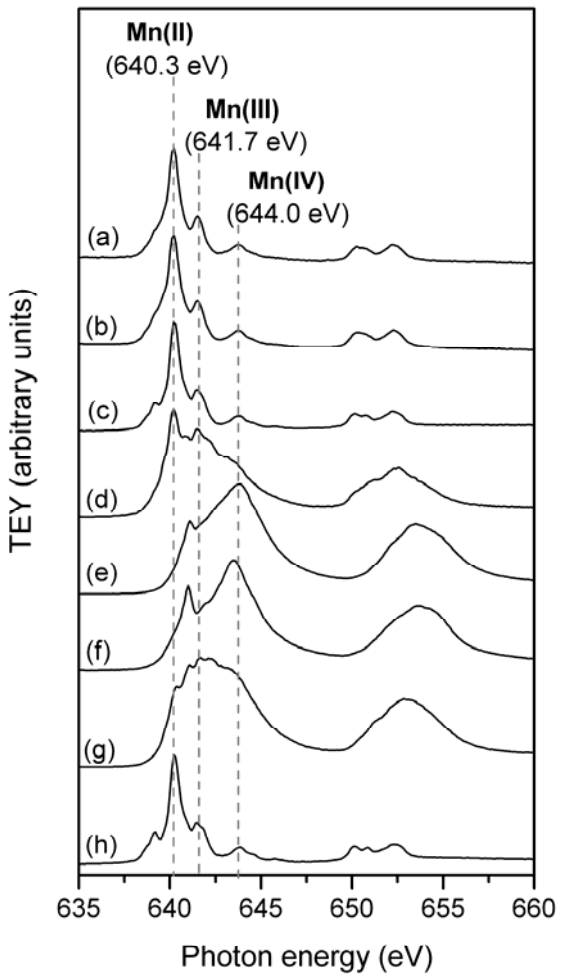

Figure 3.3.11 Mn $L_{2,3}$-edges NEXAFS spectra of solid residues formed in the presence of birnessite from selected integrated polyphenol-Maillard reaction and polyphenol only reaction systems, and pure Mn oxide and carbonate mineral standards: (a) equimolar pyrogallol-Maillard (b) pyrogallol only, (c) equimolar resorcinol-Maillard, and (d) resorcinol only reaction systems, and (e) MnO_2, (f) unreacted birnessite, (g) Mn_2O_3 and (h) $MnCO_3$. The dotted lines indicate the photon energy of the maximum absorption peak of Mn in divalent, trivalent or tetravalent states, on the Mn L_3 edge.

Manganese L-edge NEXAFS spectroscopy

The Mn $L_{2,3}$-edges NEXAFS spectra of the solid residues from selected pyrogallol, resorcinol, and integrated pyrogallol- and resorcinol-Maillard systems, as well as, reference di-, tri- and tetra-valent Mn oxide and carbonate compounds are shown in Figure 3.3.11. The Mn $L_{2,3}$-edges spectra of the solid residues from the pyrogallol only, equimolar pyrogallol- and resorcinol-Maillard reaction systems show that Mn was principally in the divalent form in these systems (Fig. 3.3.11a-c). The spectra of the solid residues from the equimolar pyrogallol-

Maillard reaction system (Fig. 3.3.11a) and pyrogallol only system (Fig. 3.3.11b) look similar to each other, in that the minor absorption peak to the left of the maximum absorption peak is not resolved, compared to pure $MnCO_3$ (Fig. 3.3.11h). This corresponds to Mn(II) that is covalently bonded to either O or N and in octahedral conformation (Grush et al. 1996), indicating that the Mn(II) in the solid residues from the pyrogallol systems (Fig. 3.3.11a, b) is covalently bonded to humic polymers. However, the spectrum of the solid residue of the equimolar resorcinol-Maillard system (Fig. 3.3.11c) looks more similar to that of pure $MnCO_3$ (Fig. 3.3.11h), which is in accord with the XRD data (Fig. 3.3.7d) showing that the solid residue consisted predominantly of $MnCO_3$ and some humic substances. The resorcinol only system residue (Fig. 3.3.11d) appears to be a mixture of Mn(II) and Mn(III), with possibly a small amount of (MnIV) present. This is also in agreement with the XRD (Fig. 3.3.7f) data which show the presence of a mixture of Mn(II), Mn(III) and Mn(IV) minerals.

Carbon K-edge NEXAFS spectroscopy

The C K-edge NEXAFS spectra of the solid residues from the Maillard reaction, pyrogallol only and pyrogallol-Maillard reaction systems are shown in Figure 3.3.12. Spectroscopic assignments are based on the absorption maxima of the reference compounds (glucose, glycine and pyrogallol) and on values reported by previous C NEXAFS studies (Myneni 2002; Urquhart and Ade 2002; Dhez et al. 2003; Cooney and Urquhart 2004; Hitchcock and Mancini 2004). The NEXAFS narrower and sharper core (C 1s) → π* transitions have been found to be the most useful for chemical analyses and identification of organic compounds due to their chemical sensitivity based on the chemical energy shifts (Urquhart and Ade 2002).

The lowest absorption bands at around 284.0 eV usually correspond to molecules with low energy π* states, such as quinones (Francis and Hitchcock 1992). Absorption bands near 285 eV are generally ascribed to C 1s (C-H) → $1\pi^*_{C=C}$ transitions (Urquhart and Ade 2002; Cooney and Urquhart 2004), which are characteristic of C=C unsaturation. The transitions of aromatic C bound to carbonyl (e.g., terephthalate species) tend to overlap with unsaturated aromatic C-H transitions due to the strong electronic interactions between the benzene π* density and carbonyl π* density, and are generally found in the 284.4-285.0 eV range (Cooney and Urquhart 2004). The absorption bands near 286-288 eV are characteristic of functionalized aromatic groups C 1s (C-R) → $1\pi^*_{C=C}$ transitions (R = functional group), such as aromatic C bound to aldehyde (286.0

eV), ketone (286.4 eV), urea (286.4 eV), carbamate (286.6-286.8 eV), amine (286.8-286.9 eV), phenol (287.0-287.3 eV) and ester (287.1 eV) groups (Urquhart and Ade 2002; Dhez et al. 2003; Cooney and Urquhart 2004; Hitchcock and Mancini 2004). Heterocyclic N compounds C 1s (C-N) → $1\pi^*_{C=C}$ transitions also occur in the ~286-287 eV range, e.g., pyridine (285.7 eV) and pyrrole (286.3 eV) (Dhez et al. 2003; Hitchcock and Mancini 2004). The C=N and C≡N π^* transitions usually occur around 286.3 eV (Myneni 2002). Generally speaking, a stronger electron withdrawing substituent on the aromatic ring, will result in a higher energy shift of the C 1s (C-R) → $1\pi^*_{C=C}$ transition.

The carbonyl C 1s (C-R) → $1\pi^*_{C=O}$ transitions usually occur between 286-291 eV, and can be used to distinguish between groups such as aldehydes (286.2-286.4 eV), ketones (286.6-286.8 eV), amide (287.8-288.2 eV), acetic/acetate (288.1-288.6 eV), urea (289.2-289.8 eV), carbamate (289.9.0-290.1 eV) and carbonate (290.2-290.6 eV) (Urquhart and Ade 2002). The main cause of the shifts observed in C 1s (C-R) → $1\pi^*_{C=O}$ transitions is the inductive effect of the neighbouring atoms on the carbonyl C 1s binding energy (Urquhart and Ade 2002). Low lying σ^* orbitals also provide valuable information in identifying aliphatic functionalities. Saturated aliphatic C exhibits C 1s (C-H) → σ^*_{C-H} transitions in the 287.1-287.9 eV range, while aliphatic alcohol C 1s (C-H) → σ^*_{C-O} transitions are found shifted to a higher energy in the 289.2-289.5 eV range (Dhez et al. 2003).

The C K-edge NEXAFS spectra of the solid residue from the Maillard reaction system (Fig. 3.3.12a) clearly show that carbonate C=O (290.2 eV) and carboxylic C=O (acetic/acetate, i.e., aliphatic) (288.6 eV) are the dominant functionalities present, which is in agreement with the FTIR data (Fig. 3.3.9a). As shown by the XRD (Fig. 3.3.6b-d) data, increasing the molar ratio of pyrogallol to Maillard reagents resulted in a decrease in $MnCO_3$ in the integrated pyrogallol-Maillard reaction system (Fig. 3.3.12b-e). Furthermore, it can be seen that the organic substances in the solid residues of the pyrogallol-Maillard and pyrogallol only systems (Fig. 3.3.12c-f) were dominated by aliphatic carboxylic C=O functionalities (288.6 eV). They also contained some aromatic functionalities, including quinone (284.0 eV), aromatic C-H (285.0-285.3 eV), possibly aromatic C bound to ketone, O or N (including heterocyclic N) (286.4 eV), and phenolic (287.0-287.1 eV) groups. It is also interesting to note that the dominant functional group of glucose, which is aliphatic alcohol groups (289.4 eV), is not evident in any of the spectra from the solid residues.

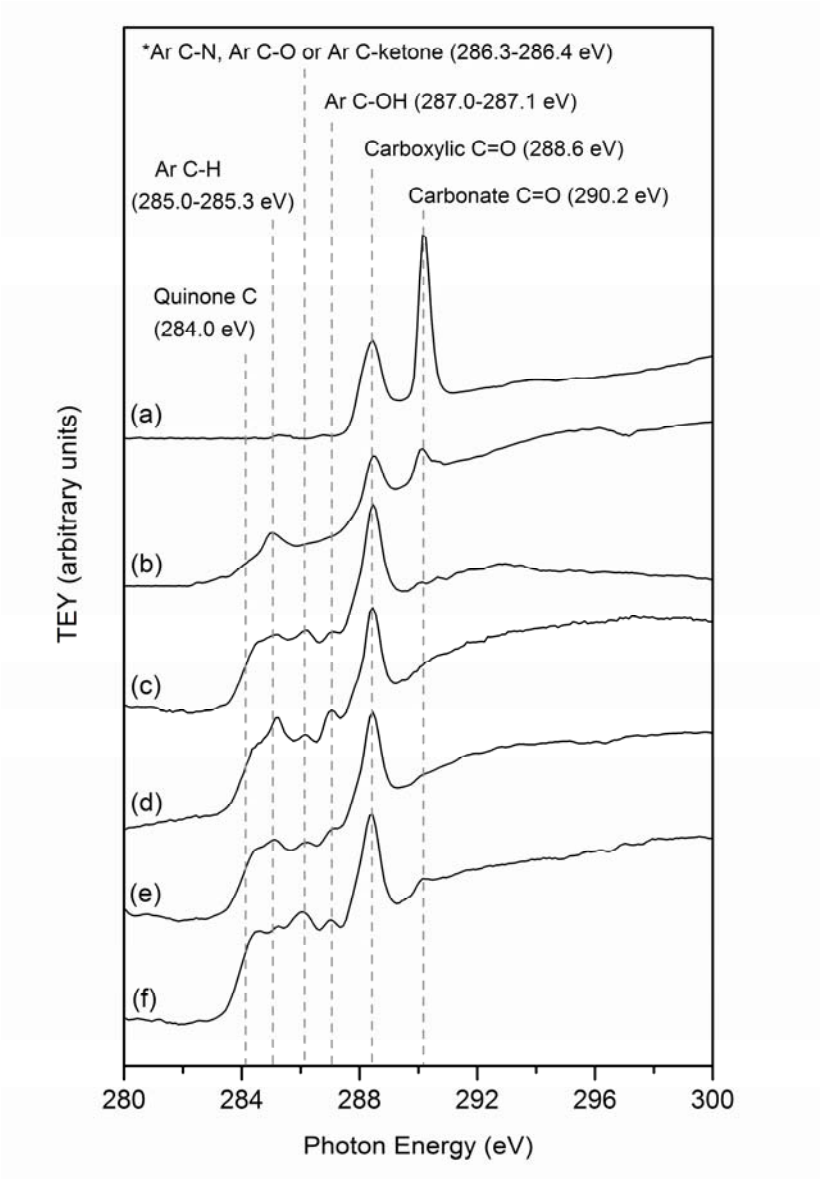

Figure 3.3.12 Carbon K-edge NEXAFS spectra of solid residues formed in the presence of birnessite in (a) the Maillard reaction system (0.05 mole glucose + 0.05 mole glycine); and selected pyrogallol-Maillard reaction systems with: (b) 0.0025 mole pyrogallol, (c) 0.025 mole pyrogallol, (d) 0.05 mole pyrogallol and (e) 0.1 mole pyrogallol; and (f) 0.05 mole pyrogallol only system. *Ar = aromatic.

(ii) Humic acid fraction isolated from supernatant

Carbon K-edge NEXAFS spectroscopy

The C K-edge NEXAFS spectra of the peat and soil HA standard materials of the International Humic Substance Society (IHSS) and the HA isolated from the supernatant of selected reaction systems (Maillard reaction, pyrogallol- and resorcinol-Maillard, pyrogallol and

resorcinol only) are shown in Fig. 3.3.13. The HA isolated from the supernatant of the Maillard reaction system were dominated by carboxylic type C (288.5-288.6 eV), and also contained aromatic C-H functionalities (285.0-285.3 eV) and possibly either aromatic ketone, aromatic C bound to N (including heterocyclic N) or other aromatic C bound to O functional groups (286.3-286.4 eV) (Fig. 3.3.13c). The spectra of the pyrogallol-Maillard and pyrogallol only systems (Fig. 3.3.13d-f) show more broad and less defined peaks than the Maillard (Fig. 3.3.13c) and resorcinol systems (3.3.13g-i), which indicates that the HA formed in the pyrogallol systems is more heterogeneous in nature than the Maillard reaction and resorcinol systems. The pyrogallol systems were dominated by aromatic C-H, phenolic and carboxylic C (Fig. 3.3.13d-f). The peaks of the quinone (284.0 eV) and aromatic C bound to ketone, N or O (286.3-286.4 eV) are more prominent in the HAs from the pyrogallol systems (Fig. 3.3.13d-f) than the resorcinol systems (Fig. 3.3.13g-i). Increasing the amount of pyrogallol in the pyrogallol-Maillard reaction system from 0.05 mole to 0.10 mole did not result in a significant change in the nature of the humic acid (Fig 3.3.13d and e). The HAs from the pyrogallol only system (Fig. 3.3.13f) appear to have a stronger presence of aromatic C bound to ketone or O than the HAs from the pyrogallol-Maillard reaction systems (Fig 3.3.13d and e). The resorcinol-containing systems' HA spectra (Fig.3.3.13g-i) show sharper peaks, indicative of more homogeneous reaction products, which are dominated by aromatic C-H and phenolic and aliphatic carboxylic C=O functional groups. Increasing the amount of resorcinol in the resorcinol-Maillard system from 0.05 mole to 0.10 mole resulted in a decrease in the intensity of the aliphatic carboxylic C peak at 288.5-288.6 eV (Fig. 3.3.13g and h). The resorcinol only system was also dominated by aromatic C-H and phenolic peaks and contained very little carboxylic C (Fig. 3.3.13i). The pyrogallol only system (Fig. 3.3.13f) contained more carboxylic C than the resorcinol only system (Fig. 3.3.13i).

The C K-edge NEXAFS spectra of the IHSS soil and peat HAs (Fig. 3.3.13a and b) look basically similar to the HAs isolated from the Maillard reaction and pyrogallol-Maillard reaction systems in that they contain quinone, aromatic C, functionalized aromatic C and carboxylic C. Similar to the spectra of the natural HAs (Fig. 3.3.13a and b), the spectra of the HA from the Maillard reaction system (Fig. 3.3.13c) is also dominated by carboxylic C (288.5-228.6 eV). The intensity of the peak between aromatic C-OH and aromatic ketone, aromatic C-N or C-O appears to be lower in the soil HA (Fig. 3.3.13a) compared to the peat HA (Fig. 3.3.13b).

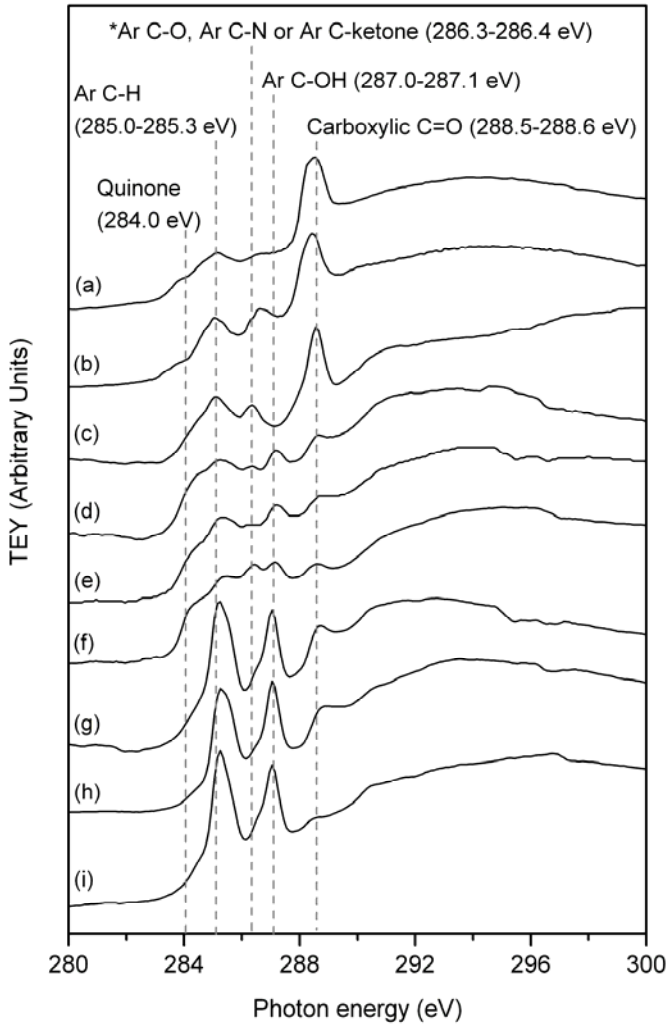

Figure 3.3.13 Carbon K-edge NEXAFS spectra of the IHSS (a) soil and (b) peat humic acids, and the humic acids extracted from the supernatants of reaction systems catalyzed by birnessite: (c) Maillard reaction; pyrogallol-Maillard reaction with: (d) 0.05 mole pyrogallol and (e) 0.10 mole pyrogallol; (f) 0.05 mole pyrogallol only; resorcinol-Maillard reaction with: (g) 0.05 mole resorcinol and (h) 0.10 mole resorcinol; and (i) 0.05 mole resorcinol only system. *Ar = aromatic.

FTIR spectroscopy

The FTIR spectra of the HA isolated from the supernatants of the Maillard reaction, selected polyphenol-Maillard reaction, and polyphenol only reac tion systems are shown in Figure A1 and A2 (Section 6 – appendices). Comprehensive assignments of the absorption bands are provided in Table A1 (Section 6 – appendices). The FTIR results of the HA from these systems support the findings of C NEXAFS analyses of these systems (Fig. 3.3.13).

3.3.4 Discussion

3.3.4.1 Characterization of the reaction systems at the end of the reaction period

Effect of birnessite and temperature

It is well-established that birnessite significantly accelerates the polymerization of polyphenols (Shindo and Huang 1982), as well as, the polycondensation of polyphenols and amino acids (Shindo and Huang 1984b). The surfaces of redox active metal oxides, such as birnessite, are very reactive in promoting the polymerization of phenolic compounds. They can act as oxidants by accepting electrons from hydroxyphenolics, leading to the formation of highly reactive semiquinone radicals which readily undergo coupling reactions with other semiquinones, phenolics, amino acids or existing humus (Huang 2000; Park et al. 2000). Electron transfer between polyphenolics and Mn oxides is facilitated by direct surface complexation of the phenolic OH-group or carboxylic group of the aromatic compound to the surface of the metal oxide. Subsequently, the reduced metal is released into solution, uncovering more metal oxide sites for reaction (Stone and Morgan 1984a, 1984b). Matocha et al. (2001) studied the kinetics of the reduction of birnessite by catechol (*o*-dihydroxybenzene) and confirmed that the reaction occurs and is controlled by precursor surface complex formation, as the electron transfer itself is very rapid. They also confirmed that release of Mn(II) into solution was directly related to *o*-quinone production.

Jokic et al. (2001c) reported that the reaction between D-glucose and glycine is very slow at room temperature due to the high potential energy barrier. Jokic et al. (2001b) showed that birnessite can significantly accelerate the Maillard reaction between glucose and glycine. Furthermore, Jokic et al. (2004b) demonstrated that birnessite significantly enhances humification in the integrated catechol-glucose-glycine system. Our results show that birnessite was able to significantly enhance the degree of browning in the pyrogallol- and resorcinol-glucose-glycine reaction systems (Fig. 3.3.2b and d), as well as moderately enhancing the degree of browning in the resorcinol only system (Fig. 3.3.2c). The pyrogallol only system appeared to show the least response to the presence of birnessite (Fig. 3.3.2a). This could be, in part, due to the highly reactive nature of pyrogallol which enables it to polymerize itself quite readily without the presence of a catalyst such as birnessite. More importantly is the fact that a substantial

amount of humified organic material is found in the solid phase of the birnessite-catalyzed pyrogallol system, based on evidence from the Mn $L_{2,3}$-edges (Fig. 3.3.11b) and C K-edge NEXAFS (Fig. 3.3.12f) data of the solid residues. Thus, the humic substances in the solid phase are not taken into account by visible absorbance readings of the supernatant. The reaction systems in the presence of birnessite had lower final pH + pE (indication of dissolved oxygen in the system) values at the end of the reaction period than the control systems (Table 3.3.1). This is attributed to increased oxidative polymerization of polyphenols which consumes oxygen, as indicated by the visible absorbance values. The systems in the presence of birnessite had higher final pH values (Table 3.3.1) due to the reductive dissolution of birnessite by the biomolecules, glucose, glycine and or pyrogallol/resorcinol, which resulted in the consumption of protons (Eq. 3.3.1).

$$MnO_2 + 4H^+ + 2e^- \rightarrow Mn^{2+} + 2H_2O \text{ ..... } (3.3.1)$$

Temperature was shown to significantly affect the humification processes as indicated in the visible absorbance, pH and pH + pE values of the integrated pyrogallol- and resorcinol-Maillard reactions both in the presence and absence of birnessite (Table 3.3.1). Jokic et al. (2004b) also showed that increasing temperature enhanced the extent of humification in the catechol-glucose-glycine reaction. They found that the E_4/E_6 ratio of humic acid isolated from the supernatant of the system incubated at 25° C was lower (4.46) than that of humic acid produced at 45° C (7.43), which indicated that the humic substances produced at 45° C were more aliphatic in nature and less condensed due to enhanced cleavage at a higher temperature.

Effect of the molar ratio of polyphenol to Maillard reagents on reaction systems incubated at 45° C in the presence of birnessite

Stone and Morgan (1984b) found that polyhydroxyphenolics with OH groups in the *ortho* or *para* positions could form direct surface complexes with Mn (III, IV) oxides much more readily than polyphenols with OH groups in the *meta* position. They determined the relative second-order rate constants for the dissolution of Mn (III, IV) oxide at pH 7.2 by various polyhydroxyphenolics, including catechol (*o*-OH group) 2×10^1 L mol^{-1} s^{-1}, hydroquinone (*p*-OH group) 2.33×10^0 L mol^{-1} s^{-1} and resorcinol (*m*-OH group) 4.9×10^{-3} L mol^{-1} s^{-1}. Direct surface

complexation significantly enhances electron transfer reactions, and subsequently the dissolution of Mn oxide and the formation of free radicals (semi-quinones) which readily participate in polymerization reactions. Thus pyrogallol with three hydroxyl groups all in the *ortho* position to one another would be able to react with birnessite far more readily than resorcinol which has two OH groups in the *meta* position. Shindo (1992) clearly showed that pyrogallol reaction with birnessite yielded more humic polymers than resorcinol reaction with birnessite. This is indicated in our data by the steady decrease in the pH with increasing moles of pyrogallol added in the reaction systems (Fig. 3.3.3). Pyrogallol, which is able to participate in direct electron transfer reactions more readily, has higher polymerization reactivity and thus more protons would be generated in pyrogallol-containing systems. Resorcinol, with an OH group in the *meta* position, is not able to participate in direct electron transfer reactions as readily, which means a lower oxidative polymerization reactivity, and less protons generated. However, in the resorcinol-Maillard reaction system, glucose (a reducing sugar) and glycine are able to carry out the reductive dissolution of birnessite (Jokic et al. 2001b), which consumes protons, and ultimately controls the final pH of the systems. This explains why the final pH values of the resorcinol-Maillard reaction systems were very close to that of the Maillard reaction (Fig. 3.3.3). Furthermore, it is clear that in the resorcinol only system (Fig. 3.3.11d), the extent of reduction of Mn in birnessite to Mn(II) was substantially less, compared with the pyrogallol only, pyrogallol- and resorcinol-Maillard reactions systems (Fig. 3.3.11a-c), as shown by the presence of a mixture of Mn(II), Mn(III) and Mn(IV) oxides in the solid phase of the resorcinol only system (Fig. 3.3.7f and 3.3.11d).

The pyrogallol-Maillard reaction systems with the lowest amounts of pyrogallol (0.00125 and 0.0025 mole) to Maillard reagents (0.05 mole glucose + 0.05 mole glycine) showed a net increase from the starting pH of 7.00 to the pH values of 7.8 to 8.0 which were close to that of the Maillard reactions system (Fig. 3.3.3). This indicates that in these systems the reductive dissolution of birnessite predominantly driven by the Maillard reaction was the dominant process controlling the final pH. Further increase in the amount of pyrogallol added resulted in a net drastic decrease in the pH of the systems, indicating the oxidative polymerization of biomolecules was the dominant process. This is also confirmed by the visible absorbance of the supernatants of pyrogallol-Maillard reaction system (Fig. 3.3.5), where initially there was a decrease in the visible absorbance, but above the 0.0125 mole pyrogallol treatment the increasing

pyrogallol added resulted in a significant and steady increase in the absorbance. This indicates that the addition of a sufficient amount of pyrogallol to Maillard reagents resulted in a large increase in the degree of humification. This trend of the increase of the absorbance with increasing molar ratios of resorcinol to Maillard reagents was also observed (Fig. 3.3.5).

The comparison of trends in the Mn concentration (Fig 3.3.4) and visible absorbance (Fig. 3.3.5) of the supernatants from the pyrogallol- and resorcinol-Maillard reaction systems cannot be properly explained without first discussing the nature of the humic substances formed in these systems, which follows below.

3.3.4.2 Characterization of reaction products from reaction systems incubated at 45° C in the presence of birnessite

Humic substances

Another important impact of the relative ability of pyrogallol and resorcinol to form direct surface complexes with birnessite is aromatic ring cleavage. Wang and Huang (1994) clearly showed that pyrogallol is far more easily cleaved by nontronite (Fe-bearing smectite) than the diphenols, catechol (*o*-dihydroxybenzene) or hydroquinone (*p*-dihydroxybenzene), which is related to their relative ability to form direct surface complexes with the minerals surface. They also concluded that the greater the ease of ring cleavage of a polyphenol, the more CO_2 was released and more aliphatic fragments were incorporated into the resultant humic substances. Furthermore, Wang and Huang (2000b) showed that there was substantial ring cleavage of pyrogallol by birnessite. Increased ring cleavage and the resultant increase in aliphatic fragment incorporation leads to humic substances with more aliphatic nature and more COOH functional groups (Wang and Huang 2000a). These groups have a much higher affinity for binding divalent cations, such as dissolved Mn(II), than phenolic OH groups, and it is well known that COOH functionalities give humic substances most of their cation complexing capacity (Stevenson 1994). The logarithm of the stability constant (K) (μ = 0.1, 25° C) of the complex of glycine and Mn(II) is +2.80, whereas for catechol and Mn(II) its log K is -14.70 (Martell and Smith 2004). This indicates that the humic substances produced in the pyrogallol containing systems, which posses more carboxylic functionalities, would be able to sorb Mn(II) to a much greater extent than polymers with more aromatic or phenolic character. Increased metal complexation would eventually result in the coprecipitation of humic substances out of

solution due to decreased solubility as a result of increase in molecular size and charge neutrality (McBride 1994). Direct evidence for this is provided by the FTIR and C and Mn NEXAFS spectra of the solid residues and the HAs isolated from the supernatant of the pyrogallol-Maillard reaction and pyrogallol only systems in the present study. It is clear that the humified organic substances found precipitated in the solid residues are dominated by carboxylic functional groups (Fig. 3.3.10 and 3.3.12), compared to the HAs from the supernatant (Fig. 3.3.13) which possess a significant aromatic and phenolic character. The Mn L-edge NEXAFS spectra of the equimolar pyrogallol-Maillard reaction and pyrogallol only systems provide further evidence in that the Mn(II) in the solid residue is covalently bonded to either O or N (Fig. 3.3.11a and b). It appears that the solid residues of the pyrogallol-Maillard reaction system containing a concentration of 0.025 mole pyrogallol or above (Fig. 3.3.9c-e) consisted completely of humified organic materials complexed with Mn, as there is no evidence of $MnCO_3$ or any other Mn mineral. This is also indicated by the Mn L-edge NEXAFS spectra (Fig. 3.3.11a). The chemical fractionation of HA from a humic gleysol by divalent and trivalent metal cations was demonstrated by Christl and Kretzschmar (2007) using C 1s NEXAFS spectroscopy. They concluded that the cation-induced coagulation of humic acid resulted in the preferential removal of humic acid with functional groups involved in metal-cation binding, in particular, aliphatic carboxylic groups. The conclusions from this afore-mentioned study (Christl and Kretzchmar 2007) using natural humic acid are in complete agreement with our findings.

Recently, it has been proposed that humic substances are collections of diverse, relatively low molecular mass components that are associated by mere hydrophobic interactions and hydrogen bonds (Sutton and Sposito 2005). This view has questioned the formation of humic substances by polymerization of phenolic compounds. Our study of the polyphenol-Maillard reaction clearly shows that a significant amount of aliphatic material is formed, due to ring cleavage of phenols, as well as, the incorporation of Maillard reagents into the humic acid fraction through condensation reactions. Furthermore, the NEXAFS spectra show that the humification products of biomolecules and IHSS standard humic substances also contain substantial aromatic characteristics (Fig. 3.3.12 and 3.3.13). Therefore, the data indicate that the polycondensation reactions and the formation of aliphatic fragments through ring cleavage proceed concomitantly. The present findings would partially account for the aliphaticity of humic substances in soils (Schnitzer 1977; Stevenson 1994) and the variation of their

characteristics, including carboxylic group contents, with soils in different climatic zones (Schnitzer 1977).

Resorcinol is not able to readily form a direct surface complex with birnessite due to an OH group in the *meta* position (Stone and Morgan 1984b). Therefore it is unable to readily participate in electron transfer reactions like pyrogallol, and thus does not undergo substantial ring cleavage or polymerization through direct electron transfer. It is possible that electron transfer might occur through outer-sphere reactions (Stone and Morgan 1984b) or due to reaction with Maillard reagents, particularly glycine, or Maillard reaction products, which include a range of aromatic compounds including various polyphenols (Haffenden and Yaylayan 2005), heterocyclic N (Jokic et al. 2004a), and highly reactive furfural compounds (Ikan et al. 1996). It is evident from the C K-edge NEXAFS spectra of the HAs from the supernatant of the resorcinol-Maillard reaction (Fig 3.3.13g and h) that these HAs contained more carboxylic functionalities than the HAs from the resorcinol only system (Fig. 3.3.13i), which would be due to the influence of Maillard reagents in the system. Decreased ring cleavage in the resorcinol system would mean that the resultant humic substances would have less aliphatic fragment incorporation, compared to pyrogallol. This is very evident from the C NEXAFS spectra of the HAs from the pyrogallol and resorcinol systems, where the pyrogallol systems' HAs (Fig. 3.3.13d-f) were far more heterogeneous and poorly defined compared to the resorcinol systems' HAs which were dominated by aromatic C-H and phenolic C-OH functionalities (Fig. 3.3.13g-i). In complete contrast to the pyrogallol-Maillard systems in which $MnCO_3$ was absent when the amount of pyrogallol added was 0.025 mole or higher (Fig 3.3.6c and d), the solid residues of the resorcinol-Maillard systems consisted predominantly of $MnCO_3$ (Fig. 3.3.7 b-e) and some Maillard reaction-type humic substances (Fig. 3.3.10). This indicates that the bulk of the humic polymers produced in the resorcinol-Maillard reaction system remained in the supernatant, and not precipitated in the solid residue complexed with Mn(II) as in the pyrogallol containing systems. This reasoning is in accord with the Mn L-edge NEXAFS spectra of the solid residues of the integrated resorcinol- and pyrogallol-Maillard reaction systems; the data show that Mn(II) was bound to carbonate in the former system and covalently bound to organics in the latter system (Fig. 3.3.11a and c). This further substantiates the view that the strongly aromatic/phenolic polymers formed in the resorcinol-Maillard reaction system had a lower affinity for Mn(II) and hence remained suspended in the supernatant. These findings also provide

an explanation for the contrasting trends observed in the Mn concentration (Fig. 3.3.4) of the supernatant of the resorcinol- and pyrogallol-Maillard reaction systems, and the substantially higher dissolved Mn concentration and visible absorbance values in the former than the latter (Fig. 3.3.5). The results indicate less Mn(II) sorption and more humic polymers in the supernatant in the resorcinol-Maillard reaction systems compared with the pyrogallol-Maillard systems. Therefore, the ability of the polyphenols to form direct surface complexes with birnessite not only affects the extent of their oxidative polymerization reactions, but also the nature of the humic substances formed and ultimately their partition in the solution and solid phases in the system, whether remaining in solution or coprecipitating with metals out of solution.

Manganese carbonate

The formation of $MnCO_3$ in the polyphenol-Maillard reaction system as influenced by the structure and functionality of polyphenols and their molar ratio to Maillard reagents is clearly shown by the XRD, Mn L-edge NEXAFS and FTIR data (Fig. 3.3.6, 3.3.7, 3.3.9, 3.3.10 and 3.3.11). It has been previously shown that CO_2 is produced during the oxidation of glycine (Wang and Huang 1987, 2005), catechol (Majecher et al. 2000), pyrogallol (Wang and Huang 2000b) and glucose (Jokic et al. 2004b) by birnessite. Carbon dioxide released from these biomolecules dissolves in solution to form carbonic acid (Eq. 3.3.2):

$$CO_2 + H_2O \leftrightarrow H_2CO_3 \ldots (\text{Log K} = -1.46) \text{ (Lindsay 1979) } \ldots\ldots\ldots\ldots\ldots \quad (3.3.2)$$

Carbonic acid dissociates to form bicarbonate and eventually carbonate depending on the pH of the solution (Eq. 3.3.3 and 3.3.4):

$$H_2CO_3 \leftrightarrow H^+ + HCO_3^- \ldots (\text{Log K} = -6.36) \text{ (Lindsay 1979)} \ldots\ldots\ldots\ldots\ldots\ldots (3.3.3)$$

$$HCO_3^- \leftrightarrow H^+ + CO_3^{2-} \ldots (\text{Log K} = -10.33) \text{ (Lindsay 1979)} \ldots\ldots\ldots\ldots\ldots\ldots (3.3.4)$$

The partial pressure of CO_2 in the atmosphere is usually 0.0003 atm, however in a water-logged system the partial pressure can be as high as 0.3 atm, thus resulting in much higher CO_3^{2-} concentrations (Lindsay 1979). The CO_2 released from the oxidation of biomolecules (glucose,

glycine, pyrogallol and resorcinol) would enhance the partial pressure of CO_2 and dissolution of CO_2 in water to form H_2CO_3. Reduction of birnessite by the biomolecules resulted in substantial release of Mn (Fig. 3.3.1). Mn is present as Mn(II) in solution as shown in previous studies using EPR spectrometry (Wang and Huang 2000b; Jokic et al. 2001b; Matocha et al. 2001). Thus, $MnCO_3$ (rhodochrosite) can form in the system when the activity product of Mn^{2+} and CO_3^{2-} (Eq. 3.3.5) exceeds the Ksp of $MnCO_3$ (1.8×10^{-18}) (Lindsay 1979):

$$Mn^{2+}{}_{(aq)} + CO_3^{2-}{}_{(aq)} \leftrightarrow MnCO_3{}_{(s)} \text{……..(3.3.5)}$$

Therefore the biomolecule-induced formation of $MnCO_3$ is considered as a mechanism for the formation of rhodochrosite, as the CO_2 is derived from oxidation of biomolecules and the XRD (Fig. 3.3.6a, b and e, and 3.3.7b-e), Mn L-edge NEXAFS (Fig. 3.3.11c) and FTIR (Fig. 3.3.9a and b, and 3.3.10a-e) data show the formation of $MnCO_3$ in the reaction systems. Okita et al. (1988) hypothesized that the $MnCO_3$ deposit at Molango, Mexico, formed due to the reduction of manganese oxides by organic materials and that the organic-derived CO_2 resulted in negative $\delta^{13}C$ values and manganese carbonate formation. Furthermore, rhodochrosite-like $MnCO_3$ has been identified as one of the dominant Mn-bearing minerals in a naturally occurring palustrine emergent wetland (La Force et al. 2002). The present findings provide experimental evidence for substantiating the hypothesis of the biogenic formation of $MnCO_3$ deposits and for interpreting the presence of rhodochrosite-like $MnCO_3$ in wetlands.

Increasing the pyrogallol concentration in the pyrogallol-Maillard reaction systems resulted in less $MnCO_3$ formation (Fig. 3.3.6a-d). This is, in part, attributed to the lower solution pH values (Fig. 3.3.3), due to increased oxidative polymerization reactions, which decreased the CO_3^{2-} concentration in solution. In addition, the larger amounts of humic polymers apparently had an inhibitory effect on $MnCO_3$ formation, due to perturbation of the crystallization of pure $MnCO_3$ (Fig. 3.3.6a-d) and also the competing effect of humic polymers for Mn^{2+} through complexation as indicated in the drastic decrease in the solution Mn concentration with increase in the amount of pyrogallol present in the systems (Fig. 3.3.4). The high solution pH (Fig. 3.3.3) and Mn concentration (Fig. 3.3.4) of the resorcinol-Maillard reaction systems favoured the formation of $MnCO_3$ in the solid residues. The XRD (Fig. 3.3.7b-e) data indicate that increasing the resorcinol concentration in the resorcinol-Maillard reaction system promoted the formation

of crystalline $MnCO_3$. The FTIR spectra of the solid residues (Fig. 3.3.10b-e) also clearly showed that the formation of Maillard-reaction type organic substances in the solid residue of the resorcinol-Maillard reaction systems decreased with increasing amount of resorcinol added to the system. This could be due to the formation of more aromatic/phenolic polymers in the resorcinol-Maillard reaction system (Fig. 3.3.13g-i) with increasing amount of resorcinol added to the system, which had a lower affinity for Mn(II) and thus increased the concentration of Mn(II) in solution (Fig. 3.3.4) and the amount of polymers in the supernatant (Fig 3.3.5). At the same time, increasing the resorcinol concentration in the resorcinol-Maillard reaction system would result in increased competition for glycine by resorcinol versus the Maillard reaction. This would, in turn, result in less Maillard reaction type reaction products which are rich in carboxylic functional groups, and thus have a high affinity for Mn(II). Therefore, the reaction conditions in the resorcinol system were more favourable for the formation of $MnCO_3$. In the resorcinol only system, the birnessite was only partially reduced to both Mn(III) and Mn(II) (Fig. 3.3.11d); the formation of $MnCO_3$ was hindered due to the partial dissolution of birnessite and competitive formation of a number of relatively poorly crystalline Mn(II) and Mn(III) mineral species (Fig. 3.3.7f).

3.3.5 Conclusions

The results obtained in the present study have demonstrated that there is a significant difference in the reactivity of pyrogallol and resorcinol in the integrated polyphenol-Maillard reaction humification pathway. Pyrogallol (1,2,3 trihydroxybenzene), with three OH groups in the *ortho* position, is able to form direct surface complexes with birnessite far more readily than resorcinol (1,3 dihydroxybenzene), with two OH groups in the *meta* position. This significantly affected the extent of direct electron transfer reactions, such as reductive dissolution of birnessite, and oxidative polymerization and cleavage of biomolecules, which, in turn, affected the nature of the humic substances formed. The humic acids formed in the pyrogallol-Maillard reaction (glucose-glycine) systems were more heterogeneous in nature and contained more aliphatic and carboxylic fragments than those from the resorcinol-Maillard reaction systems, which contained more aromatic polymers. Partitioning of organic material in the solution and solid phases occurred, whereby the more aliphatic/carboxylic polymers were found precipitated in the solid phase due to stronger complexation with Mn(II), whereas more aromatic polymers

were present in the supernatant due to their lower affinity for Mn(II). Increasing the molar ratio of pyrogallol or resorcinol to Maillard reagents enhanced humification and resulted in the formation of humic substances with more aromatic character.

The structure and functionality of pyrogallol and resorcinol and their molar ratio to Maillard reagents also affected inorganic C formation. The biomolecule-induced formation of rhodochrosite ($MnCO_3$) was observed in the polyphenol-Maillard reaction humification pathway, as a result of the oxidation of the biomolecules, glucose, glycine, pyrogallol and resorcinol by birnessite. The integrated pyrogallol-Maillard reaction systems contained the least $MnCO_3$ and were more enriched in humic substances in the solid phase than the integrated resorcinol-Maillard reaction systems. There was an increase in the amount of crystalline $MnCO_3$ with increasing amount of resorcinol present in the reaction system; the opposite trend was true in the integrated pyrogallol-Maillard reaction humification pathway.

The data obtained in this study show that the position and/or number of -OH groups on the benzene ring of polyphenols and the molar ratio of polyphenol to Maillard reagents substantially affected not only the degree of humification and nature of humic polymers formed but also the extent of $MnCO_3$ formation which was a competing reaction to the genesis of humic substances. The findings obtained in this study clearly show the importance of the nature and abundance of biomolecules, such as polyphenols, sugars and amino acids in influencing abiotic humification and carbonate formation in natural environments. The results of this study also have relevance to treating phenolic wastes using Mn oxides or soils, as the chemical structure of phenolic compounds significantly affect their ability to be polymerized or cleaved (detoxified), or their reaction products to be complexed with metals.

3.4 Research Unit 4: *The role of glucose in the integrated polyphenol-Maillard humification pathway as catalyzed by birnessite*

3.4.1 Introduction

Sugars and amino acids are among the most abundant biomolecules in terrestrial and aquatic environments (Anderson et al. 1989). Glucose is one of the primary decomposition products arising from the natural degradation of cellulose (Koivula and Hanninen 2001), one of the most abundant substrates in the terrestrial environment. However, the role that sugars play in abiotic humification reactions is not yet fully understood.

The Maillard reaction, involving condensation reactions between sugars and amino acids (Maillard 1913), is regarded as an important pathway in natural humification processes (Ikan et al. 1996; Arafaioli et al. 1999; Bosetto et al. 2002). Even though the Maillard reaction between glucose and glycine is kinetically sluggish under normal environmental conditions (Jokic et al. 2001c), Jokic et al. (2001b) showed that birnessite substantially catalyzes the Maillard reaction under environmentally relevant conditions (25 and 45° C at pH 7.0), resulting in the formation of humic substances very similar to that of natural humic substances. This includes the formation of amide and heterocyclic N functional groups (Jokic et al. 2004a). It was also shown that birnessite catalysis of the Maillard reaction (glucose and glycine) occurs both in the presence and absence of light (Jokic et al. 2001a) which is relevant to top- and subsoil environments. Jokic et al. (2004b) studied the integrated catechol-Maillard system (equimolar concentrations of catechol, glucose and glycine) under environmentally relevant conditions catalyzed by birnessite, and found that the addition of catechol to the Maillard system was far more effective in promoting humification (browning) than the Maillard system alone. The influence of various polyphenols, with different structures and functionalities, and their molar ratio to Maillard reagents (glucose and glycine) on humification processes as catalyzed by birnessite has also been studied (Hardie et al. 2007). Increasing the molar ratio of polyphenols to Maillard reagents substantially enhanced humification reactions and promoted the formation of humic substances with a stronger aromatic character.

Although the Maillard reaction and the influence of polyphenols on the Maillard reaction as catalyzed by birnessite (δ-MnO_2) have been reported (Jokic et al. 2001a, 2001b, 2004b; Hardie et al. 2007), the role of sugars in influencing the the polyphenol humification pathway

and the integrated polyphenol-Maillard humification pathway as catalyzed by birnessite remains to be uncovered. Therefore, the objective of this study was to examine the effect of the molar ratio of glucose to catechol and glycine in the integrated polyphenol-Maillard pathway on humification processes and reaction products, as well as, the effect of the molar ratio of glucose to catechol on catechol-humification processes, as catalyzed by birnessite.

3.4.2 Materials and Methods

3.4.2.1 Materials

Birnessite has been found to be one of the most powerful catalysts of abiotic humification reactions (Huang 2000) and was thus selected as the mineral catalyst in this study. Birnessite (δ-MnO_2) was synthesized according to one of the methods described by McKenzie (1971), which involves reducing boiling $KMnO_4$ by slowly adding concentrated HCl. The precipitate was washed by means of repeated filtration using distilled deionized water (henceforth referred to as water) on a 0.1 μm pore Millipore membrane filter, until the wash water was tested free from chloride ($AgNO_3$ test). It was then freeze-dried, and finally lightly ground using a mortar and pestle. The synthesized birnessite was characterized by means of X-ray diffraction (XRD) (Rigaku Rotaflex 200SU, Tokyo, Japan), Fourier transform infrared (FTIR) spectroscopy (Bruker Equinox 55, Ettlingen, Germany), Mn L-edge near edge X-ray absorption fine structure (NEXAFS) spectroscopy on the SGM (Spherical Grating Monochromator) beamline at the Canadian Light Source (Saskatoon, SK, Canada) and BET specific surface area analysis (Quantachrome Autosorb-1, Syosset, NY, USA) using N_2 gas. Catechol, D-glucose (Sigma-Aldrich ACS reagent grade >99%) and glycine (Sigma Ultra pure grade >99%) were obtained from Sigma Aldrich Canada Ltd (Oakville, ON, Canada). The Mn reference compounds, $MnCO_3$ (99.99%) and Mn_2O_3 (>98%) were obtained from Sigma Aldrich (Oakville, ON, Canada) and MnO (>99.99%) and MnO_2 (>99%) from Alfa Aesar, Johnson Matthey Catalog Company, Inc. (Ward Hill, MA, USA). These were used in the Mn L-edge NEXAFS studies. Elliot soil (1S102H) and Suwannee River (1S101H) humic acid standards were purchased from the International Humic Substances Society (IHSS), St. Paul, MN, USA, and used in the C K-edge NEXAFS study.

3.4.2.2 Incubation experiment.

Sterile conditions were maintained throughout the experiment in order to establish the role of abiotic processes. All glassware, birnessite, water and apparatus were autoclaved prior to the experiments. In addition to this, thimerasol, an antiseptic agent, was added to each flask (0.02 %, w/v) before any of the reagents were added. Thimerasol does not affect the oxidation process of phenolic compounds (Wang et al. 1983a). In order to investigate the effect of the molar ratio of glucose to catechol and glycine, a number of treatments were employed with increasing amounts (0, 0.00125, 0.0025, 0.0125, 0.0250, 0.0500, 0.1000 moles) of glucose added to a fixed amount of catechol (0.05 mole) and glycine (0.05 mole) using birnessite as catalyst. There was also a set of treatments containing a fixed amount of catechol (0.05 mole) with increasing amounts of glucose added (0, 0.00125, 0.0025, 0.0125, 0.0250, 0.0500, 0.1000 moles) using birnessite as catalyst. Two and a half grams of birnessite were suspended in 75 mL of the reaction solutions in a 250 mL flask. There were selected control treatments in which birnessite was absent, i.e., the catechol only system (0.05 mole catechol), the glucose only system (0.05 mole glucose), the Maillard reaction system (0.05 mole glucose + 0.05 mole glycine), the catechol-glycine system (0.05 mole catechol + 0.05 mole glycine) and the equimolar catechol-Maillard system (0.05 mole glucose + 0.05 mole glycine + 0.05 mole catechol). All the reaction systems were adjusted to an environmentally relevant pH 7.0 using 0.1 M HCl or 0.1 M NaOH. The final volume of the flasks was made up to 100 mL using autoclaved water.

The flasks were then tightly sealed and placed in a constant temperature water bath at 45°C for a period of 15 days while gently shaking. Forty-five degrees centigrade is an environmentally relevant temperature as it is common in tropical and subtropical areas, and has also been reported in temperate areas as the approximate temperature of an exposed sunlit soil surface on a day when the ambient air temperature is 25°C (Jury et al. 1991). All treatments were performed in triplicate. The absence of microbial growth was verified by culturing aliquots of selected samples at the end of the incubation period. Aerobic microbial growth was tested for by culturing on Tryptocase Soy Agar (TSA) plates, while anaerobic microbial growth was tested for on TSA plates in a BBL GasPak 150 Large Anaerobic System. All cultures were incubated for a period of 5 and 9 days at 28° C (Jokic et al. 2004b).

3.4.2.3 Characterization of reaction systems at the end of the incubation period and isolation of humic acids.

At the end of the reaction period, the final pH and Eh of the suspensions were measured. The samples were then centrifuged at 25,000 g for 40 min to separate the solid residue from the solution. The absorbance of the supernatant was measured between 400 and 600 nm on a UV-visible spectrophotometer (Beckman DU 650 microprocessor controlled spectrophotometer, Fullerton, CA, USA). The visible absorbance at 400 and 600 nm provides an indication of the extent of polymerization which has taken place in the reaction systems (Shindo and Huang 1982, 1984a, 1984b). Shindo and Huang (1984a) studied the polymerization of polyphenols by short-range ordered Mn, Fe, Al and Si oxides, and showed that the yield of humic polymers was directly related to the visible absorbance. Likewise, with natural humic substances, Gan et al. (2007) showed that visible absorbance can be used to determine the concentration of fulvic acid in solution. The supernatant was diluted with water prior to absorbance determination and the values obtained were subsequently multiplied by the dilution factor. The Mn content of the supernatant was determined using atomic absorption spectroscopy at 279.5 nm (Varian Spectra AA 220, Walnut Creek, CA, USA).

The solid residue was repeatedly washed with water using centrifugation at 25,000 g for 40 min until the wash water was clear. These water extracts were collected and added to the supernatant. The washed residue was then freeze-dried. The combined water extracts and supernatant was then acidified to pH 1.0 using 6 M HCl and allowed to stand for 24 h to precipitate the humic acid (HA) fraction out of the solution (Swift 1996). The acidified suspensions were then centrifuged at 25,000 g for 45 min to separate the HA fraction from the rest of the solution containing the fulvic acid (FA) fraction and non-humic substance fraction. The HA residue was then resuspended in a 0.1 M HCl and 0.3 M HF solution and shaken for 48 h. It was then centrifuged again as described before and dialyzed in 1000 molecular weight cut off dialysis tubing for 5 days in distilled deionized water until the water tested free from chloride ($AgNO_3$ test). The purified HA was then freeze-dried. A HA sample isolated from the supernatant of the equimolar catechol-Maillard system, without the HCl/HF treatment to remove sorbed metals, was used in the Mn L-edge NEXAFS studies to investigate the nature of Mn bonding in the HA sample.

3.4.2.4 Characterization of reaction products

Total carbon analysis. Total carbon analysis of the solid residues was performed using a dry combustion method on a Leco CR-12 Carbon Analyzer (Leco Corporation, St. Joseph, MI, U.S.A.) as described by Wang and Anderson (1998).

X-ray diffraction (XRD). The solid residues were examined using X-ray diffractometry on a Rigaku Rotaflex 200SU (Tokyo, Japan) with a rotating Fe anode and graphite monochromator. The samples were lightly ground and then mounted on glass slides by making a slurry of the ground sample with acetone and allowing it to dry. The scans were performed at 40 kV and 160 mA, from 4 to 80 °2θ, at a step size of 0.02 °2θ at a scanning rate of 0.1 °2θ sec^{-1}.

Near edge X-ray absorption fine structure (NEXAFS) spectroscopy. The speciation of C and Mn was investigated in selected solid residues and supernatant HA fractions using C K-edge and Mn L-edge NEXAFS on the SGM (Spherical grating monochromator) beamline (Regier et al. 2007) at the Canadian Light Source (Saskatoon, SK, Canada). A number of pure reference Mn compounds ($MnCO_3$, MnO, Mn_2O_3, MnO_2) and IHSS soil and river HA standards, were also examined. Samples which were investigated for Mn were lightly ground and mounted on carbon tape. Samples, which were investigated for C, were mounted on gold (Au)-coated (~400 Å) silicon (Si) wafers by making dilute suspensions of the samples in distilled deionized water and then placing a droplet of the suspension on the wafer and allowing it to dry. An exit slit width of 20 μm and a dwell time of 0.3s were used to minimize damage due to exposure to radiation. These spectra were recorded by total electron yield (TEY) at an energy step size of 0.1 eV. The Mn L-edge spectra were normalized to the TEY of a gold I_0 mesh which was fixed in front of the sample in the path of the beam. The C K-edge spectra were normalized to a clean Au-coated Si wafer, so that the signals from C in the beamline and C contamination on the gold I_0 mesh would not interfere with the signal from our samples (Watts et al. 2006). Spectra obtained were analyzed using aXis2000 software (Hitchcock et al. 2005). The energy scale of the C and Mn spectra were internally calibrated using glycine and MnO, respectively, based on calibrated values reported from previous studies (Garvie and Craven 1994; Boese et al. 1997). All the spectra were normalized to each other, with the maximum intensity of each spectrum fixed at 1.

3.4.3 Results and Discussion

3.4.3.1 Effect of the presence of birnessite on the reaction systems

In all the reaction systems studied, no aerobic or anaerobic microbial growth was observed. Thus, all the processes studied were abiotic in nature. The X-ray diffractogram of the synthesized birnessite had characteristic d-values at 7.21, 3.61 and 2.45 Å as reported by McKenzie (1989). The FTIR spectrum of the synthesized birnessite showed typical birnessite absorption bands at 3400, 1621, 509 and 466 cm^{-1} (Potter and Rossman 1979).

Fig. 3.4.1 shows the effect of the presence of birnessite on the visible absorbance (400-600 nm) of the supernatant of the catechol-glycine, catechol-Maillard, catechol only and catechol-glucose reaction systems. The presence of birnessite significantly enhanced browning (humification) in all of the reaction systems, most notably in the integrated catechol-Maillard system (Fig. 3.4.1b).

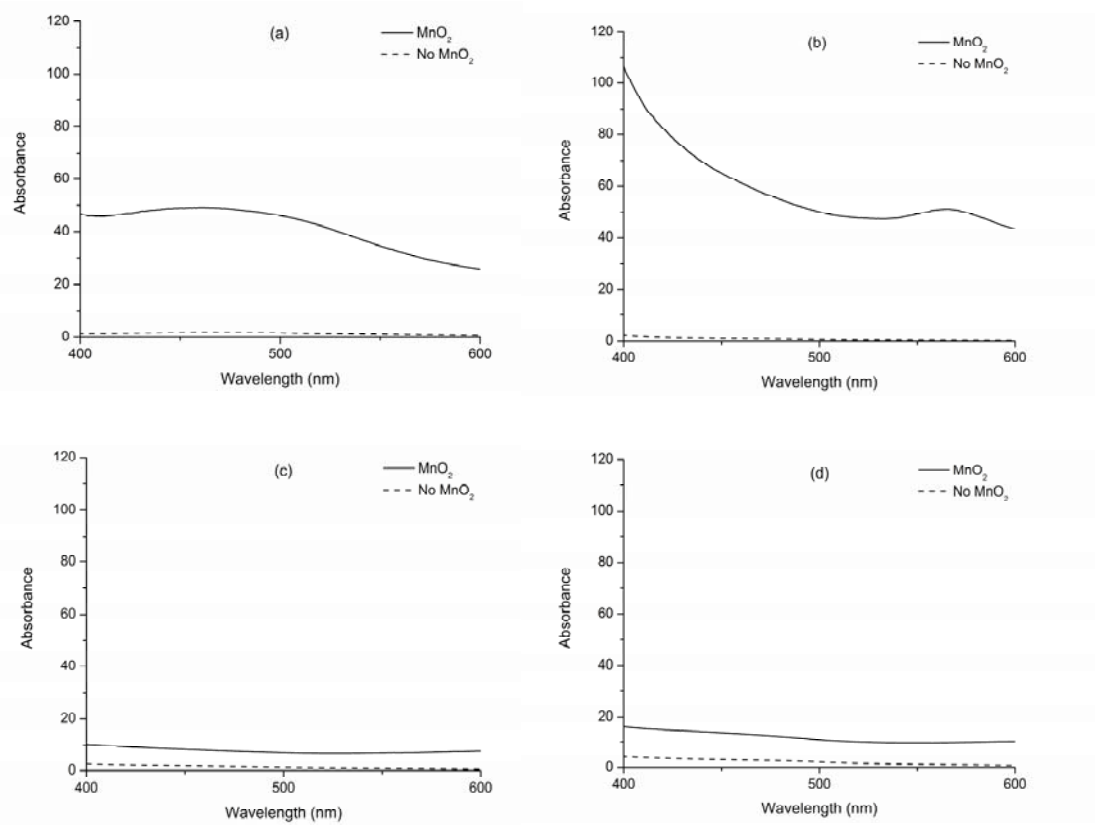

Figure 3.4.1 The effect of the presence of birnessite on the visible absorbance (400-600 nm) of the supernatant from (a) the catechol-glycine system, (b) the catechol-glucose-glycine system, (c) the catechol only system and (d) the catechol-glucose system. The amount of each reagent added was 0.05 mole in the reaction systems. The absorbances are scaled by the dilution factor.

Table 3.4.1 Comparison of the effect of the presence of birnessite on the visible absorbance, pH and redox potential (pH + pE), and Mn concentration of the supernatant of selected reaction systems.

Treatment*	Visible absorbance		pH	pH + pE	Mn
	400 nm	600 nm			(mmol L^{-1})
Presence of birnessite					
Catechol	10.29 ±4.21	6.97±4.06	7.27 ±0.04	8.59 ±0.12	17.3 ±0.2
Catechol-glycine	55.92 ±6.91	31.58 ±5.54	7.13 ±0.12	7.54 ±0.86	31.6 ±4.6
Catechol-glycine-glucose	100.59 ±6.37	44.21 ±5.34	6.85 ±0.01	6.74 ±0.19	92.0 ±4.9
Catechol-glucose	15.65 ±0.45	10.63 ±0.25	6.80 ±0.18	6.88 ±0.13	19.7 ±0.8
Glucose only	0.07 ±0.02	0.04 ±0.01	7.49 ±0.22	12.80 ±0.92	13.3 ±2.4
Absence of birnessite					
Catechol	2.04 ±0.33	0.62 ±0.26	4.17 ±0.29	10.45 ±0.72	-
Catechol-glycine	1.71 ±0.75	0.78 ±0.16	6.52 ±0.04	9.91 ±0.40	-
Catechol-glycine-glucose	2.84 ±0.57	0.42 ±0.09	5.49 ±0.07	8.78 ±0.52	-
Catechol-glucose	3.12 ±1.13	0.38 ±0.41	3.93 ±0.15	10.67 ±0.31	-
Glucose only	0	0	5.07 ±0.09	11.56 ±0.25	-

*Amount of each reagent added was 0.05 mole in the reaction systems

Table 3.4.1 provides a summary of the solution characteristics of selected reaction systems in the presence and absence of birnessite. The glucose only system showed the least browning both in the presence and absence of birnessite. However, the addition of glucose to catechol (compare the visible absorbance of the catechol only systems with that of the catechol-glucose system) enhanced the browning in the presence of birnessite (Table 3.4.1). This indicates that catechol and glucose in the presence of birnessite reacted together in browning reactions. Likewise, the addition of glucose to the catechol-glycine system substantially enhanced browning in the presence of birnessite. The addition of glycine to catechol also significantly enhanced browning reactions in the presence of birnessite, but not in the absence. The pH + pE value is a function of the dissolved oxygen concentration in solution, and is thus an indication of the redox status of a system (Lindsay 1979). The addition of glucose in the catechol or catechol-glycine system consistently decreased the pH and the pH + pE, indicating the generation of more protons and consumption of more oxygen. This is in accord with the enhancement of the absorbance at both 400 and 600 nm with the addition of glucose to the catechol or catechol-

glycine systems. Except for the glucose only system, the systems reacted in the presence of birnessite had lower final redox status (pH + pE) values than in the absence, which indicates more oxygen was consumed and thus oxidative polymerization reactions were enhanced. Systems in the presence of birnessite also had higher final pH values, as a result of the reductive dissolution of birnessite by the biomolecules which results in the consumption of protons.

3.4.3.2 Influence of the molar ratio of glucose to catechol with or without glycine on reactions systems incubated in the presence of birnessite

The effect of the molar ratio of glucose to glycine and catechol in the catechol-Maillard system, and that of glucose to catechol in the catechol-glucose system, on the visible absorbance of the supernatant at 400 and 600 nm is shown in Fig. 3.4.2. Increasing the molar ratio of glucose to catechol and glycine in the catechol-Maillard system resulted in a substantial increase in the visible absorbance of the supernatant at 400 nm (Fig. 3.4.2a) but not to the same extent at 600 nm (Fig. 3.4.2b). This indicates that increasing the molar ratio of glucose enhanced the formation of lower molecular weight humic polymers. This is attributable to the enhanced formation of Maillard reaction products which are relatively lower molecular weight products (Section 3.1).

Increasing the molar ratio of glucose to catechol resulted in an increase in the visible absorbance at both 400 and 600 nm. Therefore, adding increasing amounts of glucose to catechol enhanced browning reactions but to a lesser extent than in the integrated catechol-Maillard system. The absorbance results (Fig. 3.4.2) also indicate the important role that glycine plays in enhancing browning reactions; glycine readily undergoes polycondensation with polyphenols such as catechol or reducing sugars such as glucose in the presence of birnessite to form darkly coloured polymers (Shindo and Huang 1984b; Wang and Huang 1987; Wang and Lin 1993; Wang and Huang 1997; Jokic et al. 2001b).

The effect of the molar ratio of glucose to glycine and catechol in the catechol-Maillard system, and that of glucose to catechol in the catechol-glucose system, on the final pH and Mn concentration of the supernatants is shown in Fig. 3.4.3. The pH of the reaction systems is controlled by two dominant processes, namely the proton-consuming reduction of birnessite (Eq 3.4.1), and the proton-generating oxidative polymerization reactions of catechol (Eq. 3.4.2) (Stone 1987) and other reactive aromatic compounds generated by the Maillard reaction or dehydration of glucose (e.g., polyphenols, furfural and hydroxymethylfurfural compounds)

(Lourvanij and Rorrer 1994; Ikan et al. 1996; Haffenden and Yaylayan 2005; Furlani et al. 2006; Gonzalez and Laird 2006).

$$MnO_2 + 4H^+ + 2e^- \rightarrow Mn^{2+} + 2H_2O \qquad (3.4.1)$$

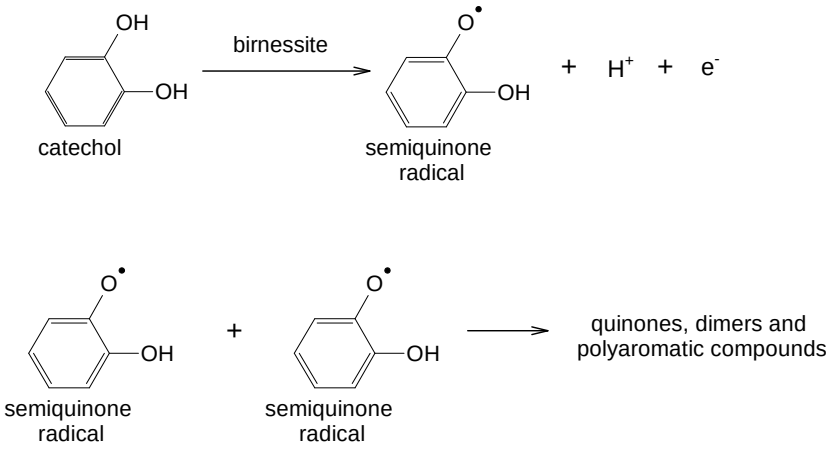

(3.4.2)

Polycondensation reactions, such as the condensation of glucose and glycine or quinone and glycine or the dehydration of glucose to form hydroxymethylfurfural (Lourvanij and Rorrer 1994), result in the release of H_2O and thus do not affect the pH of the system. Increasing the amount of glucose in the catechol-Maillard system resulted in a decrease in the pH value of the system, whereas increasing the amount of glucose resulted in an initial decrease in the pH in the catechol-glucose system (Fig. 3.4.3a). It was found that birnessite was completely dissolved (reduced) in the catechol-Maillard and catechol-glucose reaction systems studied (FTIR data of the solid residues not shown). This indicates that the extent of oxidative polymerization reactions would have a greater influence on the net final pH of reaction systems than the dissolution of birnessite, which occurred to the same extent in all the systems studied. Increasing the concentration of glucose in the catechol-Maillard system resulted in a substantial increase in the Mn concentration in the supernatant (Fig. 3.4.3b). However, increasing the amount of glucose in the catechol-glucose system resulted in an initial increase (up to 0.0025 mole glucose added), but then the Mn concentration tended to level off in the supernatant (Fig. 3.4.3b). As all the birnessite in the reaction systems was dissolved, the complexation of Mn(II) and humic products

and formation of Mn(II) phases such as $MnCO_3$ in the reaction systems controls the amount of Mn in solution. This will be discussed in further detail in section 3.4.3.3.2.

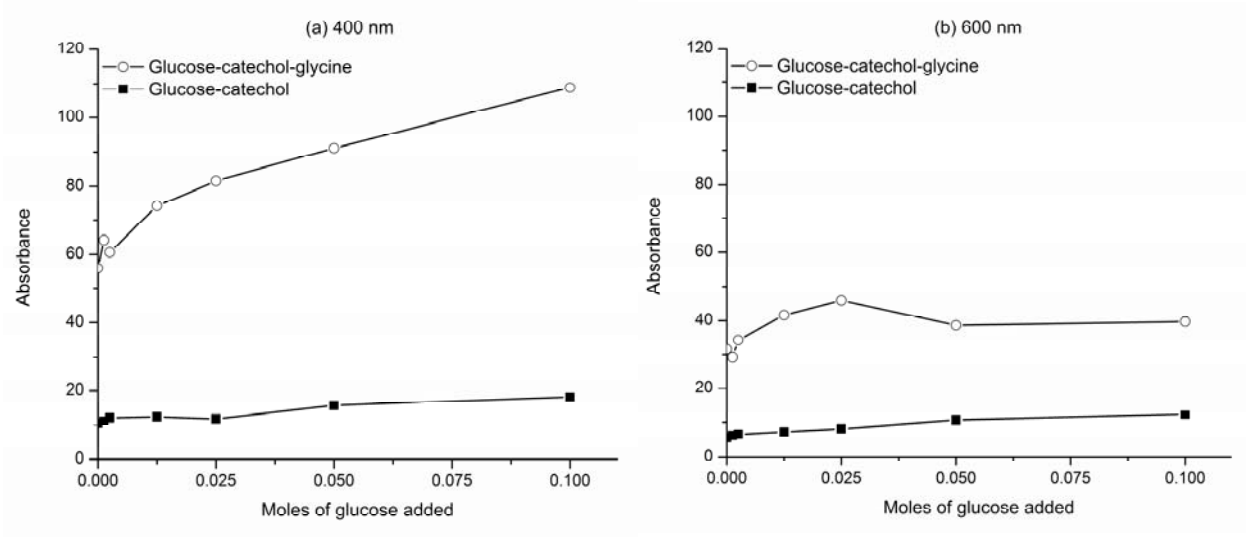

Figure 3.4.2 Comparison of the absorbances of the supernatants at (a) 400 and (b) 600 nm of the integrated catechol-Maillard (0.05 mole catechol + 0.05 mole glycine + varying mole glucose) and glucose-catechol (0.05 mole catechol + varying mole glucose) systems reacted in the presence of birnessite with increasing amount of glucose added to the system. The absorbances are scaled by the dilution factor.

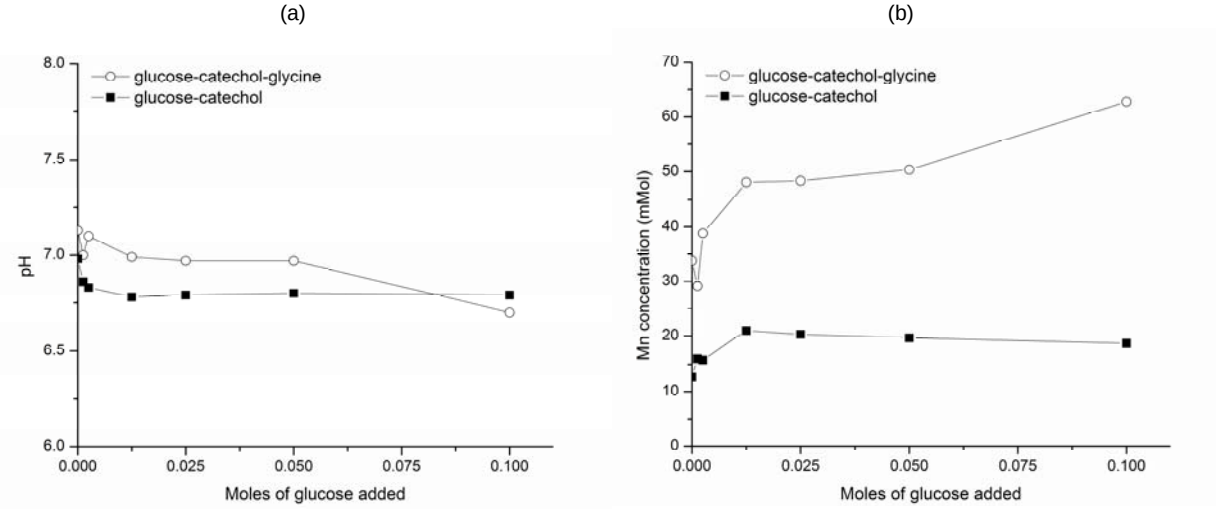

Figure 3.4.3 Comparison of (a) the final pH and (b) the Mn concentration of the supernatant of the integrated catechol-Maillard (0.05 mole catechol + 0.05 mole glycine + varying mole glucose) and glucose-catechol (0.05 mole catechol + varying mole glucose) reaction systems catalyzed by birnessite, with increasing amount of glucose added.

3.4.3.3 Characterization of reaction products from reaction systems incubated in the presence of birnessite

3.4.3.3.1 Humic acid isolated from the supernatant

Carbon K-edge NEXAFS spectroscopy

The C K-edge NEXAFS spectra of the HA isolated from the supernatant of selected reaction systems and natural IHSS soil and river HA standards are shown in Fig. 3.4.4. Spectroscopic assignments are based on the absorption maxima of the reference compounds (glucose, glycine and pyrogallol) and on values reported by previous C NEXAFS studies (Myneni 2002; Urquhart and Ade 2002; Dhez et al. 2003; Cooney and Urquhart 2004; Hitchcock and Mancini 2004). The NEXAFS narrower and sharper core (C 1s) → π* transitions have been found to be the most useful for chemical analyses and identification of organic compounds due to their chemical sensitivity based on the chemical energy shifts (Urquhart and Ade 2002).

The lowest absorption bands at around 284.0 eV usually correspond to molecules with low energy π* states, such as quinones (Francis and Hitchcock 1992). Absorption bands near 285 eV are generally ascribed to C 1s (C-H) → $1\pi^*_{C=C}$ transitions (Urquhart and Ade 2002; Cooney and Urquhart 2004), which are characteristic of C=C unsaturation. The transitions of aromatic C bound to carbonyl (e.g., terephthalate species) tend to overlap with unsaturated aromatic C-H transitions due to the strong electronic interactions between the benzene π* density and carbonyl π* density, and are generally found in the 284.4-285.0 eV range (Cooney and Urquhart 2004). The absorption bands near 286-288 eV are characteristic of functionalized aromatic groups C 1s (C-R) → $1\pi^*_{C=C}$ transitions (R = functional group), such as aromatic C bound to aldehyde (286.0 eV), ketone (286.4 eV), urea (286.4 eV), carbamate (286.6-286.8 eV), amine (286.8-286.9 eV), phenol (287.0-287.3 eV) and ester (287.1 eV) groups (Urquhart and Ade 2002; Dhez et al. 2003; Cooney and Urquhart 2004; Hitchcock and Mancini 2004). Heterocyclic N compounds C 1s (C-N) → $1\pi^*_{C=C}$ transitions also occur in the ~286-287 eV range, e.g., pyridine (285.7 eV) and pyrrole (286.3 eV) (Dhez et al. 2003; Hitchcock and Mancini 2004). The C=N and C≡N π* transitions usually occur around 286.3 eV (Myneni 2002). Generally speaking, a stronger electron withdrawing substituent on the aromatic ring, will result in a higher energy shift of the C 1s (C-R) → $1\pi^*_{C=C}$ transition.

The carbonyl C 1s (C-R) → $1\pi^*_{C=O}$ transitions usually occur between 286-291 eV, and can be used to distinguish between groups such as aldehydes (286.2-286.4 eV), ketones (286.6-286.8 eV), amide (287.8-288.2 eV), acetic/acetate (288.1-288.6 eV), urea (289.2-289.8 eV), carbamate (289.9-290.1 eV) and carbonate (290.2-290.6 eV) (Urquhart and Ade 2002). The main cause of the shifts observed in C 1s (C-R) → $1\pi^*_{C=O}$ transitions is the inductive effect of the neighbouring atoms on the carbonyl C 1s binding energy (Urquhart and Ade 2002). Low lying σ* orbitals also provide valuable information in identifying aliphatic functionalities. Saturated aliphatic C exhibits C 1s (C-H) → σ^*_{C-H} transitions in the 287.1-287.9 eV range, while aliphatic alcohol C 1s (C-H) → σ^*_{C-O} transitions are found shifted to a higher energy in the 289.2-289.5 eV range (Dhez et al. 2003).

The natural soil and river HA (Fig. 3.4.4a and b) were dominated by aliphatic carboxylic functionalities (288.6 eV), and also contained quinone C (284.0 eV), aromatic C-H (285.0-285.3 eV), and functionalized aromatic C, such as aromatic C bound to N, O or ketone, and phenolic groups (286.4-287.1 eV). The HA isolated from the supernatant of the Maillard reaction system (Fig 3.4.4c) was also strongly aliphatic carboxylic (288.6 eV) in nature, and also contained aromatic C-H (285.0-285.3 eV) and aromatic C bound to N, O or ketone groups (286.4-287.1 eV). The HA isolated from the catechol only system was strongly aromatic (285.0 – 287.1 eV) with a small amount of aliphatic carboxylic functional groups (288.6 eV) (Fig 3.4.4h). In the catechol-glycine system (Fig. 3.4.4g), the HA isolated from the supernatant was dominated by aromatic C-H (288.6 eV) and phenolic groups (287.0-287.1 eV), but contained relatively more aliphatic carboxylic groups than the catechol only system HA (Fig. 3.4.4h). The addition of glucose (0.025 mole) to the catechol-glycine system (Fig 3.4.4f) significantly enhanced the relative intensity of the aliphatic carboxylic group peak (288.6 eV). Increasing the molar ratio of glucose to catechol and glycine in the catechol-Maillard system (Fig. 3.4.4f-d) promoted the formation of aliphatic carboxylic (288.6 eV) and aromatic C bound to N, O or ketone groups (286.3-286.4 eV), which are similar to the functionalities observed in the natural HA (Fig. 3.4.4a and b).

The C K-edge NEXAFS spectra of the HA isolated from the supernatant of selected catechol-glucose reaction systems is shown in Fig. 3.4.5. In comparison to the HA from the catechol-Maillard system (Fig. 3.4.5a), the HA from the catechol-glucose systems (Fig. 3.4.5b to d) and catechol only (Fig. 3.4.5e) contained very little aliphatic carboxylic groups (288.6 eV).

Furthermore, the spectra of the HA from catechol-glucose systems (Fig. 3.4.5b to d) were very similar to that of the catechol only system (Fig. 3.4.5e), regardless of the amount of glucose added to the system. There appears to be a slight increase in the relative intensity of the phenolic group peak (287.0-287.1 eV) in the HA from catechol-glucose systems with high amounts of glucose (0.05 mole and 0.1 mole glucose) (Fig. 3.4.5b and c) compared to the HA from the catechol-glucose system with 0.025 mole glucose and the catechol only system (Fig. 3.4.5d and e).

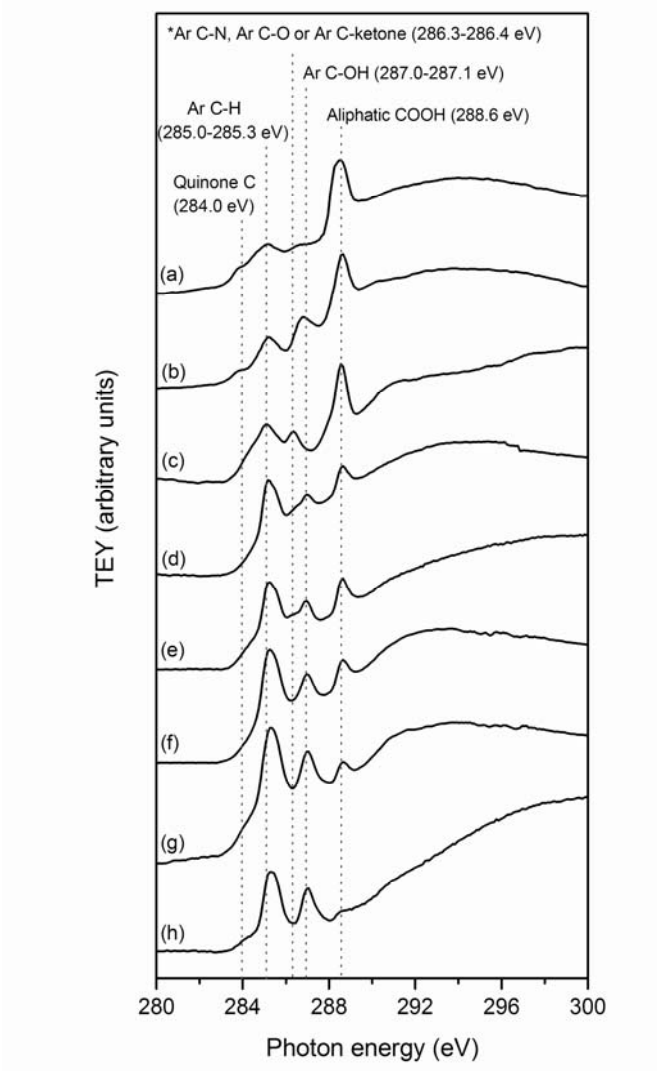

Figure 3.4.4 Carbon K-edge NEXAFS spectra of the IHSS (a) soil and (b) river humic acids, and the HA extracted from the supernatants of systems reacted in the presence of birnessite: (c) the Maillard reaction system (0.05 mole glucose + 0.05 mole glycine); the integrated catechol-Maillard reaction system (0.05 mole catechol + 0.05 mole glycine) with: (d) 0.1 mole glucose, (e) 0.05 mole glucose, (f) 0.025 mole glucose; (g) the catechol and glycine reaction system (0.05 mole catechol + 0.05 mole glycine); and (h) the 0.05 mole catechol only system. *Ar = aromatic.

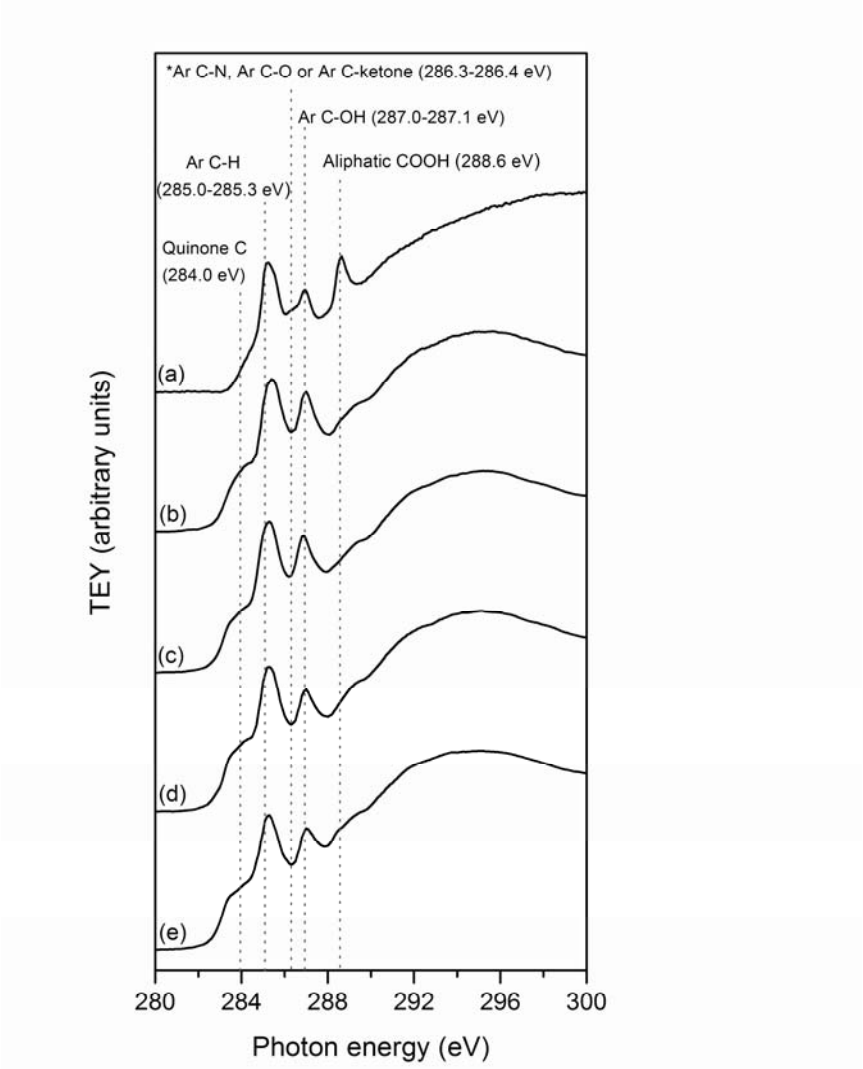

Figure 3.4.5 Carbon K-edge NEXAFS spectra of the HA extracted from the supernatants of systems reacted in the presence of birnessite: (a) the equimolar catechol-Maillard reaction (0.05 mole catechol + 0.05 mole glucose + 0.05 mole glycine); the catechol-glucose reaction system (0.05 mole catechol) with (b) 0.1 mole glucose, (c) 0.05 mole glucose, (d) 0.025 mole glucose; and (e) the catechol only system. *Ar = aromatic.

It can be concluded from the C K-edge spectra in Figs. 3.4.4 and 3.4.5, that it is the reaction of glucose and glycine (i.e., the Maillard reaction) in the integrated catechol-Maillard system (Fig. 3.4.4d-f and Fig. 3.4.5a) that significantly promotes the formation of aliphatic carboxylic functional groups in the HA fraction isolated from the supernatant. The HA from catechol-glycine system (Fig. 3.4.4g) and glucose-catechol systems (Fig. 3.4.5b-d) did not contain relatively as high amounts of aliphatic carboxylic functional groups as the HA from the

integrated catechol-Maillard systems. It can be further concluded that increasing the molar ratio of glucose to catechol and glycine in the integrated catechol-Maillard system (Fig. 3.4.4g-d) promoted the formation of Maillard reaction type functional groups (aliphatic carboxylic and aromatic C bound to N, O or ketone functional groups (Fig. 3.4.4c) in the HA fraction isolated from the supernatant of the reactions systems .

3.4.3.3.2 Solid Phase

X-ray diffraction

The X-ray diffractograms of the solid residues from the catechol only, catechol-glycine and selected catechol-Maillard systems catalyzed by birnessite, are shown in Fig. 3.4.6. The reaction products of the catechol only system (Fig. 3.4.6a) appear quite crystalline compared to the other systems. Manganese carbonate is the only identifiable product in the residue, with a typical d-value at 2.84 Å (Joint Committee on Powder Diffraction Standards 1974). When glycine was added to catechol the reaction product became less crystalline (Fig. 3.4.6b), and the peaks at 10.8 and 2.84 Å which were present in the catechol only system can still be seen. Three new peaks appear at 5.39, 4.71 and 4.06 Å, which also do not match any of the starting organic compounds, any known organic or organometallic compounds (International Centre for Diffraction Data 2006) or Mn-bearing minerals (Joint Committee on Powder Diffraction Standards 1974). When glucose was introduced into the glycine and catechol system (Fig. 3.4.6c), there was a further decrease in the crystallinity of the reaction products; and with increased addition of glucose to the system, the solid reaction products became even more disordered (Fig. 3.4.6d-f).

The X-ray diffractograms of unreacted birnessite and the solid residues from the catechol only, selected catechol-glucose systems, and glucose only system, reacted in the presence of birnessite, are shown in Fig. 3.4.7. The reaction products of the catechol only (Fig. 3.4.7a) and catechol-glucose systems (Fig. 3.4.7b-e) appear to be quite crystalline, and the strong peak at around 13.2 Å appears in all of the diffractograms. The peak at 9.49 Å appears to diminish in intensity with increasing amount of glucose added to the systems (Fig. 3.4.7a-e). Other than the d-value of 2.84 Å which is from $MnCO_3$, the rest of the d-values do not match any known organic or organometallic compounds (International Centre for Diffraction Data 2006) or Mn-

bearing minerals (Joint Committee on Powder Diffraction Standards 1974). The glucose only system (Fig. 3.4.7f) appears to contain some birnessite (7.21 and 2.14 Å), and a small amount of $MnCO_3$ (2.84 Å).

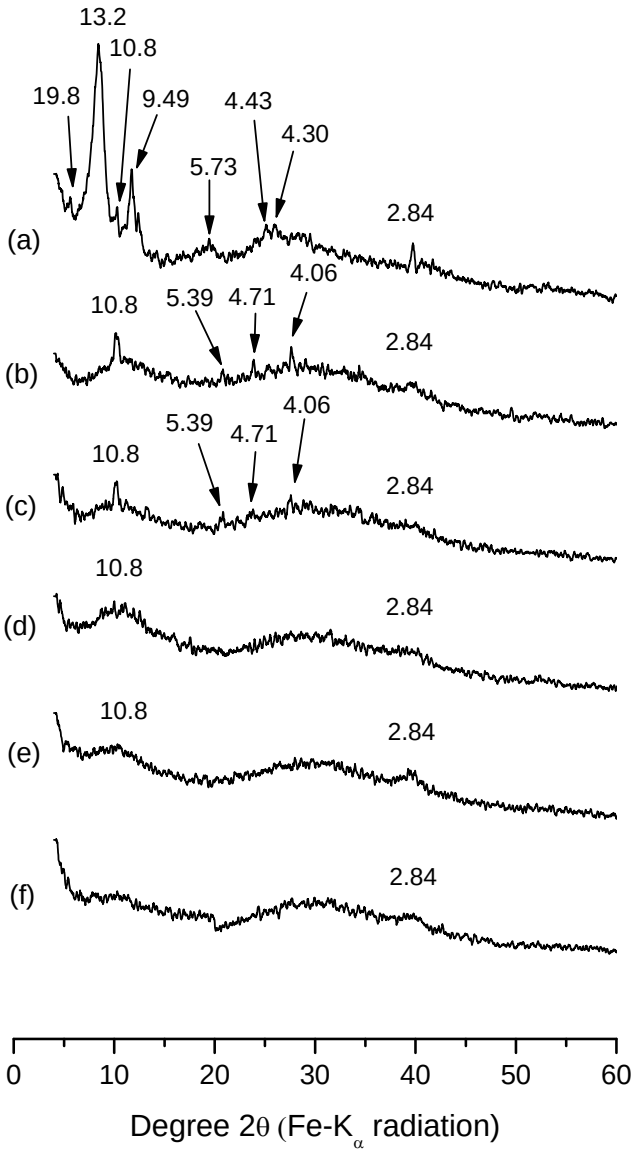

Figure 3.4.6 X-ray diffractograms of the solid residues from selected systems reacted in the presence of birnessite: (a) the catechol only system (0.05 mole catechol); (b) the catechol-glycine system (0.05 mole catechol + 0.05 mole glycine); the integrated catechol-Maillard reaction system (0.05 mole catechol + 0.05 mole glycine) with (c) 0.0025 mole glucose, (d) 0.025 mole glucose, (e) 0.05 mole glucose, and (f) 0.1 mole glucose. The d-values are indicated in angstrom.

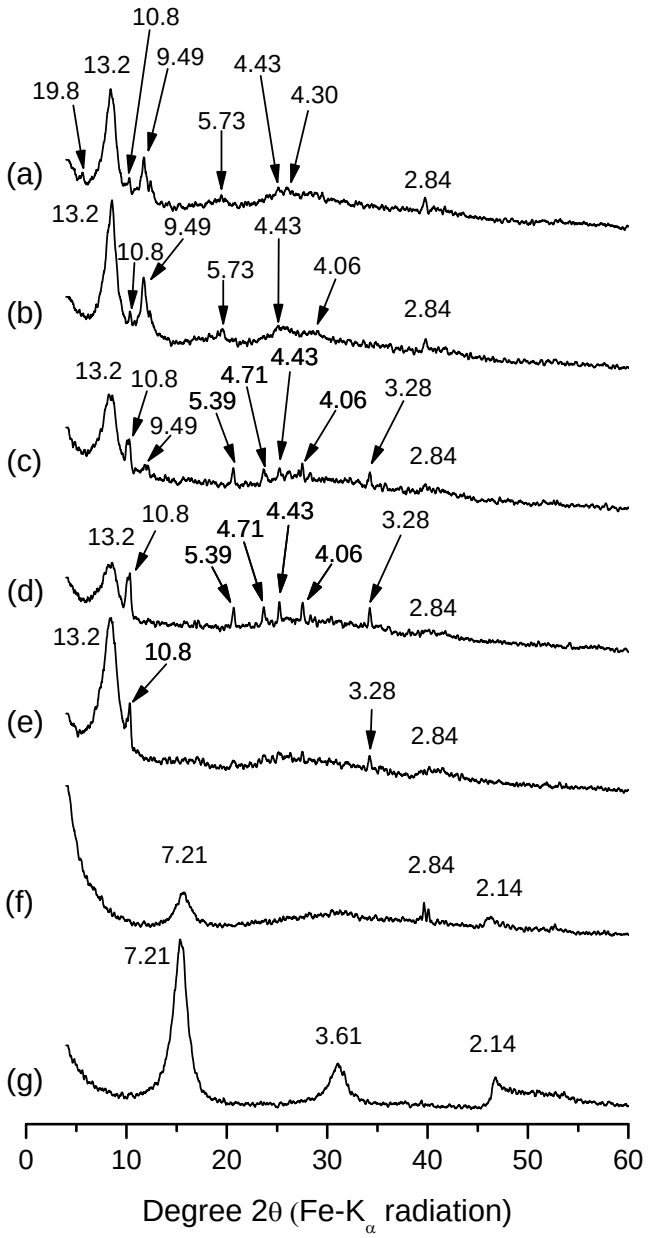

Figure 3.4.7 X-ray diffractograms of the solid residues from selected systems reacted in the presence of birnessite: (a) the catechol only system (0.05 mole catechol); the catechol-glucose reaction system (0.05 mole catechol) with (b) 0.0025 mole glucose, (c) 0.025 mole glucose, (d) 0.05 mole glucose, and (e) 0.1 mole glucose; (f) the glucose only system (0.05 mole glucose); and (g) unreacted birnessite. The d-values are indicated in angstrom.

Total carbon analysis

The total C contents of the solid residues from selected catechol-Maillard and catechol-glucose systems catalyzed by birnessite are shown in Table 3.4.2. Rhodochrosite ($MnCO_3$) was identified in solid residues (Fig. 3.4.6 and 3.4.7). It was not possible to differentiate between organic and inorganic C using the LECO analyzer as it is based on a dry combustion method to measure the CO_2 released at 841 °C and 1100 °C to distinguish between CO_2 released from organic C (841° C) and total C , i.e., inorganic C + organic C (1100° C). Manganese carbonate decomposes at temperatures above 200°C, which is substantially lower than the melting point of $CaCO_3$ (825° C) (Perry and Phillips 1995). Calcium carbonate is considered the most common form of inorganic C in soils and sediments. Thus, the C from $MnCO_3$ would be included in the "organic C" fraction using the conventional dry combustion method. Increasing the amount of glucose in the catechol-Maillard and catechol-glucose systems slightly decreased the percentage of total C in the residues. This could be attributed to the formation of humic substances with more unsaturated character which have a lower total C content (e.g., glucose % C = 40.0% vs. catechol % C = 65.5%) or to the formation of $MnCO_3$ (% C = 10.4%).

Table 3.4.2 Total carbon contents of the solid residues from selected catechol-Maillard and catechol-glucose reaction systems catalyzed by birnessite.

Treatment	Total C content (%)[a]
Integrated catechol-Maillard system	
Catechol-glycine system (0.05 mole catechol + 0.05 mole glycine)	37.3
Catechol-glycine-glucose system with 0.0025 mole glucose	37.2
Catechol-glycine-glucose system with 0.025 mole glucose	36.3
Catechol-glycine-glucose system with 0.05 mole glucose	35.9
Catechol-glycine-glucose system with 0.1 mole glucose	35.9
Catechol-glucose system	
Catechol only system (0.05 mole catechol)	41.7
Catechol-glucose system with 0.0025 mole glucose	41.5
Catechol-glucose system with 0.025 mole glucose	41.0
Catechol-glucose system with 0.05 mole glucose	40.8
Catechol-glucose system with 0.1 mole glucose	39.8

[a]Average standard deviation was ±0.02%

Carbon K-edge NEXAFS spectroscopy

The C K-edge NEXAFS spectra of the solid residues from the Maillard reaction, selected catechol-Maillard, catechol-glucose, catechol only and glucose only systems, reacted in the presence of birnessite are shown in Fig. 3.4.8. All the spectra show the strong presence of aliphatic carboxylic groups (288.6 eV), in particular the glucose only system (Fig. 3.4.8g). This is in strong contrast to the spectra of HA isolated from the supernatant of the catechol-glucose and catechol only systems (Fig. 3.4.5b-e). This is attributable to the chemical partitioning of humic products between the solution and solid phases based on the stronger relative affinity of divalent metals such as Mn(II) for carboxylic than phenolic functional groups (Christl and Kretzchmar 2007; Hardie et al. 2007). Thus, there is more aliphatic carboxylic material in the solid phase than in the HA in the solution phase. There is also abundant evidence for the presence of quinone C (284.0 eV), aromatic C-H (285.0-285.3 eV) and C-OH (287.0-287.1 eV) functionalities in the solid residues. Although, the C K-edge spectra of the HA from the supernatant of the catechol-glucose systems did not show appreciable differences between each other as the amount of glucose was varied in the system (Fig. 3.4.5b-e), the molar ratio of glucose in the catechol-glucose system did affect the nature of the humic substances in the solid residues (Fig. 3.4.8d-f). Increasing the amount of glucose in the catechol-glucose and catechol-Maillard systems decreased the formation of quinone C (284.0 eV); in contrast the formation of aromatic C-H (285.0-285.3 eV) and aromatic C-OH (287.0-287.1 eV) was enhanced by increasing the amount of glucose added to the system (Fig. 3.4.8b-f).

The solid residues from the catechol-Maillard and catechol-glucose systems containing 0.1 mole glucose (Fig. 3.4.8b and f) contained relatively more carbonate (290.2 eV), than the catechol-Maillard and catechol-glucose systems containing 0.05 mole glucose (Fig. 3.4.8c and e). This trend was also confirmed by FTIR spectroscopy (Fig. A3 and A4). This indicates that increasing the molar ratio of glucose in these systems enhanced the formation of $MnCO_3$. This is not related to the pH of the systems as the catechol-Maillard system with 0.1 mole glucose actually had a lower pH than the catechol-Maillard system containing 0.05 mole glucose (Fig. 3.4.3a). This is instead attributed to the increase in the oxidation of glucose by birnessite (Bose et al. 1959) which results in the release of CO_2 (Jokic et al. 2004b). The released CO_2 is subsequently dissolved and converted to CO_3^{2-} in solution which apparently promotes the

formation of $MnCO_3$. The increased formation of $MnCO_3$ also explains why the total C content of the solid residues decreased with increasing amount of glucose added to the system (Table 3.4.2), as the total C in $MnCO_3$ is 10.4% which is much lower than that of humic substances (about 45% C).

The solid residue from the glucose only system was dominated by aliphatic carboxylic C (288.6 eV) and smaller amounts of aromatic C-H (285.0-285.3 eV) and aromatic O-H functional groups (287.0-287.1 eV) (Fig 3.4.8g). This is to be expected as the dominant organic products arising from the oxidation of glucose by Mn(IV) oxides are carboxylic acids (Bose et al. 1959), predominantly formic acid with minor amounts of glycolic, glyceric, and gluconic acids, as well as aromatic furfural compounds (Furlani et al. 2006). Lourvanij and Rorrer (1994) showed that microporous clays pillared with Fe(III), Cr(III) and Al reacted with glucose at 150° C could promote the isomerization of glucose to fructose, the partial dehydration of glucose to 5-(hydroxymethyl)-2-furaldehyde (Eq. 3.4.3), and the cleavage of 5-(hydroxymethyl)-2-furaldehyde to form carboxylic acids, in particular formic acid which is the final product in the reaction. They found that Fe(III), which is the strongest oxidant of the three metals investigated, was the strongest catalyst of the dehydration and cleavage of the glucose to formic acid. Gonzalez and Laird (2006) showed that smectites can catalyze the formation of hydroxymethylfurfural and furfural compounds from glucose at relatively low temperatures (37° C).

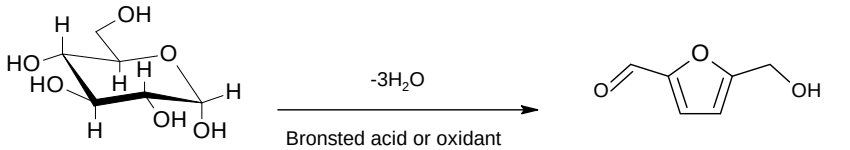

α-D-glucose 5-(hydroxymethyl)-2-furaldehyde (3.4.3)

Therefore the glucose-induced effects on the nature of the humified products in the solid residues of the catechol-glucose and catechol-Maillard systems (Fig. 3.4.8b-f) are ascribed to the oxidation of glucose by Mn(IV) oxide and the resultant formation of aliphatic carboxylic groups and the aromatization products which contain aromatic C-H and –OH functional groups. The peak which appears between 296 and 298 eV in the glucose only system residue (Fig. 3.4.8g) is due to the presence of potassium [the potassium $L_{2,3}$-edge (295-300 eV) overlaps with the last

part of the C K-edge] from any remaining birnessite in the residue, as shown in the XRD data (Fig. 3.4.7f). This is because the K-birnessite used in this study was synthesized by adding concentrated HCl to boiling $KMnO_4$ (McKenzie 1971).

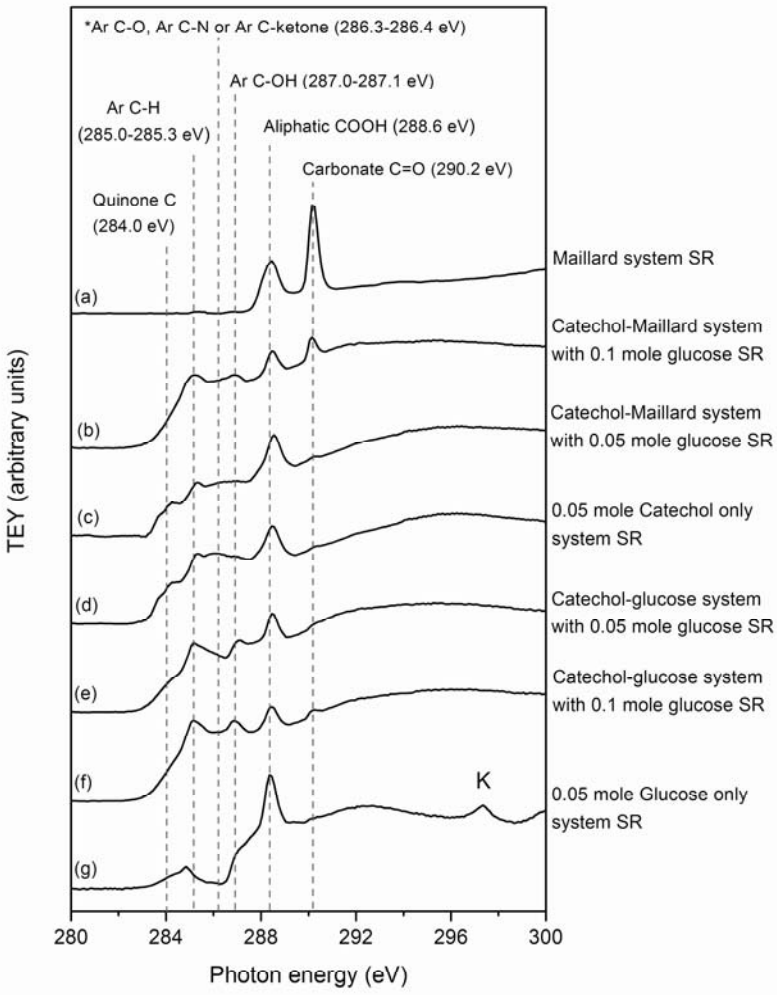

Figure 3.4.8 Carbon K-edge NEXAFS spectra of the solid residues from selected systems reacted in the presence of birnessite: (a) the Maillard reaction (0.05 mole glucose + 0.05 mole glycine); the catechol-Maillard system with (b) 0.1 mole glucose, and (c) 0.05 mole glucose; (d) the 0.05 mole catechol only system; the catechol-glucose system with (e) 0.05 mole glucose, and (f) 0.1 mole glucose; and (g) the 0.05 mole glucose only system. *Ar = aromatic.

Mn L-edge NEXAFS spectroscopy

The Mn $L_{2,3}$-edge NEXAFS spectra of the solid residues from selected reaction systems, HA from the equimolar catechol-Maillard system (unpurified), pure reference compounds and unreacted birnessite are shown in Fig. 3.4.9.

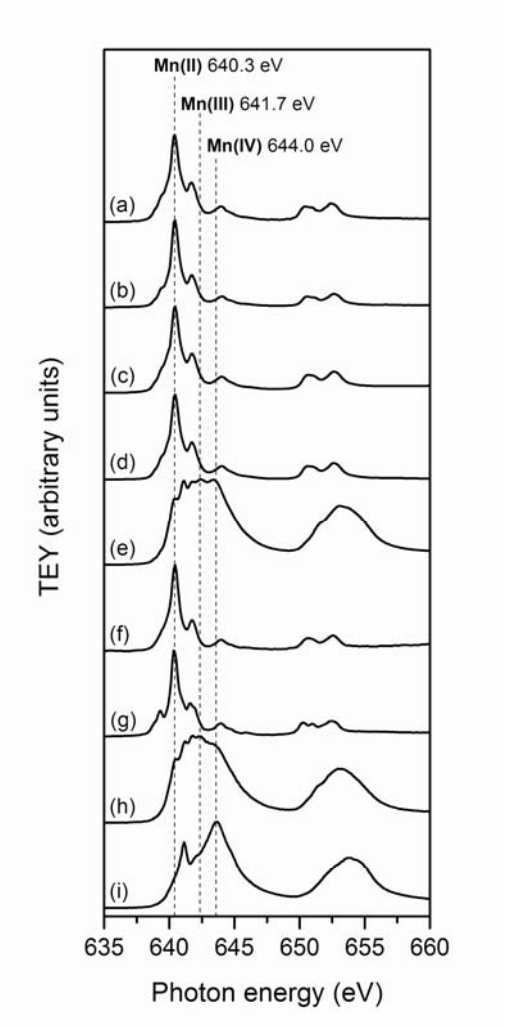

Figure 3.4.9 Mn L-edge NEXAFS spectra of the solid residues of selected treatments reacted in the presence of birnessite: the catechol-Maillard system (0.05 mole catechol + 0.05 mole glycine) with (a) 0.05 mole glucose and (b) 0.1 mole glucose added; the catechol-glucose system (0.05 mole catechol) with (c) 0.05 mole glucose and (d) 0.1 mole glucose added; (e) the 0.05 mole glucose only system; (f) unpurified HA from the equimolar catechol-Maillard system; (g) pure $MnCO_3$; (h) pure Mn_2O_3 and (i) unreacted birnessite. The dotted lines indicate the photon energy of the maximum absorption peak of Mn in divalent, trivalent or tetravalent states, on the Mn L_3 edge.

The Mn in the solid residues from the catechol-Maillard (Fig. 3.4.9a and b) and catechol-glucose (Fig. 3.4.9c and d) systems was in the Mn(II) form. By comparing the shape of the L_3 edge (638-648 eV) of the solid residues from the catechol-Maillard and catechol-glucose systems (Fig. 3.4.9a-d) to that of pure $MnCO_3$ (Fig. 3.4.9g) and Mn(II) bound to humic acid (Fig. 3.4.9f), it can be deduced that the solid residues from the catechol-Maillard and catechol-glucose systems contained a mixture of $MnCO_3$ and Mn(II) bound to humic products. The XRD (Fig.

3.4.6 and 3.4.7), C K-edge NEXAFS (Fig. 3.4.8) and FTIR (data not shown) spectroscopic data confirm the presence of $MnCO_3$ and organic products.

The solid residue of the glucose only system (Fig. 3.4.9e) appears to contain a mixture of Mn(II), Mn(III) and Mn(IV); but judging from the overall shape of the L_3- (638-648 eV) and L_2- (650-660 eV) edges, it appears to be predominantly in the (MnIII) form (compared with the spectra of pure Mn_2O_3 - Fig. 3.4.9h). The XRD (Fig. 3.4.7f) and C K-edge NEXAFS (Fig. 3.4.8g) spectra indicate the presence of $MnCO_3$ and birnessite in the glucose only system solid residue. This shows that glucose alone was not able to reductively dissolve all of the birnessite initially added to the system, in contrast with the other systems containing catechol or catechol and glycine.

3.4.4 Conclusions

The Maillard reaction and the influence of polyphenols on the Maillard reaction as catalyzed by birnessite (δ-MnO_2) were previously reported. However, the role of glucose in influencing the polyphenol humification pathway and the integrated polyphenol-Maillard humification pathway as catalyzed by birnessite remained to be uncovered. The results of the present study show that glucose enhanced humification (browning) reactions in the catechol and especially in the integrated catechol-Maillard reaction systems under the catalysis of birnessite. Increasing the molar ratio of glucose to catechol and glycine in the integrated catechol-Maillard system resulted in a substantial increase in the visible absorbance of the supernatant at 400 nm but the increase was less at 600 nm. This indicates that increasing the molar ratio of glucose to catechol and glycine resulted in increased formation of lower molecular weight humic polymers. This is attributable to the enhanced formation of Maillard reaction products, which are relatively lower molecular weight products, with the increase in the molar ratio of glucose to catechol and glycine.

Increasing the amount of glucose in the catechol-glucose system under the catalysis of birnessite slightly enhanced the formation of aromatic C-OH functionalities and did not affect the formation of aliphatic carboxylic functional groups in the HA fraction isolated from the supernatant of the reaction systems. Increasing the amount of glucose in the integrated catechol-Maillard system under birnessite catalysis promoted the formation of Maillard reaction-type functionalities in the supernatant HA fraction, i.e., aromatic C bound to N, O or ketone and

aliphatic carboxylic groups, which were similar to the functionalities observed in the natural soil and river HA. Therefore, glucose-glycine interaction (i.e., Maillard reaction) in the integrated catechol-Maillard system is predominantly responsible for the enhanced formation of the aliphatic carboxylic functionalities in the HA fraction isolated from the supernatant.

The C K-edge NEXAFS spectroscopic data show that increasing the amount of glucose in the catechol-glucose and catechol-Maillard reaction systems promoted the formation of aromatic C-H and aromatic C-OH but decreased the formation of quinone C and aliphatic COOH in the solid residues. Furthermore, the spectroscopic data also show that glucose promoted the formation of carbonate ($MnCO_3$) at the expense of the aliphatic carboxylic groups in the solid residues of both humification pathways. These transformations are attributable to the dehydration and oxidation of glucose by birnessite, which results in the formation of aromatization products and also the release of CO_2 through decarboxylation and its subsequent conversion to carbonate.

It is thus concluded that sugars, such as glucose, which are one of the most abundant biomolecules in the environment, can make a significant contribution to influence the formation and nature of humic substances and the genesis of carbonates. The findings obtained in this study demonstrate the importance of sugars in influencing abiotic humification pathways and related products in natural environments.

3.5 Research Unit 5: *Catalysis of the Maillard and polyphenol-Maillard humification pathways by poorly crystalline Al and Fe oxides*

3.5.1 Introduction

The formation of humic substances in the environment is a result of selective preservation processes and biotic (enzymatic) and abiotic (mineral) catalytic mechanisms (Stevenson 1994; Bollag et al. 1998; Huang 2004; Clapp et al. 2005). The surfaces of metal oxides are very reactive in promoting the polymerization of phenolic compounds. Metal oxides such as Fe, Mn, Al and Si oxides can act as catalysts by accepting electrons from phenolics leading to the formation of highly reactive semiquinone radicals which readily undergo coupling reactions with other semiquinones, phenolics, amino compounds or existing humus (Huang 2000; Park et al. 2000). Sesquioxides, especially poorly crystalline Fe and Al oxides play an important role in long-term carbon stabilization in soils (Torn et al. 1997; Rasmussen et al. 2005; Mikutta et al. 2006). They are able to form strong chemical bonds with organic molecules via ligand exchange (Mikutta et al. 2007; Kögel-Knabner et al. 2008) as well as being able to physically protect organic molecules from oxidative and biological degradation (Mikutta et al. 2005; Kögel-Knabner et al. 2008).

Shindo and Huang (1984a) investigated the catalytic ability of short-ranged ordered Mn(IV), Fe(III), Al and Si oxides in the oxidative polymerization of the diphenols, catechol, resorcinol and hydroquinone. They found that Mn(IV) oxides (birnessite, cryptomelane, and pyrolusite) were the most powerful catalysts of oxidative polymerization reactions, compared to Fe(III), Al and Si oxides. Manganese(IV) oxide has the strongest catalytic power in promoting catechol humification (compared with Fe(III) and Al oxides) due to the lower electronegativity of Mn and the higher redox potential of the Mn(IV) oxide system (Liu and Huang 2001). Short-range ordered oxides of Al and Si, and especially Fe(III) and Mn(IV), can also promote the formation of aliphatic and carboxylic groups in humic substances through ring cleavage of polyphenols (Wang and Huang 2000b). Birnessite (δ-MnO_2) has been shown to catalyze polycondensation reactions between amino acids and phenolic compounds in the abiotic formation of organic N complexes (Shindo and Huang 1984b). Birnessite is also able to promote the deamination and decarboxylation (Wang and Huang 1987), and dealkylation (Wang and Huang 1997) of glycine. Wang and Huang (1997, 2005) showed that birnessite promotes the

incorporation of carboxyl and especially alkyl C of glycine into the polycondensates formed with pyrogallol.

The Maillard reaction (Maillard 1913) (condensation reactions between sugars and amino acids) is also regarded as an important pathway in natural humification processes (Ikan et al. 1996; Arafaioli et al. 1999; Bosetto et al. 2002). The Maillard reaction pathway under environmentally relevant conditions had been previously investigated using birnessite (Jokic et al. 2001a, 2001b, 2004a) and crystalline goethite (Gonzalez and Laird 2004) as catalysts. In nature it is likely that the polyphenol and Maillard reaction pathways interact with each other since sugars, amino acids and polyphenols all coexist in soil solutions and aquatic environments. The integrated polyphenol-Maillard humification pathway was first studied by Jokic et al. (2004b) using birnessite as catalyst in a reaction system containing glucose, glycine and catechol. They reported that birnessite significantly accelerates the integrated polyphenol-Maillard humification process at temperatures and a pH typical of natural environments. They found that the isolated humic materials have complex spectral and physical characteristics similar to naturally occurring soil humic materials. However, the ability of short-range ordered Al and Fe(III) oxides in influencing the Maillard and integrated polyphenol-Maillard humification pathways remains to be uncovered.

The objective of the present study was, thus, to examine the catalytic abilities of poorly ordered Al and Fe(III) oxides in the Maillard reaction and integrated polyphenol-Maillard humification pathways. These poorly ordered oxides are ubiquitous in natural environments (Bigham et al. 2002; Huang et al. 2002). A further aim of the study was to compare the reaction processes and products of the Al- and Fe-oxide-catalyzed Maillard and catechol-Maillard reaction systems with that of the previously investigated birnessite-catalyzed reaction systems.

3.5.2 Materials and Methods

3.5.2.1 Materials

Poorly crystalline Al and Fe(III) oxides were synthesized according to the method described in Huang et al. (1977). They were characterized using X-ray diffraction analysis as described below and shown to be poorly crystalline. The BET specific surface area and microporosity of the oxides were determined using N_2 gas (Micromeritics Accelerated Surface

Area and Porosimetry ASAP 2000 Analyzer, Micromeritics Instrument Corporation, Norcross, GA, USA).

Catechol (Sigma-Aldrich ACS reagent grade >99%), D-glucose (Sigma-Aldrich ACS reagent grade >99%) and glycine (Sigma Ultra pure grade >99%) were obtained from Sigma Aldrich Canada Ltd (Oakville, ON, Canada). The Fe reference compounds [>99.5% FeO, >98% Fe_3O_4, >99% α-Fe_2O_3, >99% γ-Fe_2O_3 and >99% α-FeO(OH)], which were used in the Fe L-edge NEXAFS spectroscopic study, were obtained from Alfa Aesar, Johnson Matthey Catalog Company, Inc. (Ward Hill, MA, USA). The Al reference compound, >99% $AlPO_4$, used in Al K- and L-edge NEXAFS spectroscopic studies, was obtained from Sigma Aldrich Canada Ltd (Oakville, ON, Canada). Furthermore, for the Al K-edge NEXAFS study, synthetic gibbsite [γ-$Al(OH)_3$] was obtained from Ward's Natural Science (Rochester, NY, USA), and synthetic pseudoboehmite was obtained from BASF Catalysts LLC (Iselin, NJ, USA). The identity of all inorganic reference compounds were confirmed using XRD and NEXAFS spectroscopy as described below. Elliot soil (1S102H) and Suwannee River (1S101H) humic acid standards were purchased from the International Humic Substances Society (IHSS), St. Paul, MN, USA, and used in the C K-edge NEXAFS study.

3.5.2.2 Incubation experiment

Distilled deionized water was used in all the experiments and is henceforth referred to as water. Sterile conditions were maintained throughout the experiment in order to establish the role of abiotic processes. All glassware, birnessite, water and apparatus were autoclaved prior to the experiments. In addition to this, thimerasol, an antiseptic agent, was added to each flask (0.02 %, w/v) before any of the reagents were added. Thimerasol does not affect the oxidation process of phenolic compounds (Wang et al. 1983a).

Two and a half grams of Al or Fe oxide were suspended in each of the reaction solution systems: (i) the Maillard reaction (0.05 mole glucose + 0.05 mole glycine) and (ii) the equimolar integrated catechol-Maillard system (0.05 mole catechol + 0.05 mole glucose + 0.05 mole glycine) in a 250 mL flask. There were control Maillard reaction and catechol-Maillard reaction treatments in which metal oxide was absent. All the reaction systems were adjusted to an environmentally relevant pH 7.0 using 0.1 M HCl or 0.1 M NaOH. The final volume of the reaction solutions was made up to 100 mL using autoclaved water. The flasks were then tightly

sealed and placed in a constant temperature water bath at 45° C for a period of 15 days while gently shaking. Forty-five degrees centigrade is an environmentally relevant temperature as it is common in tropical and subtropical areas, and has also been reported in temperate areas as the approximate temperature of an exposed sunlit soil surface on a day when the ambient air temperature is 25° C (Jury et al. 1991). All treatments were performed in triplicate. The absence of microbial growth was verified by culturing aliquots of selected samples at the end of the incubation period. Aerobic microbial growth was tested for by culturing on Tryptocase Soy Agar (TSA) plates, while anaerobic microbial growth was tested for on TSA plates in a BBL GasPak 150 Large Anaerobic System. All cultures were incubated for a period of 5 and 9 days at 28° C (Jokic et al. 2004b).

3.5.2.3 Characterization of reaction systems at the end of the incubation period and isolation of humic acids.

At the end of the reaction period, the final pH and Eh of the suspensions were measured. The samples were then centrifuged at 25,000 g for 40 min to separate the solid residue from the solution. The absorbance of the supernatant was measured between 400 and 600 nm on a UV-visible spectrophotometer (Beckman DU 650 microprocessor controlled spectrophotometer, Fullerton, CA, USA). The visible absorbance at 400 and 600 nm provides an indication of the extent of polymerization which has taken place in the reaction systems (Shindo and Huang 1982, 1984a, 1984b). Shindo and Huang (1984a) studied the polymerization of polyphenols by short-range ordered Mn, Fe, Al and Si oxides, and showed that the yield of humic polymers was directly related to the visible absorbance. Likewise, with natural humic substances, Gan et al. (2007) showed that visible absorbance can be used to determine the concentration of fulvic acid in solution. The supernatant was diluted with water prior to absorbance determination and the values obtained were subsequently multiplied by the dilution factor. The Al and Fe content of the supernatant was determined using atomic absorption spectroscopy (Varian Spectra AA 220, Walnut Creek, CA, USA).

The solid residue was repeatedly washed with water using centrifugation at 25,000 g for 40 min until the wash water was clear. These water extracts were collected and added to the supernatant. The washed residue was then freeze-dried. The combined water extracts and supernatant was then acidified to pH 1.0 using 6 M HCl and allowed to stand for 24 h to

precipitate the humic acid (HA) fraction out of the solution (Swift 1996). The acidified suspensions were then centrifuged at 25,000 g for 45 min to separate the HA fraction from the rest of the solution containing the fulvic acid (FA) fraction and non-humic substance fraction. The HA residue was then resuspended in a 0.1 M HCl and 0.3 M HF solution and shaken for 48 h. The suspension was then centrifuged again as described before and the sedimented HA was dialyzed in 1000 molecular weight cut off dialysis tubing for 5 days in distilled deionized water until the water tested free from chloride ($AgNO_3$ test). The purified HA was then freeze-dried.

3.5.2.4 Characterization of the reaction products

X-ray diffraction (XRD). The solid residues, unreacted catalysts and reference compounds were examined using X-ray diffractometry on a Rigaku Rotaflex 200SU (Tokyo, Japan) with a rotating Fe anode and graphite monochromator. The samples were lightly ground and then mounted on glass slides by making a slurry of the ground sample with acetone and allowing it to dry. The scans were performed at 40 kV and 160 mA, from 4 to 80 °2θ, at a step size of 0.02 °2θ at a scanning rate of 0.1 °2θ sec^{-1}.

Organic carbon analysis. Organic carbon analysis of the solid residues was performed using a dry combustion method on a Leco CR-12 Carbon Analyzer (Leco Corporation, St. Joseph, MI, U.S.A.) as described by Wang and Anderson (1998).

Near edge X-ray absorption fine structure (NEXAFS) spectroscopy. The speciation of C, Al, and Fe was investigated in selected solid residues and supernatant HA fractions using C and Al K-edge and Fe L-edge NEXAFS spectroscopy on the SGM (Spherical grating monochromator) beamline (Regier et al. 2007) and Al L-edge NEXAFS spectroscopy on the VLS-PGM (variable line spacing plane grating monochromator) beamline (Hu et al. 2007) at the Canadian Light Source (Saskatoon, SK, Canada).

The reference compounds [pseudoboehmite, gibbsite, $AlPO_4$, FeO, α-Fe_2O_3, γ-Fe_2O_3, Fe_3O_4 and α-FeO(OH)], unreacted oxide catalysts and solid residues were finely ground and mounted on C-tape and then examined using Al K-edge and Al and Fe L-edge NEXAFS. The photon energy step size used was 0.1 eV. An exit slit width of 50 μm and a dwell time of 0.3s were used. All spectra were normalized against the beamline current measured by a Ni or Au mesh (90% transmission). An additional spline baseline was applied to the Al L-edge spectra due

to distortions caused by sample self-absorption. The Al K-edge, and Al and Fe L-edge spectra were recorded by total electron yield (TEY) and fluorescence yield (FLY).

The reference compounds (glycine, IHSS soil and river HA standards) and solid residue and HA samples which were investigated using C K-edge NEXAFS were mounted on gold (Au)-coated (~400 Å) silicon (Si) wafers. The samples were mounted on the Au-coated Si wafers by making dilute suspensions of the samples in distilled deionized water and then placing a droplet of the suspension on a wafer and allowing it to dry. An exit slit width of 20 μm and a dwell time of 0.3s were used to minimize damage due to exposure to radiation. These spectra were recorded by total electron yield (TEY) at an energy step size of 0.1 eV. The C spectra were normalized to a clean Au-coated Si wafer, so that the signals from C in the beamline and C contamination on the gold I_0 mesh would not interfere with the signal from our samples (Watts et al. 2006). Spectra obtained were analyzed using aXis2000 software (Hitchcock et al. 2005).

The energy scale of the C, Al and Fe spectra collected on the SGM beamline were internally calibrated using glycine, gibbsite and α-Fe_2O_3, respectively, based on calibrated values of the white lines (absorption maxima) of the compounds reported from previous studies [C K-edge absorption maxima of glycine = 288.6 eV (Boese et al. 1997; Myneni 2002), Al K-edge absorption maxima of gibbsite = 1570.5 eV (Ildefonse et al. 1998), Fe L-edge absorption maxima of α-Fe_2O_3 = 709.5 eV (Garvie and Buseck 1998)]. The energy scale of the PGM was calibrated using sharp features in inert gases such as Xe and Kr (Hu et al. 2007). All the spectra were normalized to each other, with the maximum intensity of each spectrum fixed at 1.

3.5.3 Results and Discussion

3.5.3.1 Effect of the presence of metal oxide catalyst on the reaction systems

In all the reaction systems studied, no aerobic or anaerobic microbial growth was observed. Thus, all the processes studied were abiotic in nature. The BET specific surface area of the Al oxide was 221.1 $m^2\ g^{-1}$ and the Fe oxide was 164.7 $m^2\ g^{-1}$. The BET specific surface area of the Mn oxide was previously reported as 63 $m^2\ g^{-1}$ (Section 3.1). The micropore area of the Al oxide was 20.6 $m^2\ g^{-1}$ and the Fe oxide was 83.2 $m^2\ g^{-1}$. The Mn oxide did not possess any microporosity.

The effect of the presence of the Al- and Fe-oxides on the visible absorbance of the supernatants of the reaction systems compared with the Mn-oxide system is shown in Figure

3.5.1. The presence of the redox-reactive Mn and Fe oxides significantly enhanced browning (humification) in all of the reaction systems, most notably in the catechol-Maillard system (Fig. 3.5.1b). The presence of Al oxide in the Maillard system (Fig. 3.5.1a) actually appeared to decrease visible absorbance compared to the control system. This is most likely due to the sorption of humic polymers on the surface of the Al oxide, as indicated by the colour of the Al oxide which changed from pure white to a light brown after the reaction period. This was confirmed by the organic C content analysis of the solid residue which is discussed in Section 3.5.3.3.

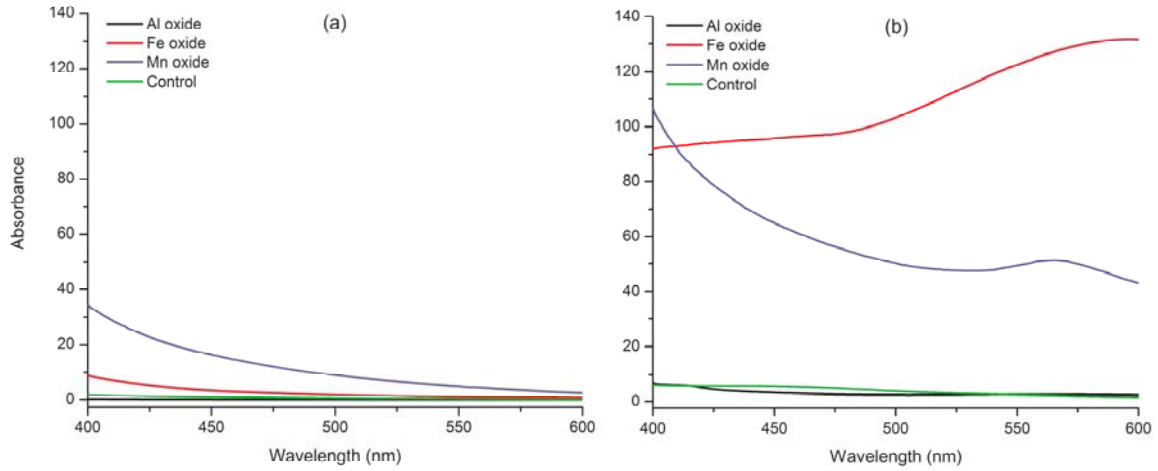

Figure 3.5.1 Comparison of the effect of the presence of Al-, Fe- and Mn-oxide on the visible absorbance (400-600 nm) of the supernatant from (a) Maillard reaction and (b) the integrated catechol-Maillard system. The absorbances are scaled by the dilution factor. The absorbances of the Mn oxide systems are cited from Section 3.1.

Table 3.5.1 provides a summary of the solution characteristics of the reaction systems in the presence and absence of the Al, Fe and Mn oxides at the end of the 15 day reaction period. The systems in the presence of the Mn oxide (birnessite) had the highest final pH values. This is attributed to the complete reductive dissolution of birnessite during the reaction period (FTIR and XRD data not shown) which results in the consumption of protons and ultimately raises the solution pH. The integrated catechol-Maillard systems had lower pH values than the Maillard reaction systems in all of the metal oxide and control systems. This is attributed to the enhancement of oxidative polymerization reactions involving catechol, which result in the generation of semiquinone free radicals and protons. The Mn oxide-catalyzed systems had the

lowest redox status (pH + pE values) which indicates that more oxygen was consumed in these systems due to oxidative polymerization reactions than in the other systems. The Fe oxide systems had the second lowest redox status, while the control and Al oxide systems were the highest.

Table 3.5.1 Comparison of pH, redox status (pH + pE) and metal concentration of the supernatants from the Al, Fe and Mn oxide-catalyzed and control systems. The Mn oxide data are cited from Section 3.1.

Treatment	pH	pH + pE	[Al] (mmol/L)	[Fe] (mmol/L)	[Mn] (mmol/L)
Metal oxide systems					
Al oxide Maillard[a]	5.48 ±0.04	11.65 ±0.02	10.7 ±2.4	-	-
Al oxide Integrated[b]	4.70 ±0.07	8.07 ±1.09	52.2 ±5.4	-	-
Fe oxide Maillard	5.46 ±0.11	7.19 ±0.40	-	34.8 ±2.5	-
Fe oxide Integrated	4.99 ±0.03	7.65 ±0.07	-	58.8 ±4.1	-
Mn oxide Mailllard	8.08 ±0.11	7.07 ±0.54	-	-	193.1 ±5.7
Mn oxide Integrated	6.85 ±0.01	6.62 ±0.33	-	-	92.0 ±8.5
Control systems					
No catalyst Maillard	6.26 ±0.13	10.72 ±0.76	-	-	-
No catalyst Integrated	5.49 ±0.12	9.05 ±0.90	-	-	-

[a]Maillard = Maillard reaction

[b]Integrated = integrated catechol-Maillard reaction

The Al and Fe oxide-catalyzed catechol-Maillard systems had higher concentrations of metal in solution than the Al and Fe oxide-catalyzed Maillard systems (Table 3.5.1). This is attributable to the presence of catechol in the integrated catechol-Maillard which favoured the dissolution of the Al and Fe oxides. The opposite trend was observed in the Mn oxide-catalyzed systems. This is attributable to the fact that all the Mn oxide was dissolved in the Maillard and catechol-Maillard systems during the reaction period, unlike the Al and Fe oxides, and that significant amounts of Mn were found sorbed in the solid residues of the Maillard and catechol-Maillard systems as Mn(II) was complexed with organic compounds and/or reacted with carbonate to form rhodochrosite [$Mn(II)CO_3$] (this will be discussed in further detail in Section 3.5.3.3).

The stronger catalytic ability of the Mn and Fe oxides compared to the Al oxide can be attributed to the higher redox potential of the Mn and Fe oxide reaction systems compared to the Al oxide system which is not subject to redox reactions (Liu and Huang 2001). The standard electrode potential values of the overall redox reaction of catechol oxidation by Mn(IV) oxide and Fe(III) oxide are +0.509 V and +0.071 V, respectively (Liu and Huang 2001). The higher positive potential of the Mn(IV) oxide system indicates that it is thermodynamically more favourable for the oxidation of catechol to quinone than the Fe(III) oxide system. This would also explain why the Mn oxide was completely reduced and consumed in the integrated catechol-Maillard system in comparison to the Fe or Al oxides. Furthermore, the lower electronegativity of Mn (1.55) versus Fe (1.83) or Al (1.61) accelerates the formation of semiquinone free radicals by promoting electron cloud delocalization from the catechol phenolic oxygen into the aromatic 2p π-orbital of catechol (Liu and Huang 2001).

3.5.3.2 Characterization of humic acid fraction isolated from the supernatant of the reaction systems

Carbon K-edge NEXAFS spectroscopy

The C K-edge NEXAFS spectra of natural IHSS HAs and the HAs isolated from the supernatant of the Maillard and catechol-Maillard systems are shown in Fig. 3.5.2. There was very little browning in the control and Al oxide-catalyzed Maillard reaction systems (Fig. 3.5.1a) and thus HA fractions could not be isolated from these systems. Spectroscopic assignments are based on the absorption maxima of the reference compounds (glucose, glycine and pyrogallol) and on values reported by previous C NEXAFS studies (Myneni 2002; Urquhart and Ade 2002; Dhez et al. 2003; Cooney and Urquhart 2004; Hitchcock and Mancini 2004). The NEXAFS narrower and sharper core (C 1s) → π* transitions have been found to be the most useful for chemical analyses and identification of organic compounds due to their chemical sensitivity based on the chemical energy shifts (Urquhart and Ade 2002).

The lowest absorption bands at around 284.0 eV usually correspond to molecules with low energy π* states, such as quinones (Francis and Hitchcock 1992). Absorption bands near 285 eV are generally ascribed to C 1s (C-H) → $1\pi^*_{C=C}$ transitions (Urquhart and Ade 2002; Cooney and Urquhart 2004), which are characteristic of C=C unsaturation. The transitions of aromatic C bound to carbonyl (e.g., terephthalate species) tend to overlap with unsaturated aromatic C-H

transitions due to the strong electronic interactions between the benzene π* density and carbonyl π* density, and are generally found in the 284.4-285.0 eV range (Cooney and Urquhart 2004). The absorption bands near 286-288 eV are characteristic of functionalized aromatic groups C 1s (C-R) → $1\pi^*_{C=C}$ transitions (R = functional group), such as aromatic C bound to aldehyde (286.0 eV), ketone (286.4 eV), urea (286.4 eV), carbamate (286.6-286.8 eV), amine (286.8-286.9 eV), phenol (287.0-287.3 eV) and ester (287.1 eV) groups (Urquhart and Ade 2002; Dhez et al. 2003; Cooney and Urquhart 2004; Hitchcock and Mancini 2004). Heterocyclic N compounds C 1s (C-N) → $1\pi^*_{C=C}$ transitions also occur in the ~286-287 eV range, e.g., pyridine (285.7 eV) and pyrrole (286.3 eV) (Dhez et al. 2003; Hitchcock and Mancini 2004). The C=N and C≡N π* transitions usually occur around 286.3 eV (Myneni 2002). Generally speaking, a stronger electron withdrawing substituent on the aromatic ring, will result in a higher energy shift of the C 1s (C-R) → $1\pi^*_{C=C}$ transition.

The carbonyl C 1s (C-R) → $1\pi^*_{C=O}$ transitions usually occur between 286-291 eV, and can be used to distinguish between groups such as aldehydes (286.2-286.4 eV), ketones (286.6-286.8 eV), amide (287.8-288.2 eV), acetic/acetate (288.1-288.6 eV), urea (289.2-289.8 eV), carbamate (289.9.0-290.1 eV) and carbonate (290.2-290.6 eV) (Urquhart and Ade 2002). The main cause of the shifts observed in C 1s (C-R) → $1\pi^*_{C=O}$ transitions is the inductive effect of the neighbouring atoms on the carbonyl C 1s binding energy (Urquhart and Ade 2002). Low lying σ* orbitals also provide valuable information in identifying aliphatic functionalities. Saturated aliphatic C exhibits C 1s (C-H) → σ^*_{C-H} transitions in the 287.1-287.9 eV range, while aliphatic alcohol C 1s (C-H) → σ^*_{C-O} transitions are found shifted to a higher energy in the 289.2-289.5 eV range (Dhez et al. 2003).

The C K-edge spectra of the natural HA samples (Fig. 3.5.2a and b) are dominated by aliphatic carboxylic functionalities (288.6 eV) and also contain aromatic functional groups (285.0-287.1 eV). The soil HA (Fig. 3.5.2a) appears more heterogeneous than the river HA (Fig. 3.2.5b). The relative intensity of the aliphatic carboxylic functional groups (288.6 eV) to aromatic functional groups (285.0-287.1 eV) was lower in the HA from the Al oxide catechol-Maillard system than the Fe oxide catechol-Maillard system (Fig. 3.5.2d and e). The HA from the supernatant of the Mn oxide catechol-Maillard system (Fig. 3.5.2g) had a relatively higher content of aliphatic carboxylic groups (288.6 eV) than the other systems. The HA from the control catechol-Maillard system was predominantly aromatic in nature (Fig. 3.5.2c) but

appeared to contain a higher relative amount of aliphatic carboxylic functionalities (288.6 eV) than the Al oxide or Fe oxide catechol-Maillard systems (Fig. 3.5.2d and e). The HA from the Fe oxide- and Mn oxide-catalyzed Maillard reaction systems appeared quite similar in nature, as both were strongly aliphatic carboxylic in nature (Fig. 3.5.2f and h).

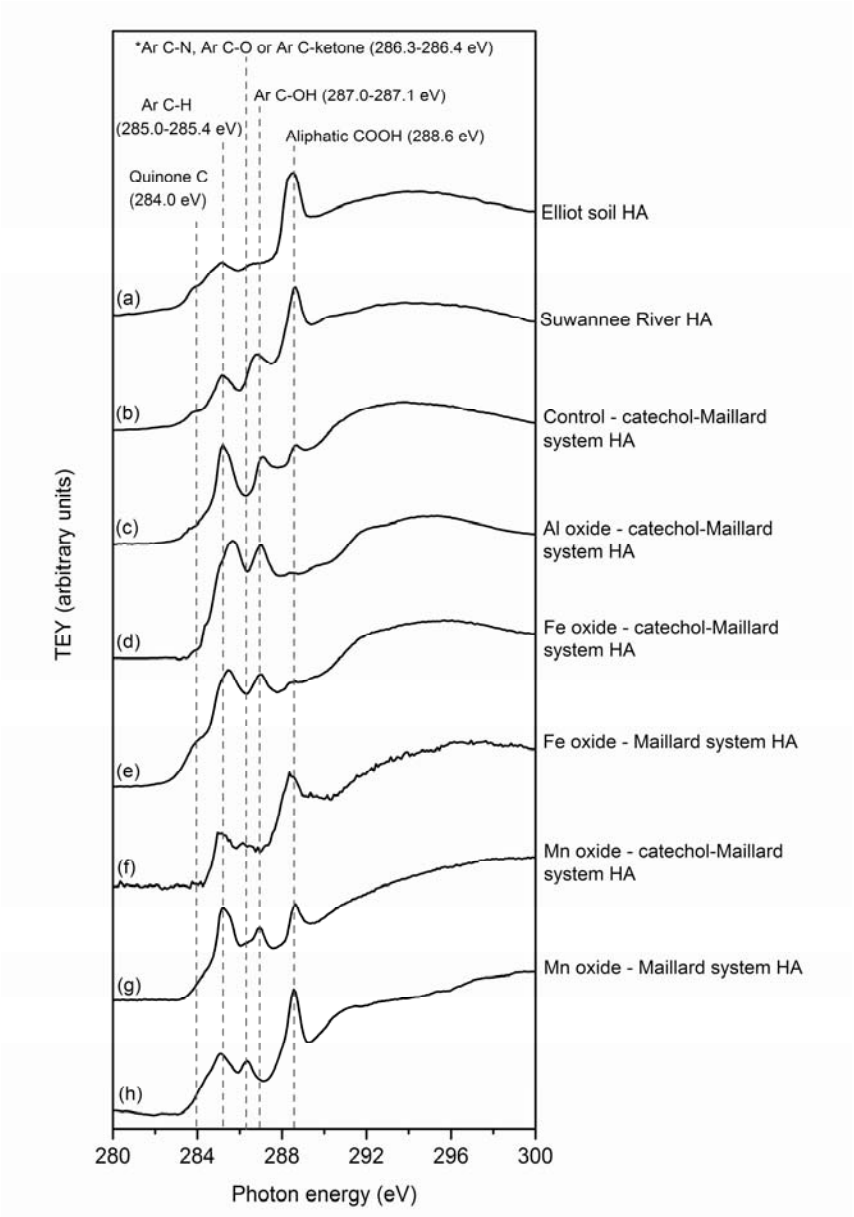

Figure 3.5.2 Carbon K-edge NEXAFS spectra of the IHSS (a) soil and (b) river HAs, and the HAs extracted from the supernatants of the: (c) control catechol-Maillard system (no catalyst), (d) Al oxide catechol-Maillard system, (e) Fe oxide catechol-Maillard system (f) Fe oxide Maillard system, (g) Mn oxide catechol-Maillard system and (h) Mn oxide-catalyzed Maillard system. *Ar = aromatic. The Mn oxide HA spectra are cited from Section 3.1.

3.5.3.3 Characterization of the solid phase reaction products from reaction systems incubated in the presence of metal oxides

X-ray diffraction

The X-ray diffractograms of the unreacted Al oxide, and solid residues of the Maillard and catechol-Maillard systems reacted in the presence of Al oxide, are shown in Fig. 3.5.3. The Al oxide used as catalyst was poorly crystalline pseudoboehmite (Fig. 3.5.3a) and appears to have become more ordered after reaction in the Maillard (Fig. 3.5.3b) and catechol-Maillard (Fig. 3.5.3c) systems. It is unclear whether the increase in crystallinity of the Al oxide (Fig. 3.5.3b and c) was due to aging at 45°C in the solution of biomolecules during the incubation period, or whether this was due to the partial dissolution of the poorly crystalline components of the Al oxide after reaction with the biomolecules, resulting in the improved stacking and ordering of the pseudoboehmite in the solid residues.

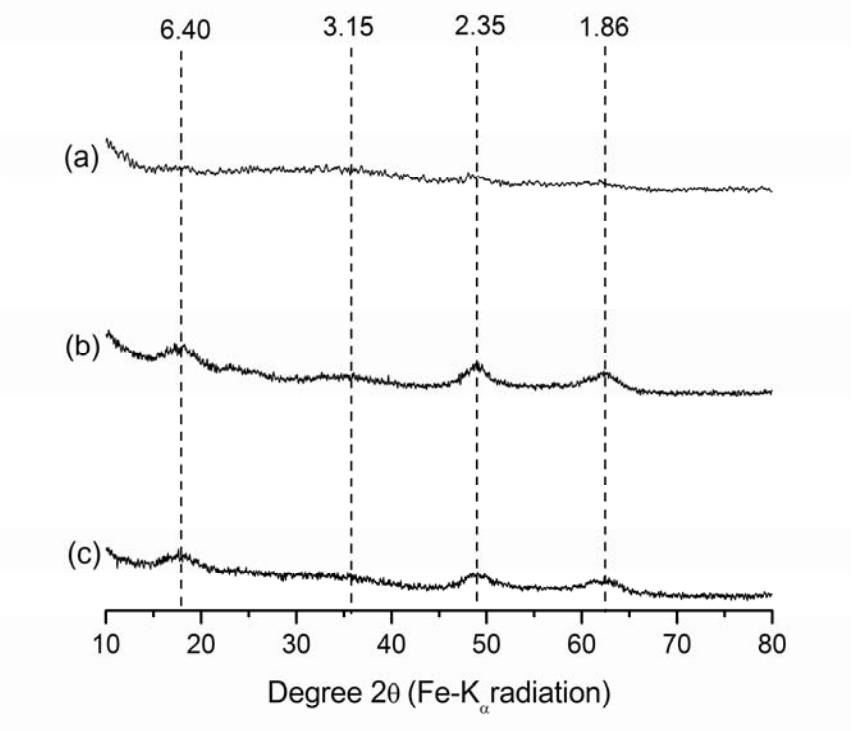

Figure 3.5.3 X-ray diffractograms of the (a) unreacted Al oxide and solid residues from the Al-oxide-catalyzed: (b) Maillard reaction system, and (c) catechol-Maillard reaction system. The d-values are indicated in angstrom.

The X-ray diffractograms of the unreacted Fe oxide, and solid residues of the Maillard and catechol-Maillard systems reacted in the presence of Fe oxide, are shown in Fig. 3.5.4. The Fe oxide used as catalyst was poorly crystalline (Fig. 3.5.4a) and had a broad band at approximately 2.52 Å, which is typical for Fe(III) oxides such as hematite (α-Fe_2O_3) and maghemite (γ- Fe_2O_3) (Joint Committee on Powder Diffraction Standards 1974). The solid residue from the Maillard system (Fig. 3.5.4b) did not appear different from that of the unreacted Fe oxide (Fig. 3.5.4a). However, the solid residue from catechol-Maillard system (Fig. 3.5.4c) contained a number of sharp peaks, in addition to the broad band at 2.52 Å. The peak at 8.86 Å can be ascribed to catechol, whereas the other sharp peaks are not characteristic of catechol or any of the other biomolecules used in the reaction system (International Centre for Diffraction Data 2006). These peaks were also not present in any of the other reaction systems studied thus far (Sections 3.1 - 3.4). These peaks do not match the d-values of any known Fe oxides or Fe carbonates (Joint Committee on Powder Diffraction Standards 1974).

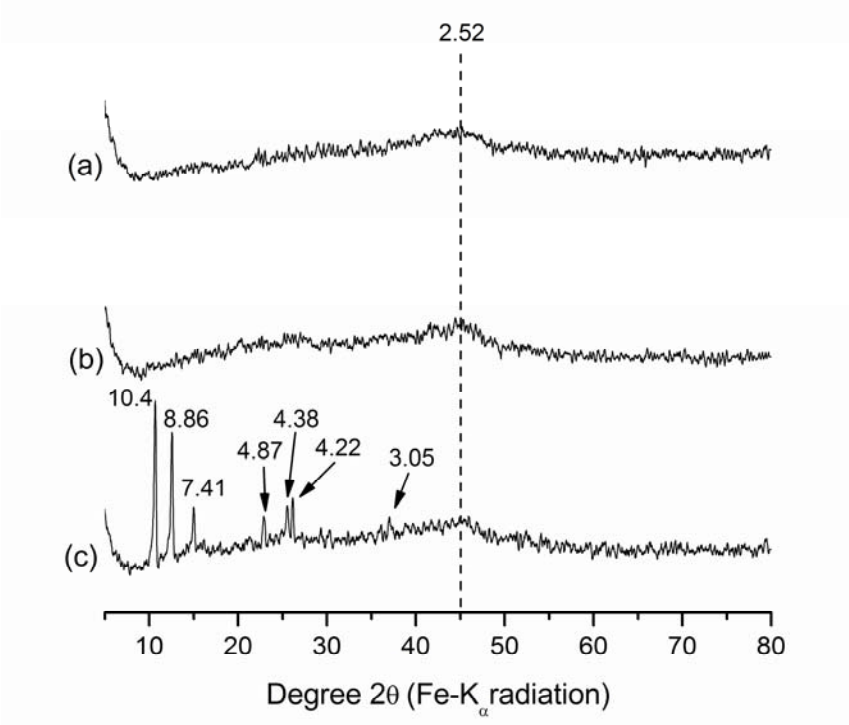

Figure 3.5.4 X-ray diffractograms of the (a) unreacted Fe oxide and solid residues from the Fe-oxide-catalyzed: (b) Maillard reaction system, and (c) catechol-Maillard reaction system. The d-values are indicated in angstrom.

Organic carbon analysis

The organic C content of the unreacted metal oxide catalysts and the solid phase from the Al, Fe and Mn oxide-catalyzed reaction systems are shown in Table 3.5.2. The enrichment of organic C (g) in the solid residues was calculated as follows: [organic C content of residue (%) – organic C content of catalyst (%)] x [Total mass of solid residue (g)] = [Enrichment of organic C (g)]

Table 3.5.2 Organic C enrichment in the solid residues (SR) from the Al, Fe and Mn oxide-catalyzed Maillard reaction and integrated catechol-Maillard systems. The Mn oxide data are cited from Section 3.1.

Sample	Organic C content (%)	Total mass of solid residue[a] (g)	Enrichment of organic C (g)
Al oxide catalyst	0.3	-	-
Al oxide Maillard system SR	5.6	2.22	0.12
Al oxide catechol-Maillard system SR	14.0	2.46	0.34
Fe oxide catalyst	0.2	-	-
Fe oxide Maillard system SR	5.6	2.34	0.13
Fe oxide catechol-Maillard system SR	18.5	2.43	0.45
Mn oxide catalyst	0.1	-	-
Mn oxide Maillard system SR	13.0[b]	1.33	0.17
Mn oxide catechol-Maillard system SR	35.9[b]	6.73	2.41

[a]The amount of metal oxide initially added to each system was 2.50 g
[b]Combustion method employed could not distinguish between organic C and $MnCO_3$

The solid residues from the Maillard reaction systems catalyzed by the Al- and Fe-oxides contained the same percentages of organic C (5.6 %). However the Fe oxide-catalyzed catechol-Maillard system contained a much higher percentage of organic C (18.5 %) than the Al oxide-catalyzed catechol-Maillard system (14.0 %). The Mn oxide-catalyzed Maillard and catechol-Maillard systems contained the highest percentages of C (13.0 % and 35.9 %, respectively) compared to the Al- and Fe-oxide-catalyzed systems. However, in contrast to the Al and Fe oxide-catalyzed systems, in the Mn oxide-catalyzed systems (Maillard and catechol-Maillard)

all of the oxide was consumed during the reaction period. At the end of the incubation period the solid phase of the Mn oxide-catalyzed system contained Mn(II) complexed with organic compounds and rhodochrosite [$Mn(II)CO_3$] (FTIR and Mn L-edge NEXAFS spectroscopic data not shown). It was not possible to differentiate between organic C and $MnCO_3$ using the LECO analyzer as it is based on a dry combustion method to measure the CO_2 released at 841 °C and 1100 °C to distinguish between CO_2 released from organic C (841° C) and total C , i.e., inorganic C + organic C (1100° C). Manganese carbonate decomposes at temperatures above 200°C, which is substantially lower than the melting point of $CaCO_3$ (825° C) (Perry and Phillips 1995). Calcium carbonate is considered the most common form of inorganic C in soils and sediments. Thus, the C from $MnCO_3$ would be included in the "organic C" fraction using the conventional dry combustion method.

The Mn oxide-catalyzed catechol-Maillard system showed the greatest enrichment of organic C in the solid residue with an increase of 2.41 g of organic C compared to the Al and Fe oxide-catalyzed systems which showed an increase of 0.34 and 0.45 g of organic C, respectively (Table 3.5.2). The visible absorbance of the supernatant from the Mn and Fe oxide systems were significantly higher than that of the Al oxide and control systems (Fig. 3.5.1b). The data indicate that most of the humic substances in the Fe oxide remained suspended in the supernatant, whereas, in the Mn oxide system, the supernatant and solid phase contained considerable amounts of humic substances. In the Al oxide system most of the humic substances were found sorbed in the solid phase as the visible absorbance of the supernatant was relatively low and appeared even lower than that of the control system.

Glycine and catechol have typical aliphatic carboxylic and phenolic functional groups, respectively. These functional groups are the dominant functional groups identified in the HA (Fig. 3.5.2) and solid phase (see later Fig. 3.5.5). Carboxylic and phenolic groups play an important role in the sorption of metals and metal oxide surfaces. The values of the logarithm of the stability constants of the complexes of the glycine and Al^{3+} and Fe^{2+} are 5.91 and 4.13, respectively, at 25°C and an ionic strength of $\mu = 0.1$ (Martell and Smith 2004). Those of the logarithm of the stability constants of the complexes of the catechol and Al^{3+} and Fe^{2+} are -6.08 and -14.3, respectively, at 25°C and an ionic strength of $\mu = 0.1$ (Martell and Smith 2004). Thus Al^{3+} has a relatively higher affinity for carboxylic and phenolic groups than Fe^{2+}. This would explain the data indicating that most of the humic products in the Al oxide-catalyzed system

were found sorbed in the solid phase, whereas, in the Fe oxide system most of the products were found in the supernatant (Fig. 3.5.1 and Table 3.5.2).

Carbon K-edge NEXAFS spectroscopy

The C K-edge NEXAFS spectra of the solid residues from the Maillard and catechol-Maillard systems catalyzed by Al, Fe and Mn oxides are shown in Fig. 3.5.5. The solid residues from all the metal oxide-catalyzed Maillard systems (Fig. 3.5.5a-c) were strongly aliphatic carboxylic (288.6 eV) in nature, which is similar to the HAs isolated from the supernatant of the Fe and Mn oxide-catalyzed systems (Fig. 3.5.2f and h). There is also evidence of aromatic C bound to carbonyl (284.5 eV), aromatic C-H (285.0-285.3 eV), aromatic C bound to N, O or ketone functional groups (286.4 eV) and phenolic C (287.0 eV) in the solid residues from the metal oxide-catalyzed Maillard systems (Fig 3.5.5a-c). In contrast to the solid residues from the Fe and Al oxide-catalyzed Maillard systems (Fig. 3.5.5a and b), the Mn oxide-catalyzed Maillard system contained a relatively large amount of Mn carbonate (290.2 eV) (Fig. 3.5.5c), which was confirmed by XRD and FTIR spectroscopy (data not shown). This was attributed to the high pH of the Mn oxide Maillard system (Table 3.5.1) as a result of the complete reductive dissolution of birnessite which is favourable for the formation of $MnCO_3$.

The solid residues from all three catechol-Maillard systems contained quinone C (284.0 eV), aromatic C-H (285.0-285.3 eV), phenolic (287.0-287.1 eV) and aliphatic carboxylic (288.6 eV) functionalities (Fig. 3.5.5). The solid residue from the Mn oxide-catalyzed catechol-Maillard system (Fig. 3.5.5f) appeared the most heterogeneous in terms of the aromatic functionalities of the three systems, and was dominated by aliphatic carboxylic functional groups, in contrast to the Al and Fe oxide systems (Fig. 3.5.5d and e). The Mn oxide-catalyzed catechol-Maillard system also contained a relatively small amount of Mn carbonate (290.2 eV) (Fig. 3.5.5f), which was confirmed by XRD and FTIR spectroscopy (data not shown). The Fe oxide-catalyzed catechol-Maillard system showed the sharpest aromatic functionality peaks (Fig. 3.5.5e).

The solid residues from the Al and Fe oxide-catalyzed catechol-Maillard reaction systems (Fig. 3.5.5d and e) contained more aliphatic carboxylic material than the HA isolated from the supernatant of the reaction systems (Fig. 3.5.2d and e). This is attributable to the chemical partitioning of the humic substances between the solution and solid phases by the preferential coprecipitation of multivalent metals with humic substances possessing aliphatic carboxylic

groups (Christl and Kretzchmar 2007; Hardie et al. 2007) or to the preferential adsorption of these functional groups on the positively charged surfaces of Al or Fe oxides (Chorover and Amistadi 2001; Kögel-Knabner et al. 2008). The HA in the control system appeared to be relatively strongly aliphatic carboxylic in nature (Fig. 3.5.2c). However, in contrast to the other systems, there were no metal oxides or dissolved multivalent metals in the control system, and therefore, the chemical partitioning of the humic polymers between the solution and solid phases based on their functional groups would not occur. Therefore, all the HA formed in the control system was found in the supernatant unlike the systems catalyzed by metal oxides, and thus it appeared more aliphatic carboxylic in nature than the other systems.

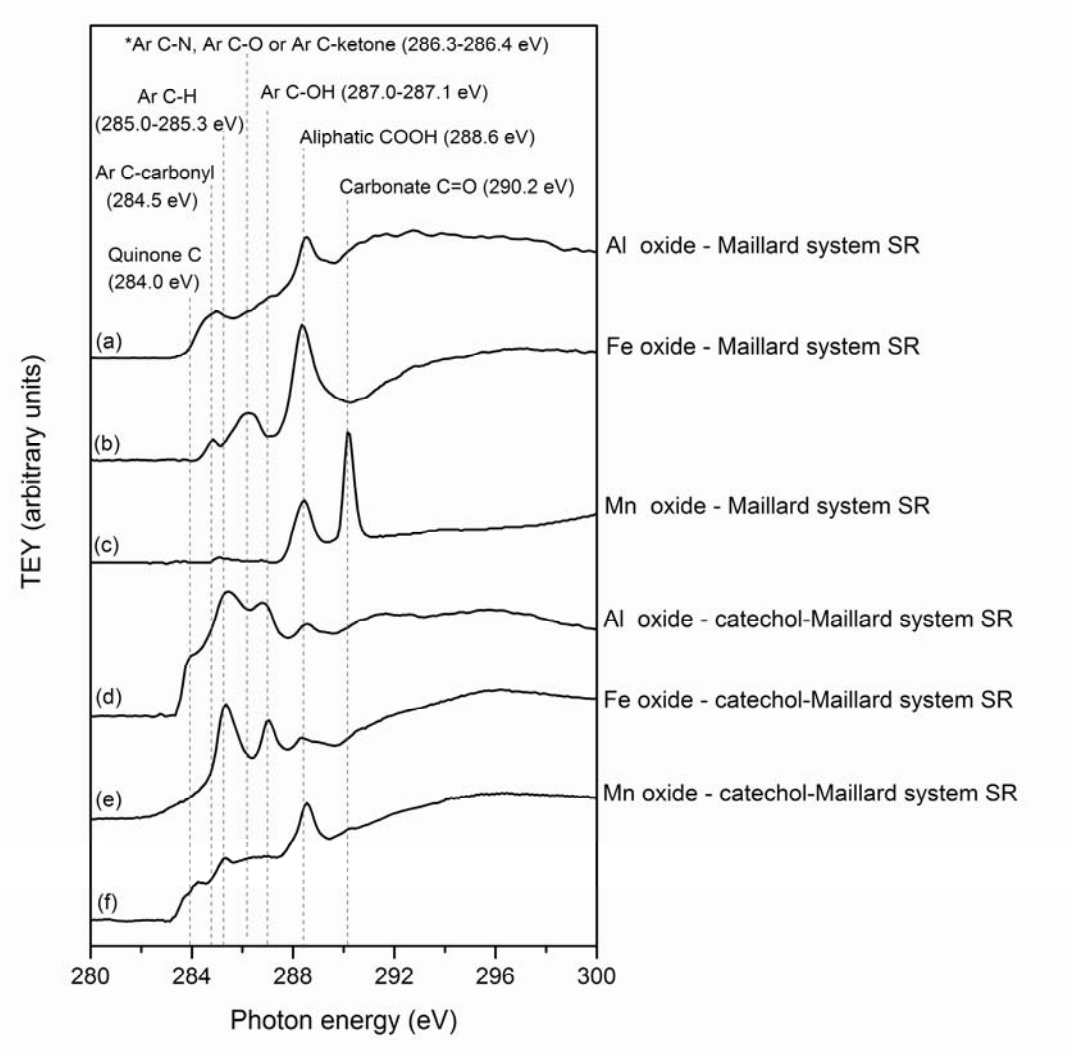

Figure 3.5.5 Carbon K-edge NEXAFS spectra of the solid residues (SR) from the Maillard reaction systems catalyzed by (a) Al oxide, (b) Fe oxide and (c) Mn oxide, and the integrated catechol-Maillard reaction systems catalyzed by (d) Al oxide, (e) Fe oxide and (f) Mn oxide. *Ar = aromatic. The Mn oxide spectra are cited from Section 3.1.

Aluminum K- and L-edge NEXAFS spectroscopy

The Al K-edge NEXAFS TEY and FLY and L-edge NEXAFS FLY spectra of selected reference compounds, the unreacted Al oxide, and the solid residues from the Maillard and catechol-Maillard systems reacted in the presence of Al oxide are shown in Fig. 3.5.6, 3.5.7 and 3.5.8, respectively. The Al L-edge NEXAFS TEY spectra of the samples and reference compounds were very weak and not meaningful (data not shown). The reference compounds were selected because they contain Al in either 4- (tetrahedral) or 6-coordination (octahedral) and would help in the identification of the Al coordination in unreacted Al oxide catalyst and residues from the reaction systems. Gibbsite contains Al in 6-coordination (Bragg and Claringbull 1965), pseudoboehmite and boehmite contain Al in 6-coordination (Yoon et al. 2004; Hu et al. 2008), and $AlPO_4$ has Al in 4-coordination (Berry and Mason 1959).

The Al K-edge (TEY) and L-edge (FLY) NEXAFS spectra of the Al oxide reacted in the catechol-Maillard system (Fig. 3.5.6c and 3.5.8c) indicate that the residue had a greater content of tetrahedral-Al (1566.1 eV and 78.2 eV, respectively) than the unreacted Al oxide (Fig. 3.5.6a and 3.5.8a). This indicates the effect of organic humic polymers bound to the Al (either through surface complexation or by co-precipitation with Al from solution) on Al speciation of the solid residues. The effect of organic ligands on the coordination of Al has recently been demonstrated by Hu et al. (2008) using Al K- and L-edge NEXAFS spectroscopy. They showed that Al oxide formed in the presence of tannic acid contained more tetrahedral Al than oxides formed in the absence (Hu et al. 2008). There was not a significant change in the nature of the Al oxide reacted in the Maillard system (Fig. 3.5.6b and 3.5.8b), other than the band at 1567.2 eV became more intense (Fig. 3.5.6b), which is similar to the shape of the spectra of pure pseudoboehmite (Fig. 3.5.6e). This is in accord with the XRD data, which showed that the pseudoboehmite in the Al oxide-Maillard system appeared more ordered after reaction in the biomolecule systems (Fig. 3.5.3).

The Al K-edge FLY spectra of the Al oxide Maillard and catechol-Maillard residues only showed a small increase in the intensity of the 1567.2 eV peak (Fig. 3.5.7b and c) in comparison to the unreacted Al oxide catalyst (Fig. 3.5.7a). The TEY is more sensitive to surface chemistry of the sample whereas the fluorescence yield is more an indication of the chemistry of the bulk sample. Thus, it can be deduced from the small change in Al speciation collected by FLY that

changes to the Al speciation of the sample occurred predominantly on the surfaces of the mineral colloids.

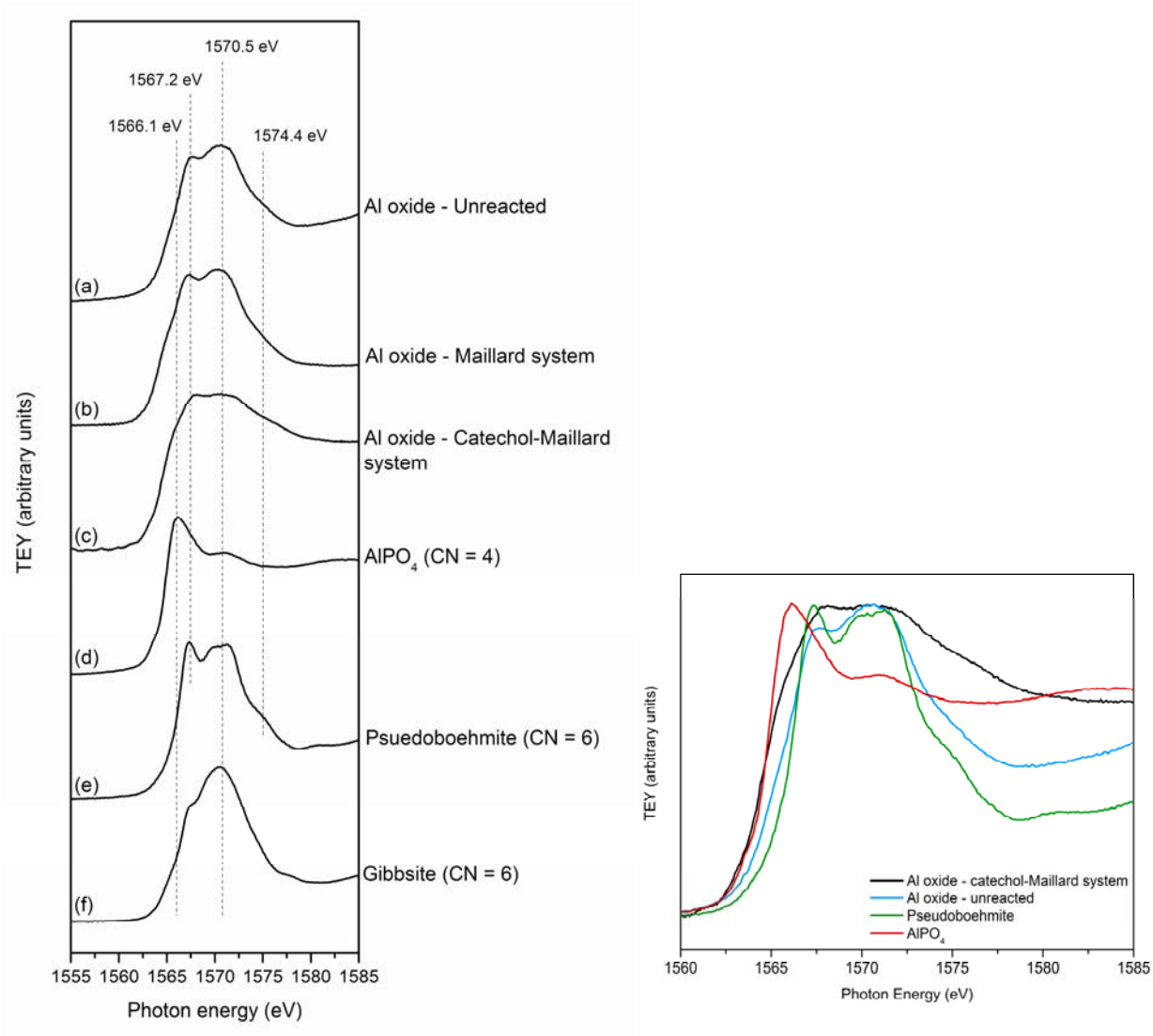

Figure 3.5.6 Aluminum K-edge NEXAFS TEY spectra of (a) the unreacted Al oxide catalyst; and the solid residues from the Al oxide-catalyzed: (b) Maillard reaction system, and (c) integrated catechol-Maillard reaction system; and pure reference compounds (d) $AlPO_4$, (e) pseudoboehmite, and (f) gibbsite. The figure on the right hand side shows a magnified view of the Al K-edge spectra of the Al oxide before and after reaction in the catechol-Maillard system, and the reference compounds $AlPO_4$ and pseudoboehmite. CN = coordination number.

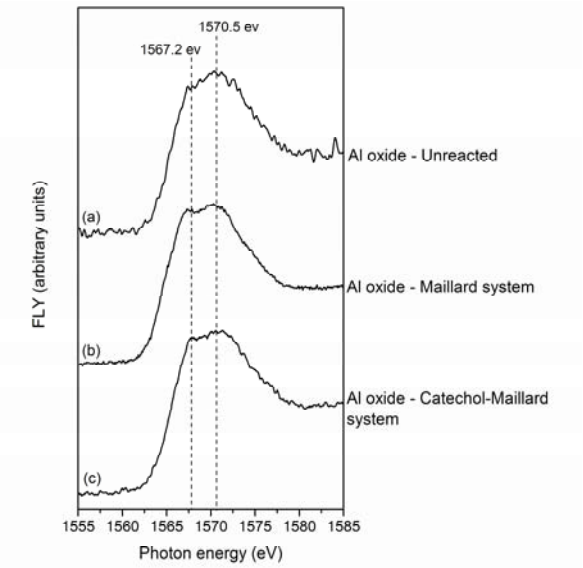

Figure 3.5.7 Aluminum K-edge NEXAFS FLY spectra of (a) the unreacted Al oxide catalyst; and the solid residues from the Al oxide-catalyzed: (b) Maillard reaction system, and (c) integrated catechol-Maillard reaction system.

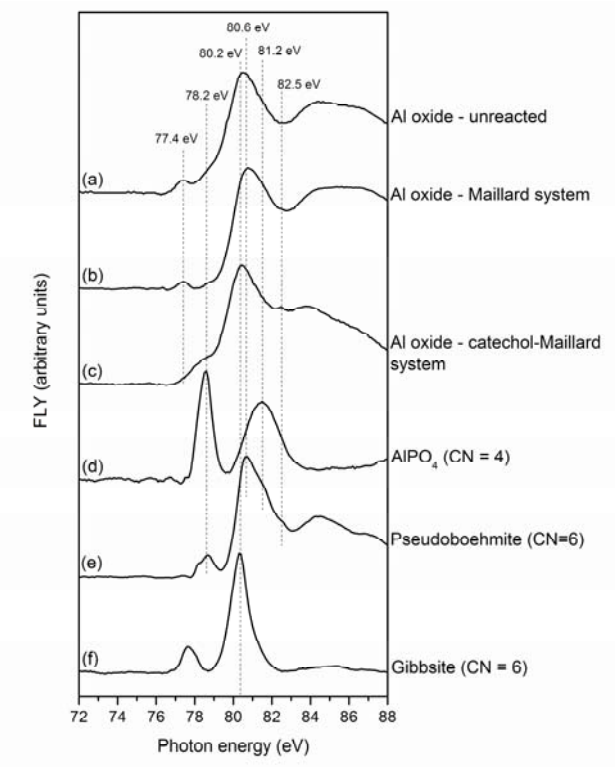

Figure 3.5.8 Aluminum L-edge NEXAFS FLY spectra of (a) the unreacted Al oxide catalyst; and the solid residues from the Al oxide-catalyzed: (b) Maillard reaction system, and (c) integrated catechol-Maillard reaction system; and the pure reference compounds (d) $AlPO_4$, (e) pseudoboehmite, and (f) gibbsite. CN = coordination number.

Iron L-edge NEXAFS spectroscopy

The Fe $L_{2,3}$-edge NEXAFS (TEY and FLY) spectra of the unreacted Fe oxide, the solid residues from the Maillard and catechol-Maillard systems reacted in the presence of Fe oxide, and selected reference compounds are shown in Fig. 3.5.9. The reference compounds were selected because of the oxidation state and coordination symmetry of the Fe that they contain. The compounds FeO (wustite) and Fe_3O_4 (magnetite) contain Fe(II) in octahedral symmetry (Wilke et al. 2001). Unfortunately the FeO was partially oxidized during the measurements (Fig. 3.5.9d) and so does not look like pure FeO containing only Fe(II) (Crocombette et al. 1995). The compounds Fe_3O_4 (magnetite) and γ-Fe_2O_3 (maghemite) contain Fe(III) in both octahedral and tetrahedral symmetry, whereas, α-Fe_2O_3 (hematite) and α-FeO(OH) (goethite) contain Fe(III) in only octahedral symmetry (Wilke et al. 2001).

The Fe L-edge NEXAFS (TEY and FLY) spectra of the unreacted Fe oxide catalyst (Fig. 3.5.9a) appears similar to that of the pure γ-Fe_2O_3 (Fig. 3.5.9f), in terms of the shape and resolution of the two major peaks (707.7 and 709.5 eV) and difference in intensity between the major peak at 709.5 eV and left side peak at 707.7 eV. The difference in intensity between the major peak at 709.5 eV and left side peak at 707.7 eV gives an indication of the ratio of Fe(II) and Fe(III) in the Fe oxide, the smaller the difference, the more Fe(II) the oxide contains (Crocombette et al. 1995; Garvie and Buseck 1998). The Fe L-edge NEXAFS (TEY and FLY) spectra of the Fe oxides reacted in the Maillard and catechol-Maillard systems (Fig. 3.5.9b and c) show that these residues contained more Fe(II) than the unreacted catalyst (Fig. 3.5.9a). The FLY NEXAFS spectra (Fig. 3.5.9 right) clearly show that there was more Fe(II) in the solid residue from the Fe oxide-catalyzed Maillard system (Fig. 3.5.9b) than the Fe oxide-catalyzed catechol-Maillard system (Fig. 3.5.9c).

The coordination symmetry of Fe can be deduced from how well-resolved the main absorption peak (709.5 eV) and smaller side peak (707.7 eV) are from each other (Crocombette et al. 1995). It can be seen in the TEY spectra (Fig. 3.5.9 left) of the reference Fe oxides with Fe(III) in octahedral symmetry (coordination number = 6), i.e., α-Fe_2O_3 (Fig. 3.5.9g) and α-FeO(OH) (Fig. 3.5.9h), that the peaks are more well-resolved than in the spectra of the Fe oxides containing Fe(III) in octahedral and tetrahedral symmetry (coordination number = 4 and 6), i.e., Fe_3O_4 (Fig. 3.5.9e) and γ-Fe_2O_3 (Fig. 3.5.9f). Therefore, the data indicate that the Fe oxide

catalyst (Fig. 3.5.9a) and the solid residues from the Fe oxide-catalyzed Maillard and catechol-Maillard systems (Fig. 3.5.9b and c) contained Fe(III) in both octahedral and tetrahedral symmetry. Since the changes in the Fe(II) content of the solid residues are apparent in the TEY and FLY spectra (Fig. 3.5.9b and c), it means that the change in the Fe oxidation state was not only in the surface of the samples but also in the bulk of the samples.

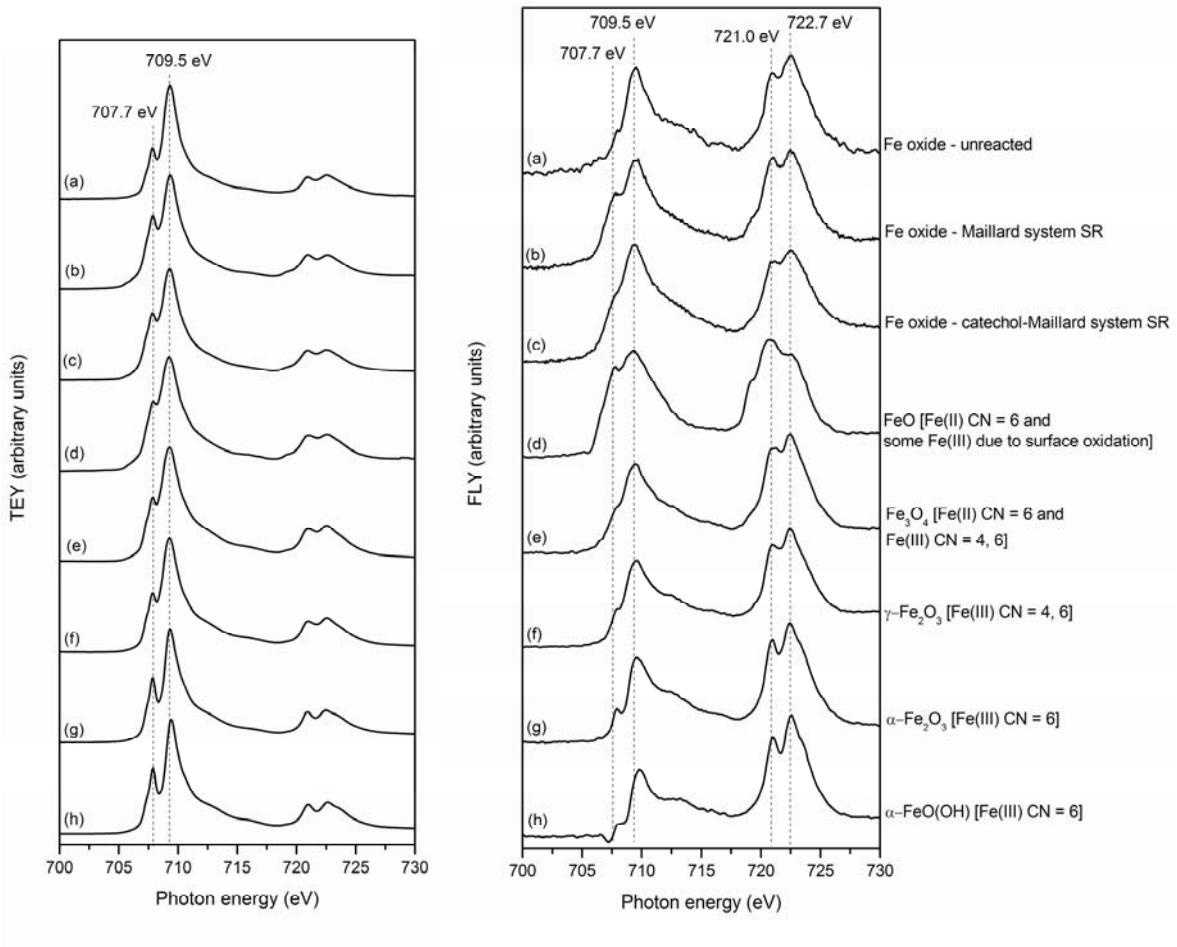

Figure 3.5.9 Iron $L_{2,3}$-edge NEXAFS TEY (left) and FLY (right) spectra of (a) the unreacted Fe oxide catalyst; the solid residues (SR) from the Fe oxide-catalyzed: (b) Maillard reaction system, and (c) integrated catechol-Maillard reaction system; and reference compounds: (d) FeO (wustite), (e) Fe_3O_4 (magnetite); (f) γ-Fe_2O_3 (maghemite); (g) α-Fe_2O_3 (hematite); and (h) α-FeO(OH) (goethite). CN = coordination number.

3.5.4 Conclusions

The abiotic catalysis of the Maillard reaction humification under environmentally relevant conditions had only previously been investigated using smectites and the metal oxides, birnessite and crystalline goethite. Only birnessite was studied as catalyst in accelerating the integrated catechol-Maillard reaction humification pathway. The present study investigated the catalytic ability of poorly crystalline Al and Fe(III) oxides, which are ubiquitous in the natural environment, on the Maillard and integrated catechol-Maillard humification pathways. The results obtained from the Al and Fe(III) oxide-catalyzed systems were compared with those from the previously investigated Mn(IV) oxide-catalyzed systems.

It was found that Al, Fe(III) and Mn(IV) oxides catalyzed humification to different extents in the Maillard and catechol-Maillard reaction systems. The Mn oxide was the strongest promoter of oxidative browning in the Maillard reaction and catechol-Maillard systems. Even though the visible absorbance (browning) was generally highest in the Fe oxide-catalyzed catechol-Maillard system, the redox status and C content of the solid phase indicated that the Mn oxide system was the strongest promoter of humification in the catechol-Maillard system. This is, in part, attributable to the higher redox potential of the Mn oxide system compared to the Fe oxide system. The lower electronegativity of Mn compared with that of Al and Fe also partially accounts for the differences. The greatest enrichment of organic C in the solid phase was found in the Mn oxide-catalyzed catechol-Maillard system (2.41 g), which was about 5 times greater than that of the Fe oxide system (0.45 g) and about 7 times greater than the Al oxide system (0.34 g). Based on the relatively high visible absorbance of the supernatant of the Fe oxide-catalyzed catechol-Maillard system and the relatively low C content in the solid residue, it appears that most of the humic substances formed in the Fe oxide system remained in the supernatant. This is partially attributable to the nature of the humic products which formed in the oxide systems.

The metal oxides substantially influenced the chemical nature of the resultant humic products in the supernatant and solid residues in the Maillard reaction and integrated catechol-Maillard reaction humification pathways. The humic products (supernatant and solid phase) from the systems catalyzed by Mn oxide had a much higher content of aliphatic carboxylic groups than those from the control and Al and Fe oxide-catalyzed systems which were more aromatic in nature. Since the humic substances in the Mn oxide system were more aliphatic carboxylic in

nature, they had a higher affinity for multivalent metal cations which would promote precipitation in the solid phase.

The humification processes also affected the surfaces of the oxides to different extents. It appears that Al oxide reacted in the catechol-Maillard system had a greater content of tetrahedral-Al than the oxide before reaction with the biomolecules, indicating the effect of organic humic polymers bound to the Al (either through surface complexation or by co-precipitation with Al from solution) on the Al coordination. The Fe oxide reacted in the Maillard and catechol-Maillard systems contained more Fe(II) than the unreacted Fe oxide. In contrast, the Mn oxide was found to be completely reduced and altered after reaction with the biomolecules. The findings obtained in this study show the significant influence of the nature of short-range ordered metal oxides on abiotic humification pathways and products in natural environments.

3.6 Research Unit 6: *Catalysis of the Maillard and polyphenol-Maillard humification pathways by pure layer silicates and natural soil clays*

3.6.1 Introduction

Clay size layer silicates have been shown to catalyze the abiotic polymerization of polyphenols, and polycondensation of polyphenols and amino acids, by acting as electron acceptors in oxidative polymerization reactions (Kumada and Kato 1970; Filip et al. 1977; Wang and Li 1977; Wang et al. 1978a; Wang and Huang 1986; Wang et al. 1986; Wang and Huang 1989b, 1989c, 1991). Wang and Huang (1989b) showed that the edge-sites of kaolinite provide all of its catalytic power in generating hydroquinone-derived humic polymers, whereas, in the case of nontronite its edge-sites only partially account for its catalytic power. Nontronite has also been shown to catalyze the polycondensation of glycine and pyrogallol (Wang and Huang 1991). Molecular O_2 chemisorbed on silicates, such as nontronite, has a strong oxidative power, and contributes partially to the ring cleavage of pyrogallol, and the decarboxylation and deamination of glycine (Wang and Huang 1991). The promoting effect of 2:1 layer silicates is higher than that of 1:1 layer silicates because of the larger specific surface area and lattice imperfections which favour the adsorption of O_2 molecules or radicals. Wang and Huang (1986) found that hydroquinone can be transformed by catalysis of Ca-saturated nontronite in aqueous solution at near neutral pH (6.5) to humic macromolecules and deposited in the interlayers of nontronite. They also found that most of the interlayer humic macromolecules are highly resistant to alkaline extraction and are, thus, humin type materials. Gonzalez and Laird (2004) showed that four different smectites saturated with various metal cations (Ca, Na, Cu(II) and Al) can catalyze the Maillard reaction between arginine and glucose at an environmentally relevant temperature (37° C). They also observed that some of the adsorbed humic substances were intercalated into the smectites. However, the abiotic catalysis of the integrated polyphenol-Maillard humification pathway (Jokic et al. 2004b) by layer silicates remains to be investigated.

The abiotic catalytic ability of soils in the formation of humic substances is attributable to their reactive components, namely Mn, Fe, and Al oxides, (oxy)hydroxides, and short-range ordered mineral colloids, clay-sized layer silicates, and some reactive primary minerals (Huang 2000). A number of studies have investigated the abiotic catalytic ability of natural soils (whole soils and clay fractions) as catalysts of polymerization of polyphenols (Wang et al. 1983a; Wang

and Huang 1989a), phenolic acids (Pohlman and McColl 1989) and the polycondensation of polyphenols and amino acids (Wang and Huang 2003). Wang and Huang (1989a) examined the catalytic ability of the sterilized Ap horizon from a Mollisol from Saskatchewan, Canada, on the ring cleavage and polymerization of pyrogallol. They reported that abiotic processes evidently cause the polymerization of pyrogallol as well as its ring cleavage and the formation of aliphatic fragments. The IR and ESR spectra of the humic substances (HS) formed closely resemble those of natural occurring HS. Wang and Huang (2003) showed that the clay fractions from a tropical Oxisol and temperate Mollisol greatly enhance the polymerization of pyrogallol and glycine, the abiotic ring cleavage of pyrogallol, and the deamination of glycine, and that these reactions increase with increasing temperature. Little is known on the abiotic catalysis of the Maillard reaction and especially the integrated polyphenol-Maillard reaction by natural soils and sediments. Further research is needed on this subject matter to advance our understanding of the role of abiotic catalysis in the formation of humic substances in natural environments.

Therefore, the objective of this study was to investigate the abiotic catalysis of clay-sized layer silicate specimens and natural soil clays in the Maillard reaction and integrated polyphenol-Maillard reaction.

3.6.2 Materials and Methods

3.6.2.1 Materials

Pure layer silicates, kaolinite (KGa-2) and nontronite (SWa-1), were obtained from the Source Repository of the Clay Mineral Society (W. Lafayette, IN, USA). Two subsoils were selected from a tropical and a temperate environment that were low in organic matter (OM), so that the inherent OM of the soils would not interfere with the characterization of the humic products formed in the reaction systems. Soil samples from a B horizon of an Oxisol (*Posic Ferrasol* – WRB) from Mpumalanga Province, South Africa, and a B horizon of a Mollisol (*Haplic Chernozem* - WRB*; Elstow Association, Orthic Dark Brown Chernozem* – Canadian Soil Classification) from Saskatchewan, Canada were used.

Catechol (Sigma-Aldrich ACS reagent grade >99%), D-glucose (Sigma-Aldrich ACS reagent grade >99%) and glycine (Sigma Ultra pure grade >99%) were obtained from Sigma Aldrich Canada Ltd (Oakville, ON, Canada). The Fe [>99.5% FeO, >98% Fe_3O_4, >99% α-Fe_2O_3, >99% γ-Fe_2O_3 and >99% α-FeO(OH)] and Mn (>99.99% MnO, >98% Mn_2O_3) reference

compounds, which were used in the Fe L-edge, Mn L-edge NEXAFS spectroscopic studies, were obtained from Alfa Aesar, Johnson Matthey Catalog Company, Inc. (Ward Hill, MA, USA). The Mn (99.99% $MnCO_3$) and Al (>99% $AlPO_4$) reference compounds, which were used in the Mn L-edge and Al K-edge NEXAFS spectroscopic studies, were obtained from Sigma Aldrich Canada Ltd (Oakville, ON, Canada). Furthermore, for the Al K-edge NEXAFS study, synthetic gibbsite [γ-$Al(OH)_3$] was obtained from Ward's Natural Science (Rochester, NY, USA), and synthetic pseudoboehmite was obtained from BASF Catalysts LLC (Iselin, NJ). The synthetic δ-MnO_2 (birnessite) used as a reference compound in the Mn L-edge NEXAFS study was synthesized according to the method described in McKenzie (1971) and was characterized and described in Section 3.1. Elliot soil (1S102H) and Suwannee River (1S101H) humic acid standards were purchased from the International Humic Substances Society (IHSS), St. Paul, MN, USA, and used in the C K-edge NEXAFS study.

Characterization of the soils. The texture class of the soils was determined using the pipette method of particle size fractionation (Gee and Bauder 1986). The organic and inorganic C contents of the soils were determined using a dry combustion method on a Leco C632 Carbon Analyzer (Leco Corporation, St Joseph, MI, USA) as described by Wang and Anderson (1998). The pH of the soils was determined in water using a 1:2.5 (w/v) soil to distilled water ratio. A summary of the chemical and physical characteristics of the whole soils are shown in Table 3.6.1.

Table 3.6.1 Summary of the physical and chemical characteristics of the whole natural soil samples.

Sample	Soil classification		Parent material	Horizon depth	Texture class	Inorg. C	Org. C	pH H_2O
	WRB[a]	ST[b]		(cm)		(%)	(%)	
Oxisol	Posic Ferrasol	Mesic Anionic Acrustox	dolomite	50-100	clay loam	0	0.33	5.8
Mollisol	Haplic Chernozem	Typic Cryoboroll	lacustrine	25-40	clay	0.19	1.04	7.2

[a]World Reference Base (IUSS Working Group WRB 2006); [b]Soil Taxonomy (Soil Survey Staff 1999)

Separation of the pure layer silicate and natural soil clay fractions. The pure layer silicate and soil samples were lightly ground and suspended in a dilute Na_2CO_3 and NaOH suspension

(pH 9.5) at a 1:10 (w/v) ratio. The suspensions were dispersed by ultrasonification at 50 W for 3 min. The clay fractions (<2 μm) were collected by sedimentation and then freeze-dried.

Characterization of the natural soil clay fractions. The organic and inorganic C contents of the soil clay fractions were determined using a dry combustion method on a Leco C632 Carbon Analyzer (Leco Corporation, St Joseph, MI, USA) as described by Wang and Anderson (1998). The dithionate-citrate bicarbonate (DCB) extractable metal content of the soil clays was determined using the method described in Jackson et al. (1986). This method determines the total content of Fe and Mn oxides (amorphous coatings and discrete phases), as well as, the amorphous alumina content. A summary of the chemical characteristics of the natural soil clay fractions are shown in Table 3.6.2. The soil clay fractions were characterized using XRD (Table 3.6.3). Identification of the crystalline minerals in the natural soil clay fractions was performed using standard methods described in Whittig and Allardice (1986).

3.6.2.2 Incubation experiment

Distilled deionized water was used in all the experiments and is henceforth referred to as water. Sterile conditions were maintained throughout the experiment in order to establish the role of abiotic processes. All glassware, birnessite, water and apparatus were autoclaved prior to the experiments. In addition to this, thimerasol, an antiseptic agent, was added to each flask (0.02 %, w/v) before any of the reagents were added. Thimerasol does not affect the oxidation process of phenolic compounds (Wang et al. 1983a). Two and a half grams of clay (kaolinite, nontronite, Oxisol, Mollisol) were suspended in 75 mL of each of the reaction solution systems: (i) the Maillard reaction system (0.05 mole glucose + 0.05 mole glycine) and (ii) the equimolar integrated catechol-Maillard system (0.05 mole catechol + 0.05 mole glucose + 0.05 mole glycine) in a 250 mL flask. There were control Maillard reaction and catechol-Maillard reaction treatments established in which clay was absent. All the reaction systems were adjusted to an environmentally relevant pH 7.0 using 0.1 M HCl or 0.1 M NaOH. The final volume of the reaction solutions was made up to 100 mL using autoclaved water. The flasks were then tightly sealed and placed in a constant temperature water bath at 45° C for a period of 15 days while gently shaking. Forty-five degrees centigrade is an environmentally relevant temperature as it is common in tropical and subtropical areas, and has also been reported in temperate areas as the approximate temperature of an exposed sunlit soil surface on a day when the ambient air

temperature is 25° C (Jury et al. 1991). The absence of microbial growth was verified by culturing aliquots of selected samples at the end of the incubation period. All treatments were performed in triplicate. Aerobic microbial growth was tested for by culturing on Tryptocase Soy Agar (TSA) plates, while anaerobic microbial growth was tested for on TSA plates in a BBL GasPak 150 Large Anaerobic System. All cultures were incuabated for a period of 5 and 9 days at 28° C (Jokic et al. 2004b).

3.6.2.3 Characterization of reaction systems at the end of the incubation period and isolation of humic acids.

At the end of the reaction period, the final pH and Eh of the suspensions were measured. The samples were then centrifuged at 25,000 g for 40 min to separate the solid residue from the solution. The absorbance of the supernatant was measured between 400 and 600 nm on a UV-visible spectrophotometer (Beckman DU 650 microprocessor controlled spectrophotometer, Fullerton, CA, USA). The visible absorbance at 400 and 600 nm provides an indication of the extent of polymerization which has taken place in the reaction systems (Shindo and Huang 1982, 1984a, 1984b). Shindo and Huang (1984a) studied the polymerization of polyphenols by short-range ordered Mn, Fe, Al and Si oxides, and showed that the yield of humic polymers was directly related to the visible absorbance. Likewise, with natural humic substances, Gan et al. (2007) showed that visible absorbance can be used to determine the concentration of fulvic acid in solution. The supernatant was diluted with water prior to absorbance determination and the values obtained were subsequently multiplied by the dilution factor. The Al and Fe contents of the supernatant were determined using atomic absorption spectroscopy at a wavelength of 309.3 and 248.3 nm, respectively (Varian Spectra AA 220, Walnut Creek, CA, USA).

The solid residue was repeatedly washed with water using centrifugation at 25,000 g for 40 min until the wash water was clear. These water extracts were collected and added to the supernatant. The washed residue was then freeze-dried. The combined water extracts and supernatant was then acidified to pH 1.0 using 6 M HCl and allowed to stand for 24 h to precipitate the humic acid (HA) fraction out of the solution (Swift 1996). The acidified suspensions were then centrifuged at 25,000 g for 45 min to separate the HA fraction from the rest of the solution containing the fulvic acid (FA) fraction and non-humic substance fraction. The HA residue was then resuspended in a 0.1 M HCl and 0.3 M HF solution and shaken for 48

h. The suspension was then centrifuged again as described before and the sedimented HA was dialyzed in 1000 molecular weight cut off dialysis tubing for 5 days in distilled deionized water until the water was tested free from chloride ($AgNO_3$ test). The purified HA was then freeze-dried.

3.6.2.4 Characterization of reaction products

X-ray diffraction (XRD). The solid residues and unreacted catalysts were examined using X-ray diffractometry on a Rigaku Rotaflex 200SU (Tokyo, Japan) with a rotating Fe anode and graphite monochromator. The samples were lightly ground and then mounted on glass slides by making a slurry of the ground sample with acetone and allowing it to dry. The scans were performed at 40 kV and 160 mA, from 4 to 80 °2θ, at a step size of 0.02 °2θ at a scanning rate of 0.1 °2θ sec^{-1}.

Inorganic and organic carbon analysis. Inorganic and organic carbon analysis of the solid residues was performed using a dry combustion method on a Leco C632 Carbon Analyzer (Leco Corporation, St. Joseph, MI, U.S.A.) as described by Wang and Anderson (1998).

Near edge X-ray absorption fine structure (NEXAFS) spectroscopy. The speciation of C, Al, Fe and Mn was investigated in selected unreacted clays, solid residues and supernatant HA fractions using C and Al K-edge and Fe and Mn L-edge NEXAFS spectroscopy on the SGM (Spherical grating monochromator) beamline (Regier et al. 2007) at the Canadian Light Source (Saskatoon, SK, Canada).

The reference compounds (pseudoboehmite, gibbsite, $AlPO_4$, FeO, α-Fe_2O_3, γ-Fe_2O_3, Fe_3O_4 and α-FeO(OH), MnO, $MnCO_3$, Mn_2O_3 and δ-MnO_2), unreacted clay catalysts and solid residues were finely ground and mounted on C-tape, and then examined using Al K-edge and Fe and Mn L-edge NEXAFS spectroscopy. The photon energy step size used was 0.1 eV. An exit slit width of 50 μm and a dwell time of 0.3 s were used. All spectra were normalized against the beamline current measured by a Au mesh. The Al K-edge and Fe and Mn L-edge spectra were recorded by total electron yield (TEY) and fluorescence yield (FLY).

The reference compounds (glycine, IHSS soil and river HA standards), solid residues and HA samples, which were investigated using C K-edge NEXAFS, were mounted on gold (Au)-coated (~400 Å) silicon (Si) wafers. The samples were mounted on the Au-coated Si wafers by making dilute suspensions of the samples in distilled deionized water and then placing a droplet

on the wafer and allowing it to dry. An exit slit width of 20 μm and a dwell time of 0.3 s were used to minimize damage due to exposure to radiation. These spectra were recorded by total electron yield (TEY) at an energy step of 0.1 eV. The C spectra were normalized to a clean Au-coated Si wafer, so that the signals from C in the beamline and C contamination on the gold I_0 mesh would not interfere with the signal from the samples (Watts et al. 2006). Spectra obtained were analyzed using aXis2000 software (Hitchcock et al. 2005).

The energy scale of the C, Al, Fe and Mn spectra collected on the SGM beamline were internally calibrated using glycine, gibbsite, α-Fe_2O_3 and MnO, respectively, based on calibrated values reported from previous studies (Garvie and Craven 1994; Crocombette et al. 1995; Boese et al. 1997; Ildefonse et al. 1998). All the spectra were normalized to each other, with the maximum intensity of each spectrum fixed at 1.

3.6.3 Results and Discussion

3.6.3.1 Characterization of the soil clay fractions

Selected chemical characteristics of the natural Oxisol and Mollisol clay fractions are shown in Table 3.6.2. The Oxisol clay contained much higher (at least one order of magnitude) amounts of DCB extractable metal concentrations than the Mollisol clay.

Table 3.6.2 The inorganic and organic C contents and DCB extractable Al, Fe and Mn contents of the natural soil clay fractions.

Sample	Inorg. C	Org. C	DCB[a] extractable metals (%)		
	(%)	(%)	Al	Fe	Mn
Oxisol	0	0.71	3.44	7.26	6.21
Mollisol	0.17	1.74	0.21	0.64	0.06

[a]Dithionite-citrate bicarbonate

The minerals identified by X-ray diffraction (XRD) in the Oxisol and Mollisol clays are shown in Table 3.6.3. The Oxisol soil was highly weathered, as indicated by the absence of layer silicates and the presence of gibbsite, hematite, maghemite and goethite. Despite the fact that the Oxisol clay contained 6.21 % DCB extractable Mn (Table 3.6.2), no Mn oxide mineral phases were detected by XRD (Table 3.6.3), indicating that the extractable Mn was present as

noncrystalline Mn oxides. The Mollisol clay contained various 2:1 layer silicates and kaolinite, and no crystalline discrete Al, Fe or Mn oxide phases were detectable (Table 3.6.3).

Table 3.6.3 Minerals identified in the natural soil clays by X-ray diffraction.

Sample	Primary minerals	Layer silicates	Oxides
Oxisol clay	quartz	not detectable	gibbsite, hematite, maghemite, goethite
Mollisol clay	quartz, mica	illite, vermiculite, smectite, kaolinite	not detectable

3.6.3.2 Effect of the presence of catalysts on the reaction systems

In all the reaction systems studied, no aerobic or anaerobic microbial growth was observed. Thus, all the processes studied were abiotic in nature. The effect of the presence of the pure layer silicates, kaolinite and nontronite, and natural soil clays, Oxisol and Mollisol, on the visible absorbance of the supernatants of the reaction systems are shown in Fig. 3.6.1 and 3.6.2, respectively. The presence of the kaolinite and nontronite clays did not greatly enhance browning in the Maillard reaction system (Fig. 3.6.1a). The layer silicate clays moderately enhanced browning in the catechol-Maillard reaction systems (Fig. 3.6.1b), compared to the pure Mn and Fe oxides (See previous Research Unit 3.5). Nontronite enhanced browning in the catechol-Maillard system to a greater extent than kaolinite (Fig. 3.6.1b).

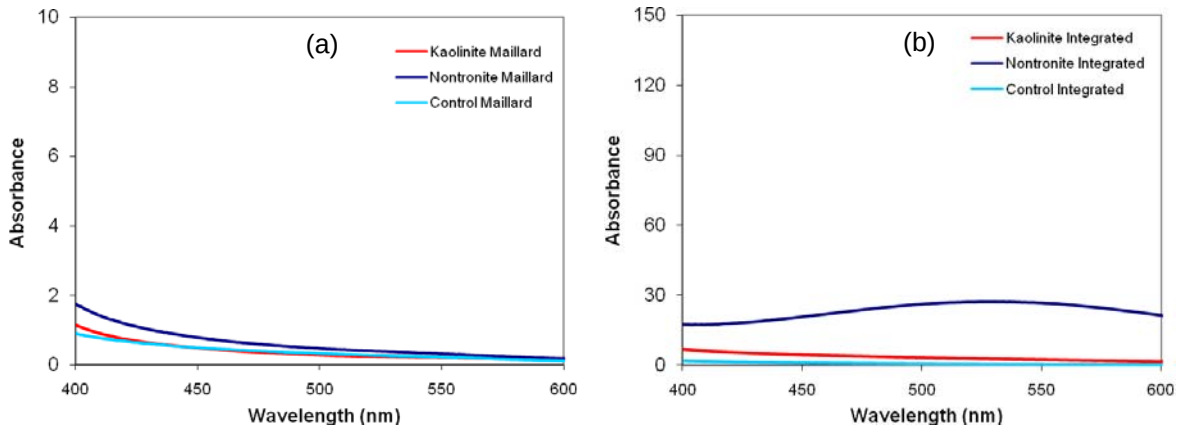

Figure 3.6.1 Comparison of the effect of the presence of the kaolinite and nontronite clays on the visible absorbance (400-600 nm) of the supernatant from (a) Maillard reaction and (b) the integrated catechol-Maillard system. The absorbances are scaled by the dilution factor.

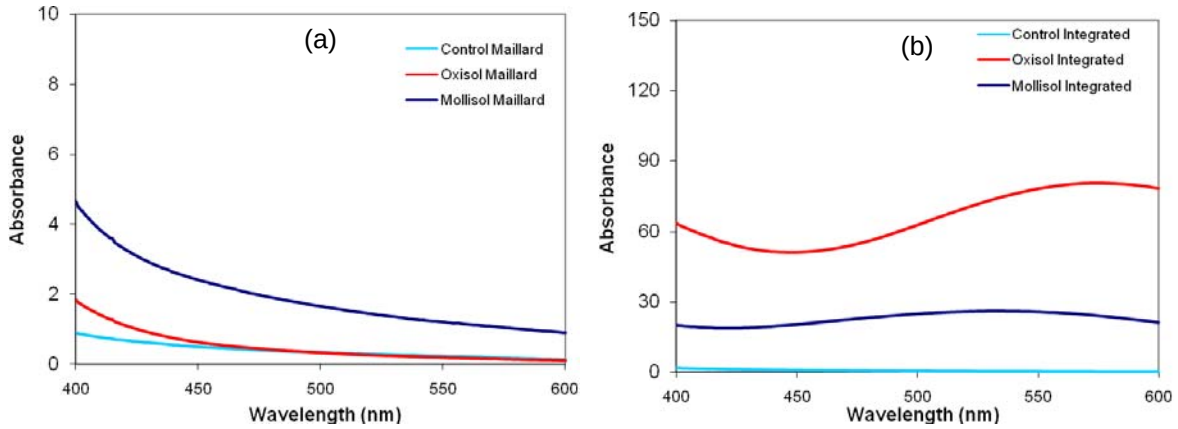

Figure 3.6.2 Comparison of the effect of the presence of the Oxisol and Mollisol clays on the visible absorbance (400-600 nm) of the supernatant from (a) Maillard reaction and (b) the integrated catechol-Maillard system. The absorbances are scaled by the dilution factor.

The presence of the natural soil clays enhanced humification in both the Maillard and catechol-Maillard systems. The Mollisol clay enhanced browning to a greater extent in the Maillard reaction system than the Oxisol clay (Fig. 3.6.2a). In contrast, the Oxisol clay enhanced browning in the integrated catechol-Maillard system to a much greater extent than the Mollisol clay (Fig. 3.6.2b).

Table 3.6.4 provides a summary of the solution characteristics of the Maillard and catechol-Maillard systems reacted both in the presence and absence of the kaolinite, nontronite, Oxisol and Mollisol clays. Kaolinite appeared to be the weakest catalyst of humification reactions in the Maillard and catechol-Maillard systems, as indicated by the low visible absorbance and high redox status values (Table 3.6.4). The Mollisol and nontronite systems had similar visible absorbance and redox status values. The Oxisol systems had the highest final pH values (Table 3.6.4), most likely due to the presence of the Mn and Fe oxides (Table 3.6.2) and their reductive dissolution (Table 3.6.4), which would result in the consumption of protons. The Oxisol systems also had the lowest redox status values of all the systems, indicating that more oxygen was consumed in these systems, and thus had more oxidative polymerization reactions.

Table 3.6.4 Comparison of visible absorbance, pH, redox status (pH + pE) and metal concentration of the supernatants of the pure layer silicate- and natural soil clay-catalyzed reaction systems.

Sample	Absorbance 400 nm	Absorbance 600 nm	pH	pH + pE	Al (mmol L^{-1})	Fe (mmol L^{-1})	Mn (mmol L^{-1})
Pure layer silicate clays							
Kaolinite M[a]	1.15 ±0.14	0.17 ±0.12	5.07 ±0.06	11.35 ±0.05	0.32 ±0.03	0	0
Kaolinite I[b]	5.82 ±0.52	1.26 ±0.15	5.93 ±0.05	8.07 ±0.25	0.96 ±0.07	0.16 ±0.07	0
Nontronite M	1.90 ±0.41	0.28 ±0.06	4.89 ±0.13	8.40 ±0.05	0	0.99 ±0.14	0
Nontronite I	19.09 ±0.90	22.68 ±1.78	5.70 ±0.07	6.30 ±0.28	0.24 ±0.07	10.74 ±0.73	0
Natural soil clays							
Oxisol M	1.85 ±0.20	1.03 ±0.21	6.88 ±0.01	7.29 ±0.05	[c]n.d.	3.27 ±0.41	19.55 ±0.33
Oxisol I	61.87 ±3.82	77.51 ±4.52	6.03 ±0.02	5.14 ±0.06	[c]n.d.	15.64 ±0.60	22.16 ±0.97
Mollisol M	4.65 ±1.38	0.77 ±0.06	5.76 ±0.11	7.79 ±0.29	[c]n.d.	0.59 ±0.21	0.06 ±0.01
Mollisol I	21.72 ±1.20	22.62 ±0.60	5.90 ±0.10	5.99 ±0.60	[c]n.d.	7.04 ±0.06	0.10 ±0.03
Control							
No catalyst M	0.74 ±0.08	0.12 ±0.02	6.26 ±0.13	10.72 ±0.76	-	-	-
No catalyst I	2.84 ±0.57	0.42 ±0.09	5.49 ±0.12	9.05 ±0.90	-	-	-

[a]M = Maillard reaction,
[b]I = integrated catechol-Maillard reaction
[c]n.d.= not determined

3.6.3.3 Characterization of reaction products from reaction systems incubated in the presence of clays

X-ray diffraction

The X-ray diffractograms of the solid residues containing the kaolinite and nontronite clays reacted in the Maillard and catechol-Maillard systems and the unreacted clays, are shown in Fig. 3.6.3 and 3.6.4. There is little difference in the X-ray diffractograms of the unreacted kaolinite clay (3.6.3a) and the kaolinite clay after the reaction with the biomolecules (Fig. 3.6.3b and c). The most intense peak (13.3 Å) of the nontronite clay (Fig. 3.6.4a) appears to have become less intense after reaction in the Maillard and catechol-Maillard systems (Fig. 3.6.4b and c). This indicates that the humic products may have coated the surfaces of the mineral, thus causing less ordering in the stacking of the nontronite particles. It also appears that the peak at 13.3 Å has become broader and the maximum has shifted to 12.1 Å in the catechol-Maillard

system (Fig 3.6.4c). This indicates that the humification reactions have affected the interlayer space of the nontronite clay.

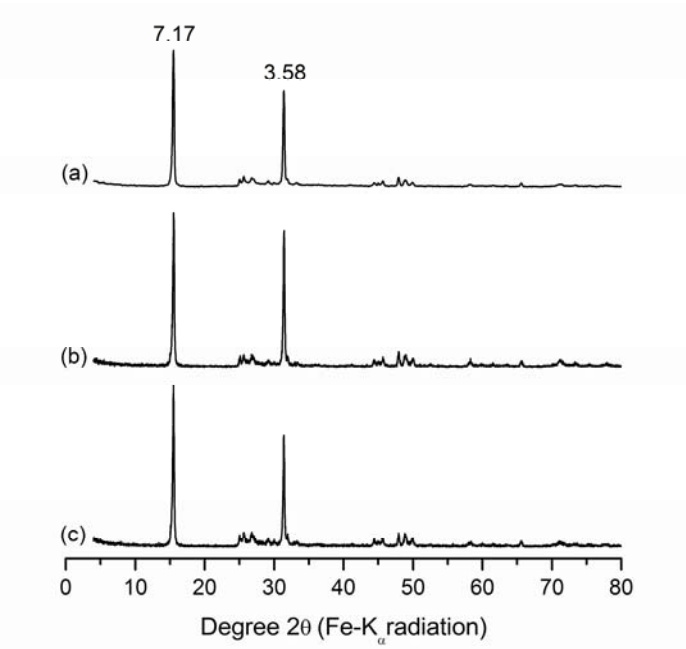

Figure 3.6.3 X-ray diffractograms of (a) the unreacted kaolinite clay and solid residues from the kaolinite-catalyzed (b) Maillard reaction and (c) catechol-Maillard reaction systems. The d-values are indicated in angstrom.

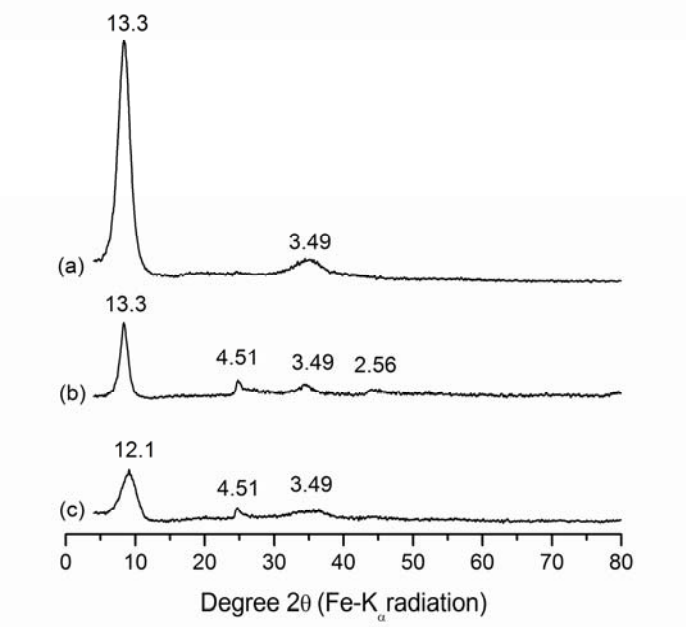

Figure 3.6.4 X-ray diffractograms of (a) the unreacted nontronite clay and the solid residues from the nontronite-catalyzed (b) Maillard reaction and (c) catechol-Maillard reaction systems. The d-values are indicated in angstrom.

The X-ray diffractograms of the solid residues of the Oxisol- and Mollisol-catalyzed Maillard and catechol-Maillard systems and unreacted clays are shown in Fig. 3.6.5 and 3.6.6. There were no significant differences between the X-ray patterns of the unreacted Oxisol clay (Fig. 3.6.5a) and the Oxisol clay reacted in the Maillard and catechol-Maillard systems (Fig. 3.6.5b and c). This indicates that the crystal structures of these crystalline components of the Oxisol clay, were not affected by the humification reactions to any significant extent. The poorly crystalline components such as the Mn oxides, which make up a significant portion of the soil (Table 3.6.2) were not detected by XRD (Fig. 3.6.5a).

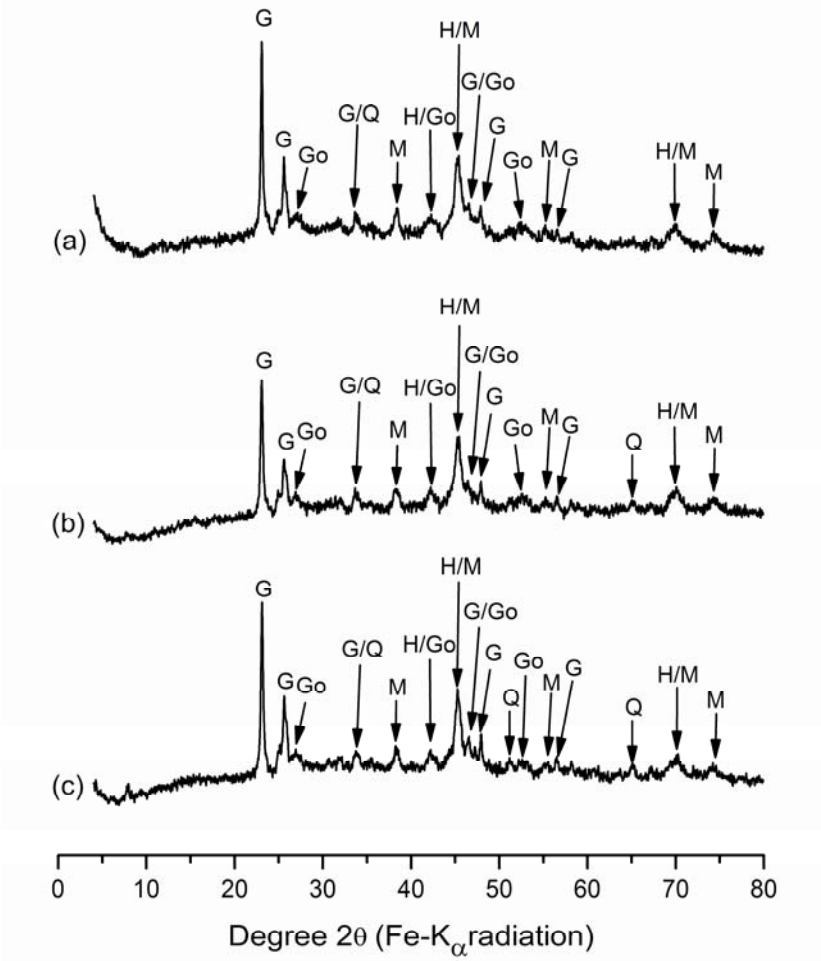

Figure 3.6.5 X-ray diffractograms of (a) the unreacted Oxisol clay and the solid residues from the Oxisol clay-catalyzed (b) Maillard reaction and (c) catechol-Maillard reaction systems. The d-values are indicated in angstrom. G = gibbsite (4.85, 4.37, 3.31, 2.45, 2.39, 2.04 Å), Go = goethite (4.18, 2.69, 2.45, 2.19 Å), Q = quartz (3.34, 1.82 Å), M = maghemite (2.95, 2.52, 2.09, 1.70, 1.61 Å), and H= hematite (2.69, 2.51, 1.69 Å).

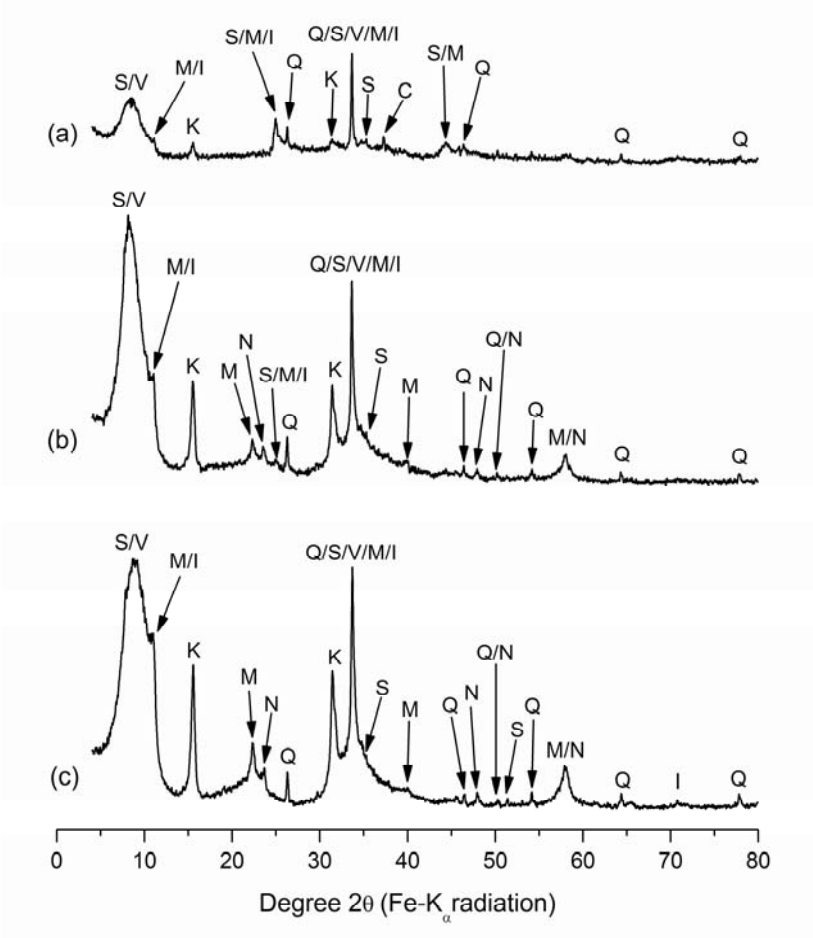

Figure 3.6.6 X-ray diffractograms of the solid residues from (a) the unreacted Mollisol clay and the Mollisol-catalyzed (b) Maillard reaction and (c) catechol-Maillard reaction systems. The d-values are indicated in angstrom. S = smectite (13.6, 4.47, 3.34, 3.23, 2.33 Å), V = vermiculite (13.6, 3.34 Å), M = mica (9.97, 4.99, 3.33, 2.88, 2.00 Å), I = illite (10.0, 4.48, 3.33, 1.67 Å), Q = quartz (4.26, 3.34, 2.46, 2.28, 2.13, 1.82, 1.54 Å), K = kaolinite (7.15, 3.58 Å), C = calcite (3.04 Å), N = nordstrandite (4.78, 2.39, 2.28, 2.02 Å). The presence of smectite and vermiculite was confirmed by K-saturation and Mg-saturation-glycerol solvation.

The peaks of the X-ray patterns of the Mollisol clay reacted in the Maillard and catechol-Maillard systems (Fig. 3.6.6b and c) became more defined and intense compared with the pattern of the unreacted Mollisol clay (Fig. 3.6.6a). In particular, the peaks of the smectite/vermiculite, illite/mica, kaolinite and quartz became more intense. This indicates that the removal of the poorly crystalline material coating on the mineral surfaces during the reaction period improved the ordering of the stacking of these minerals, thus enhancing the peak intensity. Furthermore, a new mineral phase, nordstrandite [$Al(OH)_3$] (Bosmans 1970), was identified in the Maillard and

catechol-Maillard system solid residues (Fig. 3.6.6b and c). The data indicate that nordstrandite was formed from the Al released from Al-bearing minerals during humification. The presence of organic ligands can perturb or inhibit the crystallization of $Al(OH)_3$ polymorphs. Bayerite is usually the dominant product when $Al(OH)_3$ crystallization is rapid and not perturbed by interfering ligands; gibbsite is usually the dominant product under conditions where $Al(OH)_3$ crystallization is retarded but not inhibited, and nordstrandite is formed under intermediate conditions (Violante and Huang 1985; Violante et al. 1993; Violante and Huang 1993).

Organic C content

The organic C contents of the unreacted clay catalysts and solid residues (SR) from the clay-catalyzed Maillard and integrated catechol-Maillard reaction systems are shown in Table 3.6.5. The net gain in organic C in mg was calculated as follows: [Mass of SR at end of the reaction period (g)] x [net gain in org. C (%)] x 1000 = [Net gain in organic C in SR (mg)]. Inorganic C was not detected in the unreacted kaolinite, nontronite or Oxisol clays or the solid residues from the kaolinite-, nontronite- or Oxisol-catalyzed Maillard and catechol-Maillard reaction systems. There was a small amount of inorganic C in the unreacted Mollisol catalyst, 0.17% (Table 3.6.2), but this was found to have been dissolved during reaction with the biomolecules in the Maillard and catechol-Maillard systems.

The greatest accumulation of organic C in the solid phase was observed in the Oxisol-catalyzed Maillard and catechol-Maillard systems (28.74 and 103.94 mg, respectively) (Table 3.6.5). The Mollisol-catalyzed Maillard and catechol-Maillard systems showed little or no accumulation of organic C (Table 3.6.5). The supernatant Oxisol-catechol-Maillard system had the highest visible absorbance of all the clay-catalyzed catechol-Maillard systems (Fig. 3.6.2b), as well as, the greatest accumulation of organic C in the solid phase (Table 3.6.5). This can be attributed to the high Fe and Mn oxide content of the Oxisol clay (Table 3.6.2). The visible absorbance of the supernatant of the Oxisol-Maillard system appeared lower than that of the Mollisol-Maillard system (Fig. 3.6.2a), however, there was a much greater accumulation of organic C in solid phase of the Oxisol-Maillard system (Table 3.6.5) which could account for the lower visible absorbance. The lower redox status of the Oxisol-Maillard system than the Mollisol-Maillard system (Table 3.6.4) also indicated that there was a greater extent of oxidative polymerization reactions in the Oxisol-Maillard system. The organic C (Table 3.6.5) and visible

absorbance (Fig. 3.6.2) data indicate that the majority of the humic substances formed in the Mollisol-catalyzed Maillard and catechol-Maillard systems were present in the supernatant, whereas, in the Oxisol-catalyzed systems, the humic substances were present in both the solid and solution phases. This is attributable to the presence of the abundant Fe and Mn oxides in the Oxisol system (Table 3.6.2) and the reductive dissolution of these oxides (Table 3.6.4), which facilitate the coprecipitation of humic substances (Christl and Kretzchmar 2007; Hardie et al. 2007). Furthermore, the Al and Fe oxide surfaces have a strong affinity for sorbing humic substances and play an important role in long-term C stabilization in the soil environment (Kögel-Knabner et al. 2008).

Table 3.6.5 Organic C contents of unreacted clays and solid residues (SR) from the layer silicate and natural soil clay-catalyzed Maillard and integrated catechol-Maillard reaction systems.

Sample	Organic C content (%)	Net gain in organic C (%)	Mass of SR at end of reaction period (g)	Net gain in Org. C in SR (mg)
Kaolinite catalyst	0	-	-	-
Kaolinite Maillard	0.35	0.35	2.41	8.44
Kaolinite integrated[a]	0.40	0.40	2.36	9.44
Nontronite catalyst	0.39	-	-	-
Nontronite Maillard	0.99	0.60	2.32	13.92
Nontronite integrated	0.63	0.24	2.08	4.99
Oxisol clay catalyst	0.71	-	-	
Oxisol Maillard	1.74	1.03	2.79	28.74
Oxisol integrated	5.19	4.48	2.32	103.94
Mollisol clay catalyst	1.74	-	-	-
Mollisol Maillard	1.75	0.01	2.11	0.21
Mollisol integrated	1.67	-0.07	2.05	-1.44

[a]Integrated catechol-Maillard system

The pure layer silicate clay systems showed relatively small increases in organic C in the solid phase of the Maillard and catechol-Maillard systems (Table 3.6.5). The visible absorbance

of the supernatant of kaolinite-catalyzed Maillard and catechol-Maillard systems was the lowest of the clay systems and appeared close to or even lower than the control system (Fig. 3.6.1); evidently, the humic substances generated by the system were sorbed in the solid phase accounting for the low visible absorbance of the system. The visible absorbance of the supernatant of the nontronite-catalyzed Maillard and catechol-Maillard systems was relatively higher than that of the control and kaolinite systems (Fig. 3.6.1) and similar to that of the Mollisol systems (Fig. 3.6.2). However, in contrast to the Mollisol systems, the nontronite systems showed the accumulation of some organic C in the solid phase (Table 3.6.5). It is possible that the mineral surfaces in the unreacted Mollisol clay were already saturated with organic C (1.74%) before reaction with the biomolecules, whereas, the unreacted nontronite clay contained very little organic C (0.39%) and thus could sorb organic C.

C K-edge NEXAFS spectroscopy

The C K-edge NEXAFS spectra of natural HAs, HAs isolated from the supernatant and solid residues (SR) from selected catechol-Maillard systems reacted in the presence of the clay catalysts is shown in Fig. 3.6.7. The kaolinite-catalyzed catechol-Maillard system and all of the clay-catalyzed Maillard reaction systems produced very little browning in the supernantant (Fig. 3.6.1 and 3.6.2) and therefore it was not possible to isolate a HA fraction from these samples.

Spectroscopic assignments are based on the absorption maxima of the reference compounds (glucose, glycine and pyrogallol) and on values reported by previous C NEXAFS studies (Myneni 2002; Urquhart and Ade 2002; Dhez et al. 2003; Cooney and Urquhart 2004; Hitchcock and Mancini 2004). The NEXAFS narrower and sharper core (C 1s) → π* transitions have been found to be the most useful for chemical analyses and identification of organic compounds due to their chemical sensitivity based on the chemical energy shifts (Urquhart and Ade 2002).

The lowest absorption bands at around 284.0 eV usually correspond to molecules with low energy π* states, such as quinones (Francis and Hitchcock 1992). Absorption bands near 285 eV are generally ascribed to C 1s (C-H) → $1\pi^*_{C=C}$ transitions (Urquhart and Ade 2002; Cooney and Urquhart 2004), which are characteristic of C=C unsaturation. The transitions of aromatic C bound to carbonyl (e.g., terephthalate species) tend to overlap with unsaturated aromatic C-H transitions due to the strong electronic interactions between the benzene π* density and carbonyl

π* density, and are generally found in the 284.4-285.0 eV range (Cooney and Urquhart 2004). The absorption bands near 286-288 eV are characteristic of functionalized aromatic groups C 1s (C-R) → $1\pi^*_{C=C}$ transitions (R = functional group), such as aromatic C bound to aldehyde (286.0 eV), ketone (286.4 eV), urea (286.4 eV), carbamate (286.6-286.8 eV), amine (286.8-286.9 eV), phenol (287.0-287.3 eV) and ester (287.1 eV) groups (Urquhart and Ade 2002; Dhez et al. 2003; Cooney and Urquhart 2004; Hitchcock and Mancini 2004). Heterocyclic N compounds C 1s (C-N) → $1\pi^*_{C=C}$ transitions also occur in the ~286-287 eV range, e.g., pyridine (285.7 eV) and pyrrole (286.3 eV) (Dhez et al. 2003; Hitchcock and Mancini 2004). The C=N and C≡N π* transitions usually occur around 286.3 eV (Myneni 2002). Generally speaking, a stronger electron withdrawing substituent on the aromatic ring, will result in a higher energy shift of the C 1s (C-R) → $1\pi^*_{C=C}$ transition.

The carbonyl C 1s (C-R) → $1\pi^*_{C=O}$ transitions usually occur between 286-291 eV, and can be used to distinguish between groups such as aldehydes (286.2-286.4 eV), ketones (286.6-286.8 eV), amide (287.8-288.2 eV), acetic/acetate (288.1-288.6 eV), urea (289.2-289.8 eV), carbamate (289.9.0-290.1 eV) and carbonate (290.2-290.6 eV) (Urquhart and Ade 2002). The main cause of the shifts observed in C 1s (C-R) → $1\pi^*_{C=O}$ transitions is the inductive effect of the neighbouring atoms on the carbonyl C 1s binding energy (Urquhart and Ade 2002). Low lying σ* orbitals also provide valuable information in identifying aliphatic functionalities. Saturated aliphatic C exhibits C 1s (C-H) → σ^*_{C-H} transitions in the 287.1-287.9 eV range, while aliphatic alcohol C 1s (C-H) → σ^*_{C-O} transitions are found shifted to a higher energy in the 289.2-289.5 eV range (Dhez et al. 2003).

The spectra of the natural river and soil HA samples (Fig. 3.6.7a and b) were dominated by aliphatic carboxylic functionalities (288.6 eV) and also contained quinone C and aromatic functional groups (285.0-287.1 eV). The HA isolated from the supernatant of the Mollisol system was dominated by aliphatic carboxylic functionalities (288.6 eV) and there was also evidence of aromatic C-H (285.0-285.3 eV) and phenolic functionalities (287.0 eV) (Fig 3.6.7c). In contrast, the HA isolated from the supernatant of the Oxisol system (Fig. 3.6.7d) was dominated by aromatic functionalities and the aliphatic carboxylic functionalities were relatively weaker. However, the aliphatic carboxylic C functionalities were the dominant functional group in the solid residue of the Oxisol system (Fig 3.6.7e). As was previously observed in the metal oxide systems (Unit 3.1 and 3.5), the solid residues of the Al, Fe and especially Mn oxide

systems contained relatively more aliphatic carboxylic groups than the HA isolated from the supernatant. This is attributable to the chemical partitioning of the humic substances between the solution and solid phases by the preferential coprecipitation of multivalent metals with humic substances possessing aliphatic carboxylic groups (Christl and Kretzchmar 2007; Hardie et al. 2007) or to the preferential adsorption of these functional groups of the humic substances on the positively charged surfaces of Al or Fe oxide (Chorover and Amistadi 2001; Kögel-Knabner et al. 2008). It has been shown that natural dissolved organic matter binds predominantly by means of ligand exchange to Fe oxide surfaces, whereas weaker cation bridging and van der Waals forces are the dominant mechanism for sorption to negatively charged vermiculite (Mikutta et al. 2007). Thus the association of organic C with Fe oxides surfaces would be stronger than with negatively charged layer silicates. The Oxisol clay was rich in Fe and Mn oxides (Table 3.6.2 and 3.6.3), which were dissolved during humification reactions (Table 3.6.4) and thus facilitated the chemical partitioning (coprecipitation) of the humic products based on aliphatic carboxylic C content, as well as, promoting the sorption of the humic products on the Fe and Al oxide surfaces.

In the case of the nontronite system, the aliphatic carboxylic peak was more intense in the HA isolated from the supernatant (Fig. 3.6.7f) than the humic products in the solid residue (Fig. 3.6.7g). It was also observed in the Mollisol- and nontronite-catalyzed catechol-Maillard systems that very little or no organic C was accumulated in the solid phase (Table 3.6.5) and thus most of the humic products produced in these systems were found in the solution phase (Fig. 3.6.1b and 3.6.2b). This is attributable to lower availability of multivalent metal cations in the nontronite and Mollisol systems compared with the Oxisol system (Table 3.6.4). In addition, the nontronite and the Mollisol clay were dominanted by negatively charged layer silicates (Table 3.6.3) which do not bind humic substances as strongly as Fe oxides or multivalent metal cations (Mikutta et al. 2007).

The solid residue from the kaolinite system (Fig. 3.6.7h) appears to contain even less aliphatic carboxylic C than the other systems. Wang and Huang (1991) hypothesized that molecular O_2 chemisorbed on silicates, such as nontronite, has a strong oxidative power, and partially accounts for the ring cleavage of the polyphenol pyrogallol, and the decarboxylation and deamination of glycine which leads to the formation of aliphatic humic products. This could explain the significantly aliphatic nature of the HA (in the supernatant) in the nontronite and

Mollisol systems. The promoting effect of 2:1 layer silicates, such as nontronite and montmorillonite, is higher than that of 1:1 layer silicates, such as kaolinite, because of the larger specific surface area and lattice imperfections which favour the adsorption of O_2 molecules or radicals (Huang 2000). Nontronite also contains structural Fe(III) in the octahedral sheet, which also serves as an oxidant. This would explain the weaker catalytic ability of kaolinite compared to the other catalysts, as well as weak aliphatic nature of the humic products in the solid residue of the kaolinite-catechol-Maillard system.

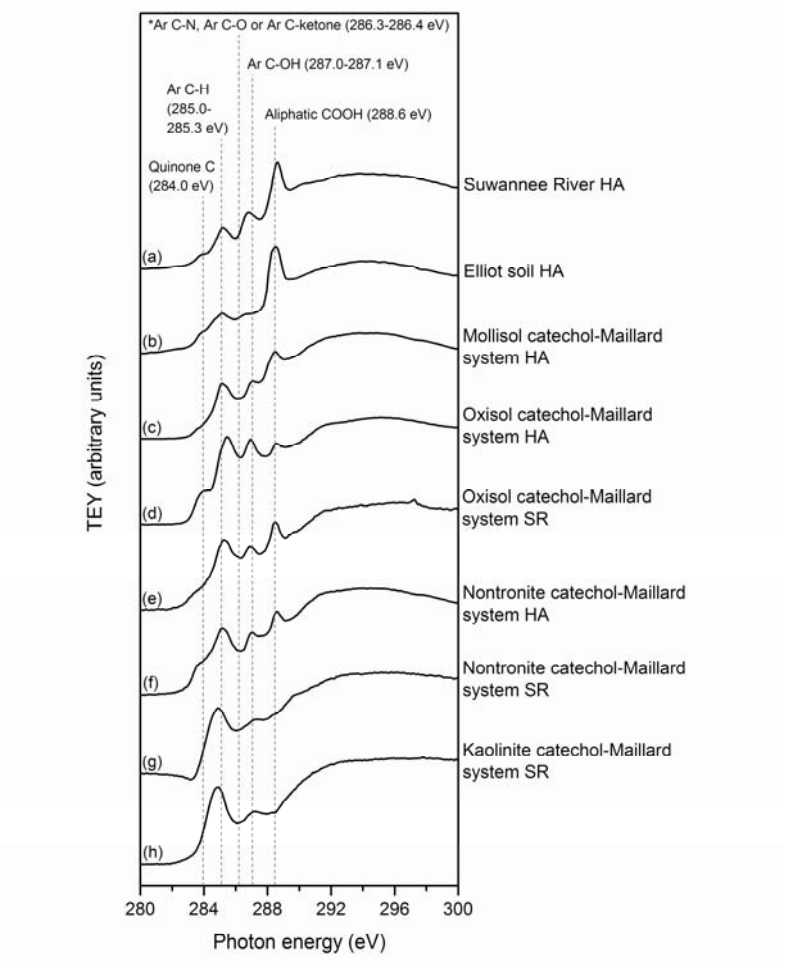

Figure 3.6.7 Carbon K-edge NEXAFS spectra of the IHSS (a) river and (b) soil humic acids (HA), and selected HA (extracted from the supernatants) and solid residue (SR) samples of the integrated catechol-Maillard reaction systems: (c) supernatant HA from Mollisol system, (d) supernatant HA from Oxisol system, (e) SR of Oxisol system, (f) supernatant HA from nontronite system, (g) SR from nontronite system, and (h) SR from kaolinite system. *Ar = aromatic.

Al K-edge NEXAFS spectroscopy

The Al K-edge NEXAFS spectra (TEY) of the nontronite and Mollisol clay systems and selected reference compounds are shown in Fig. 3.6.8. There were no apparent differences in the Al K-edge NEXAFS spectra of the nontronite and Mollisol clay systems before and after reaction with the biomolecules collected using fluorescence yield (FLY) (data not shown). The TEY is more sensitive to surface chemistry of the sample whereas the fluorescence yield is more an indication of the chemistry of the bulk sample. Thus, it can be deduced from the apparent lack of change in Al speciation collected by FLY that changes to the Al speciation of the sample only occurred on the surfaces of the mineral colloids. The Al K-edge NEXAFS spectra (TEY and FLY) of the kaolinite clay before and after reaction in the Maillard and catechol-Maillard systems appeared identical (data not shown). There were also no differences in the spectra of the Oxisol clay before or after reaction in the Maillard and catechol-Maillard systems (data not shown). Thus there were no detectable changes in the surface or bulk Al speciation of the kaolinite and Oxisol clays due to humification reactions using this technique. The reference compounds were selected because they contain Al in either 4- (tetrahedral) or 6-coordination (octahedral) and would help in the identification of the Al coordination in unreacted clays and residues from the reaction systems. Gibbsite contains Al in 6-coordination (Bragg and Claringbull 1965), pseudoboehmite and boehmite contain Al in 6-coordination (Yoon et al. 2004; Hu et al. 2008), and $AlPO_4$ has Al in 4-coordination (Berry and Mason 1959).

The nontronite and Mollisol clays appeared to contain largely octahedral and very limited tetrahedral Al (Fig. 3.6.8a and d, respectively), which is logical since they are dominated by 2:1 layer silicates which contain largely octahedral Al and some tetrahedral Al. There was a slight change in the relative intensity of the peaks at 1567.2 and 1570.5 eV in the nontronite clay (Fig. 3.6.8a) after reaction in the Maillard and catechol-Maillard systems (Fig. 3.6.8b and c). There was a much greater change in the relative intensity of the 1567.2 and 1570.5 eV peaks in the Mollisol clay (Fig. 3.6.8d) after reaction in the Maillard (Fig. 3.6.8e) and especially the catechol-Maillard systems (Fig. 3.6.8f). The peak at 1567.2 eV became much sharper and more intense than the peak at 1570.5 eV in the Mollisol-catalyzed catechol-Maillard system solid residue (Fig. 3.6.8f) than in the unreacted Mollisol clay (Fig. 3.6.8d). The coprecipitation of the dissolved Al with humified materials apparently resulted in the formation of disordered Al(oxy)hydroxides whose peak intensity at 1567.2 eV was increased relative to that at 1570.5 eV (Figure 3.6.8e and f). This trend was observed in the tannate-induced structural perturbation of Al hydroxides (Hu

et al. 2008). It also appeared that there was an increase in the intensity of the peak at 1566.1 eV (Fig. 3.6.8f). This indicates that the humification reactions resulted in the dissolution of some octahedral Al, thus enhancing the relative intensity of the 4-coordinated Al. The XRD data showed that the intensity of the peaks of the crystalline components such as quartz, mica, vermiculite/smectite, and kaolinite increased after reaction with the biomolecules (Fig. 3.6.6). Therefore, it is possible that the surface coating of poorly crystalline sesquioxides and their complexes with organics were preferentially dissolved during the humification reactions.

Fe L-edge NEXAFS spectroscopy

The kaolinite clay did not contain a sufficient amount of Fe to obtain an Fe L-edge NEXAFS spectra (TEY and FLY) of the samples. The Fe L-edge NEXAFS spectra (TEY) of the unreacted nontronite and Mollisol clays, the solid residues from the nontronite- and Mollisol-catalyzed Maillard and integrated catechol-Maillard systems, and selected reference compounds are shown in Fig. 3.6.9. There were no differences between the Fe L-edge NEXAFS FLY spectra of the unreacted nontronite and Mollisol clays and the clays reacted in the Maillard and catechol-Maillard systems (data not shown). This indicates that the changes to the Fe speciation due to humification occurred at the surfaces of the mineral colloids of these systems. The Fe L-edge NEXAFS spectra (TEY and FLY) of the unreacted Oxisol clay and the solid residues from the Oxisol-catalyzed Maillard and integrated catechol-Maillard systems and selected reference compounds are shown in Fig. 3.6.10. The reference compounds were selected because of the oxidation state and coordination symmetry of the Fe that they contain. The compounds FeO (wustite) and Fe_3O_4 (magnetite) contain Fe(II) in octahedral symmetry (Wilke et al. 2001). Unfortunately the surface of FeO was partially oxidized during the measurements (Fig. 3.6.9g) and thus does not look like pure FeO containing only Fe(II) (Crocombette et al. 1995; Garvie and Buseck 1998). In the spectra of unoxidized FeO, the peak at 707.7 eV should be the dominant peak while the peak at 709.5 eV should be weaker. The compounds Fe_3O_4 (magnetite) and γ-Fe_2O_3 (maghemite) contain Fe(III) in both octahedral and tetrahedral symmetry, whereas α-Fe_2O_3 (hematite) and α-FeO(OH) (goethite) contain Fe(III) in only octahedral symmetry (Wilke et al. 2001).

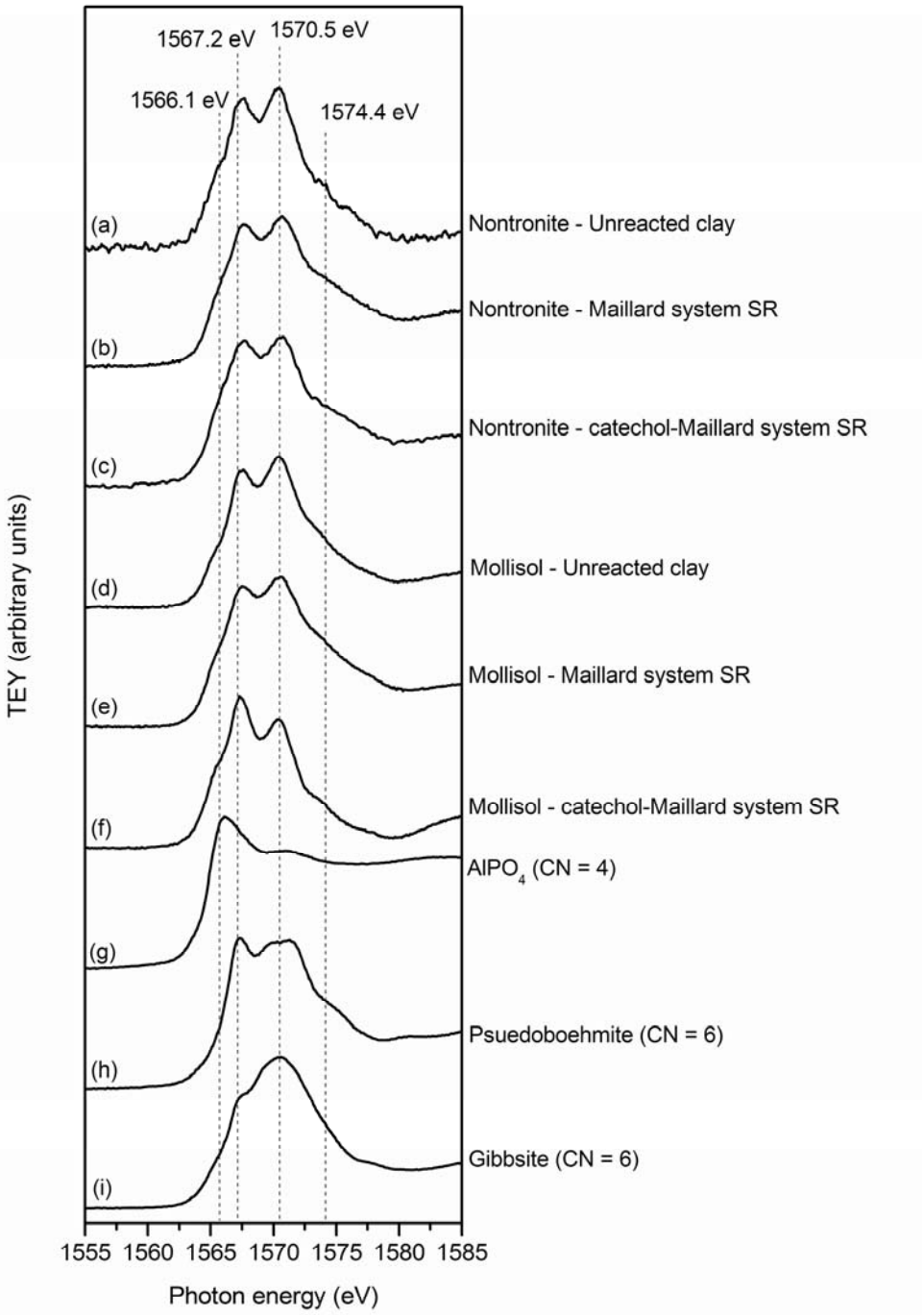

Figure 3.6.8 Aluminum K-edge NEXAFS spectra of (a) the unreacted nontronite clay; and the solid residues from the nontronite-catalyzed: (b) Maillard reaction and (c) catechol-Maillard reaction systems; (d) unreacted Mollisol clay; and the solid residues from the Mollisol-catalyzed: (e) Maillard reaction and (f) catechol-Maillard reaction systems; and pure reference compounds (g) $AlPO_4$, (h) pseudoboehmite, and (i) gibbsite. CN = coordination number.

The difference in intensity between the major peak at 709.5 eV and left side peak at 707.7 eV gives an indication of the ratio of Fe(II) and Fe(III) in the Fe oxide; the smaller the difference in intensity, the more Fe(II) the oxide contains (Crocombette et al. 1995). Thus, it is clear that the Mollisol clay (Fig. 3.6.9a) contained a greater content of Fe(II) after reaction in the Maillard and catechol-Maillard reaction systems (Fig. 3.6.9b and c). There also appeared to be a small increase in the Fe(II) content of the nontronite clay (Fig. 3.6.9d) after undergoing humification reactions in the Maillard and catechol-Maillard systems (Fig. 3.6.9e and f).

The coordination symmetry of Fe can be deduced from how well-resolved the main absorption peak (709.5 eV) and smaller side peak (707.7 eV) are from each other (Crocombette et al. 1995). It can be seen in the spectra of the reference Fe oxides with Fe(III) in octahedral symmetry (coordination number = 6), i.e., α-Fe_2O_3 (Fig. 3.6.9j) and α-FeO(OH) (Fig. 3.6.9k), that the peaks are more well-resolved than in the spectra of the Fe oxides containing Fe(III) in octahedral and tetrahedral symmetry (coordination number = 4 and 6), i.e., Fe_3O_4 (Fig. 3.6.9h) and γ-Fe_2O_3 (Fig. 3.6.9i). Therefore it appears that the Fe(III) in the Mollisol and nontronite clays is predominantly in octahedral symmetry. Nontronite is known to contain structural Fe(III) in the octahedral sheet. The Mollisol clay contained some poorly crystalline Fe oxides (Table 3.6.2) and most likely also contained some Fe substituted 2:1 layer silicates.

The Fe L_2-edge (720.9-722.6 eV) appears much stronger in the FLY spectra than the TEY spectra (Fig. 3.6.10). The Oxisol clay (Fig. 3.6.10a) contained more Fe(II) after reaction in the Maillard (Fig. 3.6.10b) and especially the catechol-Maillard system (Fig 3.6.10c). This is most apparent from the FLY results, where it can be seen that the peak at 707.7 eV is strongest in the Oxisol-catechol-Maillard system, similar to that of FeO (Fig. 3.6.10d). The Oxisol clay appeared to contain Fe(III) in the tetrahedral and especially octahedral symmetry (Fig. 3.6.10a) based on the shape of the TEY spectra. This is in agreement with the XRD results (Table 3.6.3) which show the presence of hematite, maghemite and goethite in the Oxisol clay. The Fe L-edge NEXAFS spectra of the Mollisol and nontronite clay systems (Fig. 3.6.9) and Oxisol clay systems (Fig. 3.6.10) show that Fe(III) was partially reduced to Fe(II) during the humification reactions, most noticeably in the Mollisol and Oxisol systems (Fig. 3.6.9a-c and Fig. 3.6.10a-c), and thus confirms the important role of Fe(III) in these clays as an oxidant which enhances oxidative polymerization (humification) reactions.

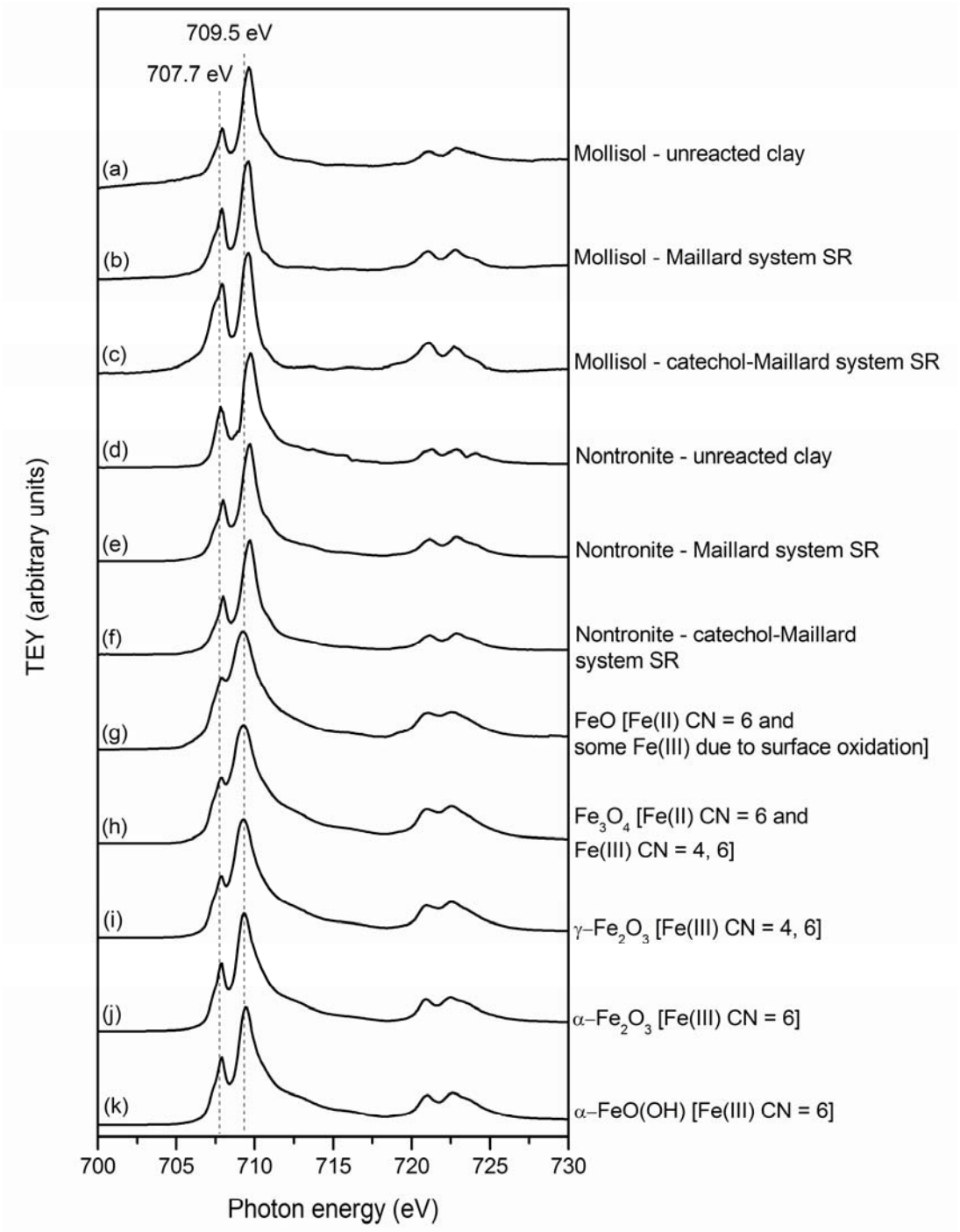

Figure 3.6.9 Iron $L_{2,3}$-edge NEXAFS spectra of (a) the unreacted Mollisol clay; the solid residues from the Mollisol-catalyzed: (b) Maillard reaction system, and (c) integrated catechol-Maillard reaction system; (d) the unreacted nontronite clay; the solid residues from the nontronite-catalyzed: (e) Maillard reaction and (f) catechol-Maillard reaction systems; and the reference compounds: (g) FeO (wustite), (h) Fe_3O_4 (magnetite), (i) γ-Fe_2O_3 (maghemite), (j) α-Fe_2O_3 (hematite), and (k) α-FeO(OH) (goethite). CN = coordination number.

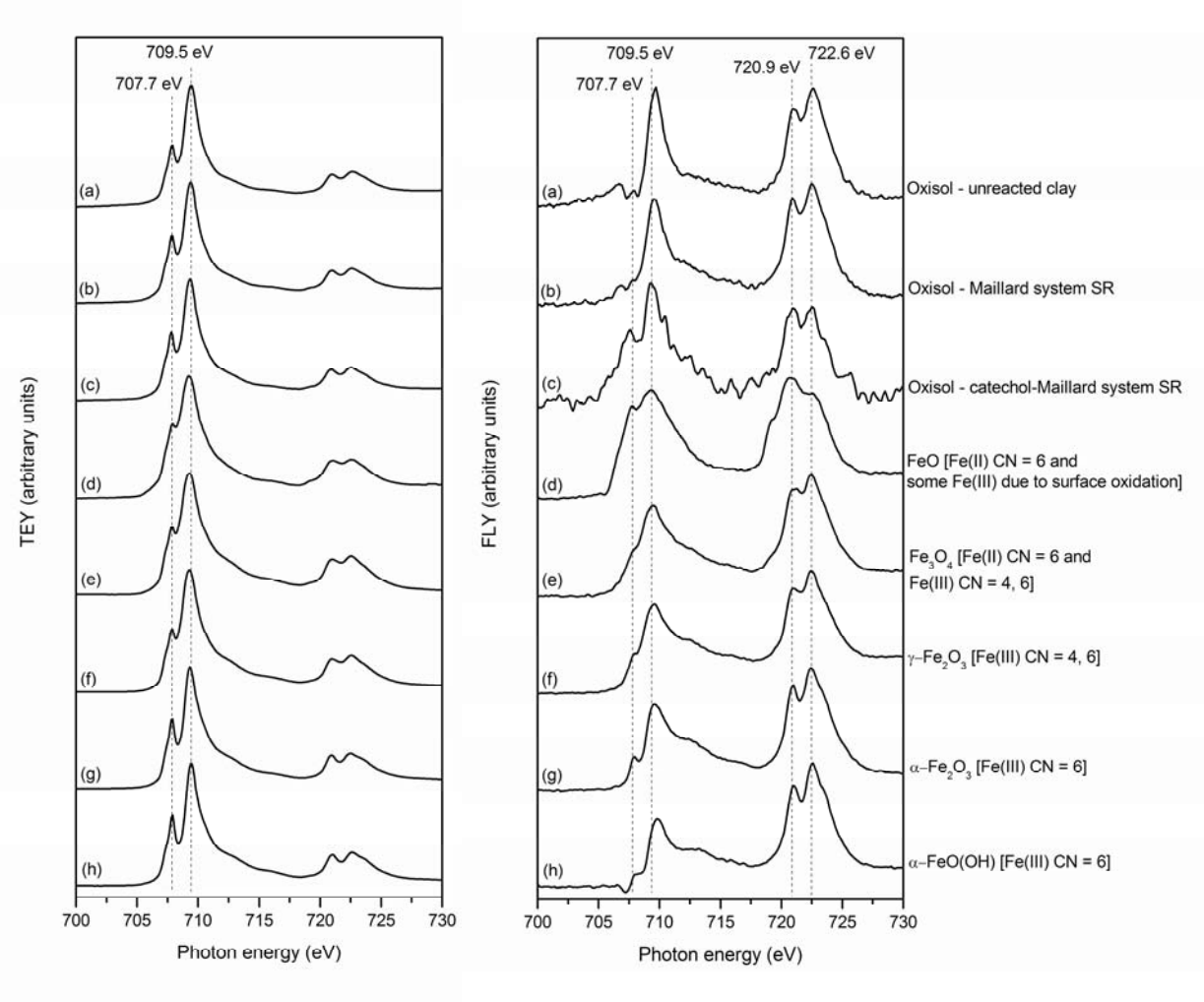

Figure 3.6.10 Iron $L_{2,3}$-edge NEXAFS spectra (TEY left and FLY right) of (a) the unreacted Oxisol clay; the solid residues from the Oxisol-catalyzed: (b) Maillard reaction system, and (c) integrated catechol-Maillard reaction system; and the reference compounds: (d) FeO (wustite), (e) Fe_3O_4 (magnetite), (f) γ-Fe_2O_3 (maghemite), (g) α-Fe_2O_3 (hematite), and (h) α-FeO(OH) (goethite). CN = coordination number.

Mn L-edge NEXAFS spectroscopy

The kaolinite, nontronite and Mollisol clays did not contain sufficient amounts of Mn to obtain meaningful Mn L-edge NEXAFS spectra (TEY or FLY) of the samples (data not shown). The Mn $L_{2,3}$-edge NEXAFS spectra (TEY) of the unreacted Oxisol clay and solid residues from the Oxisol-catalyzed Maillard and catechol-Maillard systems, HA from the birnessite-catalyzed

catechol-Maillard system and reference compounds are shown in Fig. 3.6.11. The Mn L-edge NEXAFS FLY spectra of the Oxisol systems were poor and not meaningful (data not shown).

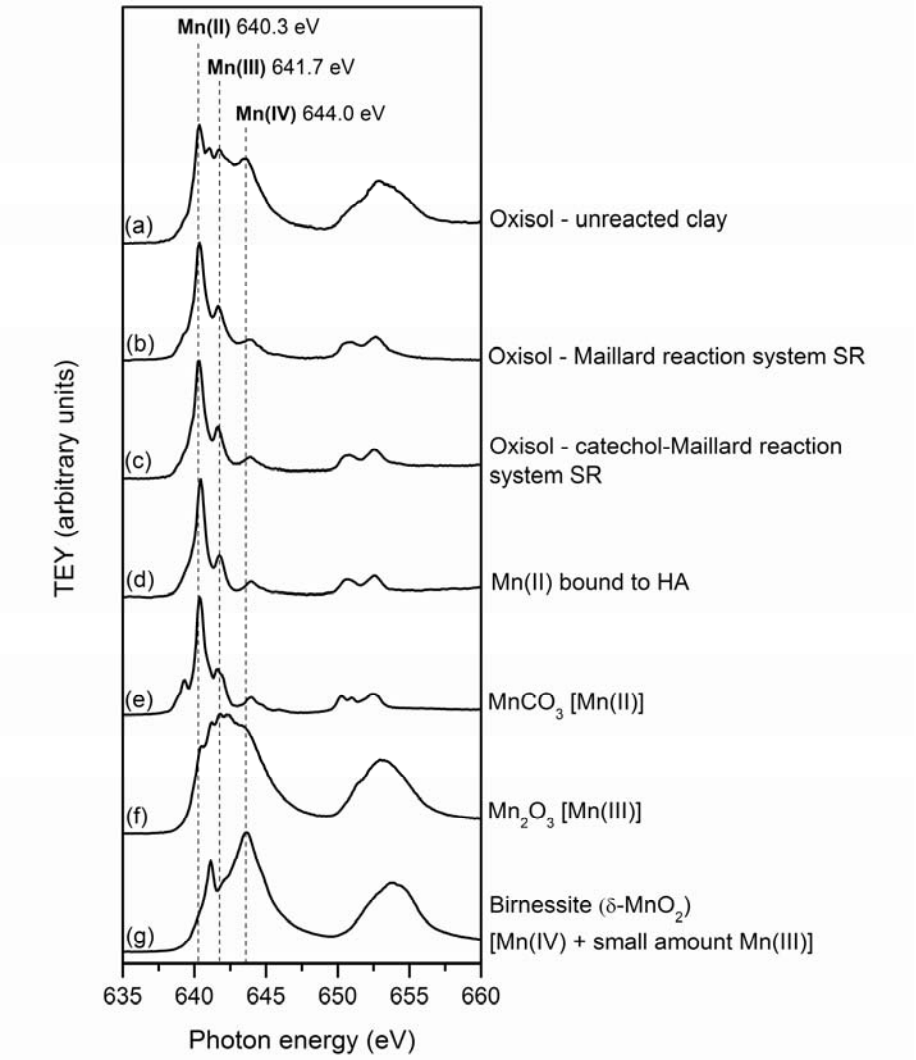

Figure 3.6.11 Mn L-edge NEXAFS spectra of (a) the unreacted Oxisol clay, (b) the solid residue from the Oxisol-Maillard system, (c) the solid residue from the Oxisol-catechol-Maillard system, (d) unpurified HA from the birnessite-equimolar catechol-Maillard system, (e) pure $MnCO_3$, (f) pure Mn_2O_3 and (g) unreacted birnessite.

The Mn in the unreacted Oxisol clay consisted of a mixture of Mn(II), Mn(III) and Mn(IV) (Fig. 3.6.11a). The Mn in the solid residues from the Oxisol-catalyzed Maillard and catechol-Maillard (Fig. 3.6.11b and c) systems was in the Mn(II) form. This indicates that all the Mn(III) and Mn(IV) species in the unreacted Oxisol clay were reduced to Mn(II) by reaction with the biomolecules in the Maillard and catechol-Maillard systems. The Mn L_3-edge of the

unpurified HA isolated from the birnessite-catalyzed catechol-Maillard reaction system from Unit 3.1 (Fig. 3.6.11d) differs from that of pure $MnCO_3$ (Fig 3.6.11e) in that the minor absorption peak (~639.1 eV) to the left of the maximum Mn(II) absorption peak (640.3 eV) is not resolved. This corresponds to Mn(II) that is covalently bonded to either O or N and in octahedral conformation (Grush et al. 1996). The shape of L_3-edge (638-648 eV) of the solid residues from the Maillard and catechol-Maillard systems (Fig. 3.6.11b and c) is very similar to the shape of the L_3-edge of Mn(II) bound to humic acid (Fig. 3.6.11d), which indicates that Mn(II) is bound to humic products in the solid residues from the Oxisol-catalyzed Maillard and catechol-Maillard systems. This confirms coprecipitation of the humic products with Mn(II) and can also account for the chemical partitioning observed in this system (Fig. 3.6.7d and e) as discussed in Section 3.1. The Mn L-edge NEXAFS results thus confirm the important role of Mn(III) and Mn(IV) oxides in the Oxisol clay in catalyzing oxidative polymerization reactions (humification) in the Maillard and catechol-Maillard reaction systems.

3.6.4 Conclusions

The abiotic catalytic ability of soils in the formation of humic substances is attributable to the reactive components, namely Mn, Fe, and Al oxides, (oxy)hydroxides, and short-range ordered mineral colloids, clay-size layer silicates, and some reactive primary minerals (Huang 2000). The Maillard reaction pathway was previously investigated using birnessite (Jokic et al. 2001b), smectites and crystalline goethite (Gonzalez and Laird 2004) as catalysts under environmentally relevant conditions, while the integrated polyphenol-Maillard pathway was investigated using birnessite (Jokic et al. 2004b). The findings of the present study show that the catalytic abilities of commonly occurring mineral colloids from temperate and tropical regions greatly differed in influencing the Maillard reaction and integrated polyphenol-Maillard humification pathways.

The natural Mollisol and Oxisol clays were relatively stronger catalysts of the Maillard reaction compared with kaolinite and nontronite. This is attributable to sesquioxide coatings on the surfaces of the natural clays and/or the presence of discrete metal oxides in soil colloids. The Mollisol clay appeared to enhance browning in the Maillard system to the greatest extent of all the clays investigated. However, the redox status of the Oxisol-Maillard system was lower than that of the Mollisol-Maillard system, which indicated that more oxygen was consumed in the

Oxisol-Maillard system, and thus more oxidative polymerization reactions took place. The organic C content results of the solid residues confirmed that a significant amount of the humic products formed in the Oxisol-Maillard system was sorbed in the solid phase, which accounts for the lower visible absorbance of the supernatant.

The Oxisol clay enhanced browning in the integrated catechol-Maillard system to a much greater extent than the Mollisol clay, which is attributed to its high content of Al and Fe oxides and especially, poorly crystalline Mn oxides. The nontronite clay enhanced browning of the catechol-Maillard system to a similar extent as the Mollisol clay. The nontronite and Mollisol clays catalyzed the formation of HA (in the supernatant) with a significant aliphatic carboxylic character in the catechol-Maillard systems, similar to that of the natural IHSS HAs. In contrast, the HA (in the supernatant) from the Oxisol-catalyzed catechol-Maillard system had stronger aromatic character; however, the humic products in the solid residue appeared to be more aliphatic carboxylic in nature. This was attributed to the chemical partitioning of humic products between the solution and solid phases by coprecipitation with multivalent cations such as Mn^{2+} and/or adsorption of aliphatic carboxylic groups of humic substances on the surfaces of the metal oxides.

The kaolinite clay was the weakest catalyst of the layer silicate clays studied in promoting the catechol-Maillard humification pathway and the humic products in the solid residue of the kaolinite catechol-Maillard system appeared to have the least aliphatic carboxylic character of all the systems. This is attributable to the greater humification promoting effect of 2:1 layer silicates, such as nontronite and other smectites, than that of 1:1 layer silicates, such as kaolinite, because of their larger specific surface area and lattice imperfections which provide reactive sites to catalyze humification.

The humification reactions affected the Al, Fe and Mn speciation in the clays to different extents. There was a significant change in the Al speciation in the Mollisol clay after reaction in the catechol-Maillard system. It was observed that, in the Mollisol and Oxisol clays, there was an increase in the Fe(II) content of the clays after reaction in the Maillard and especially integrated catechol-Maillard systems, confirming the important role of Fe(III) in catalyzing oxidative polymerization reactions. The poorly crystalline Mn(III) and Mn(IV) oxides in the Oxisol clay were reduced to Mn(II) during humification reactions in both the Maillard and catechol-Maillard systems. Furthermore, Mn(II) was coprecipitated with humic products in the

solid phase. The Oxisol-catalyzed Maillard and catechol-Maillard systems had the highest accumulation of organic C in the solid phase of all the clay systems investigated.

Highly weathered soils from tropical environments contain predominantly 1:1 minerals such as kaolinite and large quantities of Al, Fe and Mn oxides. Soils from temperate environments usually contain high amounts of expanding 2:1 layer silicates such as montmorillonite or nontronite, and smaller amounts of Al, Fe and Mn oxides and 1:1 layer silicates. The data obtained in the present study show that mineral colloids commonly occurring in temperate and tropical soils have a distinct ability to catalyze the Maillard and integrated catechol-Maillard humification pathways. The findings obtained in this study shed new light on the significance of the nature of layer silicates, and mineralogical characteristics of natural soils in temperate and tropical regions on abiotic humification pathways and products in natural environments.

4 GENERAL DISCUSSION AND CONCLUSIONS

The Maillard reaction is regarded as an important pathway in natural humification (Maillard 1913; Ikan et al. 1996; Arafaioli et al. 1999; Jokic et al. 2001b; Bosetto et al. 2002). Likewise, the polyphenol pathway of humification has been intensely studied using various soil mineral colloids as catalysts (Kumada and Kato 1970; Filip et al. 1977; Wang et al. 1986; Bollag et al. 1998; Huang 2004; Clapp et al. 2005). Jokic et al (2004b) were the first to show the significance of linking the Maillard reaction and polyphenol pathway into an integrated humification pathway, using a system containing equimolar amounts of catechol, glucose and glycine, under the catalysis of birnessite (δ-MnO_2). However, the influence of structure and functionality of polyphenols on the integrated polyphenol-Maillard humification pathway remained to be uncovered. Furthermore, the effect of the molar ratio of polyphenol to Maillard reagents in integrated polyphenol-Maillard reaction was unknown. The relative abundance of biomolecules varies with vegetation, microbial community and the environment (Stevenson 1994; Kögel-Knabner 2002). The results of the present study show that the structure and functionality of polyphenols significantly affects the humification processes and the associated carbonate formation in the integrated polyphenol-Maillard reaction catalyzed by birnessite. Among the three polyphenols investigated, pyrogallol and catechol produced more heterogeneous and aliphatic carboxylic HA in the integrated polyphenol-Maillard systems, whereas resorcinol produced more aromatic HA. These observations can be linked to the ability of the polyphenols to form direct surface complexes with birnessite. Pyrogallol and catechol, with OH groups in the *ortho*-position, are more readily able to participate in direct electron transfer reactions with birnessite than is resorcinol with OH groups in the *meta*-position. Therefore, catechol (two *ortho*-OH groups) and especially pyrogallol (three *ortho*-OH groups) are far more easily polymerized or cleaved, than is resorcinol. The chemical partitioning of the humic products between the solution and solid phases by coprecipitation with Mn(II) as influenced by their functional groups was also observed in the catechol and pyrogallol containing systems. Increasing the molar ratio of polyphenol to Maillard reagents in all of the polyphenol-Maillard systems studied resulted in a significant enhancement of humification and the formation of HA with an increasingly aromatic character.

It was previously shown that CO_2 is evolved during birnessite-catalyzed abiotic humification reactions, as a result of the oxidation of glycine (Wang and Huang 1987, 2005), catechol (Majecher et al. 2000), pyrogallol (Wang and Huang 1987, 2000b) and glucose (Jokic et al. 2004b) by birnessite. However, the abiotic biomolecule-induced formation of carbonate minerals in the environment remained to be uncovered. The present findings provide the first time evidence of the biomolecule-induced formation of $MnCO_3$ (rhodochrosite) in humification pathways as a result of the abiotic oxidation and cleavage of glucose, glycine or polyphenols by birnessite. In the catechol- and pyrogallol-Maillard systems, increasing the molar ratio of polyphenol to Maillard reagents suppressed the formation of $MnCO_3$ in the system, whereas, in the resorcinol system it enhanced $MnCO_3$ formation. This was related to the ability of the polyphenols to form direct surface complexes with birnessite. The structure of the polyphenols and the molar ratio of polyphenol to Maillard reagents substantially affected not only the degree of humification but also the extent of $MnCO_3$ formation which was a competing reaction to the genesis of humic substances in these systems. The present findings also provided experimental evidence at the molecular level for substantiating the hypothesis of the abiotic formation of $MnCO_3$ in aquatic sediments and $MnCO_3$ deposits (Okita et al. 1988; Glasby and Schultz 1999).

Sugars and amino acids are abundant in soils (Anderson et al. 1989). Glucose is one of the primary decomposition products arising from the natural degradation of cellulose (Koivula and Hanninen 2001), one of the most abundant substrates in the terrestrial environment. The Maillard reaction and the influence of catechol on the Maillard reaction as catalyzed by birnessite have been reported by Jokic et al. (2004a, 2004b). However, the role of glucose in influencing the polyphenol humification pathway and the integrated polyphenol-Maillard humification pathway as catalyzed by birnessite remained to be uncovered. The results of the present study show that glucose enhanced humification reactions in the catechol and especially catechol-Maillard reaction systems under the catalysis of birnessite. Increasing the amount of glucose in the integrated catechol-Maillard system promoted the formation of Maillard reaction-type functionalities in the supernatant HA fraction, i.e., aromatic C bound to N, O or ketone and aliphatic carboxylic groups, similar to the functionalities observed in natural soil and river HA. The C K-edge NEXAFS spectroscopic data reveal that glucose promoted the formation of aromatic C-H and aromatic C-OH but decreased the formation of quinone C in the solid residues of the catechol-glucose and catechol-Maillard reaction systems. Furthermore, the spectroscopic

data also show that glucose promoted the formation of carbonate ($MnCO_3$) at the expense of aliphatic carboxylic groups in the solid residues of both humification pathways. These transformations are in part ascribed to the dehydration and oxidation of glucose by birnessite to form aromatization products and carboxylic acids, and the subsequent release of CO_2 through decarboxylation. The present study demonstrated that sugars, such as glucose, which are one of the most abundant biomolecules in the environment, can make a significant contribution to influence the formation and nature of humic substances and genesis of carbonates such as $MnCO_3$.

The abiotic catalytic ability of soils in the formation of humic substances is attributable to the reactive components, namely Mn, Fe, and Al oxides, (oxy)hydroxides, and short-range ordered mineral colloids, clay-size layer silicates, and some reactive primary minerals (Huang 2000). The Maillard reaction humification pathway was previously investigated using birnessite (Jokic et al. 2001a, 2001b), smectites and crystalline goethite (Gonzalez and Laird 2004) as catalysts under environmentally relevant conditions, while the integrated polyphenol-Maillard humification pathway was investigated using birnessite (Jokic et al. 2004b). The results of the present study show that mineral colloids from temperate and tropical regions differ greatly in their ability to catalyze the Maillard reaction and integrated polyphenol-Maillard reaction under environmentally relevant conditions.

Among all the mineral colloids investigated, the poorly ordered Fe and especially Mn oxides were the strongest promoters of humification in the Maillard reaction. The HA produced in the Mn and Fe oxide-catalyzed Maillard reaction systems had a strong aliphatic carboxylic nature, similar to that of natural HAs. The pure layer silicate clays, kaolinite and nontronite, and Al oxide were relatively weaker catalysts of the Maillard reaction, compared with the Fe and Mn oxides. The natural Mollisol and Oxisol clays were relatively stronger catalysts of the Maillard reaction compared with kaolinite and nontronite. This is attributable to sesquioxide coatings on the surfaces of the natural clays and/or the presence of discrete metal oxides in soil colloids.

The poorly ordered Fe and Mn oxides were also the strongest catalysts of the humification in the integrated catechol-Maillard reaction system. The humic products produced in the Mn oxide-catechol-Maillard system were the most aliphatic carboxylic in nature compared to the humic products produced in all the other mineral-catalyzed catechol-Maillard reaction systems, which is largely attributed to the higher redox potential of the Mn oxide system. The crystalline

1:1 layer silicate clay, kaolinite, was the weakest catalyst of the catechol-Maillard system, whereas the 2:1 layer silicate clay, nontronite, was a relatively moderate promoter of humification in the catechol-Maillard system. The natural soil clays, from the temperate and tropical regions, significantly enhanced humification in the catechol-Maillard reaction system. The Oxisol clay was a stronger catalyst than the Mollisol clay, which is attributed to its higher content of Mn and Fe oxides.

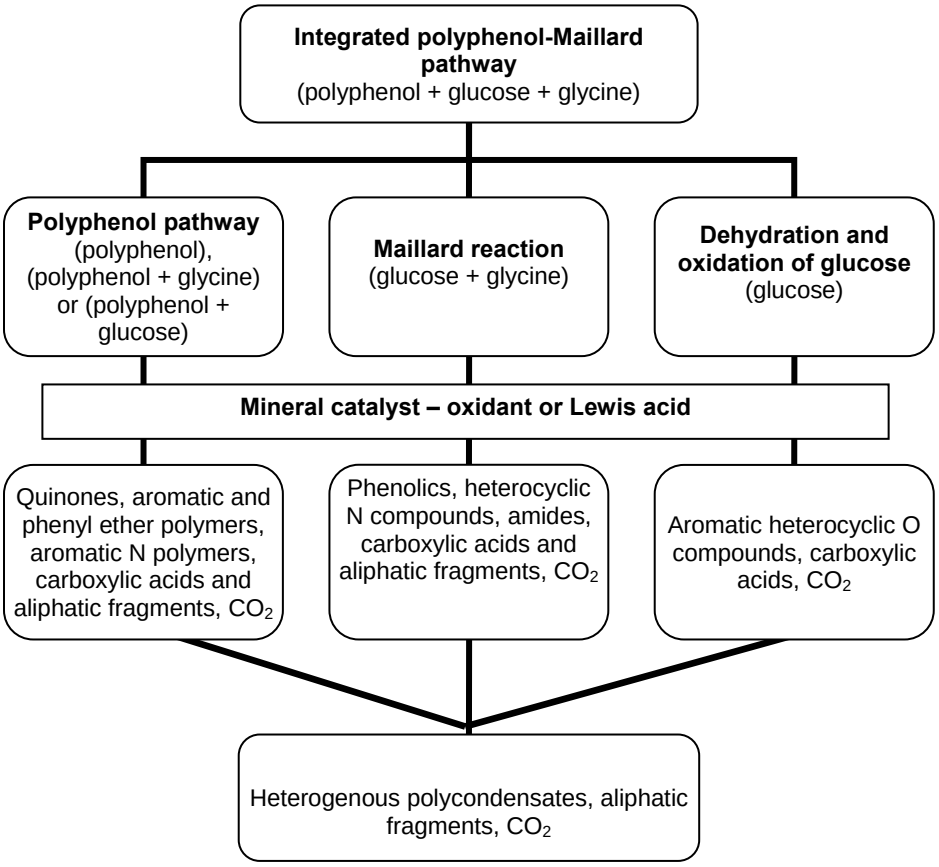

Figure 4.1 Schematic representation of the integrated polyphenol-Maillard humification pathway catalyzed by environmental mineral colloids. The type of biomolecules and mineral catalysts involved has a substantial influence on the humification processes and products.

The findings of the present study show that the catalytic abilities of commonly occurring mineral colloids in temperate and tropical regions substantially differed in influencing the Maillard reaction and integrated polyphenol-Maillard humification pathways and products. The integrated polyphenol-Maillard humification pathway catalyzed by environmental mineral

colloids is depicted in Fig. 4.1. Furthermore, the nature of the mineral colloids also affected the extent of organic C accumulation in the solid phase, and the extent of mineral surface alteration during humification. The metal oxide- and Oxisol clay-catalyzed Maillard and catechol-Maillard systems had the highest accumulation of organic C in the solid phase of all the systems investigated, which indicates the important role of metal oxides in not only promoting humification but also in C sequestration in the environment. The findings obtained in this study are of fundamental significance in understanding the importance of the nature of mineral colloids commonly occurring in temperate and tropical environments, and the nature and abundance of sugars, amino acids and polyphenols in influencing abiotic humification pathways and related reaction products in natural environments.

Our knowledge on the formation mechanisms of humic substances at the molecular level needs to be further advanced. To date, little work has been conducted on the transformation of lipids to humic substances. Lipids are one of the most refractory components of biological materials and are also a significant contributor to the humin fraction of soil humus. The role of mineral colloids as catalysts in accelerating the interactions of lipids with other biomolecules and the subsequent formation of humic substances remains to be uncovered.

Our understanding of the influence of pedogenic factors on the formation mechanisms of humic substances and carbonates, and the structural and surface chemistry of the resultant mineral-humus complexes are very limited. Application of advanced analytical methods, such as synchrotron-based X-ray and infrared spectroscopies and microscopy, atomic force microscopy, and multi-dimensional nuclear magnetic resonance spectroscopy should shed new light on the nature and properties of environmental humic substances and mineral-humus complexes. Further advancement of knowledge on this subject matter would contribute to understanding and regulating C sequestration in the Earth's Critical Zone which is the system of coupled chemical, biological, physical, and geological processes operating together to support life in the ecosystem.

5 REFERENCES

Adani, F., Ricca, G., Tambone, F. and Genevini, P. 2006. Isolation of the stable fraction (the core) of the humic acid. Chemosphere **62**: 1300-1307.

Adani, F., Spagnol, M. and Nierop, K. G. J. 2007. Biochemical origin and refractory properties of humic acid extracted from maize plants: the contribution of lignin. Biogeochem. **82**: 55-65.

Ahn, M.-Y., Martínez, C. E., Archibald, D. D., Zimmerman, A. R., Bollag, J.-M. and Dec, J. 2006. Transformation of catechol in the presence of a laccase and birnessite. Soil Biol. Biochem. **38**: 1015-1020.

Aiken, G. R., McKnight, D. M., Wershaw, R. L. and MacCarthy, P. 1985. Humic substances in soil, sediment and water: geochemistry, isolation and characterization. Wiley Interscience, New York, USA.

Aktas, N., Sahiner, N., Kantoglu, O., Salih, B. and Tanyolaç, A. 2003. Biosynthesis and characterization of laccase catalyzed poly(catechol). J. Polymers Environ. **11**: 123-128.

Alexander, M. 1997. Introduction to soil microbiology. John Wiley & Sons, New York, USA.

Allison, F. E. 1973. Soil organic matter and its role in crop production. Elsevier, Amsterdam, The Netherlands.

Allison, S. D. 2006a. Brown ground: A soil carbon analogue for the green world hypothesis? . Am. Nat. **167**: 619-627.

Allison, S. D. 2006b. Soil minerals and humic acids alter enzyme stability: implications for ecosystem processes. Biogeochem. **81**: 361-373.

Almendros, G., Dorado, J., Gonzâlez-Vila, F. J., Blanco, M. J. and Lankes, U. 2000. ^{13}C NMR assessment of decomposition patterns during composting of forest and shrub biomass. Soil Biol. Biochem. **32**: 793-804.

Ander, P. and Marzullo, L. 1997. Sugar oxidoreductases and veratryl alcohol oxidase as related to lignin degradation. J. Biotechnol. **53**: 115-131.

Andersen, J. E. T., Jensen, M. H., Moller, P. and Ulstrup, J. 1996. Perspectives for in situ scanning tunnel microscopic imaging of metalloproteins at HOPG surfaces. Electrochimica Acta **41**: 2005-2010.

Anderson, H. A., Bick, W., Hepburn, A. and Stewart, M. 1989. Nitrogen in humic substances. Pages 223-253 *in* M. H. B. Hayes, P. MacCarthy, R. L. Malcolm, R. S. Swift, eds. Humic substances II. In search of structure. Wiley-Interscience, Chichester, UK.

Arafaioli, P., Pantani, O. L., Bosetto, M. and Ristori, G. G. 1999. Influence of clay minerals and exchangeable cations on the formation of humic-like substances (melanoidins) from D-glucose and L-tyrosine. Clay Miner. **34**: 487-497.

Arafaioli, P., Ristori, G. G., Bosetto, M. and Fusi, P. 1997. Humic-like compounds formed from L-tryptophan and D-glucose in the presence of Cu(II). Chemosphere **35**: 575-584.

Baldock, J. A. 2002. Interactions of organic materials and microorganisms with minerals in stabilization of structure. Pages 85-131 *in* P. M. Huang, J.-M. Bollag, N. Senesi, eds. Interactions between soil particles and microorganisms. Impact on the terrestrial ecosystem. John Wiley & Sons, Chichester, UK.

Baldock, J. A., Masiello, C. A., Gelinas, Y. and Hedges, J. I. 2004. Cycling and composition of organic matter in terrestrial and marine ecosystems. Marine Chem. **92**: 39-64.

Baldock, J. A. and Nelson, P. N. 2000. Soil organic mattter. Pages B25-B84 *in* M. Sumner, ed. Handbook of Soil Science. CRC Press, Boca Raton, FL, USA.

Baldock, J. A. and Skjemstad, J. O. 2000. The role of soil mineral matrix in protecting natural organic materials against biological attack. Org. Geochem. **31**: 697-710.

Baldock, J. A. and Smernik, R. J. 2002. Chemical composition and bioavailability of thermally altered *Pinus resinosa* (Red pine) wood. Org. Geochem. **33**: 1093-1109.

Baldrian, P. 2006. Fungal laccases – occurrence and properties. FEMS Microbiol. Rev. **30**: 215-242.

Barnhisel, R. I. and Bertsch, P. M. 1989. Chlorites and hydroxyl-interlayered vermiculite and smectite. Pages 729-788 *in* J. B. Dixon, S. B. Weed, eds. Minerals in soil environments. Soil Science Society of America, Madison, WI, USA.

Barois, I., Villememin, G., Lavelle, P. and Toutain, F. 1993. Transformation of the soil structure through *Pontoscolex corethrurus* (Oligochaeta) intestinal tract. Geoderma **56**: 57-66.

Béguin, P. and Aubert, J. P. 1994. The biological degradation of cellulose. FEMS Microbiol. Rev. **13**: 25-58.

Berry, L. G. and Mason, B. 1959. Mineralogy. W.H. Freeman and Company, San Francisco, CA, USA.

Bigham, J. M., Fitzpatrick, R. W. and Schultz, D. G. 2002. Iron oxides. Pages 323-366 *in* J. B. Dixon, D. G. Schultz, eds. Soil mineralogy with environmental applications. Soil Science Society of America, Madison, WI, USA.

Bird, M. I., Veenendaal, E., Moyo, C., Lloyd, J. and Frost, P. 1999. Stability of elemental carbon in a savanna soil. Global Biogeochem. Cycles **13**: 993-942.

Birkel, U., Gerold, G. and Niemeyer, J. 2002. Abiotic reactions of organics on clay mineral surfaces. Pages 437-447 *in* A. Violante, P. M. Huang, J.-M. Bollag, L. Gianfreda, eds. Soil mineral-organic matter-microorganism interactions and ecosystem health: Dynamics, mobility and transformation of pollutants and nutrients. Elsevier, Amsterdam, The Netherlands.

Bittner, S. 2006. When quinones meet amino acids: chemical, physical and biological consequences. Amino Acids **30**: 205-224.

Boese, J., Osanna, A., Jacobsen, C. and Kirz, J. 1997. Carbon edge XANES of amino acids and peptides. J. Electron Spectrosc. **85**: 9-15.

Bollag, J.-M., Dec, J. and Huang, P. M. 1998. Formation mechanisms of complex organic structures in soil habitats. Adv. Agron. **63**: 237-266.

Bollag, J.-M., Myers, C., Pal, S. and Huang, P. M. 1995. The role of abiotic and biotic catalysts in the transformation of phenolic compounds. Pages 299-310 *in* P. M. Huang, J. Berthelin, J.-M. Bollag, W. B. McGill, A. L. Page, eds. Environmental impact of soil component interactions Vol 1. Natural and anthropogenic organics. Lewis Publishers, Boca Raton, FL, USA.

Bose, J. L., Foster, A. B., Stacey, M. and Webber, J. M. 1959. Action of manganese dioxide on simple carbohydrates. Nature **184**: 1301-1302.

Bosetto, M., Arafaioli, P. and Pantani, O. L. 2002. Study of the Maillard reaction products formed by glycine and D-glucose on different mineral substrates. Clay Miner. **37**: 195-204.

Bosetto, M., Arafaioli, P., Pantani, O. L. and Ristori, G. G. 1997. Study of the humic-like compounds formed from L-tyrosine on homoionic clays. Clay Miner. **32**: 341-349.

Bosetto, M., Arafaioli, P., Ristori, G. G. and Fusi, P. 1995. Formation of melanin-type compounds from L-tryptophan on Ca-saturated and Al-saturated clays. Fresenius Environ. Bull. **4**: 369-374.

Bosmans, H. J. 1970. Unit cell and crystal structure of nordstrandite, $Al(OH)_3$. Acta Crystallog. B **26**: 649-652.

Bragg, L. and Claringbull, G. F. 1965. Crystal structures of minerals. G. Bell and Sons Ltd., London, UK.

Brodowski, S. B. 2004. Origin, function, and reactivity of black carbon in the arable soil environment. PhD thesis. University of Bayreuth, Germany.

Burdon, J. 2001. Are the traditional concepts of the structures of humic substances realistic? Soil Sci. **166**: 752-769.

Burton, S. G. 2003. Laccases and phenol oxidases in organic synthesis - a review. Curr. Org. Geochem. **7**: 1317-1331.

Chefetz, B., Chen, Y. and Hadar, Y. 1998. Purification and characterization of laccase from *Chaetomium thermophilium* and its role in humification. Appl. Environ. Microbiol. **64**: 3175-3179.

Chefetz, B., Tarchitzky, J., Desmukh, A. P., Hatcher, P. G. and Chen, Y. 2002. Structural characterization of soil organic matter and humic acids in particle-size fractions of an agricultural soil. Soil Sci. Soc. Am. J. **66**: 129-141.

Chorover, J. and Amistadi, M. K. 2001. Reaction of forest floor organic matter at goethite, birnessite and smectite surfaces. Geochim. Cosmochim. Acta **65**: 95-109.

Christl, I. and Kretzchmar, R. 2007. C-1s NEXAFS spectroscopy reveals chemical fractionation of humic acid by cation-induced coagulation. Environ. Sci. Technol. **41**: 1915-1920.

Clapp, C. E., Hayes, M. H. B., Simpson, A. J. and Kingery, W. L. 2005. Chemistry of organic matter. Pages 1-150 *in* D. L. Sparks, M. A. Tabatabai, eds. Chemical Processes in Soils. Soil Science Society of America, Madison, WI, USA.

Claus, H. 2004. Laccases: structure, reactions and distribution. Micron. **35**: 93-96.

Claus, H. and Decker, H. 2006. Bacterial tyrosinases. System. Appl. Microbiol. **29**: 3-14.

Claus, H. and Filip, Z. 1988. Behavior of phenoloxidases in the presence of clays and other soil-related adsorbents. Appl. Microbiol. Biotechnol. **28**: 506-511.

Claus, H. and Filip, Z. 1990. Effects of clays and other solids on the activity of phenoloxidases produced by some fungi and actinomycetes. Soil Biol. Biochem. **22**: 483-488.

Cooney, R. R. and Urquhart, S. G. 2004. Chemical trends in the near-edge X-ray absorption fine structure of monosubstituted and para-bisubstituted benzenes. J. Phys. Chem. B. **108**: 18185-18191.

Cramer, S. P., de Groot, F. M. F., Ma, Y., Chen, C. T., Sette, F., Kipke, C. A., Eichhorn, D. M., Chen, M. K., Armstrong, W. H., Libby, F. and others. 1991. Ligand field strengths and oxidation states from manganese L-edge spectroscopy. J . Am. Chem. Soc. **113**: 7937-7940.

Crocombette, J. P., Pollack, M., Jollet, F., Thromat, N. and Gautier-Soyer, M. 1995. X-ray absorption spectroscopy at the Fe $L_{2,3}$ threshold in iron oxides. Phys. Rev. B **52**: 3143-3150.

Cullen, D. 1997. Recent advances on the molecular genetics of ligninolytic fungi. J. Biotechnol. **53**: 273-289.

Daintith, J. 1990. A concise dictionary of chemistry. Oxford University Press, Oxford, UK.

Dasgupta, J., Tyryshkin, A. M., Kozlov, Y. N., Klimov, V. V. and Dismukes, G. C. 2006. Carbonate complexation of Mn^{2+} in the aqueous phase: redox behavior and ligand binding modes by electrochemistry and EPR spectroscopy. J. Phys. Chem. B. **110**: 5099-5111.

Davison, E. A. and Janssens, I. A. 2006. Temperature sensitivity of soil carbon decomposition and feedbacks to climate change. Nature **440**: 165-173.

Dec, J. and Bollag, J.-M. 1990. Detoxification of substituted phenols by oxidoreductive enzymes through polymerization reactions. Archives Environ. Contamin. Toxicol. **19**: 543-550.

Dec, J. and Bollag, J.-M. 2000. Phenoloxidase-mediated interactions of phenols and anilines with humic materials. J. Environ. Qual. **29**: 655-676.

Dec, J., Haider, K. and Bollag, J.-M. 2001. Decarboxylation and demethoxylation of naturally occurring phenols during coupling reactions and polymerization. Soil Sci. **166**: 660-671.

Dec, J., Haider, K. and Bollag, J.-M. 2003. Release of substituents from phenolic compounds during oxidative coupling reactions. Chemosphere **52**: 549-556.

Derenne, S. and Largeau, C. 2001. A review of some important families of refractory macromolecules: composition, origin, and fate in soils and sediments. Soil Sci. **166**: 833-847.

Dhez, O., Ade, H. and Urquhart, S. G. 2003. Calibrated NEXAFS spectra of some common polymers. J. Electron Spectrosc. **128**: 85-96.

Diallo, M. S., Simpson, A., Gassman, P., Faulon, J. L., Johnson Jr., J. H., Godard III, W. A. and Hatcher, P. G. 2003. 3-D structural modeling of humic acids through experimental characterization, computer assisted structure elucidation and atomic simulations. I. Chelsea soil humic acid. Environ. Sci. Technol. **37**: 1783-1793.

Dixon, J. B. and Schulze, D. G. 2002. Soil mineralogy with environmental applications. Soil Science Society of America, Madison, WI, USA.

Dixon, J. B. and Weed, S. B. 1989. Minerals in soil environments. Soil Sci. Soc. Am., Madison, WI, USA.

Dubey, S., Singh, D. and Misra, R. A. 1998. Enzymatic synthesis and various properties of poly(catechol). Enzyme Microb. Technol **23**: 432-437.

Durán, N. and Esposito, E. 2000. Potential applications of oxidative enzymes and phenoloxidase-like compounds in wastewater and soil treatment: a review. Appl. Catalysis B. **28**: 83-99.

Eriksson, K.-E., Blanchette, R. A. and Ander, P. 1990. Microbial and enzymatic degradation of wood and wood components. Springer Verlag, Berlin, Germany.

Evershed, R. P., Bland, H. A., van Bergen, P. F., Carter, J. F., Horton, M. C. and Rowley-Conwy, R. P. 1997. Volatile compounds in archeological plant remains and the Maillard reaction during the decay of organic matter. Science **278**: 432-433.

Faust, G. T. 1940. Staining of clay minerals as a rapid means of identification in natural and beneficiation products. Report of Investigation 3522, Bureau Mines, Washington, DC, USA.

Feng, X. and Simpson, M. J. 2007. The distribution and degradation of biomarkers in Alberta grassland soil profiles. Org. Geochem **38**: 1558-1570.

Filip, Z., Flaig, W. and Ritz, E. 1977. Oxidation of some phenolic substances as influenced by clay minerals. Soil Org. Matter Stud. Proc. Symp. **2**: 91-96.

Filley, T. R., Cody, G. D., Goodell, B., Jellison, J., Noser, C. and Ostrofsky, A. 2002. Lignin demethylation and polysaccharide decomposition in spruce sapwood degraded by brown rot fungi. Org. Geochem. **33**: 11-124.

Fischer, G., Cao, X., Cox, N. and Francis, M. 2005. The FT-IR spectra of glycine and glycylglycine zwitterions isolated in alkali halide matrices. Chem. Phys. **313**: 39-49.

Flaig, W., Beutelspacher, H. and Rietz, E. 1975. Chemical composition and physical properties of humic substances. Pages 1-211 *in* J. E. Gieseking, ed. Soil components. Vol. 1 Organic components. Springer-Verlag, New York, USA.

Fox, T. R. 1995. The influence of low-molecular weight organic acids on properties and processes in forest soils. Pages 43-62 *in* W. W. McFee, J. M. Kelly, eds. Carbon forms and functions in forest soils. Soil Science Society of America, Madison, WI, USA.

Francis, J. T. and Hitchcock, A. P. 1992. Inner-shell spectroscopy of para-benzoquinone, hydroquinone, and phenol - distinguising quinoid and benzoid structures. J. Phys. Chem. **96**: 6598-6610.

Furlani, G., Pagnanelli, F. and Toro, L. 2006. Reductive acid leaching of manganese dioxide with glucose: identification of oxidation derivatives of glucose. Hydromet. **81**: 234-240.

Galliano, H., Gas, G., Seris, J. L. and Boudet, A. M. 1991. Lignin degradation by *Rigidoporus lignosus* involves synergistic action of two oxidizing enzymes: Mn peroxidase and laccase. Enzyme Microb. Technol. **13**: 478-482.

Gan, D., Kotob, S. I. and Walia, D. S. 2007. Evaluation of a spectrometrophotometric method for practical and cost effective quantification of fulvic acid. Annals Environ. Sci. **1**: 11-15.

Garvie, L. A. J. and Buseck, P. R. 1998. Ratio of ferrous to ferric iron from nanometer-sized area in minerals. Nature **396**: 667-670.

Garvie, L. A. J. and Craven, A. J. 1994. High-resolution parallel electron energy-loss spectroscopy of Mn $L_{2,3}$-edges in inorganic manganese compounds. Phys. Chem. Miner. **21**: 191-206.

Gee, G. W. and Bauder, J. W. 1986. Particle size analysis. Pages 383-411 *in* A. Klute, ed. Methods of soil analysis Part 1. Physical and mineralogical methods. American Society of Agronomy and Soil Science Society of America, Madison, WI, USA.

Gianfreda, L. and Bollag, J.-M. 1994. Effects of soils on the behavior of immobilized enzymes. Soil Sci. Soc. Am. J. **58**: 1672-1681.

Gianfreda, L. and Rao, M. A. 2004. Potential of extracellular enzymes in remediation of polluted soils: a review. Enzyme Microb. Technol. **35**: 339-354.

Gilbert, B., Frazer, B. H., Belz, A., Conrad, P. G., Nealson, K. H., Haskel, D., Lang, J. C., Srajer, G. and Stasio, G. D. 2003. Multiple scattering calculations of bonding and X-ray absorption spectroscopy of manganese oxides. J. Phys. Chem. A. **107**: 2839-2847.

Glasby, G. P. and Schultz, H. D. 1999. E_H, pH diagrams for Mn, Fe, Co, Ni, Cu and As under seawater conditions: application of two new types of E_H, pH diagrams to the study of specific problems in marine geochemistry. Aq. Geochem. **5**: 227-248.

Gonzalez, J. M. and Laird, D. A. 2004. Role of smectites and Al-substituted goethites in the catalytic condensation of arginine and glucose. Clays Clay Miner. **52**: 443-450.

Gonzalez, J. M. and Laird, D. A. 2006. Smectite-catalyzed dehydration of glucose. Clays Clay Miner. **54**: 38-44.

Goodell, B., Jellison, J., Liu, J., Daniel, G., Paszczynski, A., Fekete, F., Krishnamurthy, S., Lu, L. and Xu, G. 1997. Low molecular weight chelators and phenolic compounds

isolated from wood decay fungi and their role in the fungal biodegradation of wood. J. Biotechnol. **53**: 133-162.

Gorbaty, M. L. and Kelemen, S. 2001. Characterization and reactivity of organically bound sulfur and nitrogen fossil fuels. Fuel Process. Technol. **71**: 71-78.

Gramss, G., Ziegenhagen, C. and Sorge, S. 1999. Degradation of soil humic extract by wood- and soil-associated fungi, bacteria and commercial enzymes. Microbial Ecol. **37**: 140-151.

Granit, T., Chen, Y. and Hadar, Y. 2007. Humic acids bleaching by white-rot fungi isolated from biosolids compost. Soil Biol. Biochem. **36**: 1040-1046.

Grush, M. M., Chen, J., Stemmler, T. L., George, S. J., Ralston, C. Y., Stibrany, R. T., Gelasco, A., Christou, G., Gorun, S. M., Penner-Hahn, J. E. and others. 1996. Manganese L-edge X-ray absorption spectroscopy of manganese catalase from *Lactobacillus plantarum* and mixed valence manganese complexes. J. Am. Chem. Soc. **118**: 65-69.

Guggenberger, G. and Haider, K. M. 2002. Effects of mineral colloids on biogeochemical cycling of C, N, P and S in soil. Pages 267-322 *in* P. M. Huang, J.-M. Bollag, N. Senesi, eds. Interactions between soil particles and microorganisms. Impact on the terrestrial ecosystem. John Wiley & Sons, Chichester, UK.

Haffenden, L. J. W. and Yaylayan, V. A. 2005. Mechanism of formation of redox-reactive hydroxylated benzenes and pyrazine in ^{13}C-labelled glycine/D-glucose model systems. J. Agric. Food Chem. **53**: 9742-9746.

Haider, K. M. 1992. Problems related to the humification processes in soils of temperate climates. Pages 55-94 *in* G. Stozky, J.-M. Bollag, eds. Soil biochemistry. Vol. 7. Marcel Dekker, New York, USA.

Haider, K. M. and Martin, J. P. 1981. Decomposition in soil of specifically ^{14}C-labelled model and cornstalk lignins and coniferylalcohol over two years as influenced by drying, rewetting, and additions of an available C substrate. Soil Biol. Biochem. **13**: 447-452.

Haider, K. M. and Martin, J. P. 1988. Mineralization of ^{14}C-labelled humic acids and of humic acid-bound ^{14}C-xenobiotics by *Phanerochaete chryosporium*. Soil Biol. Biochem. **20**: 425-429.

Haider, K. M., Martin, J. P. and Filip, Z. 1975. Humus biochemistry. Pages 195-244 *in* E. A. Paul, A. D. McLaren, eds. Soil biochemistry Vol. 4. Marcel Dekker, New York, USA.

Haider, K. M., Martin, J. P. and Rietz, E. 1977. Decomposition of ^{14}C-labelled coumaryl alcohols; free and linked to dehydropolymer and plant lignins and model humic acids. Soil. Sci. Soc. Am. J. **41**: 556-562.

Hamer, U., Marschner, B., Brodowski, S. and Amelung, W. 2004. Interactive priming of black carbon and glucose mineralization. Org. Geochem. **35**: 823-830.

Hammel, K. 1997. Fungal degradation of lignin. Pages 33-45 *in* G. Cadisch, K. E. Giller, eds. Driven by nature – plant litter quality and decomposition. CAB International, Wallingford, UK.

Hardie, A. G., Dynes, J. J., Kozak, L. M. and Huang, P. M. 2007. Influence of polyphenols on the integrated polyphenol-Maillard reaction humification pathway as catalyzed by birnessite. Ann. Environ. Sci. **1**: 91-110.

Hatcher, P. G., Schnitzer, M., Dennis, L. W. and Maciel, G. E. 1981. Aromaticity of humic substances in soils. Soil Sci. Soc. Am. J. **45**: 1089-1094.

Hatcher, P. G. and Spiker, E. C. 1988. Selective degradation of plant biomolecules. Pages 45-58 *in* F. H. Frimmel, R. F. Christman, eds. Humic substances and their role in the environment. New York, USA, Wiley-Interscience.

Hauser, E. A. and Legget, M. B. 1940. Color reactions between clays and amines. J. Am. Chem. Soc. **62**: 1811-1814.

Hayes, M. H. B. 1991. Concept of the origin, composition, and structure of humic substances. Pages 3-22 *in* W. S. Wilson, ed. Advances in soil organic matter research: The impact on agriculture and the environment. Royal Society of Chemistry, Cambridge, UK.

Hedges, J. I. 1978. The formation of clay mineral reactions of melanoidins. Geochim. Cosmochim. Acta **42**: 69-79.

Hidalgo, F. J. and Zamora, R. 2000. The role of lipids in nonenzymatic browning. Grasa Aceites **51**: 35-49.

Himmelwright, R. S., Eickman, N. C., LuBien, C. D., Lerch, K. and Solomon, E. I. 1980. Chemical and spectroscopic studies of the binuclear copper active site of Neurospora tyrosinase: comparison to hemocyanins. J. Am. Chem. Soc. **102**: 7339-7344.

Hitchcock, A. P. and Mancini, D. C. 2004. Gas-phase core excitation database (Online). Available: http://unicorn.mcmaster.ca/corex/cedb-title.html [January 17, 2008].

Hitchcock, A. P., Morin, C., Zhang, X., Araki, T., Dynes, J. J., Stover, H., Brash, J. L., Lawrence, J. R. and Leppard, G. G. 2005. Soft X-ray spectromicroscopy of biological and synthetic polymer systems. J. Electron Spectrosc. **144-147**: 259-269.

Ho, C.-T. 1996. Thermal generation of Maillard aromas. Pages 27-35 *in* R. Ikan, ed. The Maillard reaction. Consequences for the chemical and life sciences. John Wiley & Sons, Chichester, UK.

Hoffmann, M. R. 1980. Trace metal catalysis in aquatic environments. Environ. Sci. Technol. **14**: 1061-1066.

Hu, W.-G., Mao, J., Xing, B. and Schmitt-Rohr, K. 2000. Poly(methylene) crystallites in humic substances detected by nuclear magnetic resonance. Environ. Sci. Technol. **34**: 530-534.

Hu, Y. F., Xu, R. K., Dynes, J. J., Blyth, R. I. R., Yu, G., Kozak, L. M. and Huang, P. M. 2008. Coordination nature of aluminum (oxy)hydroxides formed under the influence of tannic acid studied by X-ray absorption spectroscopy. Geochim. Cosmochim. Acta **72**: 1959-1969.

Hu, Y. F., Zuin, L., Reininger, R. and Sham, T. K. 2007. VLS-PGM beamline at the Canadian Light Source. AIP Conference Proceedings **879**: 535-538.

Huang, P. M. 1990. Role of soil minerals in transformation of natural organics and xenbiotics in soil. Pages 29-115 *in* J.-M. Bollag, G. Stozky, eds. Soil biochemistry Vol. 6. Marcel Dekker, New York, USA.

Huang, P. M. 2000. Abiotic catalysis. Pages B302-B332 *in* M. E. Sumner, ed. Handbook of soil science. CRC Press, Boca Raton, FL, USA.

Huang, P. M. 2004. Soil mineral-organic matter-microorganism interactions: Fundamentals and impacts. Adv. Agron. **82**: 391-472.

Huang, P. M., Wang, M. K. and Chiu, C. Y. 2005. Soil mineral-organic matter-microbe interactions: Impacts on biogeochemical processes and biodiversity in soils. Pedobiologia **49**: 609-635.

Huang, P. M., Wang, M. K., Kämpf, N. and Schultz, D. G. 2002. Aluminum hydroxides. Pages 261-289 *in* J. B. Dixon, D. G. Schultz, eds. Soil mineralogy with environmental applications. Soil Science Society of America, Madison, WI, USA.

Huang, P. M., Wang, T. S. C., Wang, M. K., Wu, M. H. and Hsu, N. W. 1977. Retention of phenolic acids on noncrystalline hydroxy-aluminum and -iron compounds and clay minerals of soils. Soil Sci. **123**: 213-219.

Hueey, J. E. 1983. Inorganic chemistry. Principles of structure and reactivity. Harper International SI Edition, London, UK.

Ibrahim, M., Alaam, M., El-Haes, H., Jalbout, A. F. and de Leon, A. 2006. Analysis of the structure and vibrational spectra of glucose and fructose. Eclet. Quím. **31**: 15-21.

Ikan, R., Rubinsztain, Y., Nissenbaum, A. and Kaplan, I. R. 1996. Geochemical aspects of the Maillard reaction. Pages 1-25 *in* R. Ikan, ed. The Maillard reaction: Consequences for the chemical and life sciences. John Wiley & Sons, Chichester, UK.

Ildefonse, P., Cabaret, D., Sainctavit, P., Calas, G., Flank, A.-M. and Lagarde, P. 1998. Aluminum X-ray absorption near edge structure in model compounds and earth's surface minerals. Phys. Chem. Miner. **25**: 112-121.

International Centre for Diffraction Data. 2006. Powder diffraction file: Organic and organometallic phases search manual for experimental patterns. JCPDS - International Centre for Diffraction Data, Newton Square.

IUSS Working Group WRB. 2006. World reference base for soil resources 2006. FAO, Rome, Italy.

Jackson, M. L., Lim, C. H. and Zelazny, L. W. 1986. Oxides, hydroxides and aluminosilicates. Pages Pages 101-150 *in* A. Klute, ed. Methods of soil analysis Part 1. Physical and mineralogical methods. American Society of Agronomy, Madison, WI, USA.

Joint Committee on Powder Diffraction Standards. 1974. Selected powder diffraction data for minerals search manual. Joint Committee on Powder Diffraction Standards, Philadelphia, PA, USA.

Jokic, A., Frenkel, A. I. and Huang, P. M. 2001a. Effect of light on birnessite catalysis of the Maillard reaction and its implication in humification. Can. J. Soil Sci. **81**: 277-283.

Jokic, A., Frenkel, A. I., Vairavamurthy, M. A. and Huang, P. M. 2001b. Birnessite catalysis of the Maillard reaction: Its significance in natural humification. Geophys. Res. Lett. **28**: 3899-3902.

Jokic, A., Schulten, H.-R., Cutler, J. N., Schnitzer, M. and Huang, P. M. 2004a. A significant abiotic pathway for the formation of unknown nitrogen in nature. Geophys. Res. Lett. **31**(L05502): 1-4.

Jokic, A., Schulten, H.-R., Cutler, J. N., Schnitzer, M. and Huang, P. M. 2005. Catalysis of the Maillard reaction by δ-MnO_2: A significant abiotic sorptive condensation pathway for the formation of refractory N-containing biogeomacromolecules in nature. Pages 127-152 *in* P. M. Huang, A. Violante, J.-M. Bollag, P. Vityakon, eds. Soil abiotic and biotic interactions and impact on the ecosystem and human welfare. Science Publishers Inc., Enfield, USA.

Jokic, A., Wang, M. C., Liu, C., Frenkel, A. I. and Huang, P. M. 2004b. Integration of the polyphenol and Maillard reactions into a unified abiotic pathway for humification in nature: The role of δ-MnO_2. Org. Geochem. **35**: 747-762.

Jokic, A., Zimpel, Z., Huang, P. M. and Mezey, P. G. 2001c. Molecular shape analysis of a Maillard reaction intermediate. SAR and QSAR Environ. Res. **12**: 297-307.

Jury, W. A., Gardener, W. R. and Gardener, W. H. 1991. Soil physics. 5 ed. John Wiley & Sons, New York, USA.

Kalbitz, K., Schmerwitz, J., Schwesig, D. and Matzner, E. 2003. Biodegradation of soil-derived dissolved organic matter as related to its properties. Geoderma **113**: 273-291.

Kassim, G., Martin, J. P. and Haider, K. M. 1981. Incorporation of a wide variety of organic substrate carbons into soil biomass as estimated by the fumigation procedure. Soil Sci. Soc. Am. J. **45**: 1106-1112.

Kelleher, B. P. and Simpson, A. J. 2006. Humic substances in soils: Are they really chemically distinct? . Environ. Sci. Technol. **40**: 4605-4611.

Kiem, R. and Kögel-Knabner, I. 2003. Contribution of lignin and polysaccharides to the refractory carbon pool in C-depleted arable soils. Soil Biol. Biochem. **35**: 101-118.

Kirk, T. K. and Farrell, R. L. 1987. Enzymatic combustion - the microbial-degradation of lignin. Annu. Rev. Microbiol. **41**: 465-505.

Knicker, H. 2004. Stabilization of N-compounds in soil and organic-matter-rich sediments – what is the difference? Marine Chem. **92**: 167-195.

Knicker, H., González-Vila, F. J., Polvillo, O., González, J. A. and Almendros, G. 2005. Fire-induced transformation of C- and N-forms in different organic soil fractions from a Dystric Cambisol under a Mediterranean pine forest (*Pinus pinaster*). Soil Biol. Biochem. **37**: 701–718.

Knicker, H. and Lüdemann, H.-D. 1995. N-15 and C-13 CPMAS and solution NMR of N-15 enriched plant material during 600 days of microbial degradation. Org. Geochem. **23**: 329-341.

Knollenberg, R. W., Merritt, R. W. and Lawson, D. L. 1985. Consumption of leaf litter by *Lumbricus terrestris* (Oligochaeta) in a Michigan woodland floodplain. Am. Midl. Nat. **113**: 1-6.

Koenigs, J. W. 1974. Fungal production of hydrogen peroxide in wood. Arch. Microbiol. **99**: 129-145.

Kögel-Knabner, I. 2002. The macromolecular organic composition of plant and microbial residues as inputs to soil organic matter. Soil Biol. Biochem. **34**: 139-162.

Kögel-Knabner, I., Guggenberger, G., Kleber, M., Kandeler, E., Kalbitz, K., Scheu, S., Esterhues, K. and Leinweber, P. 2008. Organo-mineral associations in temperate soils: Integrating biology, mineralogy, and organic matter chemistry. J. Plant Nutr. Soil Sci. **171**: 61-82.

Koivula, N. and Hanninen, K. 2001. Concentrations of monosaccharides in humic substances in early stages of humification. Chemosphere **44**: 271-279.

Kosterov, A., Federichs, T. and von Dobeneck, T. 2006. Low-temperature magnetic properties of rhodochrosite ($MnCO_3$). Phys. Earth Planet. Inter. **154**: 234-242.

Kumada, K. and Kato, H. 1970. Browning of pyrogallol as affected by clay minerals. Soil Sci. Plant Nutr. **16**: 195-200.

Kyuma, K. and Kawaguchi, K. 1964. Oxidative changes of polyphenols as influenced by allophone. Soil Sci. Soc. Am. Proc. **28**: 371-374.

La Force, M. J., Hansel, C. M. and Fendorf, S. 2002. Seasonal transformations of manganese in a palustrine emergent wetland. Soil Sci. Soc. Am. J. **66**: 1377-1389.

Ladd, J. N. and Butler, J. H. A. 1975. Humus-enzyme systems and synthetic, organic polymer-enzyme analogs. Pages 143-194 *in* E. A. Paul, A. D. McLaren, eds. Soil biochemistry, Vol. 4. Marcel Dekker, New York, USA.

Lee, J. S. K. and Huang, P. M. 1995. Photochemical effect on the abiotic transformation of polyphenols as catalyzed by Mn(IV) oxide. Pages 177-189 *in* P. M. Huang, J. Berthelin, J.-M. Bollag, W. B. McGill, A. L. Page, eds. Environmental impact of soil component interactions. Vol 1. Natural and anthropogenic organics. Lewis Publishers, Boca Raton, FL, USA.

Lehmann, J., Kinyangi, J. and Solomon, D. 2007. Organic matter stabilization in soil microaggregates: implications from spatial heterogeneity of organic carbon contents and carbon forms. Biogeochem. **85**: 45-57.

Leinweber, P., Kruse, J., Walley, F. L., Gillespie, A., Eckhardt, K. U., Blyth, R. I. R. and Regier, T. 2007. Nitrogen K-edge XANES - An overview of reference compounds used to identify 'unknown' organic nitrogen in environmental samples. J. Synchrotron Radiation **14**: 500-511.

Leonowicz, A., Cho, N.-S., Luterek, J., Wilkolazka, A., Wojtas-Wasilewska, M., Matuszewska, A., Hofrichter, M., Wesenberg, D. and Rogalski, J. 2001. Fungal laccase: properties and activity on lignin. J. Basic Microbiol. **41**: 185-227.

Leschine, S. B. 1995. Cellulose degradation in anaerobic environments. Annu. Rev. Microbiol. **49**: 339-426.

Lindsay, W. L. 1979. Chemical equilibria in soils. John Wiley & Sons, New York, USA.

Liu, C. and Huang, P. M. 2000. Catalytic effects of hydroxyl-aluminum and silicic acid on catechol humification. Pages 37-51 *in* E. Ghabbour, G. Davies, eds. Humic substances: Versatile components of plants, soil and water. Royal Society of Chemistry, Cambridge, UK.

Liu, C. and Huang, P. M. 2001. The influence of catechol humification on surface properties of metal oxides. Pages 253-270 *in* E. A. Ghabbour, G. Davies, eds. Humic substances: Structure, models and functions. Royal Chemical Society, Cambridge, UK.

Liu, C. and Huang, P. M. 2002. Role of hydroxyl-aluminosilicate ions (proto-imogolite soil) in the formation of humic substances. Org. Geochem. **33**: 295-305.

Lopez, M. J., Vargas-Garcia, M. C., Suárez-Estrella, F. and Moreno, J. 2006. Biodelignification and humification of horticultural plant residues by fungi. Intl. Biodeter. Biodegrad. **57**: 24-30.

Lourvanij, K. and Rorrer, G. L. 1994. Dehydration of glucose to organic acids in microporous pillared clay catalysts. Appl. Catalys. A. **109**: 147-165.

Lu, Y. and Pignatello, J. J. 2002. Determination of the "conditioning effect" in soil organic matter in support of a pore deformation mechanism for sorption hysteresis. Environ. Sci. Technol. **36**: 4553-4561.

Lu, Y. and Pignatello, J. J. 2004. Sorption of apolar aromatic compounds to soil humic acid particles affected by aluminum (III) ion cross-linking. J. Environ. Qual. **33**: 1314-1321.

MacCarthy, P. 2001. The principles of humic substances. Soil Sci. **166**: 738-751.

Maillard, L. C. 1913. Formation de matières humiques par action de polypeptides sur sucres. C.R. Acad. Sci. **156**: 148-149.

Majecher, E. M., Chorover, J., Bollag, J.-M. and Huang, P. M. 2000. Evolution of CO_2 during birnessite-induced oxidation of ^{14}C-labeled catechol. Soil Sci. Soc. Am. J. **64**: 157-163.

Martell, A. E. and Smith, R. M. 2004. NIST standard reference database 46. NIST critically selected stability constants of metal complexes National Institute of Standards and Technology, Gaithersburg, MD, USA.

Marthur, S. P. and Schnitzer, M. 1978. A chemical and spectroscopic characterization of some synthetic analogues of humic acid. Soil Sci. Soc. Am. J. **42**: 591-596.
Martin, J. P. and Haider, K. 1971. Microbial activity in relation to soil humus formation. Soil Sci. **111**: 54-63.
Martin, J. P. and Haider, K. M. 1980. A comparison of the use of phenolase and peroxidase for the synthesis of model humic acid-type polymers. Soil Sci. Soc. Am. J. **44**: 983-988.
Martínez, A. T. 2002. Molecular biology and structure-function of lignin-degrading heme peroxidases. Enzyme Microb. Technol. **30**: 425-444.
Martínez, A. T., Speranza, M., Ruiz-Dueñas, F. J., Ferreira, P., Camarero, S., Guillén, F., Martínez, M. J., Gutiérrez, A. and del Río, J. C. 2005. Biodegradation of lignocellulosics: microbial, chemical, and enzymatic aspects of the fungal attack of lignin. Int. Microbiol. **8**: 195-204.
Matocha, C. J., Sparks, D. L., Amonette, J. E. and Kukkadapu, R. K. 2001. Kinetics and mechanisms of birnessite reduction by catechol. Soil Sci. Soc. Am. J. **65**: 58-66.
Maurice, P. A. 1998. Atomic force microscopy as a tool for studying the reactivities of environmental particles. Pages Pages 57-66 *in* D. L. Sparks, T. J. Grundl, eds. Mineral-water interfacial interactions. American Chemical Society, Washington, DC, USA.
McBride, M. B. 1987. Adsorption and oxidation of phenolic compounds by iron and manganese oxides. Soil Sci. Soc. Am. J. **51**: 1466-1472.
McBride, M. B. 1989. Oxidation of 1,2- and 1,4-dihydroxybenzenes in aerated aqueous suspensions of birnessite. Clays Clay Miner. **37**: 470-486.
McBride, M. B. 1994. Environmental chemistry of soils. Oxford University Press, London, UK.
McKenzie, R. M. 1971. The synthesis of birnessite, cryptomelane, and some other oxides and hydroxides of manganese. Mineral. Magazine **38**: 493-502.
McKenzie, R. M. 1989. Manganese oxides and hydroxides. Pages 439-465 *in* J. B. Dixon, S. B. Weed, eds. Minerals in soil environments. Soil Science Society of America, Madison, WI, USA.
McLean, J. S., Lee, J.-U. and Beverige, T. L. 2002. Interactions of bacteria and environmental metals, fine-grained mineral development and bioremediation strategies. Pages 227-261 *in* P. M. Huang, J.-M. Bollag, N. Senesi, eds. Interactions between soil particles and microorganisms. Impact on the terrestrial ecosystem. John Wiley & Sons, Chichester, UK.
McNaught, A. D. and Wilkison, A. 1997. Compendium of chemical terminology. IUPAC recommendation. Blackwell Science, Oxford, UK.
Melillo, J. M., Aber, J. D., Linkins, A. E., Ricca, A., Fry, B. and Nadelhoffer, K. J. 1989. Carbon and nitrogen dynamics along the decay continuum: plant litter to soil organic matter. Plant Soil **115**: 189-198.
Mikutta, R., Kleber, M. and Jahn, R. 2005. Poorly crystalline minerals protect organic carbon in clay subfractions from acid subsoil horizons. Geoderma **128**: 106-115.
Mikutta, R., Kleber, M., Torn, M. S. and Jahn, R. 2006. Stabilization of soil organic matter: association with minerals or chemical recalcitrance? Biogeochem. **77**: 25-56.
Mikutta, R., Mikutta, C., Kalbitz, K., Scheel, T., Kaiser, K. and Reinhold, R. 2007. Biodegradation of forest floor organic matter bound to minerals via different binding mechanisms. Geochim. Cosmochim. Acta **71**: 2569-2590.

Mitra-Kirtley, S., Mullins, O. C., Branthauer, J. F. and Cramer, S. P. 1993. Determination of the nitrogen chemical structures in petroleum asphaltenes using XANES spectroscopy. J. Am. Chem. Soc. **115**: 252-258.

Moore, J. W. and Pearson, R. G. 1981. Kinetics and mechanisms. John Wiley & Sons, New York, USA.

Mortland, M. M. and Halloran, L. J. 1976. Polymerization of aromatic molecules on smectites. Soil Sci. Soc. Am. J. **40**: 367-370.

Muscolo, A. and Sidari, M. 2006. Seasonal fluctuations in soil phenolics of a coniferous forest: effects on seed germination of different coniferous species. Plant Soil **284**: 305-318.

Myneni, S. C. B. 2002. Soft X-ray spectroscopy and spectromicroscopy studies of organic molecules in the environment. Pages Pages 485-558 *in* P. A. Fenter, M. L. Rivers, N. C. Sturchio, S. R. Sutton, eds. Applications of synchrotron radiation in low-temperature geochemistry and environmental sciences. Mineralogical Society of America, Washington, DC, USA.

Nadelhoffer, K. J. and Fry, B. 1988. Controls on natural N-15 and C-13 abundances in forest soil organic matter. Soil Sci. Soc. Am. J. **52**: 1633-1640.

Naidja, A. and Huang, P. M. 2002. Significance of the Henri-Michaelis-Menten theory in abiotic catalysis: catechol oxidation by δ-MnO_2. Surface Sci. **506**: L243-L249.

Naidja, A., Huang, P. M. and Bollag, J.-M. 1997. Activity of tyrosinase immobilized on hydroxyaluminum-montmorillonite complexes. J. Mol. Catal. **115**: 305-316.

Naidja, A., Huang, P. M. and Bollag, J.-M. 1998. Comparison of the reaction products from the transformation of catechol catalyzed by birnessite or tyrosinase. Soil Sci. Soc. Am. J. **62**: 188-195.

Naidja, A., Huang, P. M. and Bollag, J.-M. 2000. Enzyme-clay interactions and their impact on transformations of natural and anthropogenic organic compounds in soil. J. Environ. Qual. **29**: 677-691.

Naidja, A., Huang, P. M., Dec, J. and Bollag, J.-M. 1999. Kinetics of catechol oxidation catalyzed by tyrosinase or δ-MnO_2. Pages 181-188 *in* J. Berthelin, P. M. Huang, J.-M. Bollag, F. Andreux, eds. Effect of mineral-organic-microorganism interactions on soil and freshwater environments. Kluwer Academic/Plenum Publishers, New York, USA.

Naidja, A., Liu, C. and Huang, P. M. 2002. Formation of protein-birnessite complex: XRD, FTIR, and AFM analysis. J. Coll. Interface Sci. **251**: 46-56.

Nyquist, R. A. and Kagel, R. O. 1971. Infrared spectra of inorganic compounds. Academic Press Inc., Orlando, FL, USA.

O'Brien, B. J. and Stout, J. D. 1978. Movement and turnover of soil organic matter as indicated by carbon isotope measurements. Soil Biol. Biochem. **10**: 309-317.

Oades, J. M. 1988. The retention of organic matter in soils. Biogeochem. **5**: 35-70.

Okita, P. M., Maynard, J. B., Spiker, E. C. and Force, E. R. 1988. Isotopic evidence for organic matter oxidation by manganese reduction in the formation of stratiform manganese carbonate ore. Geochim. Cosmochim. Acta **52**: 2679-2685.

Ostrofsky, A., Jellison, J., Smith, K. T. and Shortle, W. C. 1997. Changes in cation concentrations in red spruce wood decayed by brown rot and white rot fungi. Can. J. Forest Res. **27**: 567-571.

Pal, S., Bollag, J.-M. and Huang, P. M. 1994. Role of abiotic and biotic catalysts in the transformation of phenolic compounds through oxidative coupling reactions. Soil Biol. Biochem. **26**: 813-820.

Park, J.-W., Dec, J., Kim, J.-E. and Bollag, J.-M. 1999. Effect of humic constituents on the transformation of chlorinated phenols and anilines in the presence of oxidoreductive enzymes or birnessite. Environ. Sci. Technol. **33**: 2028-2034.

Park, J. W., Dec, J., Kim, J. E. and Bollag, J.-M. 2000. Dehalogenation of xenobiotics as a consequence of binding to humic materials. Arch. Environ. Contam. Toxicol. **38**: 405-410.

Paszczynski, A., Crawford, R., Funk, D. and Goodell, B. 1999. De novo synthesis of 4,5-dimethoxycatechol and 2,5-dimethoxyhydroquinone by the brown rot fungus *Gloeophyllum trabeum*. Appl. Environ. Microbiol. **65**: 674-679.

Percival, H. J., Parfitt, R. L. and Scott, N. A. 2000. Factors controlling soil carbon levels in New Zealand grasslands: Is clay content important? Soil Sci. Soc. Am. J. **64**: 1623-1630.

Pérez, J., Munoz-Dorado, J., de la Rubia, T. and Martínez, J. 2002. Biodegradation and biological treatments of cellulose, hemicellulose and lignin: an overview. Int. Microbiol. **5**: 53-63.

Perry, D. L. and Phillips, S. L. 1995. Handbook of inorganic compounds. CRC Press, Boca Raton, FL, USA.

Piccolo, A. 2001. The supramolecular structure of humic substances. Soil Sci. **166**: 810-832.

Pinnavais, T. J., Hall, P. L., Cady, S. S. and Mortland, M. M. 1974. Aromatic radical cation formation on the intracrystal surfaces of transition metal layer silicates. J. Phys. Chem. **78**: 994-999.

Pohlman, A. A. and McColl, J. G. 1989. Organic oxidation and manganese and aluminum mobilization in forest soils. Soil Sci. Soc. Am. J. **53**: 686-690.

Poirer, N., Derenne, S., Balesdent, J., Chenu, C., Bardoux, G., Mariotti, A. and Largeau, C. 2006. Dynamics and origin of the non-hydrolysable organic fraction in a forest and a cultivated temperate soil, as determined by isotopic and microscopic studies. Eur. J. Soil Sci. **57**: 719-730.

Poirer, N., Derenne, S., Balesdent, J., Rouzaud, J.-N., Mariotti, A. and Largeau, C. 2000. Chemical structure and sources of the macromolecular, resistant, organic fraction isolated from a forest soil (Lacadec, Southwest France). Org. Geochem. **31**: 813-827.

Poirer, N., Derenne, S., Balesdent, J., Rouzaud, J.-N., Mariotti, A. and Largeau, C. 2002. Abundance and composition of the refractory organic fraction of an ancient, tropical soil (Poine Noire, Congo). Org. Geochem. **33**: 383-391.

Pollack, S. S., Lentz, H. and Ziechmann, W. 1971. X-ray diffraction study of humic acids. Soil Sci. **112**: 318-324.

Ponomarenko, E. V. and Anderson, D. W. 2001. Importance of charred organic matter in Black Chernozem soils of Saskatchewan. Can. J. Soil Sci. **81**: 281-297.

Porterfield, W. W. 1983. Inorganic Chemistry. A Unified Approach. Harper International SI Edition, London, UK.

Potter, R. M. and Rossman, G. R. 1979. The tetravalent manganese oxides: Identification, hydration, and structural relationships by infrared spectroscopy. Am. Mineral. **64**: 1199-1218.

Preston, C. M., Rauthan, B. S., Rodger, C. and Ripmeester, J. A. 1982. A hydrogen-1, carbon-13, and nitrogen-15 nuclear magnetic resonance study of p-benzoquinone polymers incorporating amino nitrogen compounds ("synthetic humic acid"). Soil Sci. **134**: 277-293.

Preston, C. M. and Schmidt, M. W. I. 2006. Black (pyrogenic) carbon: a synthesis of current knowledge and uncertainties with special consideration of boreal regions. Biogeosci. **3**: 397-420.

Preston, C. M., Trofymow, J. A. and Flanagan, L. B. 2006. Decomposition, ^{13}C, and the "lignin paradox". Can. J. Soil Sci. **86**: 235-245.

Quénéa, K., Derenne, S., Largeau, C., Rumpel, C. and Mariotti, A. 2006a. Influence of change in land use on the refractory organic macromolecular fraction of a sandy spodosol (Landes de Gascogne, France). Geoderma **136**: 136-151.

Quénéa, K., Largeau, C., Derenne, S., Spaccini, R., Bardoux, G. and Mariotti, A. 2006b. Molecular and isotopic study of lipids in particle size fractions of a sandy cultivated soil (Cestas cultivation sequence, southwest France): Sources, degradation, and comparison with Cestas forest soil. Org. Geochem. **37**: 20-44.

Rasmussen, C., Torn, M. S. and Southard, R. J. 2005. Mineral assemblage and aggregation control carbon dynamics in a Californian conifer forest. Soil Sci. Soc. Am. J. **69**: 1711-1721.

Rasse, D. P., Dignac, M.-F., Bahri, H., Rumpel, C., Mariotti, A. and Chenu, C. 2006. Lignin turnover in an agricultural field: from plant residues to soil-protected fractions. Eur. J. Soil Sci. **57**: 530-538.

Regier, T., Paulsen, J., Wright, G., Coulthard, I., Tan, K., Sham, T. K. and Blyth, R. I. R. 2007. Commisioning of the spherical grating monochromator soft X-ray spectroscopy beamline at the Canadian Light Source. AIP Conference Proceedings **879**: 473-476.

Rice, J. A. 2001. Humin. Soil Sci. **166**: 848-857.

Ross, S. 1989. Soil Processes. A Systematic Approach. Routledge, London, UK.

Rouet-Mayer, M.-S., Ralambosoa, J. and Philippon, J. 1990. Roles of *o*-quinones and their polymers in the enzymic browning of apples. Phytochem. **29**: 435-440.

Ruggiero, P. and Radogna, V. M. 1988. Humic acids-tyrosinase interactions as a model of humic-enzyme complexes. Soil Biol. Biochem. **20**: 353-359.

Ruggiero, P., Sarkar, J. M. and Bollag, J.-M. 1989. Detoxification of 2,4-dichlorophenol by a laccase immobilized on soil and clay. Soil Sci. **147**: 361-370.

Rumpel, C., Alexis, M., Chabbi, A., Chaplot, V., Rasse, D. P., Valentin, C. and Mariotti, A. 2006. Black carbon contribution to soil organic matter composition in tropical sloping land under slash and burn agriculture.

Schaumann, G. E. 2006a. Review article. Soil organic matter beyond molecular structure. Part I: Macromolecular and supramolecular characteristics. J. Plant Nutr. Soil Sci. **169**: 145-156.

Schaumann, G. E. 2006b. Review article. Soil organic matter beyond molecular structure. Part II: Amorphous nature and physical aging. J. Plant Nutr. Soil Sci. **169**: 157-167.

Scheffer, F., Meyer, B. and Niederbudde, E. A. 1959. Huminstoffbildung unter katalytischer Einwirkung natürlich vorkommender Eisenverbindungen im Modelversuch. Zeit. Pflanzenern. Dueng. Bodenk. **87**: 26-44.

Schlesinger, W. H. 1990. Evidence from chronosequence studies for a low carbon-storage potential of soils. Nature **348**: 232-234.

Schmidt, M. W. I., Skjemstad, J. O. and Jäger, C. 2002. Carbon isotope geochemistry and nanomorphology of soil black carbon: Black chernozemic soils in central Europe originate from ancient biomass burning. Global Biogeochem. Cycles **16** Article no. 1123.

Schnitzer, M. 1977. Recent findings on the characterization of humic substances extracted from soils from widely differing climatic zones. Pages 77-101 Proceedings of the symposium on soil organic matter studies II. IAEA Bulletin, Vienna, Austria.

Schnitzer, M. 1978. Humic substances: chemistry and reactions. Pages 1-64 *in* M. Schnitzer, S. U. Khan, eds. Soil organic matter. Elsevier, Amsterdam, The Netherlands.

Schnitzer, M. 1986. Binding of humic substances by soil minerals. Pages 77-101 *in* P. M. Huang, M. Schnitzer, eds. Interactions of soil minerals with natural organics and microbes. Soil Science Society of America, Madison, WI, USA.

Schulten, H.-R. 2002. New approaches to the molecular structure and properties of soil organic matter: Humic-, xenobiotic-, biological-, and mineral-bonds. Pages 351-381 *in* A. Violante, P. M. Huang, J.-M. Bollag, L. Gianfreda, eds. Soil mineral-organic matter-microorganism interactions and ecosystem health. Elsevier, Amsterdam, The Netherlands.

Shindo, H. 1992. Relative effectiveness of short-range ordered Mn(IV), Fe(III), Al and Si oxides in the synthesis of humic acids from phenolic compounds. Soil Sci. Plant Nutr. **38**: 459-465.

Shindo, H., Honna, T., Yamamoto, S. and Honma, H. 2004. Contribution of charred plant fragments to soil organic carbon in Japanese volcanic ash soils containing black humic acids. Org. Geochem. **35**: 235–241.

Shindo, H. and Huang, P. M. 1982. Role of Mn(IV) oxide in abiotic formation of humic substances in the environment. Nature **298**: 363-365.

Shindo, H. and Huang, P. M. 1984a. Catalytic effects of manganese(IV), iron(III), aluminium, and silicon oxides on the formation of phenolic polymers. Soil Sci. Soc. Am. J. **48**: 927-934.

Shindo, H. and Huang, P. M. 1984b. Significance of Mn(IV) oxide in abiotic formation of organic nitrogen complexes in natural environments. Nature **308**: 57-58.

Shindo, H. and Huang, P. M. 1985a. Catalytic polymerization of hydroquinone by primary minerals. Soil Sci. **505-511**.

Shindo, H. and Huang, P. M. 1985b. The catalytic power of inorganic components in the abiotic synthesis of hydroquinone-derived humic polymers. Appl. Clay Sci. **1**: 71-81.

Shindo, H. and Huang, P. M. 1992. Comparison of the influence of Mn(IV) oxide and tyrosinase on the formation of humic substances in the environment. Sci. Total Environ. **117/118**: 103-110.

Shindo, H., Yoshida, M., Yamamoto, A., Honma, H. and Hiradate, S. 2005. $\delta^{13}C$ values of organic constituents in Japanese volcanic ash soils. Soil Sci. **170**: 175-182.

Silverstein, R. M., Webster, F. X. and Kiemle, D. 2004. Spectrometric identification of organic compounds. John Wiley & Sons, New York, USA.

Simpson, A. J. 2002. Determining the molecular weight, aggregation, structures and interactions of natural organic matter using diffusion ordered spectroscopy. Magnet. Resonan. Chem. **40**: S72-S82.

Simpson, A. J., Burdon, J., Graham, C. L., Hayes, M. H. B., Spencer, N. and Kingery, W. L. 2001. Interpretation of heteronuclear and multidimensional NMR spectroscopy of humic substances. Eur. J. Soil Sci. **52**: 495-509.

Simpson, A. J., Kingery, W. L. and Hatcher, P. G. 2003. The identification of plant derived structures in humic materials using 3-dimensional NMR spectroscopy. Environ. Sci. Technol. **37**: 337-342.

Six, J., Callewaert, P., Lenders, S., De Gryze, S., Morris, S. J., Gregorich, E. G. and Paul, E. A. 2002. Measuring and understanding carbon storage in afforested soils by physical fractionation. Soil Sci. Soc. Am. J. **66**: 1981-1987.

Sjoblad, R. D. and Bollag, J.-M. 1981. Oxidative coupling or aromatic compounds by enzymes from soil microorganisms. Pages 113-125 *in* E. A. Paul, J. N. Ladd, eds. Soil biochemistry, Vol. 5. Marcel Dekker, New York, USA.

Skjemstad, J. O., Clarke, P., Taylor, J. A., Oades, J. M. and McClure, S. G. 1996. The chemistry and nature of protected carbon in soil. Aus. J. Soil Res. **34**: 251-271.

Smernik, R. J. and Baldock, J. A. 2005. Does solid-state ^{15}N NMR spectroscopy detect all soil organic matter nitrogen? . Biogeochem. **75**: 507-528.

Smith, M. B. and March, J. 2001. March's advanced organic chemistry reactions, mechanisms, and structure. John Wiley & Sons, New York, USA.

Soil Survey Staff. 1999. Soil Taxonomy. United States Department of Agriculture, Washington, DC, USA.

Solomon, D. H. 1968. Clay minerals as electron acceptors and/or electron donors in organic reactions. Clays Clay Mineral. **16**: 31-39.

Solomon, D. H. and Hawthorne, D. G. 1983. Chemistry of pigments and fillers. John Wiley & Sons, New York, USA.

Spaccini, R., Piccolo, A., Conte, P., Haberhauer, G. and Gerzabek, M. H. 2002. Increased soil carbon sequestration through hydrophobic protection by humic substances. Soil Biol. Biochem. **34**: 1839-1851.

Sparks, D. L. 2003. Environmental soil chemistry. Academic Press, San Diego, CA, USA.

Steed, J. W. and Atwood, J. L. 2000. Supramolecular chemistry: A concise introduction. John Wiley & Sons, Chichester, UK.

Steelink, C. 1994. Application of N-15 NMR spectroscopy to the study of organic nitrogen and humic substances in the soil. Pages 405-427 *in* N. Senesi, D. Miano, eds. Humic substances in the global environment. Elsevier, Amsterdam, The Netherlands.

Steffen, K. T., Hattaka, A. and Hofrichter, M. 2002. Degradation of humic acids by the litter-decomposing basidomycete *Collybia dryophila*. Appl. Environ. Microbiol. **68**: 3442-3448.

Sternbeck, J. 1997. Kinetics of rhodochrosite crystal growth at 25° C: The role of surface speciation. Geochim. Cosmochim. Acta **61**: 785-793.

Stevenson, F. J. 1994. Humus chemistry: Genesis, composition, reactions. John Wiley & Sons, New York, USA.

Stevenson, F. J. and Schnitzer, M. 1982. Transmission electron microscopy of extracted fulvic and humic acids. Soil Sci. **133**: 179-185.

Stone, A. T. 1987. Reductive dissolution of manganeses (III/IV) oxides by substituted phenols. Environ. Sci. Technol. **21**: 979-988.

Stone, A. T. and Morgan, J. J. 1984a. Reduction and dissolution of manganese(III) and manganese(IV) oxides by organics. 1. Reaction with hydroquinone. Environ. Sci. Technol. **18**: 450-456.

Stone, A. T. and Morgan, J. J. 1984b. Reduction and dissolution of manganese(III) and manganese(IV) oxides by organics. 2. Survey of the reactivity of organics. Environ. Sci. Technol. **18**: 617-624.

Sutton, R. and Sposito, G. 2005. Molecular structure in soil humic substances: the new view. Environ. Sci. Technol. **39**: 9009-9014.

Swift, R. S. 1996. Organic matter characterization. Pages 1018-1020 *in* D. L. Sparks, ed. Methods of soil analysis. Part 3. Chemical methods. Soil Science Society of America, Madison, WI, USA.

Telysheva, G., Dobele, G., Meier, D., Dizhbite, T., Rossinka, G. and Jurkjane, V. 2007. Characterization of the transformation of lignocellulosic structures upon degradation in planted soil. J. Anal. Appl. Pyrolysis **79**: 52-60.

ten Have, R. and Theunissen, T. M. J. 2001. Oxidative mechanisms involved in lignin degradation by white-rot fungi. Chem. Rev. **101**: 3397-3413.

Thompson, T. D. and Moll, J. F. 1973. Oxidative power of smectites measured by hydroquinone. Clays Clay Miner. **21**: 337-350.

Tietjen, T. and Wetzel, R. G. 2003. Extracellular enzyme-clay mineral complexes: Enzyme adsorption, alteration of enzyme activity, and protection from photodegradation. Aq. Ecology **37**: 331-339.

Torn, M. S., Trumbore, S. E., Chadwick, O. A., Vitousek, P. M. and Hendriks, D. M. 1997. Mineral control of soil organic carbon storage and turnover. Nature **238**: 170-173.

Torres, E., Bustos-Jaimes, I. and Le Borgne, S. 2003. Potential use of oxidative enzymes for the detoxification of organic pollutants. Appl. Catalys. B. **46**: 1-15.

Tuomela, M., Oivanen, P. and Hatakka, A. 2002. Degradation of synthetic ^{14}C-lignin by various white-rot fungi in soil. Soil Biol. Biochem. **34**: 1613-1620.

Twigg, M. V. 1989. Catalyst handbook. Wolfe Publishing Ltd., London, UK.

Urquhart, S. G. and Ade, H. 2002. Trends in the carbonyl core (C 1S, O 1S) → π*C=O transition in the near-edge X-ray absorption fine structure spectra of organic molecules. J. Phys. Chem. B **106**: 8531-8538.

Vairavamurthy, A. and Wang, S. 2002. Organic nitrogen in geomacromolecules: insights on speciation and transformation with K-edge XANES spectroscopy. Environ. Sci. Tech. **36**: 3050-3056.

van Cappellen, P. and Wang, Y. F. 1996. Cycling of iron and manganese in surface sediments: A general theory for the coupled transport and reaction of carbon, oxygen, sulfur, iron, and manganese. Am. J. Sci. **296**: 197-243.

van der Merel, H. W. and Beutelspacher, H. 1976. Atlas of infrared spectroscopy of clay minerals and their admixtures. Elsevier, Amsterdam, The Netherlands.

Veldkamp, E. 1994. Organic-carbon turnover in 3 tropical soils under pasture after deforestation. Soil Sci. Soc. Am. J. **58**: 175-180.

Violante, A., Gianfreda, L. and Violante, P. 1993. Effect of prolonged aging on the transformation of short-range ordered aluminum precipitation products formed in the presence of organic and inorganic ligands. Clays Clay Miner. **41**: 353-359.

Violante, A. and Huang, P. M. 1985. Influence of inorganic and organic ligands on the formation of aluminum hydroxides and oxyhydroxides. Clays Clay Miner. **33**: 181-192.

Violante, A. and Huang, P. M. 1993. Formation mechanism of aluminum hydroxide polymorphs. Clays Clay Miner. **41**: 590-597.

von Lützow, M., Kögel-Knabner, I., Ekschmitt, K., Matzner, E., Guggenberger, G., Marschner, B. and Flessa, H. 2006. Stabilization of organic matter in temperate soils: mechanisms and their relevance under different soil conditions – a review. Eur. J. Soil Sci. **57**: 426-445.

Waksman, S. A. 1936. Humus. The Williams & Wilkins Co., Baltimore, MD, USA.

Wan, J., Tyliszczak, T. and Tokunaga, T. K. 2007. Organic carbon distribution, speciation, and elemental correlations within soil micro aggregates: Applications of STXM and NEXAFS spectroscopy. Geochim. Cosmochim. Acta **71**: 5439-5449.

Wang, D. and Anderson, D. W. 1998. Direct measurement of organic carbon content in soils by the Leco CR-12 carbon analyzer. Comm. Soil Sci. Plant Anal. **29**: 15-21.

Wang, M. C. and Huang, P. M. 1986. Humic macromolecule interlayering in nontronite through interaction with phenol monomers. Nature **323**: 529-531.

Wang, M. C. and Huang, P. M. 1987. Polycondensation of pyrogallol and glycine and the associated reactions as catalyzed by birnessite. Sci. Total Environ. **62**: 435-442.

Wang, M. C. and Huang, P. M. 1989a. Abiotic ring cleavage of pyrogallol and the associated reactions as catalyzed by a natural soil. Sci. Total Environ. **81/82**: 501-510.

Wang, M. C. and Huang, P. M. 1989b. Catalytic power of nontronite, kaolinite and quartz and their reaction sites in the formation of hydroquinone-derived polymers. Appl. Clay Sci. **4**: 43-57.

Wang, M. C. and Huang, P. M. 1989c. Pyrogallol transformations as catalyzed by nontronite, bentonite and kaolinite. Clays Clay Miner. **37**: 525-531.

Wang, M. C. and Huang, P. M. 1991. Nontronite catalysis in polycondensation of pyrogallol and glycine and the associated reactions. Soil Sci. Soc. Am. J. **55**: 1156-1161.

Wang, M. C. and Huang, P. M. 1992. Significance of Mn(IV) oxide in the abiotic ring cleavage of pyrogallol in natural environments. Sci. Total Environ. **113**: 147-157.

Wang, M. C. and Huang, P. M. 1994. Structural role of polyphenols in influencing the ring cleavage and related chemical reactions as catalyzed by nontronite. Pages 173-180 *in* N. Senesi, T. M. Miano, eds. Humic substances in the global environment and implications on human health. Elsevier, Amsterdam, The Netherlands.

Wang, M. C. and Huang, P. M. 1997. Catalytic power of birnessite in abiotic formation of humic polycondensates from glycine and pyrogallol. Pages 59-65 *in* J. Drozl, S. S. Gonet, N. Senesi, J. Webber, eds. Proceedings of the 8th conference of the International Humic Substances Society, Wroclaw, Poland.

Wang, M. C. and Huang, P. M. 2000a. Characteristics of pyrogallol-derived polymers formed by catalysis of oxides. Soil Sci. **165**: 737-747.

Wang, M. C. and Huang, P. M. 2000b. Ring cleavage and oxidative transformation of pyrogallol catalyzed by Mn, Fe, Al, and Si, oxides. Soil Sci. **165**: 934-942.

Wang, M. C. and Huang, P. M. 2003. Cleavage and polycondensation of pyrogallol and glycine catalyzed by natural soil clay. Geoderma **112**: 31-50.

Wang, M. C. and Huang, P. M. 2005. Cleavage of ^{14}C-labelled glycine and its polycondensation with pyrogallol as catalyzed by birnessite. Geoderma **124**: 415-426.

Wang, M. C. and Lin, C. H. 1993. Enhanced mineralization of amino-acids by birnessite as influenced by pyrogallol. Soil Sci. Soc. Am. J. **57**: 88-93.

Wang, T. S. C., Chen, J.-H. and Hsiang, W.-M. 1985. Catalytic synthesis of humic acids containing various amino acids and dipeptides. Soil Sci. **140**: 3-10.

Wang, T. S. C., Huang, P. M., Chou, C.-H. and Chen, J.-H. 1986. The role of soil minerals in abiotic polymerization of phenolic compounds and formation of humic substances. Pages 251-281 *in* P. M. Huang, M. Schnitzer, eds. Interactions of soil minerals with natural organics and microbes. Soil Science Society of America, Madison, WI, USA.

Wang, T. S. C., Kao, M.-M. and Ferng, Y. L. 1978a. Catalytic polymerization of phenolic compounds by clay minerals. Soil Sci. **126**: 15-21.

Wang, T. S. C., Kao, M.-M. and Li, S. W. 1978b. A new proposed mechanism of formation of soil humic substance. Pages 357-372 Studies and essays in commemoration of the golden jubilee of Academia Sinica. Academia Sinica, Tapei, Taiwan.
Wang, T. S. C. and Li, S. W. 1977. Clay minerals as heterogeneous catalysts in preparation of model humic substances. Zeit. Pflanzenern. Dueng. Bodenk. **140**: 669-676.
Wang, T. S. C., Li, S. W. and Huang, P. M. 1978c. Catalytic polymerization of phenolic compounds by a latosol. Soil Sci. **126**: 81-86.
Wang, T. S. C., Wang, M. C., Ferng, Y. L. and Huang, P. M. 1983a. Catalytic synthesis of humic substances by natural clays, silts and soils. Soil Sci. **135**: 350-360.
Wang, T. S. C., Wang, M. C. and Huang, P. M. 1983b. Catalytic synthesis of humic substances by using aluminas as catalysts. Soil Sci. **136**: 226-246.
Watts, B., Thomsen, L. and Dastoor, P. C. 2006. Methods in carbon K-edge NEXAFS: Experiment and analysis. J. Electron Spectrosc. **151**: 105-201.
Weast, R. C. 1978. CRC handbook of chemistry and physics 58th Ed. CRC Press, Boca Raton, FL, USA.
Weiss, M. S., Abele, U., Weckesser, J., Welte, W., Schiltz, E. and Schulz, G. E. 1991. Molecular architecture and electrostatic properties of a bacterial porin. Science **254**: 1627-1630.
Whittig, L. D. and Allardice, W. R. 1986. X-ray diffraction techniques. Pages 331-362 *in* A. Klute, ed. Methods of soil analysis Part 1. Physical and mineralogical methods. American Society of Agronomy and Soil Science Society of America, Madison, WI, USA.
Wilke, M., Farges, F., Petit, P.-E., Brown Jr., B. E. and Martin, F. 2001. Oxidation state and coordination of Fe in minerals: An Fe K-XANES spectroscopic study. Am. Mineral. **86**: 714-730.
Wilson, M. A. and Goh, K. M. 1977. Proton-decoupled pulse Fourier-transform ^{13}C nuclear magnetic resonance of soil organic matter. J. Soil Sci. **28**: 645-652.
Wolff, S. P. 1996. Free radicals and glycation theory. Pages 73-88 *in* R. Ikan, ed. The Maillard reaction. Consequences for the chemical and life sciences. John Wiley & Sons, Chichester, UK.
Wolters, V. 2000. Invertebrate control of soil organic matter stability. Biol. Fert. Soils **31**: 1-19.
Wong, J. W. and Shibamoto, T. 1996. Geotoxicity of the Maillard reaction products. Pages 129-159 The Maillard reaction. Consequences for the chemical and life sciences. John Wiley & Sons, Chichester, UK.
Xia, G. and Pignatello, J. J. 2001. Detailed sorption isotherms of polar and apolar compounds in a high-organic soil. Environ. Sci. Technol. **35**: 84-94.
Xing, B. 2001. Sorption of naphthalene and phenanthrene by soil humic acids. Environ. Poll. **111**: 303-309.
Xu, G. and Goodell, B. 2001. Mechanisms of wood degradation by brown-rot fungi: chelator-mediated cellulose degradation and binding of iron by cellulose. J. Biotech. **87**: 43-57.
Yavmetidinov, I. S., Stepnova, E. V., Gavrilova, V. P., Lokshin, B. V., Perminova, L. V. and Koroleva, O. V. 2003. Isolation and characterization of humin-like substances produced by wood-degrading white rot fungi. Appl. Biochem. Microbiol. **39**: 257-264.
Yaylayan, V. A. 1997. Classification of the Maillard reaction: A conceptual approach. Trends Food Sci. Technol. **8**: 13-18.

Yoon, T. H., Hohnson, S. B., Benzerara, K., Tyliszczak, T., Shuh, D. K. and Brown, G. B. J. 2004. In situ characterization of aluminum-containing mineral-microorganism aqueous suspensions using scanning transmission X-ray microscopy. Langmuir **23**: 10361-10366.

Yu, G., Saha, U. K., Kozak, L. M. and Huang, P. M. 2006. Kinetics of cadmium adsorption on aluminum precipitation products formed under the influence of tannate. Geochim. Cosmochim. Acta **70**: 5134-5145.

Zamora, R. and Hidalgo, F. J. 2005. Coordinate contribution of lipid oxidation and Maillard reaction to the nonenzymatic food browning. Crit. Rev. Food Sci. Nutr. **45**: 49-59.

Zavarzina, A. G. and Zavarzin, A. A. 2006. Laccase and tyrosinase activities in lichens. Microbiol. **75**: 546-556.

Zegouagh, Y., Derenne, S., Largeau, C., Betrand, P., Sicre, M.-A., Sliot, A. and Rousseau, B. 1999. Refractory organic matter in sediments from the north-west African upwelling system: abundance, chemical structure and origin. Org. Geochem. **30**: 83-99.

Ziechmann, W. 1959. Die Darstellung von Huminsauren im heterogenen System mit neutraler Reaktion. Zeit. Pflanzenern. Dueng. Bodenk. **84**: 155-159.

6 APPENDICES

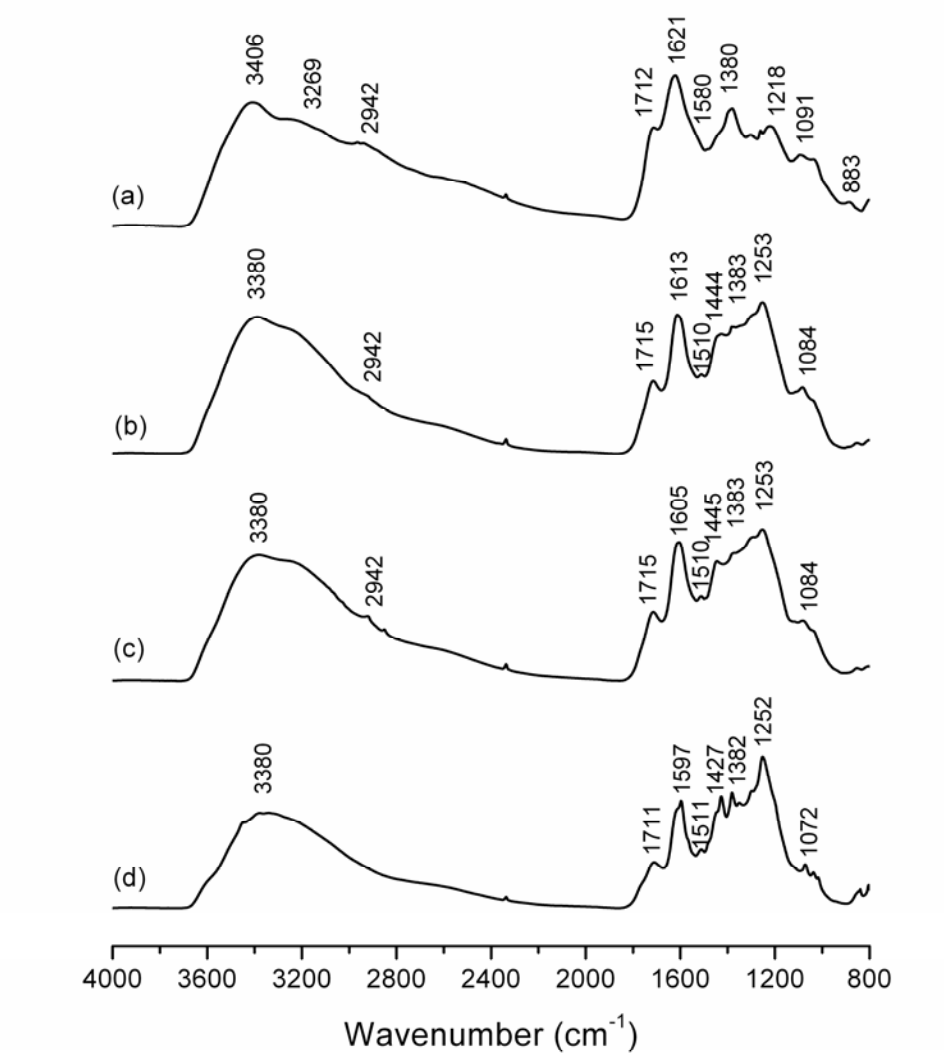

Figure A1 FTIR spectra of the humic acids isolated from the supernatants of reaction systems catalyzed by birnessite: (a) the Maillard reaction; integrated pyrogallol-Maillard reaction systems with: (b) 0.05 mole pyrogallol and (c) 0.10 mole pyrogallol; and (d) 0.05 mole pyrogallol only system.

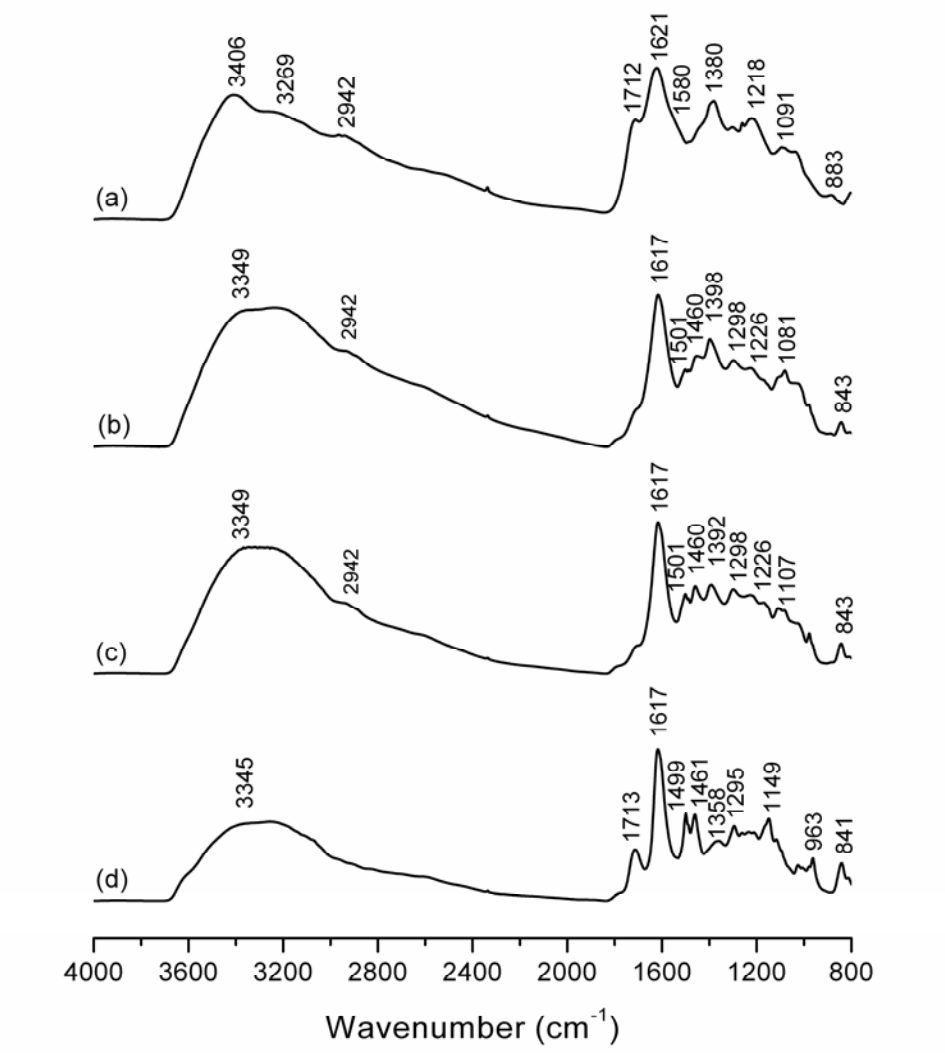

Figure A2 FTIR spectra of the humic acids isolated from the supernatants of reaction systems catalyzed by birnessite: (a) the Maillard reaction; integrated resorcinol-Maillard reaction systems with: (b) 0.05 mole resorcinol and (c) 0.10 mole resorcinol; and (d) 0.05 mole resorcinol only system.

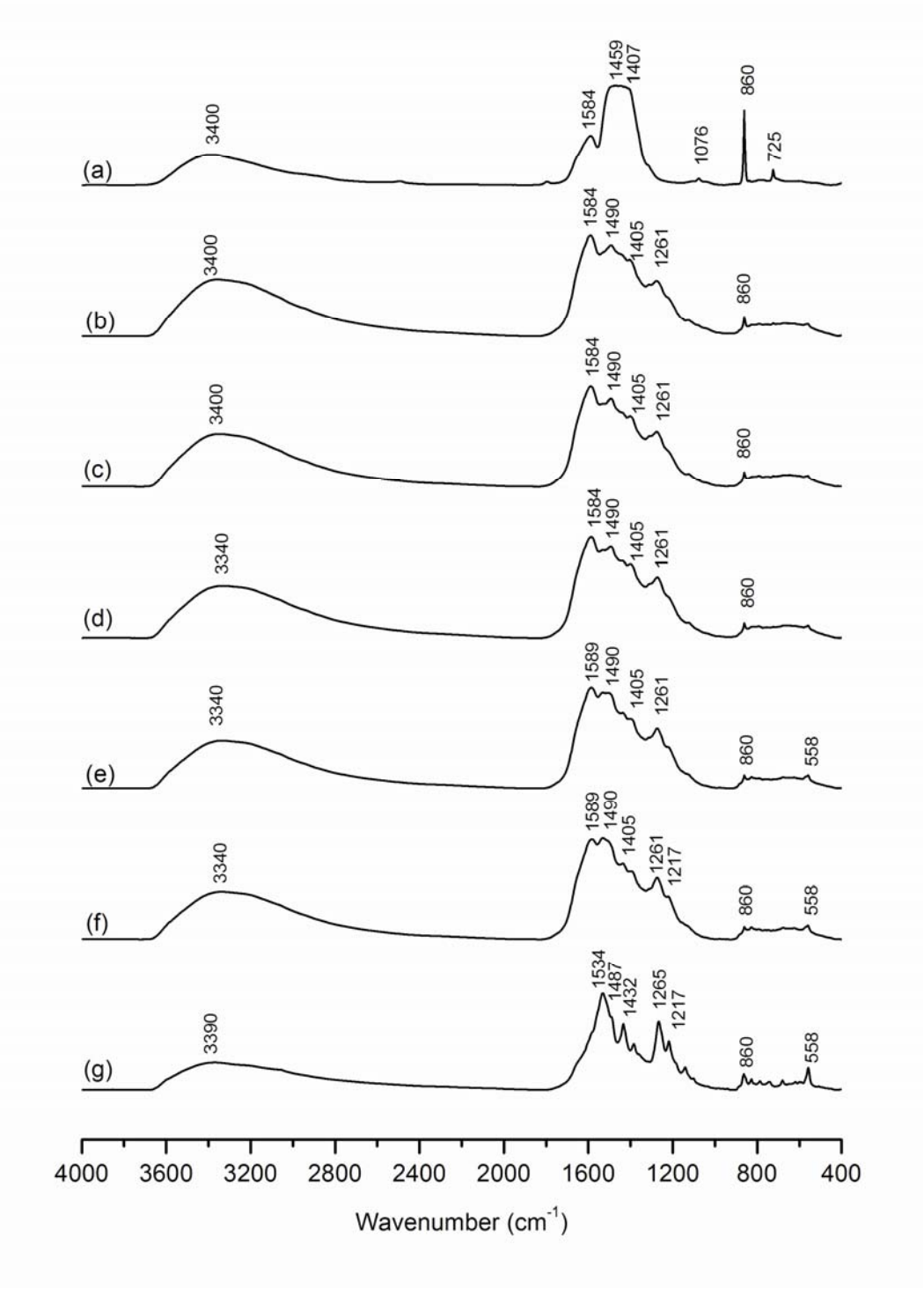

Figure A3 FTIR spectra of the solid residues isolated from the reaction systems catalyzed by birnessite: (a) the Maillard reaction; integrated catechol-Maillard reaction systems with: (b) 0.1 mole glucose, (c) 0.05 mole glucose, (d) 0.025 mole glucose and (e) 0.0025 mole glucose; (f) the catechol-glycine system (0.05 mole catechol + 0.05 mole glycine); and the catechol only system (0.05 mole catechol).

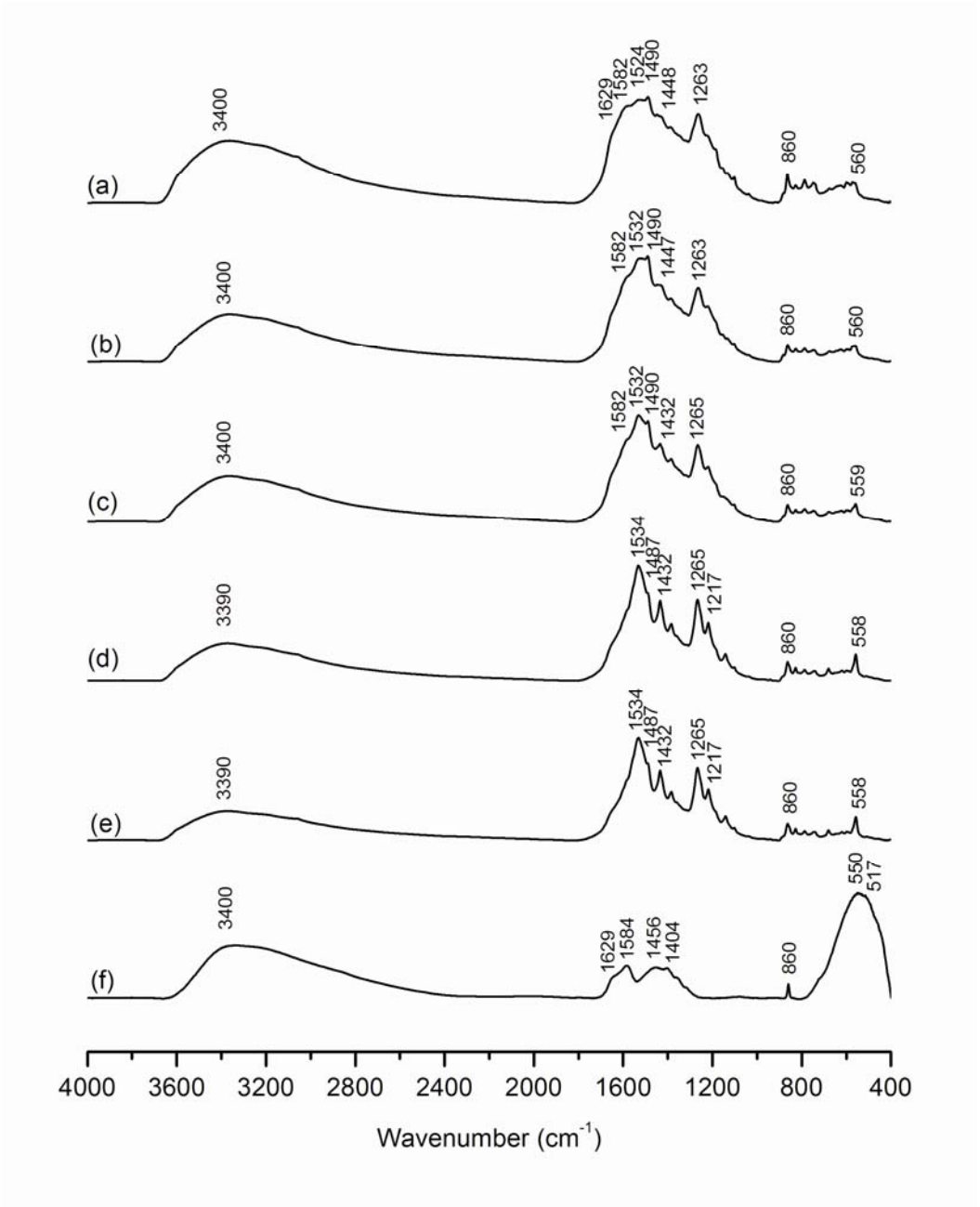

Figure A4 FTIR spectra of the solid residues isolated from the reaction systems catalyzed by birnessite: the catechol-glucose reaction systems with: (a) 0.1 mole glucose, (b) 0.05 mole glucose, (c) 0.025 mole glucose and (d) 0.0025 mole glucose; (e) the catechol only system (0.05 mole catechol); and (f) the glucose only system (0.05 mole glucose).

Table A1 Assignments of FTIR absorption bands of humic acids isolated from the supernatants of the Maillard, integrated pyrogallol-Maillard and resorcinol-Maillard, and pyrogallol- and resorcinol only systems shown in Fig A1 and A2.

Fig. A1 (a) and A2 (a) Maillard reaction system		**Fig. A1 (b) & (c) Pyrogallol-Maillard systems with 0.05 and 0.10 mole pyrogallol**		**Fig. A1 (d) 0.05 mole pyrogallol only system**		**Fig. A2 (b) & (c) Resorcinol-Maillard systems with 0.05 and 0.10 mole resorcinol**		**Fig. A2 (d) 0.05 mole resorcinol only system**	
Wavenumber (cm^{-1})		**Wavenumber (cm^{-1})**		**Wavenumber (cm^{-1})**		**Wavenumber (cm^{-1})**		**Wavenumber (cm^{-1})**	
883	Out of plane aromatic C-H bend	1084	Aliphatic C-O stretching	1072	Aliphatic C-O stretching	843, 1081-1107	Aliphatic C-O stretching	841, 963, 1149	Aliphatic C-O stretching
1091	Aliphatic C-O stretching	1253	C-O stretch and bending of COOH, C-O stretch of phenols or aryl ethers	1252	C-O stretch and bending of COOH, C-O stretch of phenols or aryl ethers	1226	C-O stretch and bending of COOH, C-O stretch of phenols or aryl ethers	1295	C-O stretch and bending of COOH, C-O stretch of phenols or aryl ethers
1218	C-O stretch and bending of COOH, C-O stretch of phenols or aryl ethers	1383	OH deformation and C-O stretch of phenols, C-H deformation of CH_2 & CH_3, asymmetrical stretch of COO^-	1382	OH deformation and C-O stretch of phenols, C-H deformation of CH_2 & CH_3, asymmetrical stretch of COO^-	1298	C-O stretch and bending of COOH, C-O stretch of phenols or aryl ethers	1358	OH deformation and C-O stretch of phenols, C-H deformation of CH_2 & CH_3, asymmetrical stretch of COO^-
1380	OH deformation and C-O stretch of phenols, C-H deformation of CH_2 & CH_3, asymmetrical stretch of COO^-	1444 - 1445	Assymetrical bending of CH_2 & CH_3, C=C aromatic ring stretch	1427	Assymetrical bending of CH_2 & CH_3 deformation band, C=C aromatic ring stretch	1392-1398	OH deformation and C-O stretch of phenols, C-H deformation of CH_2 & CH_3, asymmetrical stretch of COO^-	1461	Assymetrical bending of CH_2 & CH_3, C=C aromatic ring stretch
1580	Symmetric C-O stretch of COO^-, N-H deformation + C=N amide II band	1510	Symmetric C-O stretch of COO^-, N-H deformation + C=N amide II band	1511	Symmetric C-O stretch of COO^-	1460	Assymetrical bending of CH_2 & CH_3, C=C aromatic ring stretch	1499	Symmetric C-O stretch of COO^-
1621	Aromatic C=C ring stretch	1605-1613	Aromatic C=C stretch, symmetric C-O stretch of COO^- (shoulder)	1597	Aromatic C=C stretch, symmetric C-O stretch of COO^- (shoulder)	1501	Symmetric C-O stretch of COO^-	1617	Aromatic C=C stretch
1712	Symmetric C=O stretch of COOH	1715	Symmetric C=O stretch of COOH	1711	Symmetric C=O stretch of COOH	1617	Aromatic C=C ring stretch	1713	Symmetric C=O stretch of COOH
2942	Aliphatic C-H stretch	2942	Aliphatic C-H stretch	3380	OH stretch	1713	Symmetric C=O stretch of COOH	3345	OH stretch
3269	OH or N-H stretch	3380	OH stretch			2942	Aliphatic C-H stretch		
3406	OH stretch					3349	OH stretch		

Table A2 Assignments of FTIR absorption bands of the solid residues of the Maillard reaction, catechol-Maillard and catechol only systems shown in Fig. A3.

(a) Maillard reaction system		**(b)–(e) Integrated catechol-Maillard and (f) catechol-glycine systems**		**(g) Catechol only system**	
Wavenumber (cm^{-1})		**Wavenumber (cm^{-1})**		**Wavenumber (cm^{-1})**	
725	Carbonate C-O out of plane bend	558	Mn-O vibrations, aliphatic C-O stretches	558	Mn-O vibrations
860	Carbonate C-O stretch	860	Carbonate C-O stretch	860	Carbonate C-O stretch
1076	Carbonate C-O stretch	1217	C-O stretch of phenols or phenyl ethers	1217	C-O stretch of phenols or phenyl ethers
1407	OH deformation of phenols, C-H deformation of CH_2 & CH_3, symmetrical stretch of COO^-	1261	C-O stretch of phenols and phenyl ethers	1265	C-O stretch of phenols or phenyl ethers
1459	Carbonate symmetric C-O stretch, assymetrical bending of CH_2 & CH_3 deformation band	1405	OH deformation of phenols, C-H deformation of CH_2 & CH_3, symmetrical stretch of COO^-	1432	OH deformation of phenols, C-H deformation of CH_2 & CH_3, symmetrical stretch of COO^-
1584	Aromatic C=C stretch, Symmetric C-O stretch of COO^-, N-H deformation + C=N amide II band	1490	Symmetric C-O stretch of COO^-, N-H deformation + C=N amide II band	1487	Symmetric C-O stretch of COO^-
3400	OH stretch	1584-1589	Aromatic C=C stretch, Symmetric C-O stretch of COO^-, N-H deformation + C=N amide II band	1534	Aromatic C=C stretch, Symmetric C-O stretch of COO^-
		3340-3400	OH stretch	3390	OH stretch

Table A3 Assignments of FTIR absorption bands of the solid residues of the catechol-glucose, catechol only and glucose only systems shown in Fig. A4.

(a), (b) and (c) Catechol-glucose system with 0.1, 0.05 and 0.025 mole glucose, respectively.		**(d) Catechol-glucose system with 0.0025 mole glucose and (e) catechol only system**		**(f) Glucose only system**	
Wavenumber (cm^{-1})		**Wavenumber (cm^{-1})**		**Wavenumber (cm^{-1})**	
559-560	Mn-O vibrations, aliphatic C-O stretches	558	Mn-O vibrations, aliphatic C-O stretches	517, 550	Mn-O vibrations (birnessite and other Mn(III)/(IV) oxides
860	Carbonate C-O stretch	860	Carbonate C-O stretch	860	Carbonate C-O stretch
1263-1265	C-O stretch of phenols or phenyl ethers	1217	C-O stretch of phenols or phenyl ethers	1404	OH deformation of phenols, C-H deformation of CH_2 & CH_3, symmetrical stretch of COO^-
1432-1448	OH deformation of phenols, C-H deformation of CH_2 & CH_3, symmetrical stretch of COO^-	1265	C-O stretch of phenols or phenyl ethers	1456	Carbonate symmetric C-O stretch, assymetrical bending of CH_2 & CH_3 deformation band
1490	Symmetric C-O stretch of COO^-	1432	OH deformation of phenols, C-H deformation of CH_2 & CH_3, symmetrical stretch of COO^-	1584	Aromatic C=C stretch, Symmetric C-O stretch of COO^-, N-H deformation + C=N amide II band
1524-1532	Aromatic C=C stretch, Symmetric C-O stretch of COO^-	1487	Symmetric C-O stretch of COO^-	1629	Aromatic C=C stretch
1582	Aromatic C=C stretch, Symmetric C-O stretch of COO^-, N-H deformation + C=N amide II band	1534	Aromatic C=C stretch, Symmetric C-O stretch of COO^-	3400	OH stretch
1629	Aromatic C=C stretch	3390	OH stretch		
3400	OH stretch				